Durability of Concrete under Combined Action – Mechanical Load and Alkali-Silica Reaction

By

"Salhin Mohamed Alaud"

Dissertation presentedfor the degree of Doctor of Philosophy in Civil Engineering at Stellenbosch University

Supervisor: “Professor GPAG Van Zijl"

"Faculty of Engineering"

"December 2016"

Declaration

By submitting this dissertation electronically, I declare that the entirety of the work contained therein is my own, original work, that I am the sole author thereof (save to the extent explicitly otherwise stated), that reproduction and publication thereof by Stellenbosch University will not infringe any third party rights and that I have not previously in its entirety or in part submitted it for obtaining any qualification.

Signature:

December 2016

Acknowledgements

My deep gratitude goes first to my supervisor Professor Gideon P.A.G. Van Zijl, for his guidance and help to carry on this study in the best possible way. His unwavering enthusiasm for concrete technology kept me constantly engaged with my research and assisted me overcomes all the obstacles I have faced. Also, his financial support for materials and devices is gratefully acknowledged.

Thanks for the teams of technicians at the concrete and structures laboratory, especially, the laboratory manager, Stephen Zeranka, as well as the technical staff at our workshop for their great assistance in setting-up the test machines and conducting all the experiments.

I would also like to acknowledge the secretary and the staff of the department for their unconditional support and help.

I am also grateful to my family, my colleagues of the Civil Engineering and my friends for their continuous support and encouragement during my PhD studies.

Publications

1. **Salhin Alaud and Gideon P.A.G. Van Zijl. COMBINED MECHANICAL LOAD AND ALKALI SILICA REACTION IN CONCRETE**, Indian Concrete Institute (ICI), Article for 2th International Congress on Durability of Concrete, India, 2014.

2. **Salhin Alaud and Gideon P.A.G. Van Zijl ROLE OF PRE-CRACK FORMATION AND ALKALI SILICA REACTION ON CONCRETE**, Proceedings: 15th International Conference on Alkali Aggregate Reaction in Concrete (ICAAR), Sau Paulo, Brazil, 3-7 July, 2016, Ref: 142.

3. **Salhin Alaud and Gideon P.A.G. Van Zijl, EFFECTS ON CONCRETE PROPERTIES BY ASR DETERIORATION UNDER DIFFERENT EXPOSURE CONDITIONS**, Proceedings: 6th International Conference on Structural Engineering, Mechanics and Computation (SEMC 2016), 5-7 September 2016, Cape Town, South Africa, Ref: SEMC 2016/310.

4. **Salhin Alaud and Gideon P.A.G. Van Zijl. ASR AND MECHANICAL CRACK WIDTH IN REINFORCED CONCRETE,** Paper has submitted to 14th International Conference on Durability of Building Materials and Components (DBMC), 29-31 May 2017, Ghent, Belgium, Ref: DBMC-36.

5. **Salhin Alaud and Gideon P.A.G. Van Zijl. EFFECT OF COMBINED ASR AND CYCLIC LOADING ON CONCRETE BRIDGES**, Paper has submitted to International Conference Sustainable Civil Infrastructures: Innovative Infrastructure Geotechnology (GeoMEast 2017), 15-19 July, 2017, Sharm Elsheikh, Egypt, Ref: SUCI-D-16-00274.

Abstract

There are still many problems remaining unresolved when concrete structures exposed to combined actions are studied separately, such as, severe environment and mechanical loads. In practice, these conditions act simultaneously, and separate studies may underestimate the rates of deterioration. Alkali-Silica Reaction (ASR) is a major source of deterioration causing cracking in concrete and these cracks may lead to other problems, such as a reduced resistance to the ingress of gas, water and deleterious matter, which in turn have the potential to accelerate the ASR process, but also the carbonation, corrosion and other deterioration processes.

An experimental study has been designed to investigate the durability of normal and reinforced concrete elements subjected to the combined action of mechanical loading and degradation due to ASR. Mechanical loading is simulated by the compression, direct tensile, wedge splitting and fatigue (tensile cyclic loads) in pavements due to repeated wheel loads. The environmental action is simulated by means of ASR, induced with the crystalline reaction products. Different mixes with two types of local aggregates, reactive (Greywacke) and non-reactive (Granite) were prepared. Also, ground granulated Corex slag (GGCS) was added to half of the specimens. Reinforced prisms of concrete were prepared to calculate the combined action of mechanical and ASR expansion. Strength and modulus of elasticity under various conditions of ASR were determined from cylinders concrete. Also, wedge splitting on cubes were conducted to monitor the role of ASR on the pre-mechanical cracks. Two methods were followed to determine the ASR effects under combined action; the first was the accelerated method according to the conditions of ASTM C 1260 using a device specially made to immerse specimens in sodium hydroxide solution at 80°C; the second method was carried out over a long period of time (65weeks) according to ASTM C 1293. The specimens in the second method were made with high alkaline and exposed to two conditions, namely partially submerged and high humidity at 38°C. A comparison was made between the behaviour of the specimens exposed to combined action and others exposed to ASR only. Test results indicated that the damage due to combined action is more significant than that due to ASR only. The Granite mixes were less deteriorated than Greywacke mixes. Also the Corex slag decreases this deterioration dramatically. Mechanical cracks were the largest in Greywacke mixes with a higher ASR expansion than the others and the smallest were in Granite mixes with Corex slag. The strength and E-modulus of concrete were reduced due to ASR effects over time. The results from the two methods were different, where the accelerated method (ASTM C 1260) was not an accurate reflection of the ASR of reinforced concrete, but an indicator of the potential deterioration due to ASR. The series method of ASTM C 1293 was more accurate in identifying the changes in mechanical cracks under ASR. Finally, all the results have been reflected in graphs and have been compared and modelled.

Opsomming

Indien die effek van aksies op beton apart bestudeer word, word die invloed van gekombineerde aksie verwaarloos. As voorbeeld, veroorsaak meganiese belasting krake, wat vervolgens kan lei tot vinniger agteruitgang van beton wat blootgestel is aan aggressiewe omgewings. In die praktyk tree hierdie omstandighede terselfdertyd op, en afsonderlike studies lei tot onderskatting van die tempo van agteruitgang. Alkali-Silika Reaksie (ASR) is 'n belangrike bron van agteruitgang, wat krake in beton veroorsaak. Hierdie krake lei tot verdere probleme, soos verlaagde weerstand teen indringing van gas, water en ander nadelige stowwe, wat die potensiaal het om ASR te versnel, maar ook om karbonasie, korrosie en ander degradasie-prosesse te veroorsaak. 'n Eksperimentele studie is ontwerp om duursaamheid van normale en bewapende beton-elemente te ondersoek, wat blootgestel is aan die gekombineerde aksie van meganiese belasting en ASR degradasie. Meganiese belasting word nageboots deur belasting in druk, direkte trek, wigsplyting en vermoeidheid (sikliese trekbelastings). Laasgenoemde simuleer byvoorbeeld snelweg brugelemente wat aan herhaalde wielbelastings blootgestel word. Die omgewingsinvloede word nageboots deur gunstige toestande vir ASR, wat ingelei word deur kristallyne reaksieprodukte. Verskillende betonmenge met twee soorte lokale aggregaat, reaktief (Greywacke) en nie-reaktief (Graniet) is voorberei. Fyngemaalde granulêre Corex slagment (GGCS) is gevoeg by die helfte van die proefstukke. Dit is bekend dat GGCS 'n laer alkali-inhoud het, waardeur die ASR reaksie en -potensiaal verlaag word. Ook gewapende betonprismas is voorberei om die invloed van gekombineerde aksie te bepaal. Sterkte en styfheid van beton wat blootgestel was aan verskeie ASR toestande is bepaal op betonsilinders. Wigsplyting is ook uitgevoer op betonkubusse om die rol van ASR op vooraf gekraakte beton te toets. Twee metodes is gevolg om die effekte van ASR onder gekombineerde aksie te bepaal; die eerste is die versnelde metode volgens ASTM C 1260, waarvoor spesiaal vervaardigde apparatuur gebruik is om proefstukke te onderdompel in natriumhidroksied oplossing teen 80°C; die tweede is die metode van ASTM C 1293, uitgevoer oor 'n periode van 65 weke. In laasgenoemde metode is die proefstukke vervaardig met hoë alkali inhoud en blootgestel aan twee toestande, naamlik deels onderdompel en hoë humiditeit teen 38°C. 'n Vergelyking is gemaak tussen die gedrag van die proefstukke wat aan gekombineerde aksie onderwerp is, met dié van proefstukke wat slegs aan ASR-gunstige toestande onderwerp is. Toetsresultate het daarop gedui dat skade veroorsaak deur gekombineerde aksie meer noemenswaardig is as skade as gevolg van slegs ASR. Die Graniet-menge het minder agteruitgegaan as die Greywacke menge. GGCS lei ook tot verlaagde agteruitgang. Die invloed van meganiese krake was die grootste in Greywacke menge, met hoër ASR swelling as die ander menge. Die kleinste effek is waargeneem in Graniet-menge wat Corex slagment bevat het. Die sterkte en elastisiteitsmodulus van beton het met verloop van tyd verlaag as gevolg van ASR effekte. Die resultate van die twee metodes was verskillend. Die ASTM C 1260 toets het nie ASR in gewapende beton akkuraat gereflekteer nie, maar tog as indruk van potensiaal tot agteruitgang deur ASR gedien. Die ASTM C 1293 metode was meer akkuraat

in identifisering van die veranderinge in meganiese krake onder ASR toestande. Ten slotte is alle resultate in grafieke gereflekteer, vergelyk, en gemodelleer.

Table of Contents

List of Figures

List of Tables

Symbols and abbreviation

Symbols

Am	ASR reaction affinity
Am_0	Initial ASR reaction affinity
c	Intrinsic ASR dilation coefficient
C_{agg}	Volume fraction of all the aggregate per m^3 of concrete
C_d	Kinetic coefficient of ASR reactivity
C_u	Dimensionless parameter representing the size of the crack
C_w	Crack width
E	Elastic modulus of reactive, ASR infected concrete
E_0	Initial Young's modulus
E_d	Damaged Young's modulus
E_g	Elastic modulus of the gel
E_s	Elastic modulus of the skeleton
E_t	Young's modulus at any time
f_{cu}	Compressive strength in cyclic loading
f_{max}	Maximum of cyclic applied stress
f_t	Tensile strength in cyclic loading
g_1& q_1	Parameters of compressive cyclic loading from S-N curve
g_3& q_3	Parameters of indirect tensile cyclic loading from S-N curve
I	Identity matrix
k	Characteristic ASR rate coefficient
n_g^a	One size of aggregate
Na	The number of reactive aggregates per m^3 of concrete
P	Porosity
P_g	internal swelling pressure due to gel formation
R_a	Mean radius of aggregate
R_g	Radius of gels formed by ASR
R_p	Radius of pores
R_{REV}^a	REV radius corresponding to the aggregate size fraction a
S(x)	Area of the created crack
SC	Surrounding Concrete

t	Time
t_0	Starting reaction time
t_c	Characteristic ASR reaction time
tc	Thickness of the connected porous interface zone
t_{cr}^{m}	Time at which the mechanical crack arises
t_{ini}	Initial reaction time from starting time to mechanical crack arises
t_f	Final reaction time, i.e. when ASR reaction is completed
tr	The trace function
υ	Poisson's Ratio
V_a	Volume of sound aggregate
V_g	Volume of gel induced by ASR
V_{gel}^{mol}	Molar volume of ASR gel (in m^3/mol)
V_{por}	Volume of porosity in the concrete

Greek symbols

α	Coefficient of exponential ASR-induced reduction in E-modulus
μ	k-α, the coefficient of exponential rate of crack closure
Δl_{asr}	Length change due to ASR expansion
Δl_f	Length change after a mechanical crack arises
Δl_{ini}	Length change before a mechanical crack arises
ρ^r	Material density in the final, fully swollen state
ρ^u	Initial material density, i.e. the density in the unswollen state
Δl	Length change in concrete element due to combined action, mechanical and ASR
μ	Second parameter of Lamé's
β	ASR dilation coefficient
δ	The ratio of the gel volume to the aggregate volume
ε	Total normal strain, one-dimensional
ε_a	Expansions induced by each fraction of aggregate
ε_{asr}	Stress-free strain associated with ASR reaction
ε_m	Mechanical strain, i.e. strain leading to stress
ε_{sh}	Stress-free strain associated with hygral expansion/shrinkage
ε_T	Stress-free strain associated with thermal expansion
λ	First parameter of Lamé's

ξ	Extent of ASR, varying between 0 (no ASR) to 1 (ASR reaction completed)
ρ	Volume fraction
σ	Normal stress, here considered one-dimensional only
σ_{μ}	Tensile stress in the skeleton, here considered one-dimensional only
σ_{sc}	Stress of surrounding concrete SC

Abbreviations

AAR	Alkali aggregate reaction
ACR	Alkali carbonates reaction
ASR	Alkali silica reaction
CEM I 52.5	Ordinary Portland Cement type I with 52,5 N strength class
dnt	Micro digital camera using to measure the crack widths
ITZ	Interface transition zone
GGBS	Ground Granulated Blast Furnace slag
GGCS	Ground Granulated Corex Slag
Gn	Concrete mix made with Granite stone
Gn-co	Concrete mix made with Granite stone and 50% of the CEM I replaced by GGCS
Gw	Concrete mix made with Greywacke stone
Gw-co	Concrete mix made with Greywacke stone and 50% of the CEM I replaced by GGCS
Gn/H	Concrete mix made with Granite stone exposed to humidity
Gn-co/H	Concrete mix made with Granite stone and 50% of the CEM I replaced by GGCS exposed to humidity
Gw/H	Concrete mix made with Greywacke stone exposed to humidity
Gw-co/H	Concrete mix made with Greywacke stone and 50% of the CEM I replaced by GGCS exposed to humidity
Gn/w	Concrete mix made with Granite stone partially or totally submerged in water or NaOH
Gn-co/w	Concrete mix made with Granite stone and 50% of the CEM I replaced by GGCS partially or totally submerged in water or NaOH
Gw/w	Concrete mix made with Greywacke stone partially or totally submerged in water or NaOH
Gw-co/w	Concrete mix made with Greywacke stone and 50% of the CEM I replaced by GGCS partially or totally submerged in water or NaOH
LVDT	Linear Variable Differential Transformers
Na_2Oe	Equivalent sodium oxide

MTM	Contest materials testing machine
RC	Reinforced concrete
REV	Relative Elementary Volume
RH	Relative humidity
Series 1	Tests exposing to ASTM C 1260 standard conditions
Series 2	Tests exposing to ASTM C 1293 standard conditions
XRF	X-Ray Fluorescence

CHAPTER ONE

1. INTRODUCTION

1.1 General concept

The durability of reinforced concrete (RC) structures has been studied for decades. It relates to the ability of a structure to maintain its characteristics such as safety, efficiency and aesthetics during its service life. Mechanical and environmental actions affect concrete structures. Many studies have been done concerning the effects of mechanical loads and severe environmental conditions on concrete structures, but there are still many problems remaining unresolved regarding concrete structures exposed to combined actions of both the above effects. In practice, these loads and conditions act simultaneously and separate consideration thereof may underestimate the rates of deterioration. For example, road pavements are exposed to dynamic loads (cyclic loading) and the surrounding environment, which may interact with concrete, and cause deterioration processes such as alkali-silica reaction, carbonation, chloride-induced corrosion as well as temperature and humidity-induced shrinkage, expansion and even cracking.

Two of the most important and analysed effects that lead to the deterioration of concrete pavements and structures are the alkali-silica reaction (ASR) and repeated mechanical load. The service life of RC structures can be reduced by the effect of ASR in the presence of reactive aggregate and high relative humidity. Also by repetitive loading, the resistance of RC structures is reduced relative to a single load cycle. For the past several years, producers of concrete and concrete-materials engineers have tried finding ways to mitigate concrete damage caused by ASR. Some of them attempted to mitigate damage by adopting aggregate specifications based on predictive test methods and others, by decreasing the alkali content in the concrete, or both.

The service life of concrete structures is often limited by the crack formation in rather brittle concrete cover. So far, the durability of concrete and other cement-based materials has been studied for one or several isolated actions such as ASR, chloride penetration or carbonation. In reality, however, materials are usually exposed to a combination of mechanical and environmental loads and, hence, the durability of structural members depends essentially on the specific combination of loads and the environment (Van Zijl and Wittmann, 2011). This could imply that a combination of mechanical and environmental loads may turn out to be much more severe than that of each load case when considered separately.

An experimental study is proposed to investigate the durability of reinforced concrete elements subjected to the combined action of mechanical loading and ASR. The research has used different local ingredient materials of concrete such as aggregates and admixtures to determine the materials that will give the optimum resistance to such combined action, for instance by investigating alkali reactivity of aggregate under mechanical load. Similarly, deterioration of concrete due to ASR when exposed to high humidity according to the ASTM standard condition (ASTM C 1260-07) and (ASTM C1293-07), (accelerated method and long-term method respectively) will also be investigated. Additionally, the difference between the deterioration rates as a result of high humidity and submerging half of the sample in water and the other half in humidity will be studied.

1.2 Research objectives

The major aims of this project can be summarised as follows:

1. Understand the underlying mechanisms of the combined action of mechanical load and ASR acting simultaneously.
2. Review the applicable test methods to characterise the behaviour of concrete under combined actions such as cyclic loading, ASR and change in relative humidity and temperature.
3. Confirm the test procedures developed in the second research object above by physical experiments and subject the results to comparative analyses.
4. Recommend analytical evolution method(s) to assist designers in assessment of existing structures experiencing ASR and mechanical cracks.

1.3 Significance of research

Previous studies have taken the actions of mechanical loads and environmental effects separately, which make them different from this study. This research endeavours to contribute to increased knowledge and a clear understanding of combined actions. The study of the simultaneous influence of mechanical loads and ASR will reveal whether the total effects of individual mechanical loads and ASR are equal to the simultaneous effect of both actions or not. Identifying the implications of this research will enable the development of the basis for more realistic service-life design. More reliable prediction of the durability of reinforced concrete structures is of the utmost importance for more ecological and economical construction projects in the future. Finally, a recommendation for assessment methods to characterise durability under combined actions will be made. The expected outcome of the plan is:

1.3.1 Broad demonstrative outcome:

This study has as goal to demonstrate the validity of the assumption that:

1. The ASR chemical reaction and associated volume expansion occurs at a higher rate in the presence of damage. The specimens have been damaged by mechanical loading (70% of ultimate tensile strength to accelerate ASR testing).
2. Wider cracks in tension specimens arise due to ASR more than in those without ASR.
3. Mechanical properties of specimens made of reactive aggregate (Greywacke) were more deteriorated than that made of non-reactive aggregate (Granite), due to ASR exposure.

1.3.2 Model for prediction based on test data in section 1.3.1

1. Find ways to correlate crack width, crack spacing and ASR rate.
2. Derive a realistic micro-mechanical basis for the volume increase by ASR product formation which incorporates realistic crack pattern (width and spacing) formation. This model intends to illustrate the combined action and form a prediction model.
3. Derive a mechanical model based on the micro-mechanical basis which incorporates load transfer from concrete to reinforcing steel in RC much sooner in cracked ASR specimens than in others. The fatigue behaviour of steel will then dominate, and not the fatigue behaviour of RC.

1.4 Scope and limitations

The scope of this thesis is to develop a method to find out the effect of the combined simultaneous action of mechanical loading and ASR, seeing that they are still being tested separately in research practice. The mechanical cyclically occurring cracks assist the ingress of water and gases into the concrete which increase the rate of the reaction. The focus was on the mechanical crack-widths changing under the ASR pressure as well as their expansion under both ASR and combined action. The research is based on local concrete materials and is conducted in the Department of Civil Engineering of Stellenbosch University. The purpose is to determine the effect of ASR in structures that are placed close to or in water. Reinforced and normal concrete was cast and exposed to different conditions to obtain results. The results were the expansion procedure, the crack-width changes and the changes in the mechanical properties of the concrete. The study required a long time to retrieve the data and many stages were followed. The first stage was making the devices, and then preparing the material and concrete, exposing the specimens to different conditions, measuring and collecting the data and, finally, analysing the findings and the modelling.

1.5 Dissertation layout

The dissertation is divided into eight chapters. Chapter one is an introduction and overview of the study. Chapter two illustrates the previous studies in the scope of the research and the similarities with this

study. Research methodology and experimental design in Chapter three discuss the available methods, philosophies of the study and presents the stages and the way to implement the plan. The experiments were carried out according to a two-series test, and the results obtained are presented in Chapters four to six. In Chapter four, the deteriorations of mechanical and chemical properties of the concretes subjected to ASR were investigated. The changes in the mechanical crack-width induced by wedge-splitting load and submerged in NaOH solution are conducted in Chapter five. Chapter six studies the ASR effecting on RC beam pre-cracked by mechanical loading. Models to simulate the expansion and crack-width reduction of beams under ASR effects were devised in Chapter seven. The summary results, summary contribution and further researches are done in Chapter eight. Suggested methods to prevent and mitigate the combined action and appendices of the data results, images and graphs are attached to this thesis.

CHAPTER TWO

2. LITERATURE REVIEW

2.1 Introduction

Much research concerning the effects of mechanical loads and severe environmental conditions on concrete structures has been performed, but there are still many matters remaining unresolved regarding concrete structures exposed to combined actions, for instance, cyclic loading and ASR action. In this dissertation the following have been focused on as being major factors representing combined action: environmental effects (ASR), mechanical loads (cyclic loading), aggregate types (reactive or non-reactive), blast furnace Corex slag (BFCS) as a cement-replacing material, and crack width.

2.2 Alkali-silica reaction

Alkali–aggregate reaction (AAR) in general refers to a reaction in concrete between the highly alkaline cement paste and the reactive aggregates which occurs over time. AAR includes two more precise definitions: the most common reaction of this type is Alkali–silica reaction (ASR) and a less common related reaction is Alkali–carbonate reaction (ACR), which occurs on certain argillaceous dolomitic limestones. ASR is a reaction between the hydroxyl ions in the alkaline cement (Na and K) in the concrete and reactive forms of silica in the aggregate (e.g. chert, quartzite, opal, strained quartz crystals). This reaction can cause expansion and subsequent cracking in concrete. This reaction has been studied since 1940 and was first identified by Stanton (1940). Research on AAR has gained prominence in South Africa after the mechanism was first reported in the 1970s in the Western Cape. At present, the damage mechanism is known to exist dominantly in areas of the Western Cape, Eastern Cape and Gauteng (Ekolu, 2009). Service records of concrete structures have shown that the highest incidence of AAR in South Africa occurs in the Western Cape and that the aggregates involved are from the Malmesbury Group (Davis and Coull, 1991). Research conducted between 1978-1982 in South Africa, Scotland and Australia show that calcium hydroxide plays a significant role in the formation of an expansive gel (Hoyo, 2007). This causes increased volume and so exerts an expansive pressure ultimately resulting in deterioration and failure of the concrete. The conditions for ASR to occur are:

- The presence of sufficiently high alkali content in the cement (or from other sources).
- A reactive aggregate such as chert, quartzite, opal and greywacke stones.

- Environmental conditions being such as to promote the reaction either by exposure to water or high humidity (> 80% RH).

Alkalis in the concrete mix are defined as Sodium Oxide equivalent (Na_2Oe) (ASTM C1293, 2008). The concrete-mix designer should therefore be aware of the Na_2Oe content of all products intended to be used in the concrete mix in order to ensure that the total quantity of Na_2Oe will not exceed the acceptable or threshold amount. Limits of Na_2Oe of less than 3 kg/m^3 in concrete and 0.6% Na_2Oe in cement are recommended to minimize the possibility of ASR (Ekolu, 2009; Fulton, 2009) as summarised in Table 2-1. The type of aggregate used in concrete is a factor that determines the extent of deleterious expansion in the concrete (Fulton, 2009). Studies have found this to be true in the South African environment. For instance, in general, Granite stone in concrete is considered innocuous but since some of the Cape Granite Suite materials may be very slowly expansive, it might be prudent to work on 4.0 kg Na_2Oe per m^3 of concrete (Davis and Alexander, 1989). This is very conservative and means that, in practical terms, about 600 kg of cement per m^3 concrete (i.e. Na_2Oe = 0.7% of cement) is required before slow expansion occurs. Fulton (2009) illustrated the relation between alkali content of cement and ASR likelihood as shown in Figure 2-1.

The alkalis are expressed regarding the acid-soluble NaO and KO and are presented in the form of equivalent sodium oxide (Ekolu, 2009).

$$Na_2Oe\ \% = Na_2O\ \% + (0.658 \times K_2O\ \%) \quad (2\text{-}1)$$

Table 2-1 Limits of total alkali content derived from the clinker component of cement, per cubic meter of concrete for South African aggregates from different lithostratigraphic units (Fulton, 2009).

Rock type	Total Na_2Oe (kg/m^3)
Witwatersrand Supergroup Quartzite, Shale	2.0
Dolomite Group Chert	2.8
Malmesbury Group metasediments	2.1
Table Mountain Group orthoquartzite	2.8
Bokkeveld Group arkose	2.8
Natal Group Quartzite, Sandstone	2.8
Dwyka Formation tillite	2.8
Enon Formation Quartzite pebbles	2.8
Quaternary Quartzite gravels	2.8
Archaean Granite	Not determined
Cape Granite	4.0
Salem Granite	Not determined

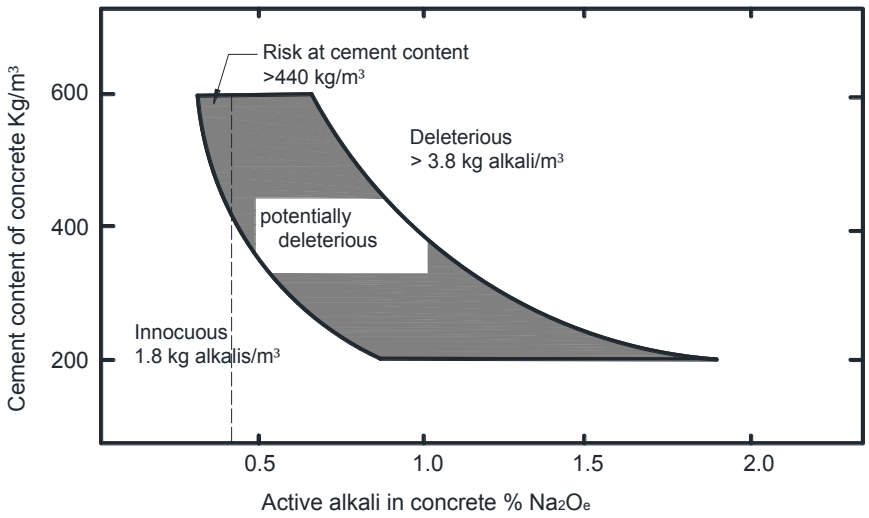

Figure 2-1 Relation between alkali content of cement and ASR likelihood (Ekolu, 2009; Fulton, 2009).

The major source of alkali in the mix is usually the cement, but some may also be contributed by mixing water, the aggregate, sea spray or chemical admixture (Fulton, 2009).

2.2.1 Laboratory standard tests for assessing ASR

The most common methods used to investigate the ASR deterioration were adopted by the American Society for Testing and Materials (ASTM) and the American Association of State Highway and Transportation Officials (AASHTO). Two common methods to assess ASR effects are (i) the ASTM C 1260 Standard accelerated Test Method for Potential Alkali-Silica Reaction of mortar bars, and (ii) the ASTM C 1293 to determine the length change of concrete due to ASR (series test 2). ASTM C 1260 incorporates a method developed at the National Building Research Institute in South Africa by Oberholster and Davies (1986). The test is based on a mortar bar cast and containing the subject aggregate (fine or crushed coarse) with standard gradation. About 24 hours after casting, the mortar bars are demolded and placed in water at a temperature which rises progressively up to 80°C for the next 24 hours. The bars are removed from the water and measured for their initial length, and then they are submerged in a 1N of NaOH solution at 80°C for 14 days. After extracting the bars, their length-changes during this storage period are measured. The total expansion used in specifications is the length measured at the end of the 14-day submersion.

ASTM C 1293 is a test on a concrete prism cast with a cement content of 420 kg/m^3. This method is most accurate in predicting the field performance of aggregates. The equivalent alkali content of the cement used should be between 0.8 and 1.0 %. This percentage is increased to 1.25 % of cement mass by adding NaOH to the mixing water and the total alkali content in the concrete mixture becomes 5.25 kg/m^3. The concrete prisms are cast and cured for 24 hours at 23±2 °C after demoulding and then stored at 38°C and

relative humidity (RH) larger than 90%. The measurement of the increases in length is taken at regular intervals for at least one year.

2.2.2 Length and volume change due to ASR

The ASR often varies throughout the components of the affected structure. In general, uneven or differential concrete swelling due to AAR may cause distresses such as relative movement, misalignment and distortion (Fournier et al., 2004). Cyr and Gibergues (2002) assumed that the expansion curve of a concrete prism affected by AAR, the general form of which is represented in Figure 2-2 (curve 1), can be characterized by three successive phases. The initial phase is where swelling begins (OA), followed by a phase of significant expansion at a nearly constant rate (AB) and ending in a decrease in the expansion rate to reach a final plateau (B1). Another form of expansion curve is also found (curve 2 of Figure 2-2) where the primary phase is not clearly separated from the expansion phase. Cyr and Gibergues (2002) also presented other curves (curves 1' and 2' shown in Figure 2-2) which start like curves 1 and 2, but end with a final slope different from zero. Different typical experimentally obtained behaviours (Giaccio et al., 2008) are shown in Figure 2-3, which represent the four previous curves in Figure 2-2. They measured this on 75×75×300 mm prisms. The concretes were prepared by adding NaOH (as granular particles) in the mixing water to achieve a total alkali content (Na_2O_e) in the concrete of 5.25 kg/m^3. The control concrete (C1) was prepared with non-reactive natural siliceous sand and Granitic crushed stone. Concrete R2 was prepared with reactive sand and concrete R3 incorporated 10% very reactive siliceous orthoquartzite and 90% non-reactive Granitic crushed stone. Finally, concrete R4 was prepared using 100% of the slow reactive Granitic crushed stone.

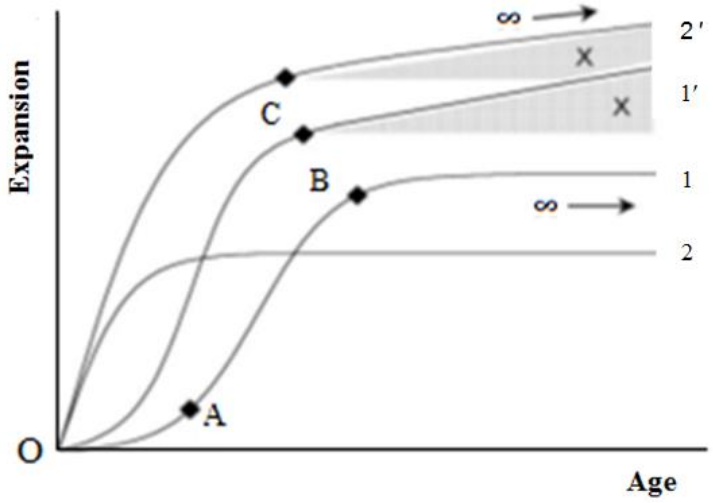

Figure 2-2 Typical expansion curves of concretes affected by AAR. X indicates the visible part of expansion characterized by phenomena independent of AAR (Gibergues and Cyr, 2002).

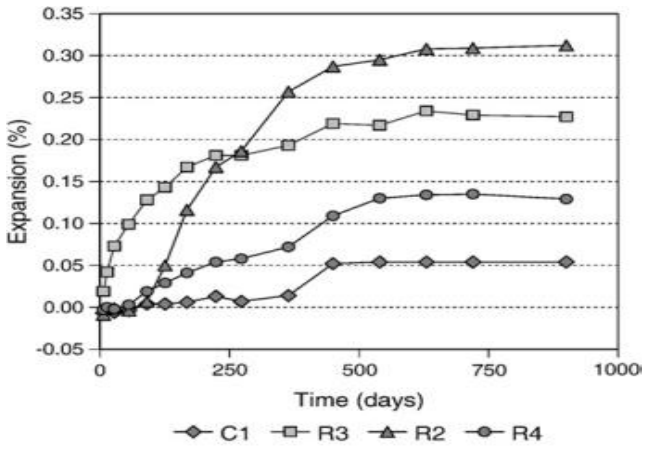

Figure 2-3 Linear expansions of prisms (Giaccio et al., 2008).

2.3 Combined action

In the context of this research, an example of combined action on a structural element is studied by application of mechanical loads and exposure to ASR inductive environmental action. Most previous studies have considered each of the actions separately. Research results of the effect of combined action are scarce. The damage under combined action has been reported to be more severe than the total damage if the actions were acting separately (Van Zijl and Wittmann, 2011). Şahmaran and Li (2008) carried out an experimental program designed to investigate the durability of engineering cementitious composite (ECC) material with regard to cracking and healing under combined mechanical loading and environmental loading. In another experimental series, reinforced concrete elements were subjected to cyclic, mechanical loading and degradation due to corrosion by Giordano et al. (2011). In their specimens, the growth of crack openings was reported to be about 45%, compared to the initial value for a specimen tested under 40 kN tensile load, and more than 100% of the initial value for the specimen tested at 60 kN tensile load. In a study on a subsea tunnel, Chen et al. (2010) investigated the durability of lining concrete under the combined action of compressive load and carbonation. The tests included a critical compressive load test, accelerated carbonation test, natural carbonation test and capillary absorption test. Their results showed that carbonation was accelerated due to prior crushing of the specimens. Capillary absorption was also increased in pre-crushed specimens. Few researchers have studied the effect of ASR on mechanically loaded concrete. The effect of ASR expansion and cracking on reinforced concrete beams was studied by Fan and Hanson (1998). In this study, beam samples were immersed in an alkali solution alternately heated to 38°C and then cooled to room temperature. After ASR expansion reached approximately 500 microstrain (at 6 months), cracking was observed on reinforced concrete beams made with the reactive aggregate. The compressive strength, indirect tensile strength, and modulus of elasticity were reduced by 24, 38, and 31%, respectively, compared with the corresponding 28-day values. The

fatigue behaviour for plain concrete subjected to ASR deterioration was studied by Ahmed et al. (1999). The objective of the investigation was to study the effect of ASR on the fatigue behaviour of concrete tested in flexure and under repeated indirect tensile load. The restraint of ASR concrete prisms produced crack patterns different from those of the unrestrained prisms. The number of cycles till failure of the unrestrained specimens was significantly reduced, greater than that subjected to indirect tensile tests. RILEM (2011) has formed a committee to find test methods to determine durability of concrete under combined environmental actions and mechanical loads. Developing test methods to characterise the behaviour of concrete under combined actions is the major aim of this proposed RILEM Technical Committee. The combined actions are such as mechanical load, freeze-thaw cycles, carbonation and chloride penetration. The validity of the recommendation of the Committee on testing methods, carried out in different countries, will be checked by a series of comparative tests.

2.4 ASR crack formation

When the alkaline porous solution of concrete reacts with reactive forms of silica minerals in the aggregate, an alkali-silica gel forms and can absorb water and swell. When the tensile stress due to the swelling pressure of the gel exceeds the tensile strength of the concrete, cracking occurs (Multon et al., 2009; Fulton, 2009). After cracking, the gel is assumed to permeate into the cracks (Multon et al., 2009) as has been observed by (Yi and Ostertag, 2005). The ASR is visible through the expansion and/or superficial cracking of macroscopic parts. Microscopically, a network of micro-cracks grows, because of swelling of reactive sites where amorphous gels are created. Micro-cracks play a significant role concerning the anisotropy of the expansion when the concrete structure is loaded (Charpin and Ehrlacher, 2012). The ASR cracks described by Giaccio et al. (2008) usually are irregular, concentrated, orientated in a parallel pattern and run through the cement paste and other fine and coarse aggregates that are close to the reactive aggregates. Local examples of severe ASR are shown in Figure 2-4.

Figure 2-4 Example of ASR cracking, left: foundation plinths of Good Hope centre, Cape Town and right: Lansdowne bridge, Cape Town.

2.4.1 ASR crack pattern and width

The growth and propagation of matrix cracks tend to start earlier due to defects produced by ASR. The period of stable crack propagation is less affected than the period of unstable crack growth, which reduces the capability of controlling crack propagation and leads to premature failure. In treating ASR-affected structures, good practise includes measuring the crack widths over time, to monitor whether the reaction has been stopped or its rate reduced by the treatment. Individual crack widths are measured at regular periods over a selected grid of cracks to gain impression of the overall continued cracking behaviour.

A method was proposed by the Institute of Structural Engineers (ISE, 1992) for crack mapping based on measuring the ASR crack widths along five parallel lines traced directly onto the concrete structure every 1 m length. Along each line, the total width of intersecting cracks is divided by the length at which they were measured. Laboratoire Central des Ponts et Chaussees (LCPC, 1997) proposed another method based on measuring the widths of any two perpendicular cracks intersecting in 1 m lines and 1.4 m of their two diagonals. Table 2-2 by Giaccio et al. (2008) presents typical characteristics of the crack pattern obtained from microscope observations. A survey was carried out of cracks located in the cement paste, in the reactive aggregate or at their interfaces. They expressed the density of cracks as the total length per unit area and considered that large defects have a major influence on the failure mechanism of concrete. The maximum crack width is also included.

There is no doubt that the crack widths in restrained concrete are less than in unrestrained concrete. The ratio of crack width at the surface to that at the reinforcement level is proportional to the ratio of the nominal strain at the surface and the reinforcement strain (ACI 224R-01, 2001). Laboratory studies were conducted by Fan and Hanson (1998) to investigate the effect of deleterious ASR expansion on the behaviour of reinforced concrete beams and on the mechanical properties of cylinders made with the same concrete. Cracking was observed on reinforced concrete beams made with the reactive aggregate after 6 months of immersion in an alkali solution heated to 38 ˚C. The dominant cracks were oriented in the direction parallel to the reinforcement. They found that due to the restraint by the reinforcement, the longitudinal expansion at the reinforcement level was greatly reduced. Reduced expansion also occurred in the transverse direction. Crack development, as well as crack width and growth, is shown in Figure 2-5. ASR cracks first appeared longitudinally on the top of the beams when the expansion reached approximately 800 microstrains.

Three categories of cracks were produced experimentally by Reinhardt and Jooss (2003) to study the effects of crack width on permeability. The crack widths were of 0.05, 0.10 and 0.15 mm with one type of HPC used. The hydraulic gradient throughout the tests amounted to 1 MPa/m. The specimens were exposed to temperature levels of 20, 50 and 80 °C. The initial flow rate reduced after 75 h approximately

30%, 10% and merely 3% for the specimen at 20, 50 and 80 °C respectively. These reductions were similar and could be plotted for all the cracks 0.05, 0.10 and 0.15 mm as in Figure 2-6.

The effect of cracking on water and chloride permeability of concrete has been studied by Aldea et al. (1999). Crack widths under indirect tensile test loading ranging from 50 to 250 μm. The water permeability was evaluated by a low-pressure water permeability test. The results showed that the chloride permeability increased with the increasing crack width and that the water permeability was significantly more sensitive than the chloride permeability.

Mechanically, the ISE (1992) proposed further investigations when the crack width was in excess of 0.15 mm. The crack width of 0.15 mm was also suggested by ACI committee 224 as a limit criterion for structures exposed to wetting and drying conditions.

Table 2-2 Typical characteristics of the crack pattern obtained from microscope observations (Giaccio et al. 2008).

Concrete	Crack width	Cement past		Interfaces		Aggregates	
		TL (mm/cm^2)	MW (mm)	TL (mm/cm^2)	MW (mm)	TL (mm/cm^2)	MW (mm)
Concrete with reactive sand		2.0	0.10	1.1	0.05	0.33	0.05
10% very reactive siliceous Orthoquartzite and 90% non-reactive Granite		3.5	0.20	2.7	0.05	1.1	0.02
				Reaction rims	2		
100% of the slow reactive Granitic crushed stone	Thin	90	0.009	0.75	0.03	1.8	0.05
	Wide	0.7	0.025				

TL= Total micro-crack length per unit area.
MW= Maximum micro-crack width.

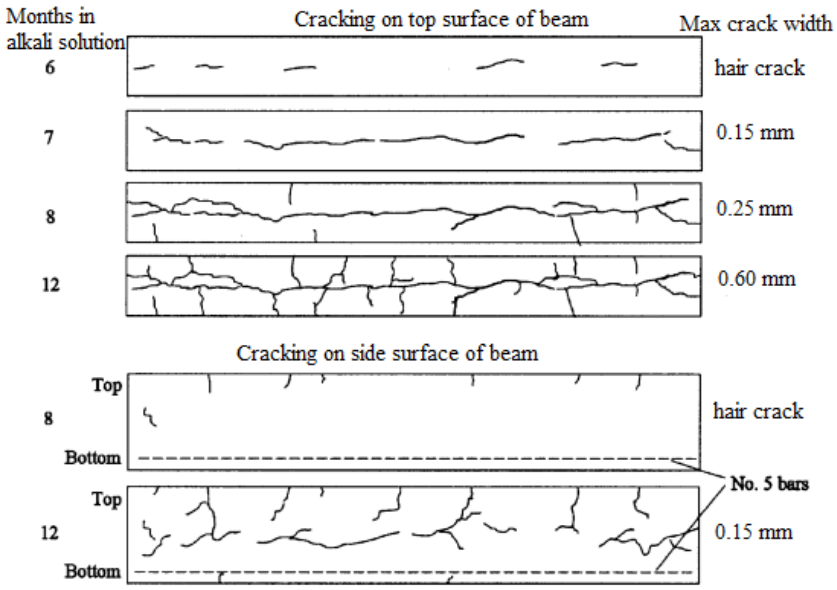

Figure 2-5 Crack width development at the top and bottom of the beam (Fan and Hanson, 1998).

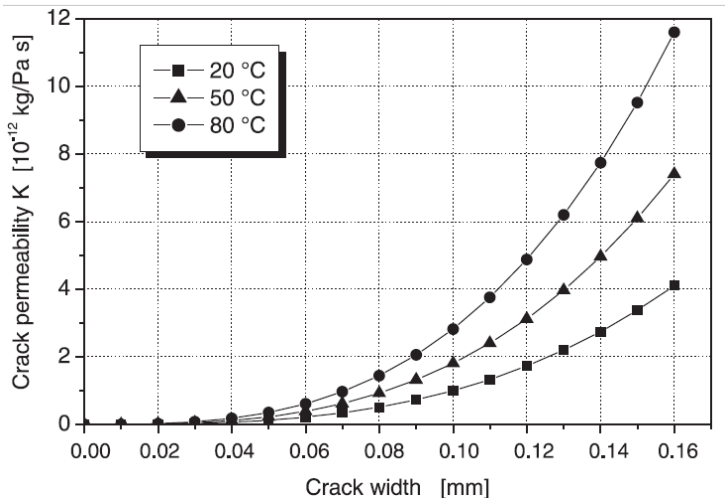

Figure 2-6 Representation of the dependency of crack permeability K on crack width and temperature (Reinhardt and Jooss, 2003).

2.4.2 Crack spacing

The crack pattern depends on many factors such as the reactivity, concrete size, concrete restraint and reinforcement direction. Crack spacing usually decreases as additional cracks develop between the initial cracks due to the reaction progresses (American Concrete Institute (ACI), 1998).

ASR tests on restrained and unrestrained concrete prisms made with Thames Valley sand, were conducted by Ahmed et al. (1999). The restrained samples were preloaded in compression by plates on the two sides and tied together. Their results showed that the restraint produced crack patterns different from those of the unrestrained prisms. Longitudinal cracks parallel to the direction of loading were observed on the surface of the restrained concrete prisms, whereas map cracks were seen on the unrestrained concrete prisms. The arrangement of crack spacing is dependent on the kind of concrete structural elements. For instance, in path slabs or road pavements, the cracks start close to free edges and joints with increased humidity access. As another example, the main cracks in reinforced members are usually parallel to the reinforcement bars (Owsiak et al., 2015).

Song and Van Zijl (2005) conducted direct mechanical tensile tests to investigate the performance of Fly Ash and Slag in ECC (FA-ECC and Slag-ECC). Random areas of weakness arise due to randomly distributed unhydrated FA particles in the concrete. These weak points lead to low limiting stress achieved over short shear transfer lengths. This caused small crack spacing in FA-ECC, ranging between 1 and 3 mm. A larger crack spacing ranging between 3 and 10 mm in Slag-ECC, were recorded. This can possibly be related to the matrix strength of Slag-ECC being higher than that of FA-ECC.

2.5 Model of ASR and mechanically induced crack formation

It has been mentioned previously that to adequately and efficiently predict the effects of ASR on a concrete structure, there must be reliable data available of the aggregate reactivity of the particular concrete mix as well as of the alkalinity (Na_2Oe) in the mix. Different models to predict the damage to concrete under the repetitive application of loads have also been developed over the years, and these models have shown significant variability in the prediction of cracks or fractures. Few models describe the behaviour of concrete under the combined action of mechanical and environmental effects and to the author's knowledge, publications dealing with models describing the simultaneous actions of cyclic loading and ASR are scarce. This study intends to model the mechanical and ASR action of reinforced and unreinforced concrete elements using the models described in the section below.

2.5.1 Modelling of ASR Expansion

The mechanism of ASR cracking was studied by Ichikawa (2009) for homogeneous and dense siliceous aggregates, in which the attack takes place gradually from the surface to the centre of the aggregate. This model takes into account the role of different kinds of precipitates according to their calcium content and hydration. It is restricted to the expansion mechanism that is related to reaction rim cracking and not to paste cracking. Figure 2-7 gives a schematic representation of the mechanism of ASR in concrete according to this model. A model proposed by Multon et al. (2009) assumes that the damage surrounding the aggregate under attack reproduces the micro-cracking induced by the pressure build-up in the gel. They assumed a representative elementary volume (REV) of concrete surrounding the reactive aggregate simplified to be spherical (Figure 2-8) and that the diffusion of the ionic species into the cement paste is instantaneous compared to relatively slow diffusion into the reactive aggregate. Therefore, the alkali concentration was assumed uniform in the paste in this model. This constitutes the main simplification in relation to Poyet's modelling (Poyet et al., 2007). The radius of the REV depends on the radius and the content of the reactive aggregate in concrete, as follows:

$$R_{REV}^{a} = \frac{\mathrm{R_a}}{\sqrt[3]{\emptyset_\mathrm{a} \,.\mathrm{C_{agg}}}} \tag{2-2}$$

with the superscript *a* depicting the size fraction of the reactive aggregate with mean radius R_a, R_{REV}^{a} the REV radius corresponding to the aggregate size fraction a, ϕ_a the volume fraction of reactive aggregates with mean radius R_a, C_{agg} the volume fraction of all the aggregate per m^3 of concrete.

The number of reactive aggregates per m^3 of concrete Na is equal to:

$$N_a = \frac{\emptyset_\mathrm{a} \,.\mathrm{C_{agg}}}{\frac{3}{4}\pi \mathrm{R_a^3}} \tag{2-3}$$

In this model, they assumed that the Na_2O/SiO_2 ratio is equal to the mean value 0.2 obtained in previous laboratory experiments; it is assumed that 1 mol of Na_2Oe reacts with 5 mol of SiO_2 to give 1 mol of ASR gel.

The volume of gel produced by one size of aggregate n_g^a is obtained by multiplying the number of moles of ASR gel produced by the aggregate by the molar volume of the gel V_{gel}^{mol}(in m^3/mol). The total volume of gel formed is then the sum of the volume of gel produced by all the aggregates (in m^3):

$$V_g = \sum_i n_g^a \times V_{gel}^{mol} \quad (2\text{-}4)$$

The volume of gel necessary to fill this porosity, which consequently does not exert pressure, is equal to the connected porosity (p):

$$V_{por} = \frac{4}{3}\pi((R_a + t_c)^3 - \mathrm{R_a^3}).\,\mathrm{p} \quad (2\text{-}5)$$

Because the aggregate was taken as spherical, the concentrations of the ionic species diffusing into the aggregate therefore depend only on time and on the radius r from the centre of the reactive aggregate (Figure 2-9).

The average deformation is considered to be proportional to the aggregate volume variation, but no computation of fracture mechanisms is proposed (Multon et al., 2009). However, the specimen size behaviour is well reproduced. Another model was proposed by Charpin and Ehrlacher (2012) who observed that aggregates of different sizes have a different impact on the overall expansion. Their assumptions of the model are that the aggregates are spherical and that the attack occurs from the surface of aggregates homogeneously. The behaviour of the aggregate surrounded by the infinite cement paste matrix is under stress-free outside boundary conditions (at infinity) as illustrated in Figure 2-10 which shows the interface transition zone (ITZ) around aggregates. The parameter $\xi \in [0;1]$ describes the degree, or extent of attack. In case the pressure is released, the undeformed radius of the sound part of the aggregate at the degree of attack ξ is $R_g(\xi)=(1-\xi)R_p$. The total undeformed remaining volume of aggregate is the sum of the volume of sound aggregate plus the remaining volume in the affected parts, representing a volume fraction of $(1-\rho)$ relatively to the original aggregate, thus:

$$V_{a0}(\xi) = \frac{4}{3}\pi \mathrm{R_p^3}[(1-\xi)^3 + (1-\rho)[1-(1-\xi)^3]] \quad (2\text{-}6)$$

Assuming that the products occupy a volume δ times bigger than the aggregate and the chemical reaction is expansive, the volume of gel at the reaction extent ξ, under zero pressure is given by:

$$V_0(\xi) = \frac{4}{3}\pi\delta\rho R_p^3[1-(1-\xi)^3] \quad (2\text{-}7)$$

When fully attacked, the smaller aggregates are shown not to cause any cracking of the cement paste. According to the energy criterion that is supplied by the release of elastic energy, the cement paste can

take such pressures when there is no initial crack or this crack is very small. The small aggregates are not sufficient to provide the energy needed to create a crack, because the elastic energy is stored in the cement paste around these aggregates.

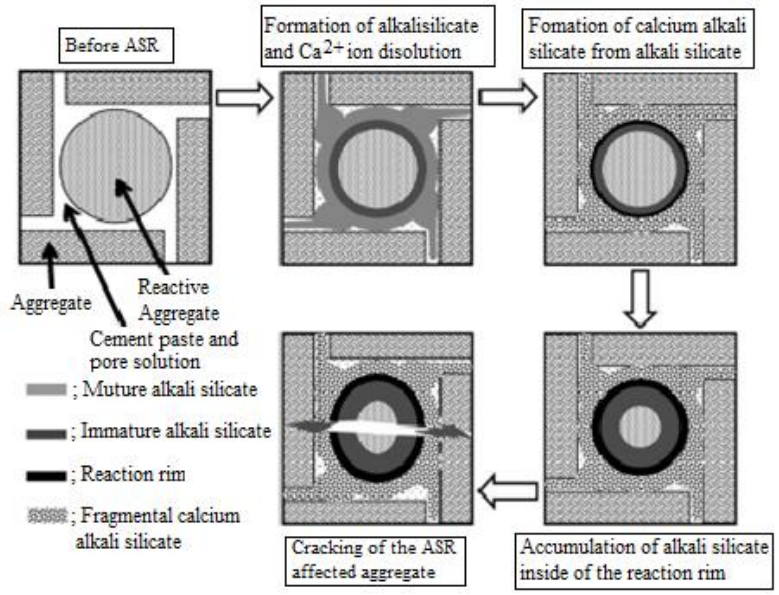

Figure 2-7 Schematic representation of the mechanism of ASR in concrete (Ichikawa, 2009).

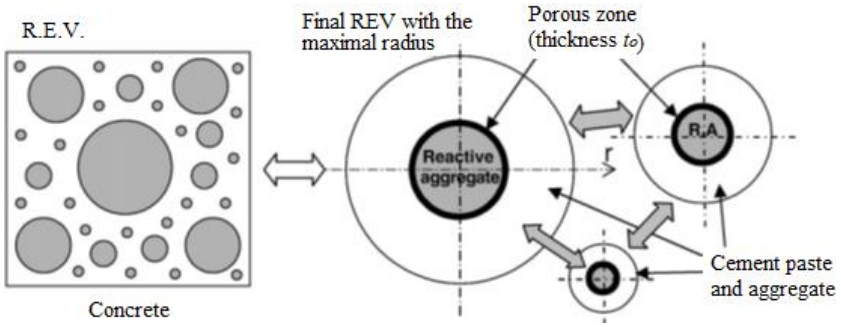

Figure 2-8 Definition of the REV for several reactive aggregate sizes (Multon et al., 2009).

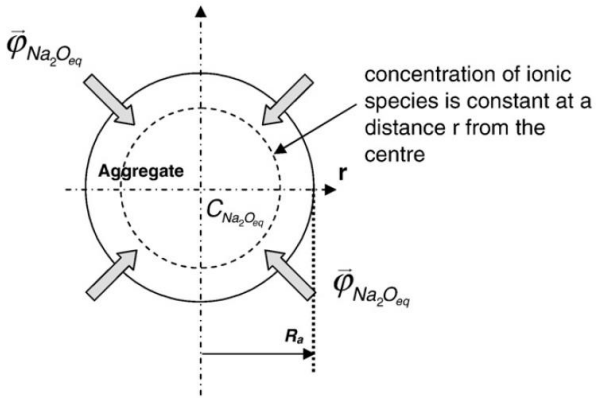

Figure 2-9 Diffusion of Na_2O_e in aggregate (Multon et al., 2009).

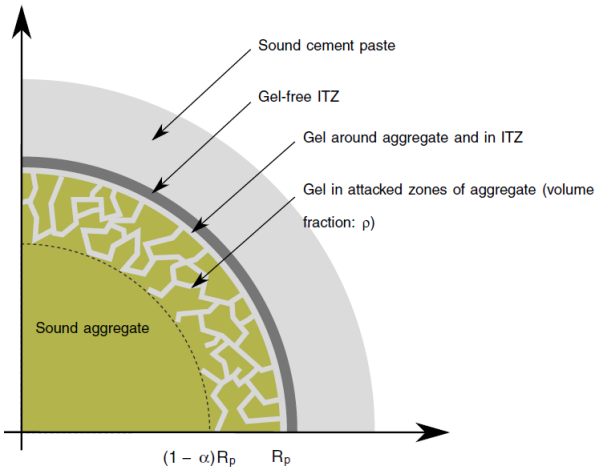

Figure 2-10 Typical reaction site of reactive aggregate (Charpin and Ehrlacher, 2012).

2.5.2 Mechanical modelling of ASR

The gel pressure causing instantaneous crack creation leads to an increase in the volume of the compressible gel and hence to a decrease in its pressure. Charpin and Ehrlacher (2012) assumed that the crack breaks the spherical symmetry of the system but keeps a cylindrical symmetry. The cement paste is cracked in a penny-shaped crack in the plane 0, e_x, e_y. The crack is concentric with the aggregate (Figure 2-11). They assume that when in the uncracked state the pressure reaches a critical value (yet unknown); a crack of finite length is instantaneously created. Hence, the crack inside radius is R_p and its outside radius is $(1+C_u)R_p$ in undeformed configuration. C_u is a dimensionless parameter representing the size of the crack. The area of the created crack is:

$$S(x) = \pi R_p^2[(1 + C_u)^2 - 1] \quad (2\text{-}8)$$

The model proposed by Multon et al. (2009) assumes that the ASR gels fill the cracks close to the aggregate. Therefore, three parts can be distinguished (Figure 2-12) namely the central aggregate (between radii 0 and R_a), the cracked zone filled by the gel (between radii R_a and R_{cz}) and that part of the REV not yet cracked. They assumed the ASR gel to be incompressible compared to the elastic properties of the cement paste and aggregate. Therefore, the ASR expansion can be taken into account as an imposed strain in the aggregate elastic constitutive law:

$$\sigma_a = \lambda_a tr\varepsilon_a . I + 2 . \mu_a . \varepsilon_a - (3\lambda_a + 2\mu_a) . \varepsilon_{asr}(t) \quad (2\text{-}9)$$

The constitutive law of the surrounding concrete (SC) only considers the elastic effect of the material:

$$\sigma_{SC} = \lambda_{SC} tr\varepsilon_{SC} . I + 2 . \mu_{SC} . \varepsilon_{SC} \quad (2\text{-}10)$$

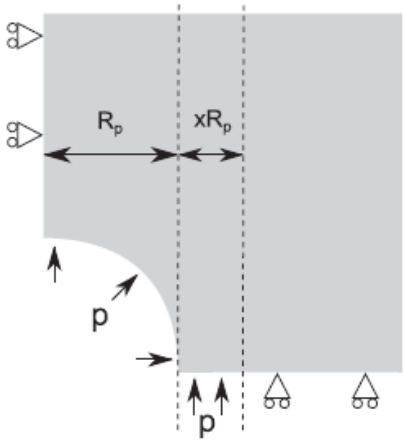

Figure 2-11 The crack considered is concentric with the aggregate (Charpin and Ehrlacher, 2012).

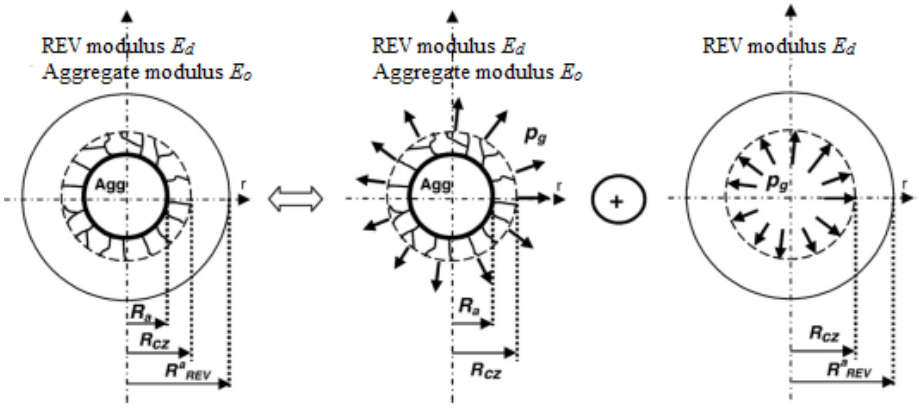

Figure 2-12 Mechanical equilibrium of the damaged REV (Multon et al., 2009).

where σ is the stress matrix for each material, ε the strain matrix for each material, I the identity matrix and tr the trace function.

The constants λ and μ are the Lamé elasticity constants. They are given in terms of other solid properties as:

$$\lambda = \frac{E\upsilon}{(1+\upsilon)(1-2\upsilon)} \tag{2-11}$$

$$\mu = \frac{E}{2\,(1+\upsilon)} \tag{2-12}$$

where υ is the Poisson's ratio. If the concrete contains several aggregate size fractions, the resulting strain is assumed to be the sum of expansions induced by each fraction:

$$\varepsilon_{asr} = \sum_a \varepsilon_a \tag{2-13}$$

According to the strain equivalence principle, the radial strain of this hollow sphere must be equal to the radial strain of the hollow uncracked sphere with inner and outer radii equal to R_a and R_{REV}^aunder pressure p but with a damaged Young's modulus E_d. The damage variable is then defined:

$$d = 1 - \frac{E_d}{E_0} \tag{2-14}$$

Where: E_0 is the initial, undamaged Young's Modulus of the concrete.

Figure 2-13 simulates modulus of E_0 in the first hollow sphere, and modulus of (1–d) E_0 in the second one, have the same stiffness.

Bangert and Meschke (2001) defined the expansive strain ε_{asr} as a function of initial material density of the skeleton ρ^u (unswollen state reaction extent ξ = 0), and final material density ρ^r(fully swollen ξ = 1):

$$\varepsilon_{asr} = \left(\frac{\rho^u}{\rho^r} - 1\right)\xi \tag{2-15}$$

Ulm et al. (2000) modelled the stress with the chemo-elastic pressure-spring device analogy of ASR swelling. Their model is based on two springs: the elastic spring of stiffness E_s, denoted by $\sigma_\mu = E_s\,\varepsilon$; and the chemical swelling pressure, denoted by $P_g = -E_g(\varepsilon - c\xi)$,where $E = E_s + E_g$. The ASR strain at free stress and neglecting the thermal expansion is thus related through a chemical dilatation coefficient β as follows:

$$\varepsilon_{asr} = \beta\xi \tag{2-16}$$

and

$$\beta = \frac{cE_g}{E} \tag{2-17}$$

Where c is the intrinsic dilatation coefficient of the reaction products and from Eqs. (2-16) and (2-17) at free stress, the chemical dilatation coefficient β can be written:

$$\beta = \frac{cE_g}{E} = \left(\frac{\rho^u}{\rho^r} - 1\right) \tag{2-18}$$

and

$$c = \frac{E}{E_g}\left(\frac{\rho^u}{\rho^r} - 1\right) \tag{2-19}$$

The ASR strain is related to the ratio of concrete to gel modulus of elasticity, and to the density of un-swollen at non-reactive to of swollen at fully reactive of concrete.

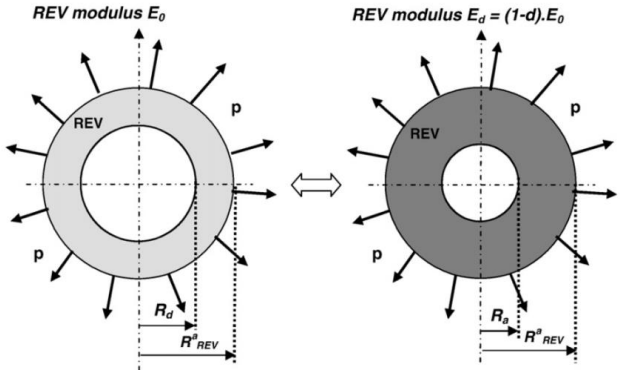

Figure 2-13 Determination of the Young's modulus of the damaged concrete (Multon et al. 2009).

2.5.3 Modelling of combined action

Expansion was measured by Giaccio et al. (2008) as a way to evaluate the ASR process. When concretes with reactive sand and that with 100% of slow reactive Granite achieved expansion in the order of 0.11% and 0.18%, they performed tests to measure stress–strain behaviour in compression on cylinders and load deflection and load-crack mouth opening displacement (CMOD) behaviour in flexure on notched beams. The energy of fracture was calculated as $G_F = W_0/A_{lig}$, where W_0 is the work of fracture (equal to the area below the load deflection plot) and A_{lig} the cross-sectional area before the test. The net bending stress at maximum load was calculated as $f_{net} = 6\ F_{max}l/4\ bh^2$ where b is the beam width, h the net depth of the beam, l the span and F_{max} the maximum load. Finally, the characteristic length parameter representative of the size of the fracture zone was calculated as $l_{ch} = EG_F/f_s^2$ using the values of the modulus of elasticity (E) obtained from 150×300 mm cylinder tests and the tensile strength (f_s) estimated as 0.6 $f_{net.}$. Ahmed et al. (1999) expressed the fatigue of ASR affected concrete in compression mathematically based on the linearity of the relationship between the number of cycles and the stress ratio in Figure 2-14:

$$log\ N = -g_1\left(\frac{f_{max}}{f_{cu}}\right) + q_1 \tag{2-20}$$

where the values of g_1 and q_1 depend on the type of aggregate used and these can be obtained from the curves equation for the mixes considered in their investigation (Figure 2-14), f_{max} is the maximum applied stress and f_{cu} is the compressive strength.

2.6 ASR-effected mechanical behaviour

The properties of concrete affected by mechanical loading and environmental conditions depend on factors such as aggregate type, temperature, degree of restraint, and the severity of the environment.

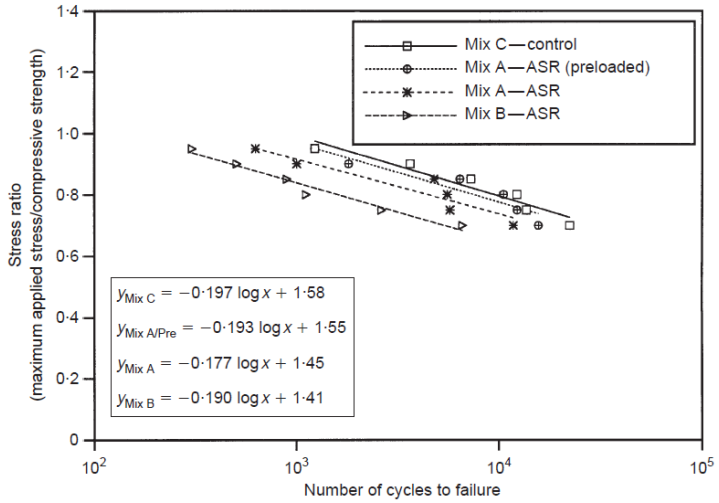

Figure 2-14 Endurance (S-N) Wohler curve for sound and ASR affected concrete prisms in compression (Ahmed et al., 1999).

Many studies have been conducted to identify the properties of concrete that has been affected by ASR deterioration. The reduction in the engineering properties of concrete affected by ASR has been studied numerically and it was found that the reduction does not occur at the same rate in different concretes. These reductions in the properties are related to the amount of expansion undergone by restrained ASR-affected concrete (Fournier et al., 2004). Relationships between the residual properties of concrete affected by ASR, and the percentage of the ASR expansion was established by the Institution of Structural Engineers (ISE, 1992). The main properties, which might be affected by ASR are elaborated in the following sections.

2.6.1 Compressive strength

One of the main properties affected by ASR is the compressive strength, which has been studied widely. Researchers have differed in the method of testing, the specimen shape, the curing and exposure conditions and the mix proportions. In Figure 2-15 the results of compressive strength change as function of ASR expansion reported by three research groups are summarised. Fan and Hanson (1998) carried out compressive tests on two reactive and two non-reactive 100 mm diameter by 200 mm high cylinders. The specimens were immersed in 0.5 N concentrations of ASR solution. The solution was made by adding 10 grams of NaOH, 14 grams of KOH and 0.1 grams of CaO per liter of tap water at 38 °C. The testing continued for one year. The specimens were quickly returned to the alkali solution after each measurement was completed for the continuation of ASR-accelerated conditioning. Under ASR accelerated conditioning, the compressive strength was reduced by 24% compared with the unaffected cylinders at 28-day values. Little further reduction occurred one year later. The ISE (1992) has reported on the development of damage in structures in the UK induced by ASR. Their study was conducted to

investigate the chemical processes and the physical effects on concrete cores taken from the same structure, but from seven different concrete pours. The work was undertaken to investigate the relationship between ASR expansion and cracks, the changes in stiffness and the stress-strain relationship in compression, to provide a basis for estimating the expansion. Prisms of 75×75×300 mm for expansion measurements were performed in accordance with ASTM C 1293 by Giaccio et al. (2008). Cylinders of 100×200 mm were made also for the compressive strength test. Their results were significantly different from those of the other research groups, where the compressive strength increased in the mix with reactive sand (as the largest expansion) at 200 days of exposure, and then decreased at 250 days of exposure. Figure 2-15 illustrates the relationship between the strength reduction and the expansion due to ASR as determined by Fan and Hanson (1998), ISE (1992) and Giaccio et al. (2008). In the first two studies (the results of laboratory controlled reactive concrete cylinders and the old concrete cores), the strength reduced with an increase in the expansion due to ASR, while in the study by Giaccio et. al, the strength increased significantly and then reduced as shown in Figure 2-15. The different results from these experiments are due to several factors, such as mix design, aggregate type, samples size, and storage conditions. Generally, a reduction in the compressive strength was caused by ASR expansion.

2.6.2 Splitting strength

Splitting tensile strength tests are commonly used to express the tensile strength of concrete. The splitting strength is affected, as are the other properties, by ASR expansion. Reduction in the direct and indirect tensile strength of concrete due to ASR expansion was found by Jones and Clark (1998). They stated that the effects of ASR in the cylinder splitting test is less sensitive than in the direct tensile strength tests. Testing of 100x200 mm cylinders that were immersed in ASR was conducted by Fan and Hanson, (1998) as mentioned in the previous paragraph. The tests were carried out on reactive and non-reactive specimens. The non-reactive specimen results did not change significantly with ASR expansion. In the 1992 ISE study (ISE, 1992) mentioned in the previous paragraph, the indirect tensile strength was measured on concrete cores. The splitting strength in reactive specimens was reduced with ASR expansion in both the studies by Fan and Hanson (1998) and ISE (1992) as shown in Figure 2-16.

2.6.3 Modulus of elasticity

Jones and Clark (1998) carried out Young's modulus testing on concrete cores. They noted that the Young's modulus was significantly reduced by ASR due to the expansion and micro-cracks. Non-destructive dynamic modulus tests were carried out on two reactive and two nonreactive cylinders by Fan and Hanson (1998). Using the same procedure of exposure as described in section 2.6.1, the dynamic modulus tests were carried out on the reactive and nonreactive cylinders. The dynamic moduli were not affected significantly up to the age of 90 days. However, just after ASR cracks were found at the age of

125 days, the concrete E-modulus was greatly reduced. Giaccio et al. (2008) performed compression tests on 100×200 mm concrete cylinders to determine the modulus of elasticity. The E-modulus was significantly reduced in concrete containing reactive sand, and which expanded more than the other mixes. Results of the dynamic modulus tests and expansion measurements of the reactive cylinders are shown in Figure 2-17 with ISE results for concrete cores mentioned previously. Both studies show that the E-modulus is reduced due to the ASR expansion. It can be concluded that ASR reduces the E-modulus significantly.

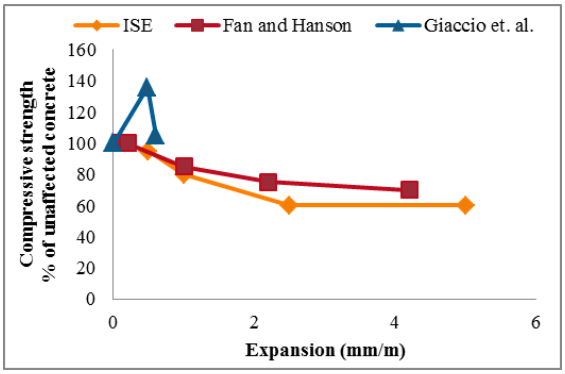

Figure 2-15 Residual compressive strength in % of values of unaffected concrete with ASR expansion.

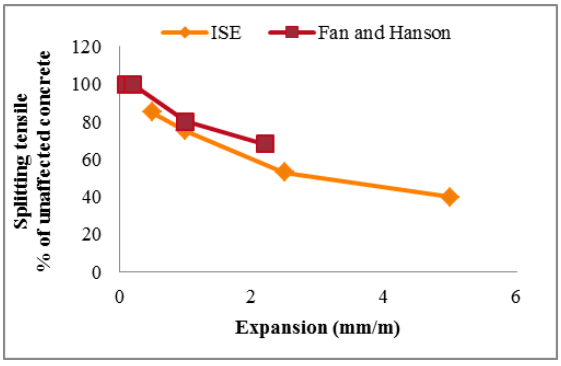

Figure 2-16 Residual splitting strength in % of values of unaffected concrete with ASR expansion.

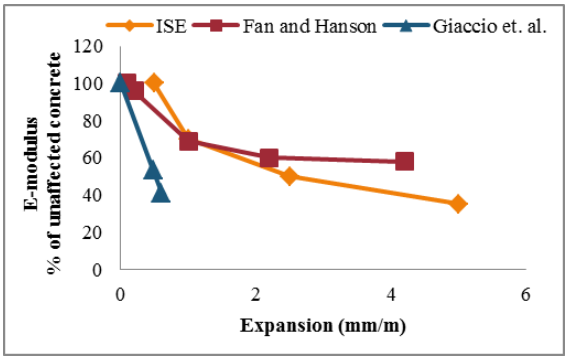

Figure 2-17 Residual E-modulus as a percentage of values of unaffected concrete with ASR expansion.

2.7 Cyclic loading and fatigue

Fatigue is a phenomenon whereby a structure fails at a lower load or load amplitude with increasing number of cyclic repetitions of those loads or load amplitudes. Attention for fatigue by design engineers is essential for structures subjected to repetitive loads of equal or varying size, including road pavements and highway bridge structures subjected to vehicle loads, as well as tall buildings and wind turbine tower structures subjected to wind fluctuations.

2.7.1 Cyclic loading

The cycle is the load variation from the minimum load to the maximum load and then back to the minimum load. Figure 2-18 illustrates basic cyclic loading parameters. Cyclic loading is mostly represented to simulate repeated loading such as vehicles on bridges and pavements. The following loadings have been defined by Euro-code (EN 1991-2, 1991) as traffic loads on bridges:

- Load Model No. 1 (FLM1): Similar to characteristic Load Model Nr. 1.

$$0.7 \times Q_{ik} - 0.3 \times q_{ik} - 0.3 \times q_{rk} \quad (2\text{-}21)$$

- Load Model No. 2 (FLM2): Set of «frequent» Lorries.
- Load Model No. 3 (FLM3): Single vehicle Load.
- Load Model No. 4 (FLM4): Set of «equivalent» Lorries.
- Load Model No. 5 (FLM5): Recorded traffic.

Where: Q_{ik}, q_{ik} and q_{rk} in Load Model Nr. 1 are as shown in Figure 2-19.

The values of the α factor in Figure 2-19 are given in the National Annexes of Euro-codes as shown in Table 2-3. These parameters depend on the class of vehicles:

First Class: international heavy vehicle traffic.

Second Class: (normal) heavy vehicle traffic.

Euro-code also identifies the number of expected vehicles per year and per slow lane for models of FLM3 and FLM4 as illustrated in Table 2-4.

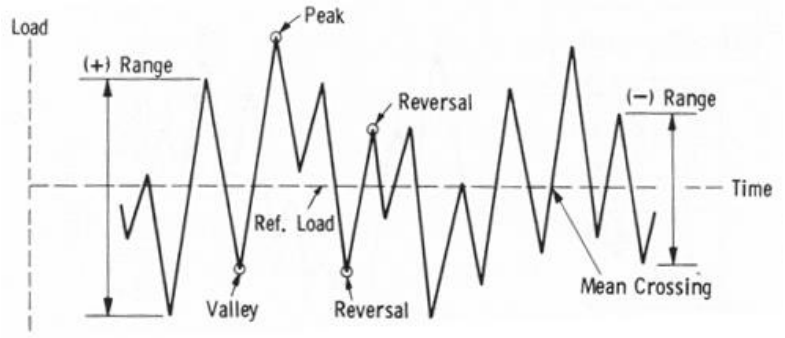

Figure 2-18 Basic fatigue loading parameters (ASTM E1049, 1997).

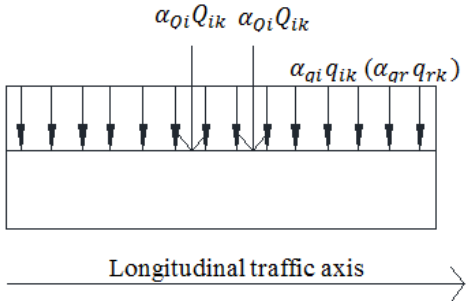

Figure 2-19 The main load model (LM1).

Table 2-3 Values of α for the description of vehicle loads (EN 1991-2, 1991).

Classes	α_{Q1}	α_{Qi} $i \geq 2$	α_{q1}	α_{qi} $i \geq 2$	α_{qr}
class 1	1	1	1	1	1
class 2	0.9	0.8	0.7	1	1

Table 2-4 Indicative number of heavy vehicles expected per year and per slow lane (FLM3 and FLM4 Models) (EN 1991-2, 1991).

	Traffic categories	*N*obs* per year and per slow lane
1	Motorways and roads with ≥ 2 lanes per direction with high flow rates of lorries	2.0×10^6
2	Motorways and roads with lorries in medium flow rates	0.5×10^6
3	Low flow rates of lorries on main roads	0.125×10^6
4	Low flow rates of lorries on local roads	0.05×10^6

***** *Nobs is the total number of Lorries crossing the bridge per year*
Note: *In each fast lane, (i.e. a traffic lane used predominantly by cars) an additional 10% Nobs may be included.*

2.7.2 Fatigue

Fatigue is defined as a process in which damage accumulates due to the repetitive application of loads that may be well below the static fracture or macroscopic damage point. The single application of the load would not produce any ill effects, and a conventional stress analysis might lead to an assumption of safety that does not exist (Roylance, 2001). The fatigue resistance of concrete is affected by factors such as water content, temperature and load level. Micro-cracks may arise during the concrete setting and hydration due to thermal strain (Olsson and Pettersson, 2010). Under cyclic loading, these micro-cracks may propagate. This may be slowly in the beginning, i.e. after a limited number of load cycles, but after a sufficiently high number of cycles they may grow to become macro-cracks. The micro or macro-cracks

lead to the ingress of water and gases into the concrete, which makes the concrete susceptible to other deterioration processes, including ASR and corrosion.

Loading rate has an effect on the static and dynamic strength of concrete. Kesler (1953) found that loading frequencies between 1 and 7 Hz did not significantly affect the fatigue resistance of the concrete. In long-term testing, time-dependent characteristics such as creep and shrinkage influence the results.

2.7.3 Fatigue curves

Fatigue generally is represented by the nominal stress amplitude S (or σ) versus the number of cycles to failure N. This is often graphically visualised as an S-N curve. Figure 2-20 shows an example of the S-N curves for aluminium and steel by Roylance (2001) and reinforced concrete by Euro-codes (EN, 1992). Using these methods, the relationship between the applied cyclic load and the fatigue life can be determined (Matsumoto et al., 2008). Another visualisation of fatigue is presented by Satoh et al. (2007) for a RC deck slab in Figure 2-21a. The stage where the displacement turns near vertical as function of the number of wheel loads depicts fatigue failure. Figure 2-21b illustrates a wheel loading test conducted in an incremental loading pattern which is recommended by the Japanese Ministry of Land, Infrastructure and Transport (Satoh et al., 2007).

The effect of ASR on the fatigue behaviour of concrete was studied in flexure and under repeated indirect tensile load by Ahmed et al. (1999). They found that the average number of cycles to failure of the restrained concrete beams cast from Thames Valley sand (mix A) was about 50% higher than for the unrestrained specimens cast from the same mix. On the other hand, the restrained beams showed an average drop of 40% in their number of cycles compared with the control specimens. The results in Table 2-5 are presented in an S-N curve in Figure 2-22 as the logarithm of the number of cycles versus the ratio of stress (in percentage) applied.

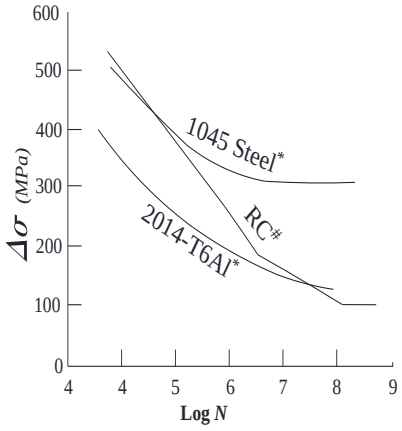

Figure 2-20 An example of S−N curves for aluminium, low-carbon steel and RC;*Roylance (2001) and #Typical design line in EN 1991(Croce, Pietro n.d.).

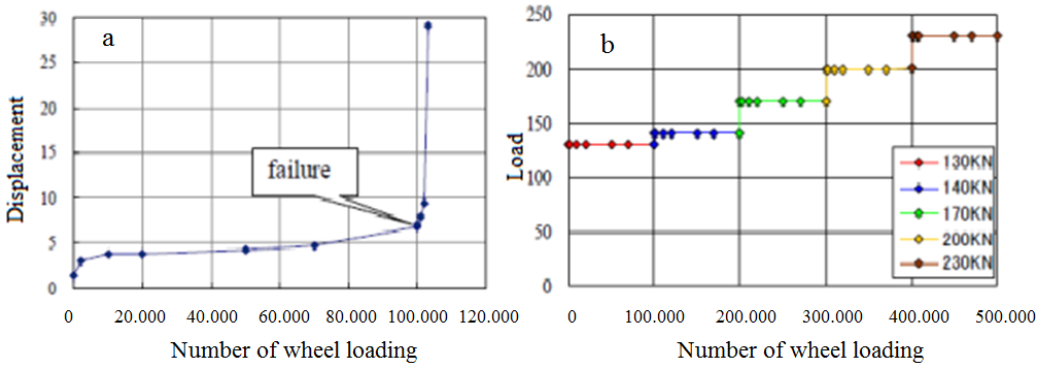

Figure 2-21 Number of wheel loadings and (a) Displacement and (b) Load.

Table 2-5 Average results for concrete fatigue in compression (Ahmed et al., 1999).

Maximum applied stress σ_{max}	Number of cycles to failure (prism, 100×100×500 mm)			
	Mix C	Mix A (preloaded)	Mix A	Mix B
0.70	22205	15571	11719	6589
0.75	13586	12237	5700	2626
0.80	12213	10494	5539	1115
0.85	7248	6394	4769	895
0.90	3625	1803	1001	506
0.95	1230	1225	625	304

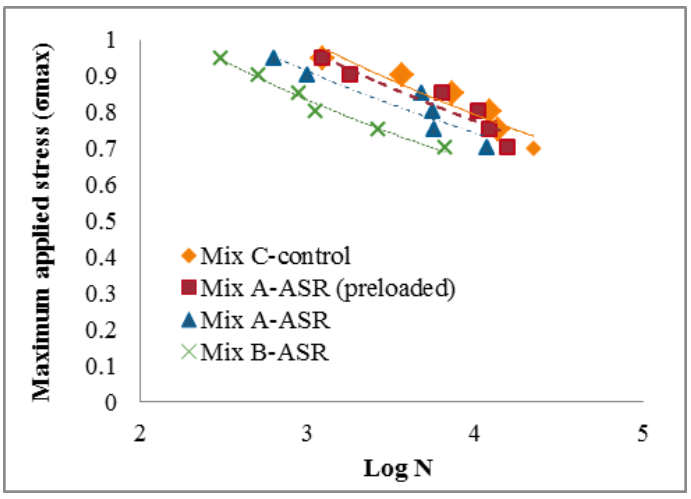

Figure 2-22 The ratio of stress (in percentage) applied versus number of load cycles to failure as the logarithm (Ahmed et al., 1999).

2.8 Concrete materials

In typical concrete, aggregate forms about 70% of the concrete volume. Also included in concrete are cement and pozzolans such as blast furnace slag, silica fume and fly ash. The following sections describe the ingredient materials.

2.8.1 Aggregate types

Aggregates such as sand, gravel, crushed stone, slag and recycled concrete are the types of coarse particulate material used in concrete. These materials are obtained from three main sources namely from the mining of mineral aggregate deposits (sand, gravel, and stone), waste slag from the manufacture of iron and steel and from the recycling of concrete. Light weight aggregates from materials such as clay, pumice, perlite, and vermiculite are used for special applications. Chemically, the aggregates can be classified into reactive and non-reactive aggregates, in respect of ASR. Reactive aggregates contain reactive silica that will react with alkalis in cement (Na, K, or in terms of Na_2Oe as described in Section 2.2) to form an alkali-silica gel less dense than the aggregate. This expansion causes pressure build-up in the vicinity of the aggregates in concrete. Due to the irregular distribution of aggregate in concrete, ASR-induced volume increase causes irregular crack patterns often in orthogonal bands referred to as map-cracking. The situation in South Africa is that considerable investigations were carried out as reported in a local South African technical publication (Davis and Coull, 1991) according to which the main base rock types were categorised in terms of non-reactive and reactive types, as summarised in Table 2-6. Chemical, physical and mechanical tests were performed on the aggregates to determine their properties with particular reference to ASR, which will assist in the design of concrete and future predictions of ASR deterioration.

2.8.2 Ground Granulated Corex Slag (GGCS) as a replacement

Ground granulated blast-furnace slagment powder (GGBS) is made from blast-furnace slag, a by-product of the iron and steel manufacturing process. Slag was initially used as a coarse aggregate, but with better understanding of its behaviour under different curing methods to improve its properties, it then became used as replacement cementitious materials for cement. Today, slag has become an important part of the international cement market.

A new process in the production of iron, the so-called Corex process, is more environmentally friendly than others. This system replaces coke ovens and blast furnaces with a direct reduction shaft and the injection of oxygen into a smelter-gasifier (Alexander et al., 2003). This plant also yields a quenched slag as a by-product of the iron making process. Upon processing, this slagment product is called ground granulated Corex slag (GGCS). This process has been installed in the Saldanha steel manufacturing plant in the Western Cape, South Africa. The different manufacturing process leads to differences between

blast furnace and Corex slag. Alexander et al. (2003) studied the properties of GGCS and compared them with GGBS. Chemical and physical analyses comparing GGBS, GGCS and ordinary Portland cement (OPC) are shown in Tables 2-7 and 2-8. In Germany, Portland blast furnace cement is regarded as a low-alkali cement if:

• For a slag content of at least 50%, the total Na_2O_e is not more than 1.1%.

• For a slag content of at least 65 %, the total Na_2O_e is not more than 2.0%. (Fulton, 2009)

To prevent deleterious expansion when using an alkali-reactive aggregate in combination with high alkali cement, the cementitious material should contain an extender complying with SANS 1491 using slag as at least 40% replacement of cement by mass (Fulton, 2009). Alexander et al. (2003) have found that 50% cement replacement by GGCS is the best percentage, considering the durability of concrete.

Table 2-6 Potential alkali-reactivity of aggregates (Davis and Coull, 1991).

Rock type and source	**Potential alkali-reactivity**
Orthoquartzite* (Coedmore Quarry)	Not deleteriously reactive
Witwatersrand Quartzite#	Potentially deleteriously reactive at an alkali content of 2.4 kg Na_2O equivalent/m^3 of concrete
Granite (Juksei Quarry)	Not deleteriously reactive
Dolomite (Olifantsfontein Quarry)	Not deleteriously reactive
Felsite (Zeekoewater Quarry)	Not deleteriously reactive
Meta-quartzite (Ferro Quarry)	Not deleteriously reactive
Dolerite (Natal Quarry)	Not deleteriously reactive
Meta-mela-andesite (Eikenhof Quarry)	Not deleteriously reactive
Meta-Greywacke (Malmesbury shale) (Peninsula Quarry)●	Potentially deleteriously reactive at an alkali content of 2.1 kg Na_2O equivalent/m^3 of concrete
Granite◊ (Rheebok Quarry)	Not deleteriously reactive
Ortho-Quartzite (Mossel Bay Quarry)	Potentially deleteriously reactive at an alkali content of 2.8 kg Na_2O equivalent/m^3 of concrete

Note: ** Quartzite of the Table Mountain group (Cape supergroup) in Natal are not all non-reactive and the DBT (CSIR) recommend (Nov. 1987) that for a conservative margin of safety a value of 2.8 kg Na_2O equivalent/m^3 of concrete be used.*

 # All witwatersandsupergroup quartzite should be regarded as suspect. Based on recent data the Division of Building Technology (DBT) of the CSIR recommends that a value of 2.0 kg Na_2O equivalent/m^3 be used for a greater margin of safety.

◊ All Malmesbury shales/Homfels/Meta-Greywackes in the Western cape should be regarded as suspect.

● Granites of the Cape granite suite are not all non-reactive and the DBT (CSIR) recommended a value of 4.0 kg Na_2O equivalent/m^3 concrete be used for a greater margin of safety.

Table 2-7 XRF analysis of binders oxide used in experimental work (in % of mass) (Alexander et al., 2003).

Oxides	OPC	GGCS	GGBS
CaO	67.2	37.2	34.0
SiO_2	22.3	30.8	35.5
$Al2O_3$	4.4	16.0	15.4
MgO	1.01	13.7	9.4
TiO_2	0.22	0.51	1.2
Fe_2O_3	3.4	0.87	0.98
MnO	0.08	0.09	0.88
K_2O	0.56	0.35	0.87
Na_2O	0.21	0.12	0.16
SO_3	0.58	3.19	2.49

Table 2-8 Physical properties of Portland cement and slag powders (Alexander et al., 2003).

Method	PC	GGCS	GGBS
BET fineness (m^2/kg)	-	1145	991
Blaine fineness (m^2/kg)	310	467	390
% passing 1 micron	-	7	6
% passing 10 micron	-	51	45

2.9 Mitigation of ASR cracks

Main sources of cracks in concrete are ASR, corrosion, shrinkage, sulfate attack and freezing and thawing. Often, concrete structures deteriorate prematurely due to various deterioration mechanisms, and need remedial measures to reinstate their serviceability. Consequently, the need for structural repair and rehabilitation has increased considerably in recent years. The deterioration of concrete has become a major concern for owners and engineers, because of the cost of repair or replacement.

Applying the wrong material and the wrong specification could be a costly exercise and may not lead to the required long-term solution for the structure. The annual cost of concrete deterioration of bridges in the USA alone has been estimated to be more than $8.3 billion (Gerhardus et al., 2002; Kessy et al., 2015). According to Knudsen et al. (1999), in Western Europe, the annual costs were estimated as early as 1998 to be $5 billion for repair of reinforced concrete (RC) structures.

2.9.1 Mitigation cracks in new concrete

There are several options to prevent or limit ASR in concrete, including limiting the total alkali content of the concrete by using supplementary cementing materials, and avoiding or limiting the use of reactive aggregates. Chemical admixtures or SCMs such as fly ash, slag, silica fume and lithium compounds (such as lithium nitrate) are known to mitigate ASR. Fibres are used to mitigate ASR too, and their mechanism is by bridging cracks and controlling the expansion.

2.9.1.1 Lithium compounds

Many researchers confirm that using lithium compounds can prevent ASR expansion or at least mitigate it. Kawamura and Fuwa (2003) have studied the effect of Li_2CO_3 and LiOH on concrete mortars, and they found that the addition of relatively small amounts (0.3 and 0.5%) of LiOH and Li_2CO_3 resulted in increased expansion while the results show that the expansions of mortars were completely suppressed by the addition of 1.0% LiOH and 1.5% Li_2CO_3 of the cement weight to the mix (see Figure 2-23). Feng et al. (2010) have monitored the expansion testing of mortar bars in accordance with ASTM C1260 and concrete prisms by ASTM C 1293 with two representative reactive coarse aggregates (Rhyolite with 85% devitrified glass and Greywacke with 8% microcrystalline quartz). They used different alkaline solutions with or without $LiNO_3$ at 100% standard Li dose (100% standard Li dose means a Li/(Na+K) molar ratio of 0.74) and in the presence or absence of $Ca(OH)_2$ at 80 °C. They summarized that adding 100% of $LiNO_3$ to the bars and in the solutions could completely inhibit the deleterious expansion in the accelerated mortar bar tests for both Rhyolite and Greywacke aggregates as shown in Figure 2-24. However, in the concrete prism tests which used larger reactive aggregate particles, $LiNO_3$ could only mitigate the deleterious expansion for the Rhyolite aggregate, but not completely for the Greywacke aggregate due to the reactive silica in the Greywacke aggregate, being less accessible than in the Rhyolite aggregate.

2.9.1.2 Corex slag

The use of slag in concrete is accepted worldwide as a means of eliminating the risk of expansion due to ASR (Alexander et al., 2003). At appropriate cement replacement levels, slag is the extender of choice to reduce ASR. Figure 2-25 (left) shows the impact of slag on the 2-year expansion of concrete prisms with alkali content 1.25% Na_2O_e in cement and containing moderately to highly reactive aggregates (Thomas and Innis, 1998). Alkali content in cement is affected to expansion level. An example in Figure 2-23 (right) of Greywacke with different amounts of Na_2O_e shows the expansion with increased Na_2O_e and decrease with increased slag amount (Slag Cement Association, 2013).

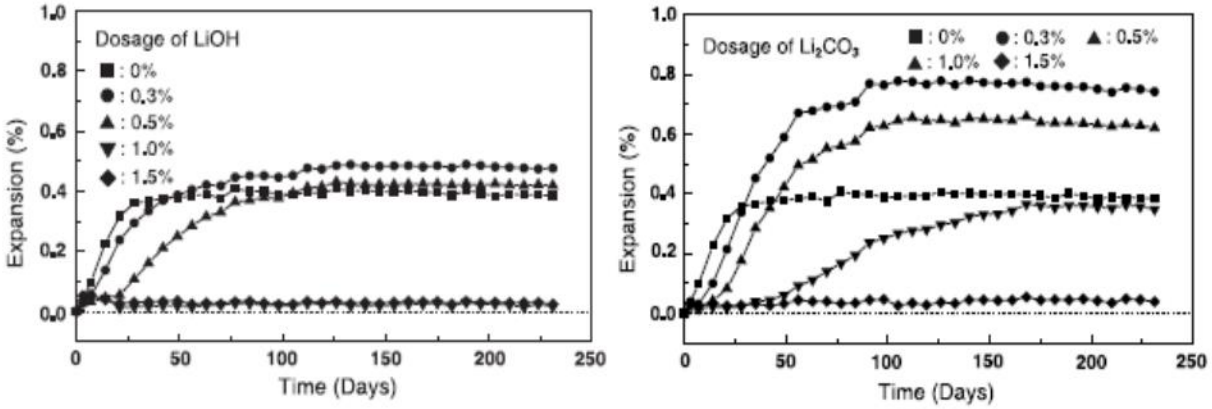

Figure 2-23 Expansion curves of mortars with LiOH (left) and Li_2CO_3 (right) (Kawamura and Fuwa, 2003).

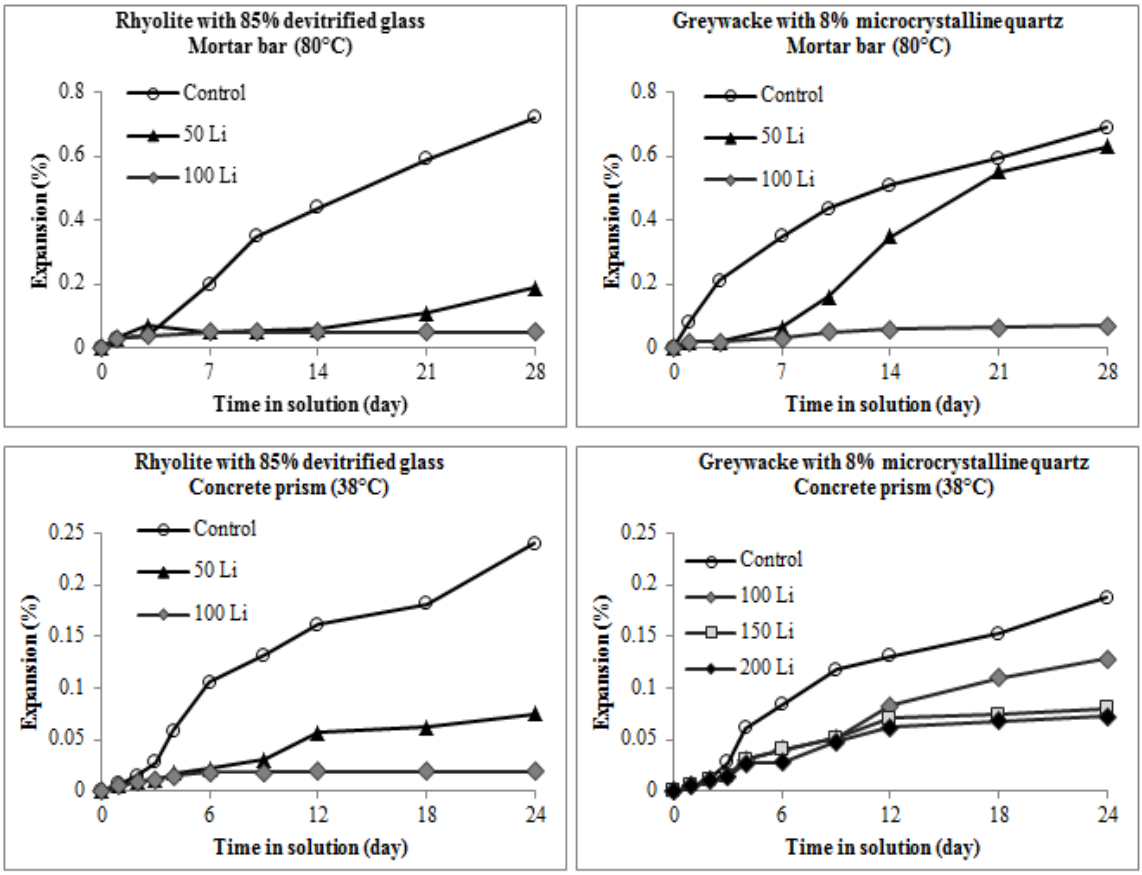

Figure 2-24 Expansion tests of mortar and prisms with two aggregates in different Lithium dose (for mortar bar tests, the bars contained 100% of the standard lithium dose, and the solution contained either 50% or100% of the standard dose) (Feng et al., 2010).

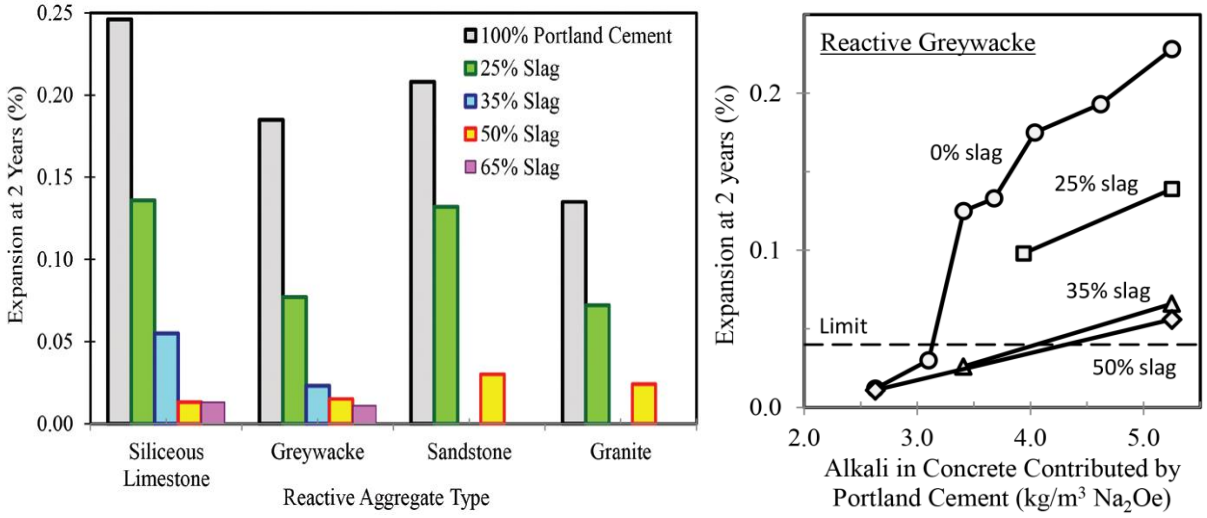

Figure 2-25 Expansion of concrete with various amounts of slag, left: different types of aggregates (Thomas and Innis 1998) and right: different amounts of Na_2O_e in concrete made with Greywacke stone (Slag Cement Association 2013).

2.9.1.3 Fly ash

The largest produced industrial waste in the world is fly ash which is produced from combustion of coal. Only about 20% of this product is used to form blended cement (Williams et al., 2002). At moderate levels of low-calcium (Class F) fly ash replacement (20% to 30%), it is capable of controlling damaging alkali-silica reaction (ASR) in concrete and the effect has been attributed to the reduced concentration of alkali hydroxides in the pore solution when fly ash is present (Thomas, 2007). Figure 2-26 illustrates the role of fly ash to mitigate ASR expansion as studied by Shehata and Thomas (2000).

2.9.1.4 ASR Crack control

Two examples from the literature address ASR crack control. Yi and Ostertag (2005) proposed that using microfiber in concrete for crack control on the microscale in close vicinity to the reaction site reduced the alkali-silica reaction rate in an ASR test series, and the corrosion rate in a chloride-induced corrosion test series. Figure 2-27 left shows the Yi and Ostertag-model to mitigate the crack widening over time by using hybrid fibre reinforced concrete (HYFRC), in either NaOH (ASR) exposed specimens, or NaCl-exposed specimens causing corrosion of the embedded reinforcing bar.

Self-healing is studied widely as a means of mitigating cracks in concrete. Amongst several options, capsule based self-healing materials have been proposed, which sequester a healing agent inside discrete capsules (Tittelboom and Belie, 2013). The capsules are triggered when they are ruptured by damage or a crack, to release the healing agent in the region of harm. Figure 2-27 right illustrates the reaction of spherical and cylindrical encapsulated agent (dark-coloured inclusions) upon contact with (A&B)

moisture or air or due to heating; (C&D) the cementitious matrix; (E&F) a second component present in the matrix (small, light-coloured inclusions) or (G&H) a second component provided by additional capsules (big, light-coloured inclusions).

2.9.2 Repairing the damage in existing concrete

It is not simple to halt the ASR reaction once it begins, but it may be possible by limiting the ingress of water into the concrete.

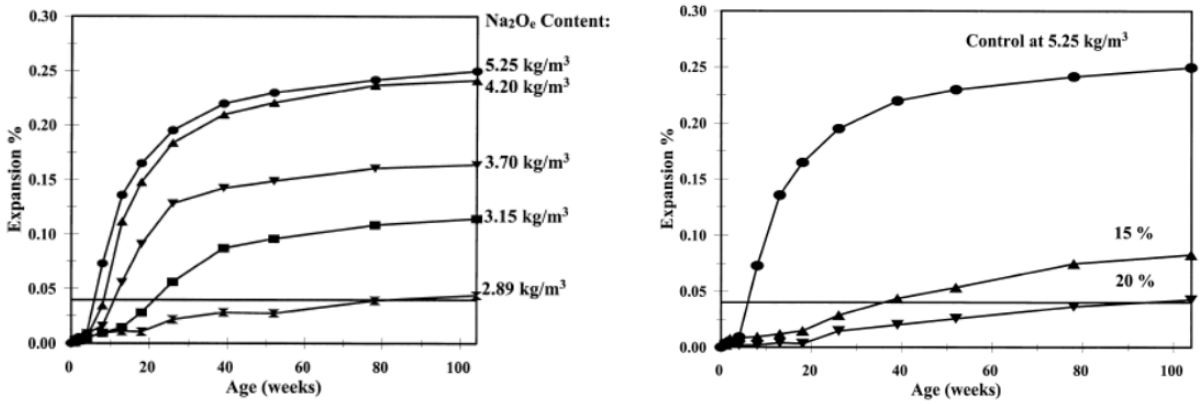

Figure 2-26 Measured expansions using various levels of total alkalis and fly ash replacement (Shehata 2000).

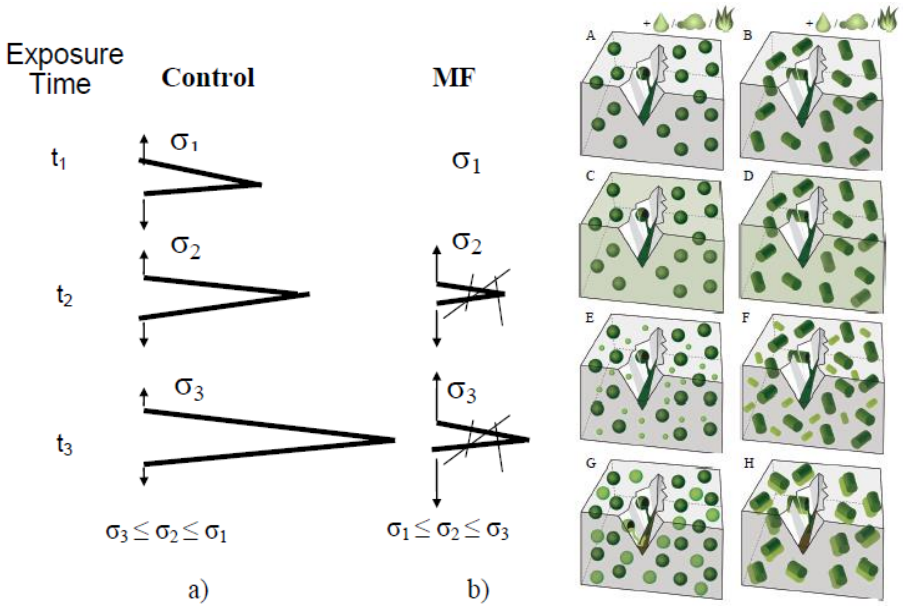

Figure 2-27 Crack control, left: difference in crack growth behaviour of a) control and b) microfiber (MF) reinforced specimens with increasing exposure time (Yi and Ostertag, 2005) and right: capsule based self-healing approaches. Leakage of healing agent from the capsules into the crack due to gravitational and capillary forces (Tittelboom and Belie, 2013).

2.9.2.1 Use of Lithium compounds

Research that has been carried out by some authors refers to the role lithium can play in mitigating the expansion in existing ASR affected concrete. It may be possible to introduce lithium into the hardened concrete in certain circumstances and change the nature of the reaction (Thomas et al., 2013). Although lithium reduces ASR expansion, it does not have the added benefit of protecting against other forms of deterioration, because it is not a hydrophobic sealer (Eskridge et al., 2005).

2.9.2.2 Use of chemical compounds

Studies have been conducted on the use of chemical compounds such as polymer cement mortar (PCM), epoxy coatings and silane. Fujii et al. (1989) have subjected specimens to outdoor conditions and cycles of wetting and drying. Silane- and urethane-coated specimens subjected to these conditions did not swell, but in fact showed volume reduction, perhaps drying shrinkage. Epoxy-coated and methyl-methacrylate-coated specimens expanded severely, and the coatings cracked. The specimens coated by sodium silicate showed expansion equal to that of the uncoated reactive. It was found that expansion decreases when the ratios of surface area to volume or treated surface area to total surface area increase. Another series of tests by the same authors was a comparison of the performance of silane, silane with a PCM cover, and silane with a methyl-methacrylate cover under cycles of wetting and drying. Silane/PCM-coated specimens had four times the expansion of specimens with the other two coatings after 32 weeks of exposure, but still less than all specimens from the first series of tests. Abe et al. (1992) have addressed the comparative effectiveness of two coatings that are water impermeable, and water vapor permeable, in reducing ASR-related expansion. The water impermeable coating consisted of three layers of epoxy. The vapor permeable coating consisted of silane followed by a flexible PCM. The control specimens were uncoated. Specimens with the vapor-permeable coating showed continuous negative expansion after two years outdoors, whereas the specimens with the impermeable coating after six months had much greater expansion than the uncoated samples.

2.9.2.3 Repair with Engineered Cementitious Composites concrete (ECC)

Li (1993) developed Engineered Cementitious Composites (ECC), which has strain-hardening behaviour under tensile loading. Existing cracks induced by ASR in a retaining wall in Japan had been unsuccessfully repaired in 1994 and was repaired again in 2003 with sprayed high-performance fiber reinforced cement composite (HPFRCC) (Kunieda and Rokugo, 2006). 50 to 70 mm thickness of two types of this HPFRCC material and conventional repair mortar were applied. Furthermore, different types of crack pre-treatment were conducted. The wall was divided into 10 sections of 1.8 m wide and 5 m high (see Figure 2-28). Table 2-9 gives the rehabilitation methods for each block. The existing cracks in blocks

4 and 8 were sealed with a polyurethane sealant (30 mm in width, 5 mm in thickness) to make an unbonded region between SHCC and surface crack. An acrylic surface coating material (paint type) was applied to an area of 2 m from the bottom throughout the blocks two days after the repair to prevent penetration of water from outside. Two years after this repair, a fine mesh of cracks developed on the HPFRCC surface. It was found that in blocks reinforced with welded bar mesh, crack patterns resembled the shape of bar mesh with crack intervals similar to the bar spacing (100 mm). On blocks without steel reinforcement and those reinforced with expanded metal, cracks were randomly distributed. However, little cracks could be observed when the acrylic was painted over the HPFRCC surface (Rokugo et al., 2005). The potential of repair overlays to limit water ingress into the substrate concrete, as a mitigating measure for ASR affected structures, was also studied by Mechtcherine and Lieboldt (2011). They investigated water and gas permeability and absorption tests for specimens made of Textile Reinforced Concrete (TRC) to quantify the effects of the type of textile, yarn coating, and TRC cracking thereon. No further measurable volume flow could be observed after a few weeks of storage of the cracked specimens in water. The textile reinforcement is a very effective crack bridging and makes for good crack distribution when positioned near the concrete surface, and leads to narrow crack widths. These narrow cracks might affect the transport properties of TRC considerably. However, they found that cracked TRC is less permeable in comparison with cracked ordinary concrete due to the small crack width and spacing in the reinforcing TRC layer.

Table 2-9 Conditions for the trial application (Rokugo et al., 2005).

Repair materials	Block No.	Reinforcement	Unbonded region at crack
Repair material A	1	Welded bar mesh	None
Fiber: PVA+ High strength PE	2	Expanded metal	None
Volume fraction of fiber: 1.5%	3	None	None
Matrix: Premixed polymer cement mortar	4	None	Present
Repair material B	5	Welded bar mesh	None
Fiber: High strength PVA	6	Expanded metal	None
Volume fraction of fiber: 2.1%	7	None	None
Matrix: Premixed cement mortar	8	None	Present
Repair material C Fiber: None Matrix: Premixed cement mortar	9	Welded bar mesh	None
No repair	10	None	None

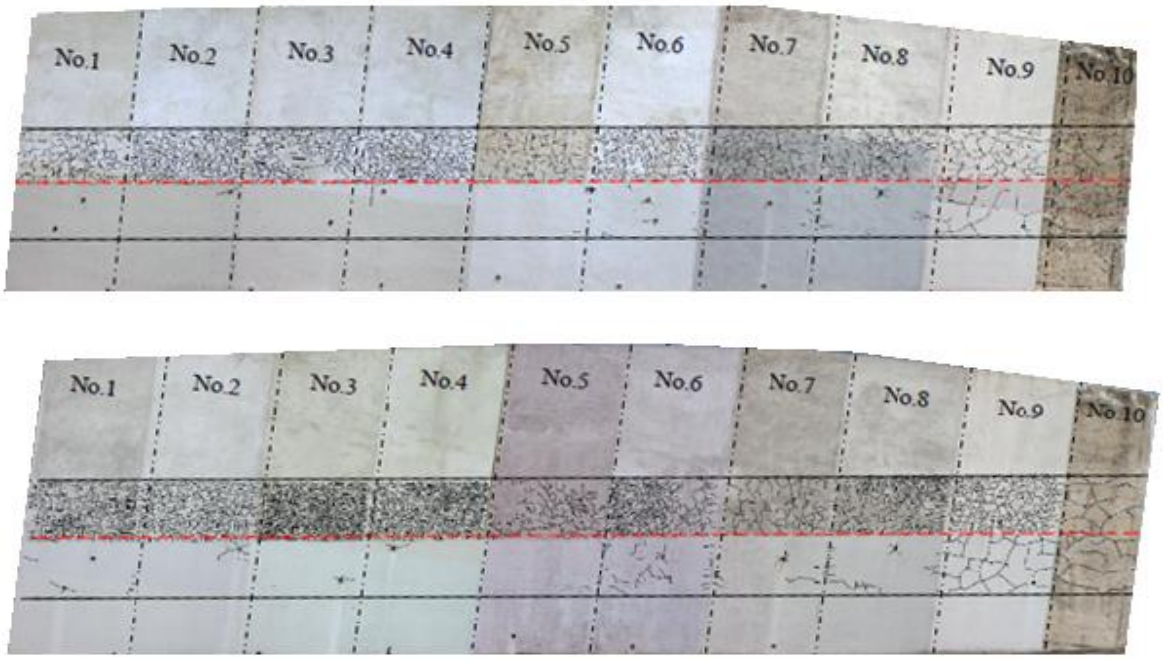

Figure 2-28 Crack Patterns 12 months after repair (top), and 24 months after repair (bottom) (Kunieda and Rokugo 2006).

CHAPTER THREE

3. RESEARCH DESIGN AND METHODOLOGY

3.1 General

Studying the effects of combined mechanical load and ASR deterioration on concrete is the main purpose of this research. Testing strategies, for instance, cyclic loading, are aimed at reinforced concrete bridge structures subjected to cyclic loading. In this chapter, the details of the experimental methodology to achieve the objectives of this study are described.

3.2 Materials

3.2.1 Aggregate

In South Africa, certain aggregate sources have been identified as potentially alkali-reactive through service records and by laboratory testing (Fulton, 2009). Meta-greywacke and Malmesbury shale sourced from Peninsula Quarry and Contermanskloof in the Western Cape have been specified as aggregates with the potential for rapid expansion when Na_2Oe of concrete is 2.1 kg per m^3 or greater (Davis and Coull, 1991; Multon et al., 2009). Similarly, Malmesbury Granite obtained from Rheebok Quarry and used for almost all concrete work in the region, is innocuous but since some of the Cape Granite Suite materials may be very slowly expansive, it might be prudent to work on 4.0 kg/m^3 Na_2Oe (Davis and Coull 1991).

In this study, two types of coarse aggregate have been used in the mixes, namely Greywacke stone as a reactive aggregate and Granite stone as a non-reactive aggregate. Greywacke contains abundant quartz-feldspar and rock fragments, and the individual units have a poorly sorted nature (Pellant, 2000). In the same reference, the white Granite has been defined as a high silica content (contains over 65% of total silica and not less than 20% quartz) and classified as an acid rock. The picture on the left, in Figure 3-1, shows the Greywacke aggregate used in mixes, and the picture on the right shows the Granite aggregate used. Fine aggregates were Malmesbury and Philippi sand. The Malmesbury sand is supplied from the Malmesbury area in the Western Cape and contains more than 98% silica according to chemical tests that have been done and reported on later in this chapter. The Philippi sand is supplied from the Philippi area in Cape Town. It is finer than Malmesbury sand and contains less silica (about 80%) according to the mentioned test. Figure 3-2 shows the Malmesbury sand on the left side and Philippi sand on the right.

Figure 3-1 Coarse aggregate used: left, Greywacke and right, Granite.

Figure 3-2 Fine aggregate used: left, Malmesbury and right, Philippi sand.

3.2.2 Cement

Pretoria Portland Cement (PPC) CEM I 52.5 N has been used in this research. The product data sheet of PPC describes CEM I 52.5 N as made from high-quality raw materials with the clinker being inter-ground with gypsum to control setting. Grinding is carefully controlled to ensure consistent performance in the 52.5 N strength class. It is general-purpose cement for building and civil engineering work.

3.2.3 Corex Slag

In assessing the need to control the alkali content of the concrete or to use GGBS or any admixture, it is assumed that the specifier has knowledge of the potential alkali reactivity of the aggregate to be used (Fulton, 2009). It is known that by using GGBS or GGCS to replace cement, the total alkali content in concrete is significantly reduced and that the ASR potential of concrete containing significant amounts of GGBS or GGCS is low. By reference to the chemical results in Table 2-7, it can be noted that the content of sodium oxide and potassium oxide in GGCS is less than that in GGBS. GGCS has been used in some samples as a replacement cementitious material at 50% of the binder weight. The slag was chosen because it is an available material in the local market and can be used as a replacement for cement. GGCS will be referred to under the generic term slag (Co) in this research.

3.3 Concrete mix

Two main concrete mixes for two series of tests were designed for the research reported in this dissertation. The first was designed for an accelerated ASR test method and for the second, intended for long-term ASR tests, sodium hydroxide was added to the mix to increase the alkali amount in the concrete. In both mixes, half of the specimens contained only CEM I cement, while in the other half 50% of the cement was replaced by Co. Coarse aggregate of particle size 9.5 mm, 13 mm and 19 mm of Greywacke and Granite stones were used, while the fine aggregates were Malmesbury sand and Philippi sand. The cement alkali content, expressed as Na_2Oe according to chemical test results (mentioned later in Table 3-6) and using Equation (2-1), is 0.6%. The water-binder content was chosen in this research to obtain a medium workability for a typical concrete class (30 to 40 MPa) of cylinder strength. The amounts of water absorption by the aggregate were included within the w/c ratio which were obtained from previous tests of aggregates by Davis and Alexander (1989). The proportions of two series mixes are shown in Table 3-1. It can be noted that the lower w/c ratio in Gw mixes is due to the fact that Greywacke aggregate absorbs less water than the Granite aggregate. In the mix of series test 1, the specimens are denoted Gw, Gn, Gw-co and Gn-co for Greywacke mix, Granite mix, Greywacke with Corex slag and Granite with Corex slag respectively. In the mix of series test 2, the specimens are denoted Gw/w, Gn/w, Gw-co/w and Gn-co/w for the specimens submerged in water and Gw/H, Gn/H, Gw-co/H and Gn-co/H for the specimens subjected to high humidity. The specimens were cured and exposed to different conditions, as is elaborated later in Section 3.5 and Table 3-3.

A mix according to Standard test ASTM C1260 was also performed as described in Section 3.7.1. This mix was used for the mortar bars of four coarse and fine aggregates, namely Greywacke (Gw) and Granite (Gn) stone and Philippi (Ph) and Malmesbury (Ma) sand. CEM I 52.5N was used as in Table 3-1. Sieve analyses of the crushed aggregates were carried out with results given in Table 3-2.

3.4 Test specimens

Four moulds were used to form the specimens in this research as follows:

3.4.1 Cylinders specimens

Unreinforced cylinders concrete of 100 mm diameter and 200 mm high were cast in two series mixes. These specimens were prepared to observe the deterioration of mechanical properties (compressive strength and modulus of elasticity) due to ASR.

3.4.2 Wedge-splitting Cube specimens

Plain concrete specimens in the form of notched cubes with sides of 100x100x100 mm were pre-cracked by wedge splitting tests and exposed to accelerated ASR conditions. To prepare for the test, a slot of

30 mm wide and 20 mm deep was made along the top side of the cubes. In order to ensure that crack formation will occur in the middle of a cube, a notch was made along the central length of the slot of 30 mm deep and 3 mm wide. These specimens were used for the observation of the change in the mechanical cracks under ASR exposure (see Figure 3-3a).

3.4.3 Prism specimens

Reinforced concrete prisms for tension and cyclic loads are used for this research to observe the expansion and crack reduction due to ASR. The prisms were made with a length of 350 mm, a square section with sides of 100 mm and reinforced by a single 16 mm Ø ribbed hig tensile strength steel bar as shown in Figure 3-3b. The bar in the tension-loaded sample is threaded on both ends of the bar to assist in the process of tension testing, and the middle section of the bar was reduced to 13mm Ø over a length of 50 mm to ensure that failure occurs in that middle region. Figure 3-3c shows the preparation of the beam moulds. The same prisms were prepared but unreinforced to determine the thermal coefficient of concrete described later in Section 3.7.2.

3.4.4 Bar specimens

Moulds of 265x25x25 mm were prepared to cast mortar bars. These mortars are immersed in NaOH according to the procedure of the ASTM C 1260 standard test.

Table 3-1 Concrete mix proportions of test series (kg).

Series	Mix	Cement CEM I 52.5	Corex slag	Granite stone	Greywacke stone	Philippi sand	Malmesbury sand	water	NaOH
Mix of test series 1	Gw	440	-	-	1000	-	815	184	-
	Gn	440	-	1000	-	815	-	220	-
	Gw-co	220	220	-	1000	-	815	202	-
	Gn-co	220	220	1000	-	815	-	226	-
Mix of test series 2	Gw/w Gw/H	440	-	-	1000	815	-	208	5.63
	Gn/w Gn/H	440	-	1000	-	815	-	212	5.63
	Gw-co/w Gw-co/H	220	220	-	1000	815	-	212	5.63
	Gn-co/w Gn-co/H	220	220	1000	-	815	-	216	5.63
ASTM C 1260 mix	Gn	440	-	990	-	-	-	206.8	-
	Gw	440	-	-	990	-	-	206.8	-
	Ph	440	-	-	-	990	-	206.8	-
	Ma	440	-	-	-	-	990	206.8	-

Table 3-2 ASTM C 1260 standard grading requirements of aggregates

Retained between sieves (sieve number)	Mass (%)
4.75 mm (No.4) to 2.36 mm (No.8)	10
2.36 mm (No.8) to1.18 mm (No. 16)	25
1.18 mm (No. 16) to 600 µm (No. 30)	25
600 µm (No. 30) to 300 µm (No. 50)	25
300 µm (No. 50) to 150 µm (No. 100)	15

3.5 Experimental plans

It is necessary to characterise the concrete as completely as possible to understand its mechanical behaviour. This will enable a better understanding of crack formation due to mechanical loads, which is one of the actions to be studied in this research. Once this is understood, and also once the potential of cracking due to ASR is understood, the possible synergetic effect of ASR and mechanically induced cracking can be distinguished. Tension, compression, cyclic load and splitting tests have been performed to represent the mechanical loads. An aggressive alkali-silica environment will be simulated by:

1. Immersing the samples in 1N of NaOH solution; and
2. By the presence of the alkalis in the concrete mix water.

Table 3-3 illustrates the experimental programme plans.

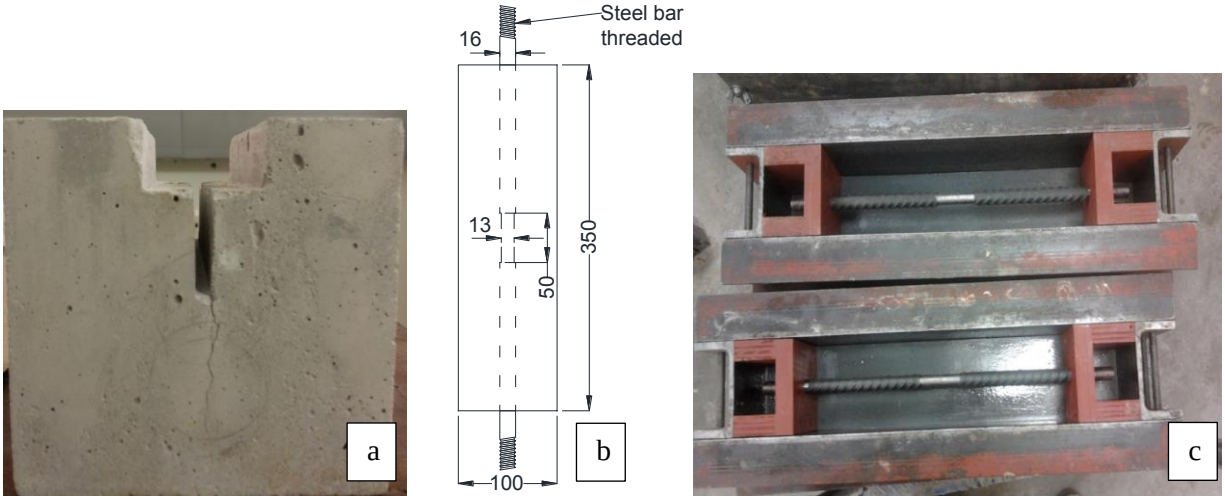

Figure 3-3 Test specimens, a. Wedge splitting specimens, b. Beam details and c. Prepared moulds for beam specimens.

Table 3-3 Experimental work plan.

Work	Plan one			Plan two	Plan three		
Specimens	Cylinders 200x100 mm			Cubes 100x100x100mm	Prisms 350x100x100 mm		
Concrete	NC			NC	RC		
	Normal	Containing high alkali		Normal	Normal	Containing high alkali	
Series test	1	2		1	1	2	
Exposure	Immersing in NaOH	Immersing in water	High humidity	Immersing in NaOH	Immersing in NaOH	Partially Immersing in water	High humidity
Condition	80°C	38°C	38°C RH>90%	80°C	80°C	38°C RH>90%†	38°C RH>90%
Mechanical action	No action during the exposure			Wedge splitting	Tensile* load up to 62 kN	Cyclic* load up to 62 kN	Cyclic* load up to 62 kN
Specimens names	Gw, Gn, Gw-co Gn-co	Gw/w, Gn/w, Gw-co/w, Gn-co/w	Gw/H, Gn/H, Gw-co/H Gn-co/H	Gw, Gw-co	Gw, Gn, Gw-co Gn-co	Gw/w, Gn/w, Gw-co/w, Gn-co/w	Gw/H, Gn/H, Gw-co/H Gn-co/H
Studying	Mechanical Properties of concrete under ASR action			Crack width changing affected by ASR	Combined tensile loading and ASR	Combined cyclic loading and ASR	

† *= the upper half of the specimens exposed to humidity*

**= 70% of yield load of direct tension*

Gw= Greywacke mix, Gn= Granite mix, -co= Corex slag added to the mix, /w= submerged in water and /H exposed to humidity.

3.5.1 Work plans

This study can be divided into three stages to study the effect of mechanical loads and ASR on normal and reinforced concrete as follows:

1. Plain concrete cylinders were used in two series tests: i. Immersed in 1N NaOH at 80°C, then compressive strength and E-modulus tests were conducted at the ages of 14, 28 and 56; and ii. Concrete containing high alkali (NaOH) was then subjected to two conditions (partially submerged in water and exposed to high humidity) and also, compressive strength and E-modulus tests were performed at ages of 1, 3, 7 and 12 months.
2. Cubes were immersed in 1N NaOH at 80 °C and subjected to a wedge-splitting test to obtain specific cracks, and then submerged in the same condition to observe the effects of mechanical crack formation on ASR progress in concrete, or vice versa.
3. Concrete beams reinforced by one bar were subjected to the two series tests: i. reinforced concrete prisms were subjected to tensile mechanical loading and subsequently exposed to 1N NaOH at 80 °C to determine the expansion of difference mixes; and ii. the specimens including high alkali content were subjected to two conditions (relative humidity and submerged partially in water) to study their

effects (expansion and crack width) on ASR under simultaneous mechanical action (cyclic mechanical loading).

From these result the expansion and crack width were studied to determine the following:

1. The effect of ASR on crack width (increasing, decreasing) caused by mechanical loading.
2. The mechanism of crack width and spacing under combined action.
3. The role of relative humidity or water and mechanical loading in increasing ASR effects on concrete.
4. Deterioration of mechanical properties under ASR in two series tests.
5. Comparison between the series tests (effect of temperature and submersion/humidity conditions).

3.5.2 Compressive strength and E-modulus of cylinders specimens (part one)

This plan has been designed to study the effect of ASR on the mechanical properties (strength and E-modulus). The study has been conducted under two terms, a short-term test (immersing the specimens in 1N NaOH at 80˚C) and a long-term test (submerging the specimens in water and/or exposing them to high humidity). Two cases were considered in each term test as follows:

1. Immersing samples in 1N NaOH at 80˚C and the others in hot water at 80˚C to compare the effect of temperature with ASR effects. Strength and E-modulus were tested at 14, 28, 56 days.
2. Exposing samples containing alkalis to high RH according to the condition of ASTM-C.1293 and others submerged in water at 38˚C. Strength and E-modulus tests were conducted at 1, 3, 7 and 12 months.

The effects on the mechanical concrete properties induced by ASR under different conditions and the duration of the test have been studied.

3.5.3 Wedge splitting and ASR of cubes specimens (part two)

Cubes were subjected to wedge-splitting loading to obtain particular crack widths and subsequently submerged in 1N NaOH at 80 °C. To perfom the wedge-splitting test, a slot was made on the top of the cube and a notch was made along the central length. The crack width obtained from the wedge splitting was monitored over weeks of exposure in the NaOH and hot water at the same temperature (80°C).

3.5.4 Reinforced concrete prisms in series tests 1 and 2 (part three)

Two stages are performed: firstly, static tensile load is progressively (monotonically) applied to determine the yield and ultimate strength; secondly, applying pre-loading on other specimens up to 70% of ultimate tensile static load. In series test 1, 62 kN tension load was applied to each prism specimen to simulate the mechanical load before immersion in NaOH aqueous solution at 80 ˚C, according to the ASTM standard condition (ASTM C1260, 2007). A comparison between the expansion of specimens subjected to ASR and the others pre-loaded and then subjected to ASR, have been carried out on the different mixes. In

series test 2, sufficient alkali content was added to the concrete mix. The same samples as in the last section were subjected to static loads in tension up to 70% of the ultimate load (62 kN), and then 100 000 cycles with the same load were applied. The range of cyclic load between the peak and minimum was 20 kN at a frequency of 5 Hz. The mechanical crack width was changed by the subsequent ASR, thermal and hygral expansion of the concrete under conditions of partially submersion in water and exposed to high humidity.

3.6 Tests devices and machines

Several devices and machines were used in this research. All the tests were performed in the Structures Laboratory of the Department of Civil Engineering, Stellenbosch University.

3.6.1 Mechanical testing machines

The mechanical machines used in this research are as follows:

1. The testing machine for steel bars was a Zwick Z250 hydraulic machine (Figure 3-4a).
2. For pre-tension and cyclic loading of reinforced concrete testing, an Instron hydraulic actuator 500B device was used (Figure 3-4b).
3. The contest machine (Figure 3-4c) was used to conduct the compressive test. The steel bar was threaded and prepared in the workshop.

3.6.2 Measurement devices

The following devices were used to measure the deformations and crack widths:

1. For deformations and strains over a 100 mm gauge length, an electronic strain gauge called Marcator 1075R was used to accurately measure the distances between the pins as shown in Figure 3-5.
2. The deformations over a 200 mm gauge length were measured by using a DEMEC gauge with an accuracy of $5x10^{-6}$ (mm/mm) (Figure 3.6). Both of these two strain gauges included the spacer bar, and calibrating bar.
3. LVDTs were used with a data acquisition system (Spider 8) to measure the displacement during compression tests. Catman software was provided at the interface between the Spider 8 and LVDTs. A load cell was also placed under the specimens and connected to the Spider 8 to record the load changing during the compression test.
4. A Digi Micro Mobile Portable Camera (dnt) (see Figure 3-7) was used to take photos of the crack at different times. The dnt camera is a microscope with 10 x to 500 x magnification and 12 megapixels. A spatial analysis program was used to measure the cracks on the pictures using the same magnification during the photo taken.

5. An infrared thermometer gun (Fluke 62 Mini) was used to determine the temperature of the concrete surface in thermal expansion coefficient tests. The device showed in Figure 3-8 measures the temperature of single points with accuracy ±1.5% and a wide temperature range from -30 °C to 500 °C.

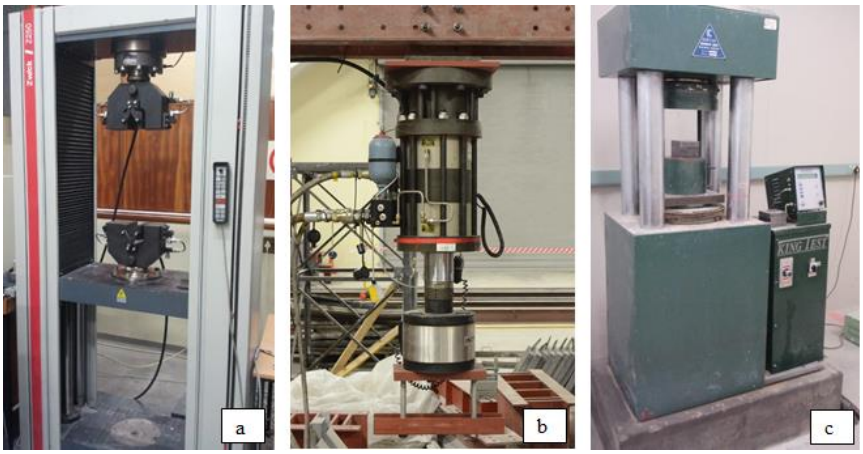

Figure 3-4 Test machines used for experiments: a. Zwick Z250, b. Instron MTM and c. Contest.

Figure 3-5 Strain gauge (Marcator 1075R) of 100 mm length with a resolution of 1 μm.

Figure 3-6 Strain gauge (DEMEC) of 200 mm length with an accuracy of 1 μm.

Figure 3-7 Digital camera (dnt) to measure the crack widths.

Figure 3-8 Fluke 62 Mini Infrared thermometer gun.

3.6.3 Curing devices

Different chambers with various conditions were used in this research. The conditions consist of different temperatures, and humidity versus submersion.

1. For the immersion of the specimens in NaOH and hot water, a new device was made to suit the test condition (chemical solution, high temperature and pressure). The device illustrated in Figure 3-9 is a custom-designed tank with sides of stainless steel covered by timber for insulation and a Perspex lid. To stir the solution, a special pump and piping material were used. A condenser with oil bubbler was placed in the top of the tank to reduce the pressure inside and a small pump was used to circulate water through it. Elements and thermostats were installed on two opposite sides to control the temperature. Perspex was used to make a base to hold the specimens upright without touching the sides. The device is divided into two parts; part 1 for hot water and part 2 for the NaOH solution. Chemical tests were conducted on all materials before the test to ensure that the experiment would not be delayed.

2. In series test 2, a chamber illustrated in Figure 3-10 was designed to expose the specimens to two conditions. In the first, the specimens were submerged totally or partially in water; while in the second; the specimens were exposed to high humidity (> 90%) at a temperature of 38˚C. The chamber was made of stainless steel covered by timber for insulation. The lids were padded by polystyrene sheets and rubber sealing compound was applied on the sides. Elements and thermostats were installed on the two parts to control the temperature. A data logger was placed on the chamber and connected with a probe in the side to measure the temperature and humidity. In part 1, a float was installed to ensure that the water stays on the same level for the duration of the test, while in part 2, the water level was kept under the bottom of samples. The specimens were placed in the chamber on a Perspex base in a specially-built chamber at a height of 100 mm from the bottom.
3. Climate and cooling rooms, as well as the normal water-curing tanks were also used to place the samples at a specific temperature and humidity.

Chambers 1 and 2 were designed for this research and the steel body was manufactured in the workshop of the department of Civil Engineering which also undertook the set-up and installation.

3.7 Preparatory Tests

For preparing the experiments, some preliminary tests were carried out on samples to assess important mechanisms of ASR and to preliminarily design appropriate tests for ASR.

3.7.1 ASTM C 1260 standard test

The ASTM C 1260 standard test is a test for potential alkali-silica reaction in concrete. This test was conducted on the mortar bars described in Section 3.4.4. The procedure of the test was performed on four coarse and fine aggregates as mentioned in Section 3.3. After the mortar cast, all the moulds were removed immediately to the moist room for 24 hours. The specimens were demoulded after 24 hours and the initial strains between each two datum disks (pins) set on the specimens were taken, using the 200 mm DEMEC. The specimens with the pins are illustrated in Figure 3-11. Three intermediate readings were taken for each mix. The specimens made with each aggregate sample were stored for the next 24 hours in the special chamber in part 1 containing tap water and totally immersed at 80 °C. After the specimens had been extracted from the hot water, the zero readings (reference) on the strain gauge were taken after drying the specimens with a towel. The bars were then placed in part 2 of the same chamber containing IN NaOH, to be totally immersed at 80 °C. The time from removing the bar from the hot water and measuring until placing it in the NaOH was 15±5 seconds. The specimens were extracted from the solution after 14 days, and the final reading of strain was recorded. Each reading was performed within

10±2 s, and the next sample was extracted after the reading of the previous sample was completed. All the results are given in Table 3-4.

According to Oberholster and Davies (1986) and Hooton and Rogers (1989) referred to in ASTM C 1260-07, the expansion at 16 days after casting is categorised as follows:

1. Less than 0.10% is indicative of innocuous behaviour in most cases.
2. More than 0.20% it to be potentially nocuous and deleterious expansion may occur in field condition.
3. Between 0.10 and 0.20% include both aggregates that are known to be innocuous and deleterious in field performance.

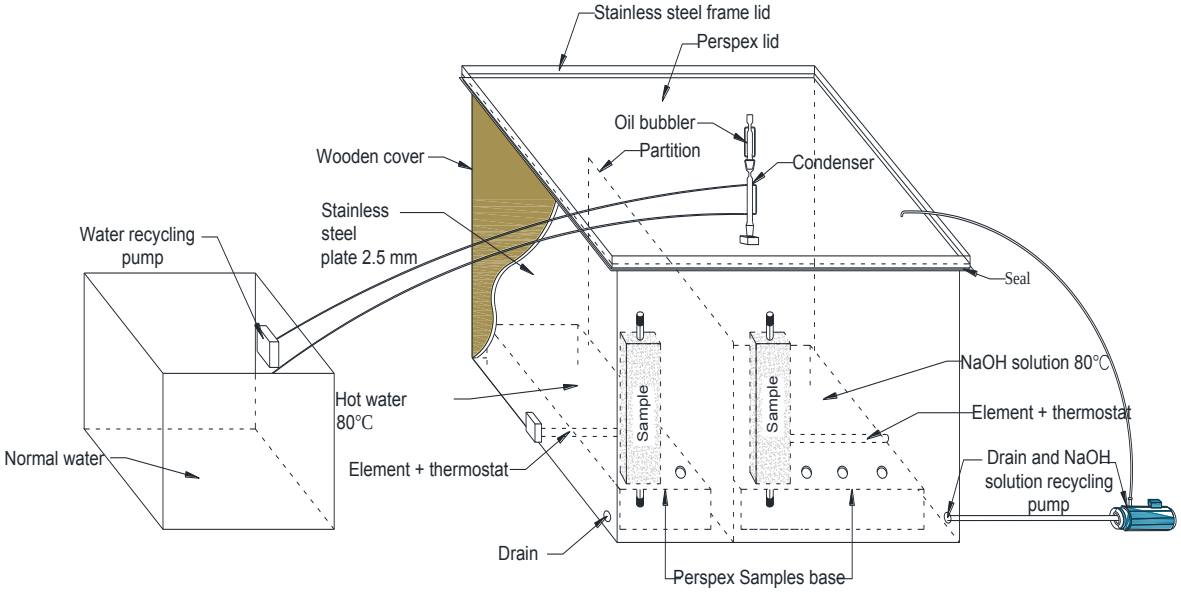

Figure 3-9 NaOH and water, high temperature device to immerse the specimens.

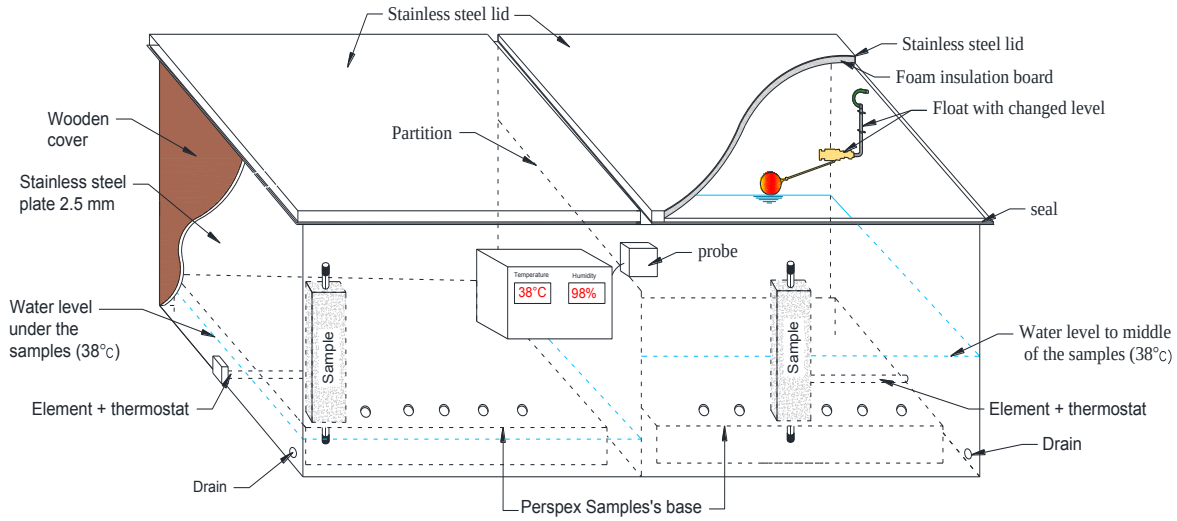

Figure 3-10 Chamber details and placed of specimens under two conditions and two actions.

Figure 3-11 Specimens prepared to ASTM C 1260 and datum discs glued on.

Table 3-4 Expansion due to ASR in aggregate types according to ASTM C 1260 (%).

Age at reading	Greywacke (Gw)	Granite (Gn)	Malmesbury (Ma)	Philippi (Ph)
Initial reading at 24 hours from cast	0	0	0	0
Strain after 1 day in hot water at 80 ˚C	0.11	0.08	0.14	0.14
Strain at 16 days (14 days in ASR at 80 ˚C)	0.41	0.11	0.08	0.11
Strain due to ASR after 14 days in solution (80 ˚C)	0.30	0.03	-0.06	-0.03
Strain after 1 week in laboratory temperature (mm)	0.32	-0.01	-0.01	0.00

The ASR expansion is equal to the gauge reading at 14 days in ASR minus the Zero reading (after 1 day in hot water). The deformation measured is divided by the gauge length (200 mm) to obtain strain. ASTM C1260 requires a gauge length of 250 mm, but a mechanical strain gauge for 200 mm length only was available.

The results in Table 3-4 indicate that only Greywacke had a residual strain equal to 0.3%, which may indicate it to be potentially nocuous and cause deleterious expansion in field performance. Granite had ASR strain equal to 0.03% which means less than 0.1%, and this leads one to classify it as innocuous behaviour in most cases. Philippi and Malmesbury mortar showed shrinkage after 14 days in ASR. The ASTM C 1260 test cannot be relied upon to identify the ASR but is an indication of the probability of the reactivity of the aggregate.

3.7.2 Coefficient of thermal expansion test

The thermal expansion is the extension due to change in temperature, which leads to a change in the shape of materials. Generally, in concrete, the coefficient of thermal expansion (CTE) is determined linearly and expressed in microstrain (10^{-6}) per degree Celsius (με/°C). The CTE of concrete is an important parameter in analysing thermally induced stresses in concrete during the hydration and over the service life (Neeraj and Jahangirnejad, 2008). The magnitude of CTE is important to determine the

amount of expansion induced by temperature. To obtain CTE, several test methods are being used such as AASHTO TP60-00 test, the Strain Gage method (CRD-C 39-81) from the US Army Corps of Engineers, and the Danish T1-B method. Test specimens used in these methods are different. The Danish T1-B method consists of prisms of 100x100x400 mm cast with datum disks placed on the sides. The length changes are taken with variations in temperature from 5 °C to 30 °C. This method was chosen, because the sample dimensions are close to the ASR samples used in this research. The minimum temperature used in this test was 11°C as an average winter temperature, and the maximum was 30 °C as an average summer temperature. The reference as an average annual temperature was 20 °C. Plain and reinforced concrete prisms were cast. The reinforced specimens were used to study the effect of steel restraint on the thermal expansion.

3.7.2.1 Concrete mix and specimens preparation

Two mixes of Greywacke and Granite stones were prepared. Six prisms (reinforced and unreinforced) were cast as in Section 3.4.3 (for each mix design). Each mix was divided into three samples of normal concrete and three of reinforced concrete. The preparation of the mixes is shown in Table 3-1 as Gw and Gn mixes of series test 2. Figure 3.12 shows the reinforced and normal specimens with datum discs (pins) glued on the two opposite sides.

3.7.2.2 Test procedure

CTE tests were conducted according to the Danish T1-B method (Standard Test). The CTE test apparatus consists of a temperature-controlled water bath and strain gauge to measure the change in specimen length between the two pins.

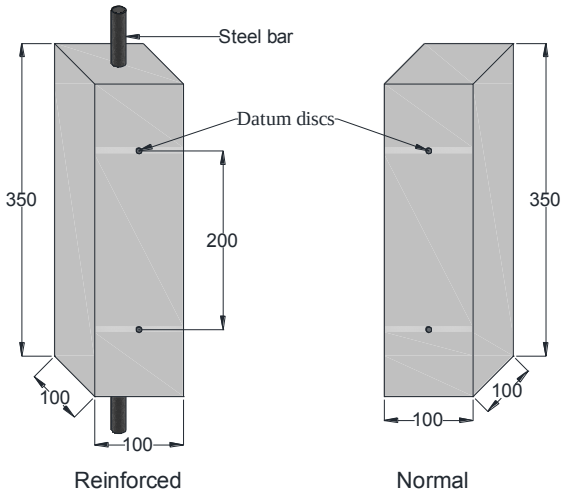

Figure 3-12 Specimens of thermal expansion test with datum discs glued on.

Once the specimens had been demoulded after 24 hours, the pins were glued on the specimens with 200 mm spacing and left for 4 to 6 hours to dry. The specimens were then placed in heavy plastic bags and placed in a water bath at 20 °C for one week. After 7 days, specimens were extracted one by one and the initial measurements (T0) were taken as a reference measurement. The device used to measure the CTE of the specimen is a DEMEC gauge described in Section 3.6.2 and shown in Figure 3-6. The specimens were then placed in the plastic bags and in a water bath at 11 °C for 24 hours to ensure that thermal balance will occur. The specimens were removed from the water bath and plastic bags one by one and the measurements were conducted (TL). The specimens were placed inside plastic bags and placed in the water bath at 20 °C. After 24 hours, the specimens were removed from the water bath and plastic bags and the strain was recorded using the strain gauge (T1). The specimens were returned to the plastic bags and water baths and the temperature was set to 30 ºC for about 24 hours. Once thermal balance occured, the specimens were again extracted from the bath and plastic bags and the measurements were conducted (TH). Now the samples were returned to the plastic bags again and the water bath set to 20 °C. Once thermal equilibrium occurred, the specimens were removed and the final measurements were taken (T2).

3.7.2.3 Results and calculation

The results of CTE at 7 days were calculated through the following equations:

$$\text{Extension} = 0.81 \times R \times 0.002 \tag{3-1}$$

where the 0.81 is a calibration factor of the strain gauge, R is the reading measured and 0.002 is the division of the strain gauge. The strain then can be determined as:

$$strain\ (\varepsilon) = \frac{extension\ (\Delta l)}{gauge\ length\ (l_o)} \tag{3-2}$$

where, Δl is the change in length equal to measured length at 30 °C (l_H) minus that measured at 11 °C (l_L), l_0 is the actual measured length at 20 °C at the beginning of the test.

The strains were then plotted at each temperature and the CTEs were calculated from the following equation:

$$CTE = \frac{\Delta l}{l_0 * \Delta T} \tag{3-3}$$

and ΔT is the difference in temperature at the high and low of measured lengths (T_H-T_L =*30-11* °C).

The results of *CTE* obtained from this test are concluded in Figure 3-13. It can be noted that the CTE of the restrained samples (reinforced) are less than those of plain concrete.

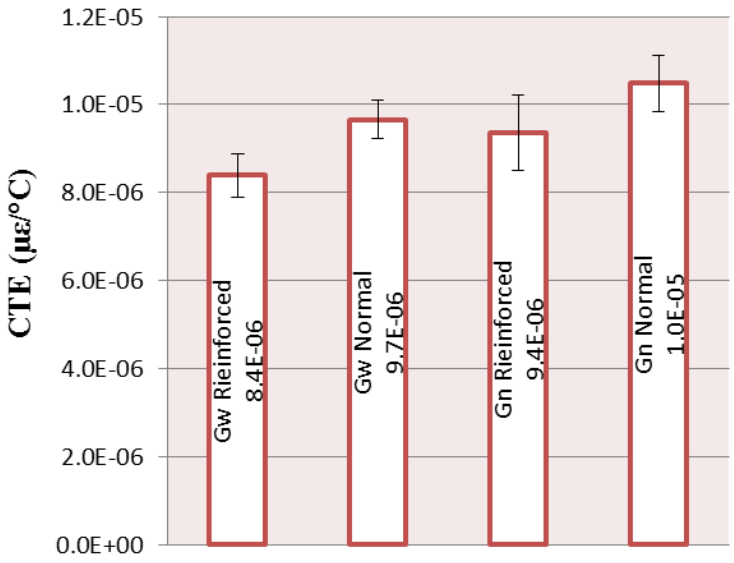

Figure 3-13 CTE of restraint and un-restraint concrete made with Greywacke and Granite.

3.7.3 Steel bar test

A steel bar with 16 mm diameter threaded at both ends to assist tensioning and reduced in the middle to a diameter of 13 mm over a 50 mm length was tested. This was done to induce a crack in the RC at a particular location where a crack is expected to develop so that the crack width can be measured during ASR cyclic loading tests. The nut of the thread was M14. The mechanical characteristics of the steel were: elastic modulus E_s =202 GPa, yield strength f_y = 480 MPa, ultimate strength f_t = 531 MPa and ultimate strain ε_u = 3.8%.

3.7.4 Aggregate and cementitious tests

Sieve analysis testing of aggregates has been carried out in this research to establish their grading. Chemical tests were also conducted to determine the basic components of aggregates, cement and Corex slag. Table 3-5 gives the chemical results of materials by Environmental Analysis Laboratory. Major element analysis was conducted by X-Ray Fluorescence (XRF).

3.7.5 Perspex and rubber test

An investigation was carried out to determine the effect of sodium hydroxide on Perspex material, which is used as a base under the specimens at high temperature in the alkaline solution. Testing of Perspex in NaOH at 90 ˚C was carried out for two weeks. The results showed that Perspex was not affected by the NaOH solution. The same test was conducted on the rubber that was used as a cap to cover the external part of the steel bar of the prism specimens. Also, the results showed that this kind of rubber has a high resistance to alkali chemical action at high temperature.

Table 3-5 The main components of mixing material (%).

Sample name	Al_2O_3	CaO	Fe_2O_3	K_2O	MgO	Na_2O	SiO_2	TiO_2
Philippi sand	0.36	10.40	0.10	0.15	0.18	0.24	79.73	0.09
Malmesbury sand	0.50	0.06	0.16	0.06	0.08	0.17	98.55	0.13
Granite stone	13.15	1.17	1.81	5.23	0.25	2.87	73.30	0.22
Greywacke stone	12.55	1.11	4.92	2.79	1.92	2.08	71.04	0.74
Greywacke crushed dust	14.23	1.16	6.11	3.17	2.54	2.02	65.28	0.79
Cement CEM I 52.5	3.91	65.45	3.28	0.52	1.46	0.25	20.13	0.19
Corex slag	14.31	38.13	1.35	0.61	10.85	0.13	30.50	0.52

Major element analysis by XRF, Rh Tube, 2.4kWatt
Cr_2O_3, MnO and P_2O_5were determined at less than 0.2%

CHAPTER FOUR

4. CONCRETE PROPERTIES UNDER ASR DETERIORATION

Abstract

Mechanical and chemical tests of concrete affected by ASR were conducted to identify the changes in concrete properties over time. Two methods of accelerated testing were followed. The first was according to ASTM C 1260, where cylinders of normal concrete were cast and submerged in 1N NaOH at 80 °C and then tested to determine their compressive strength (f_c) and modulus of elasticity (E_c) at a specific time. The second was according to ASTM C 1293, where cylinders of concrete containing high alkaline (7 kg/m^3 of Na_2O_e) were also cast and tested at a specific time by mechanical means to determine f_c and E_c and by chemical means to determine the components of concrete. The degradation of the properties of ASR-affected concrete is studied by comparing four different mixes made of Greywacke and Granite stones with and without Corex slag. The compressive strength and stiffness, as well as chemical composition, were also determined at different exposure times. Different results have been obtained from the two methods. The change in strength and stiffness of concrete under ASTM C 1260 conditions is significantly different from that under ASTM C 1293 conditions, due to the different exposure conditions.

4.1 Introduction

Chemical degradation processes can affect the properties of concrete structures during their service life by producing a hydrophilic and expansive ASR gel. These properties change due to these progressive formations of ASR expansion. Many researchers studied the property changes of concrete under ASR effects, but most of them did not compare the results of the two most common ASR test methods (ASTM C 1260 and ASTM C 1293). Tests were carried out for compressive strength and stiffness (modulus of elasticity) to determine the change in these properties due to ASR deterioration. Chemical tests were also performed to study the components of concrete before and during ASR action. The concrete cylinders were exposed to the conditions prescribed by ASTM C 1260 and ASTM C 1293.

4.2 Experimental program

Two experimental series were carried out to determine the change in concrete properties; the first was based on ASTM C 1260 and the second on ASTM C 1293. For both tests, concrete cylinders of 100 mm diameter and 200 mm high were used. Greywacke and Granite stones were used in all cases, but where Philippi and Malmesbury sands were used for the first series, only Philippi sand was used for the second series. Corex slag was added to half of the samples in both cases. The samples were denoted as in Section 3.3 and the mix proportions of both series are given in Table 3-1. The water content mentioned in this table include the aggregate absorption that was recorded in a Hippo Quarries report by Davis and Alexander (1989). Figure 4-1 shows the flow chart of the experimental work for the two series.

4.2.1 Specimens and devices of test series 1

For series test 1, four mixes as in Table 3-1 were made. For each mix, 27 specimens were cast, giving a total of 108 specimens for the four mixes. The specimens were subjected to three different conditions as mentioned; the first was in 1N NaOH aqueous solution at 80 ˚C; the second was in hot water at 80 ˚C; and the third condition was in normal water at 23±2 ˚C. Those specimens which were placed in high-temperature water were tested to determine whether temperature contributes to a change of concrete properties with ASR accelerated testing. For the immersion of the specimens in NaOH and hot water, the device illustrated in Figure 3-9 was used. The specimens were placed into the two parts (hot water and NaOH solution). The specimens in the third condition were immersed in a separate tank. Other laboratory facilities used in this experiment were mixers, sieves and slump test apparatuses. The Contest materials testing-machine (MTM) of 2 MN compressive capacity shown in Figure 3-4 was used to conduct the compressive tests. An electronic pressure gauge is built in to measure the applied load. All the tests were performed in the Structures Laboratory of the Department of Civil Engineering, Stellenbosch University. The compressive strength and modulus of elasticity tests of the cylinders were conducted after 14, 28 and 56 days of exposure.

4.2.2 Specimens and devices of test series 2

Four mixes, in total 96 specimens, 24 of each mix were made and placed into two conditions. The first condition was submerged in water denoted (/w) and the second was exposed to RH>90% denoted (/H) as in Table 3-1. For concrete curing, the specimens were placed in the chamber illustrated in Figure 3-10 on a Perspex base at a height of 100 mm from the bottom. The specimens were placed in the parts of the chamber (submerged in water and exposed to high humidity). The same Contest MTM machine (Figure 3-4) was used to conduct the compressive test. The compressive and E-modulus tests were performed on these series specimens after 1, 3, 7 and 12 months of exposure, and XRF chemical tests were performed on the same series specimens after 1, 8 and 12 months of exposure.

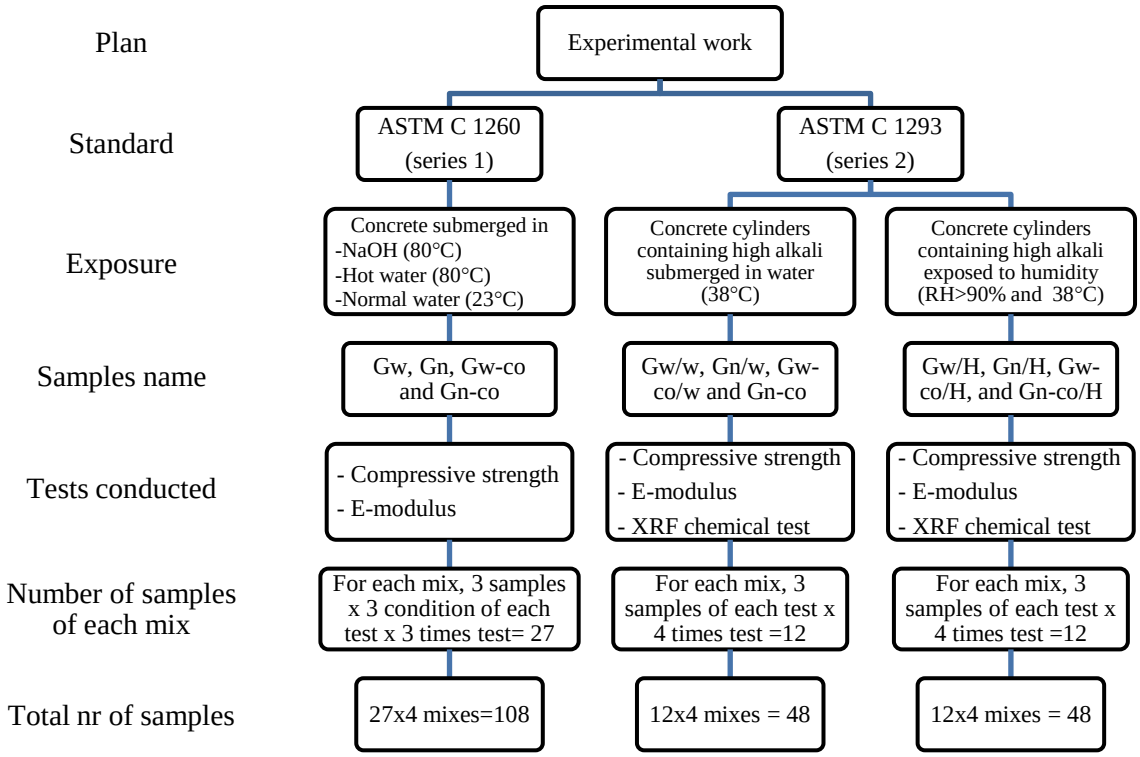

Figure 4-1 Flow chart of the experimental program.

4.3 Mechanical properties of series 1 (subjected to ASTM C 1260 conditions)

The ASTM C 1260 standard test is called the potential alkali reactivity test of aggregate and crushed aggregates. Specific particle sizes of aggregate used in the mortar bar have been described in Section 3.7.1. In this experiment, normal concrete mixes were made with coarse reactive aggregate (Greywacke) and non-reactive aggregate (Granite), as outlined in Section 4.2.

4.3.1 Test procedures

After the concrete mixtures had been cast, a slump test was conducted according to BS EN 12350-2 and the result was 65±5 mm for all mixes as shown in Figure 4-2. The specimens were placed in the cylinder moulds and covered by plastic sheets at laboratory temperature. After 24 hours, the specimens were demoulded and submerged under the three conditions described in Section 4.2.1; 1N NaOH at 80 °C, hot water at 80 °C and normal water at 23±2 °C. One-third of the specimens were extracted from their chamber at 14 days, and compression tests were performed to calculate the strength of concrete (f_c) and the modulus of elasticity (E_c). To calculate the E_c, 3 LVDTs placed at 120% with respect to each other were used to determine the average compressive strain. Three cycles up to about one-third of the ultimate load were applied, before the fourth cycle was applied until failure. The rate of the load application was

180 kN/min. The same procedures were followed on similar specimens at 28 days and 56 days. Figure 4-3 shows the set-up of the compressive test. The results were recorded by LVDTs and load cell through Spider 8 and Catman software.

4.3.2 Tests results and discussion

The stresses and strains were determined from loads and displacements, and a stress-strain curve was drawn. The stresses were calculated by dividing the recorded compressive force by the nominal cross-sectional area of the 100 mm diameter cylindrical specimens. To determine the strain, the average LVDT deformation was divided by the gauge length, which was the vertical space between the bases of the LVDTs (70 mm). From this curve, the ultimate stress and E-modulus were determined.

Figure 4-2 Slump test procedure.

Figure 4-3 Compressive strength test set-up.

The results illustrated in Figure 4-4 are the cylinder compressive strengths for all mixtures after 14, 28 and 56 days in normal water (23±2 ˚C), hot water (80 ˚C) and NaOH solution (at 80 ˚C). Figure 4-5 shows the E-modulus for the same mixes and at the same conditions. The results summarised in Table 4-1 show that for the Gw, Gw-co specimens and Gn-co with GGCS added, the strength in hot water was higher than that at normal temperature at 14 days by 21.5%, 10.7% and 23.9% respectively, while for Gn specimens this strength was less in hot water by 27% at the same age.

The strength in NaOH is slightly more than in hot water (at the same temperature of 80 ˚C) at least at the early age (14 days) in Gw, Gn, Gw-co and Gn-co by 10.7%, 15.4%, 5.0% and 13.3% respectively. At 56 days, the strength of Gw in NaOH became almost the same as in hot water, while the strength of Gn-co reduced by 4.3%. These results show that in the accelerated test, the NaOH and high temperature have an affect on the strength of Gn specimens. E-moduli shown in Figure 4-5 are slightly affected by ASR, where in Gw, Gn, Gw-co and Gn-co, they were less than those in normal water by 2.8%, 24.4%, 6.3% and 1.2% respectively at 14 days, while at 56 days they were less by 15.8%, 71.8%, 2.9% and 0.73% respectively. It is noted that the E-modulus in Gn decreases over time. At 56 days the E-moduli for specimens in hot water was lower for Gw, Gn and Gw-co by 9.3%, 42.1% and 0.4% respectively than those in normal water, but in Gn-co it was higher by 4.9%. Figure 4-6 shows the comparison of the properties of all mixes submerged in NaOH solution. Compressive strength as shown in Figure 4-6a slightly increases over the time, and the strength of the Gn mix was the lowest affected by the high temperature. In Figure 4-6b the E-modulus in Gn mix decreased with age and also for Gw-co it slightly decreased after 28 days, while in the other mixes it slightly increased after the same number of days. According to some previous studies, the mechanical properties of some aggregates are affected over time by ASR, based on the reactivity of aggregate.

Marzouk and Langdon (2003) conducted tests on normal and high strength concrete using potentially highly reactive and moderately reactive aggregates. The specimens were immersed in NaOH at 80˚C for a period of 12 weeks. They found that the compressive strength is less sensitive to ASR effects on concrete than the modulus of elasticity. Shenfu and Hanson (1998) carried out compressive and splitting tensile strength tests on 100x200 mm cylinders immersed in NaOH. They found that the compressive strength, splitting tensile strength and dynamic modulus were not affected significantly for up to 90 days and just after ASR cracks (at an age of 125 days) were found, the concrete mechanical properties were significantly reduced. For non-reactive concrete, according to Fournier et al. (2004), a reduction in the modulus of elasticity can occur even at a low level of ASR expansion or even when compressive strength of the affected concrete is still increasing due to continued hydration.

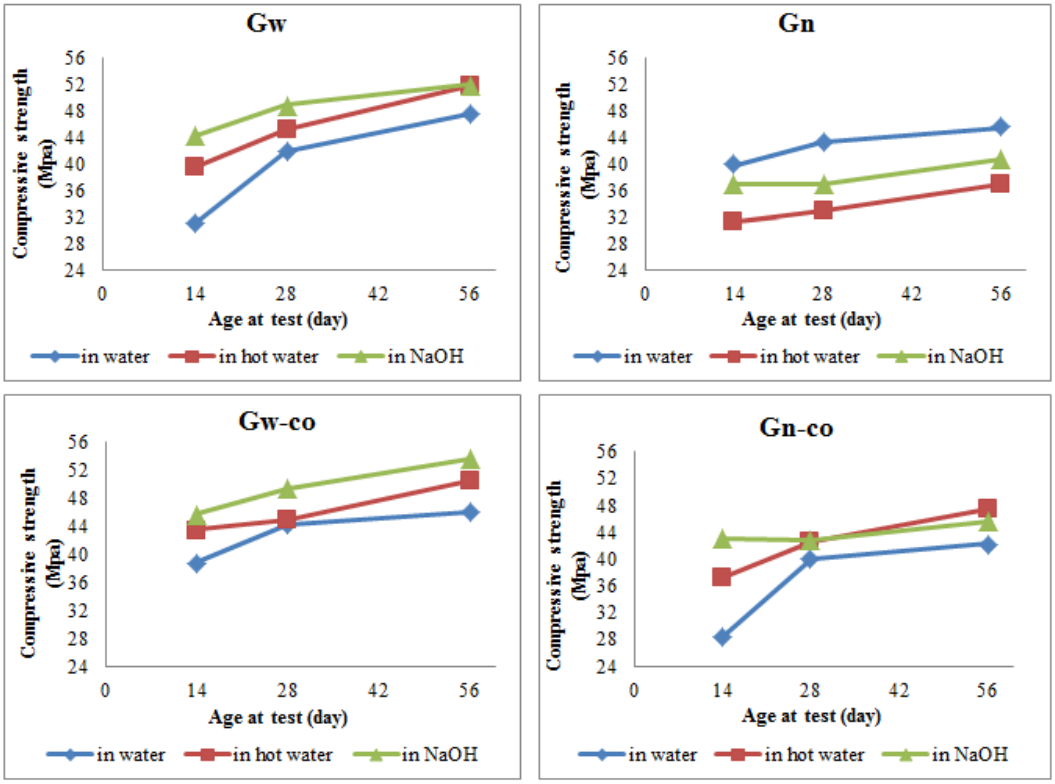

Figure 4-4 Cylinders compressive strength for all mixtures at different ages in different conditions.

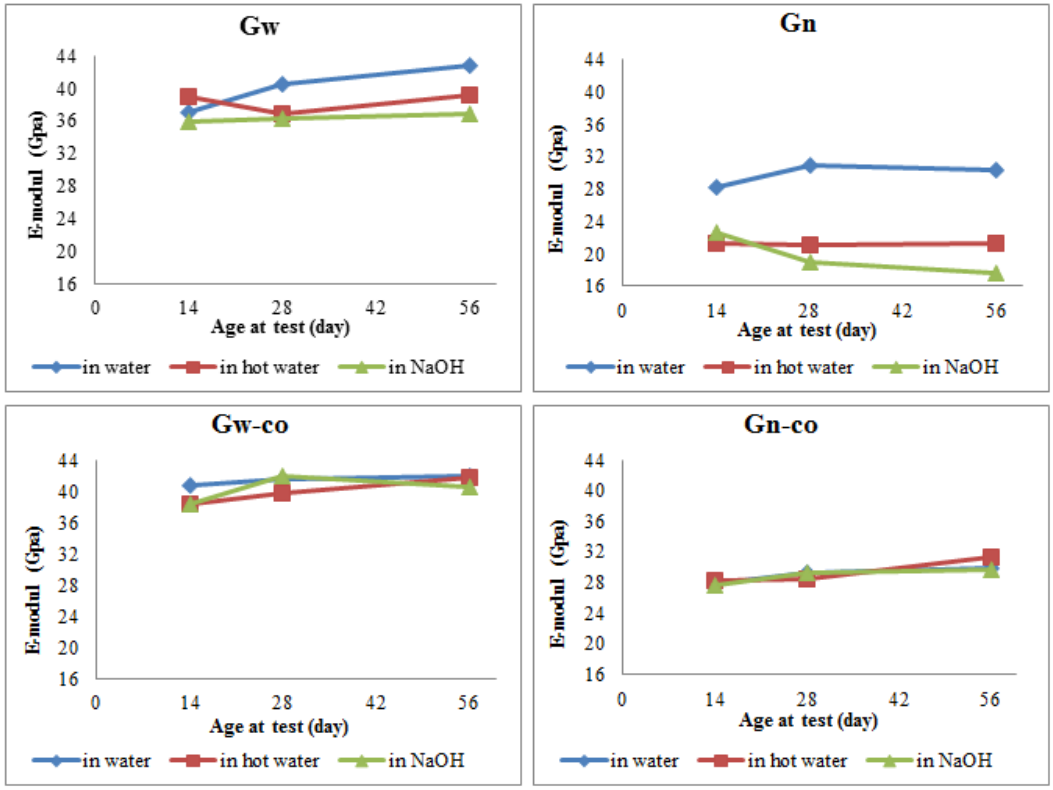

Figure 4-5 Modulus of elasticity for all mixtures at various exposure ages in different conditions.

Table 4-1 Summary of Mechanical Test Results Performed on Laboratory Specimens.

Condition in		Ultimate strength (MPa)			E-modulus (GPa)		
	Sample	14	28	56	14	28	56
Normal water	Gw	31.0 (4.7)	41.9 (5.2)	47.6 (3.5)	37.0 (2.3)	40.5 (2.6)	42.7 (3.0)
	Gn	39.9 (4.1)	43.3 (4.2)	45.6 (2.1)	28.2 (1.7)	30.9 (0.5)	30.3 (1.6)
	Gw-co	38.8 (4.4)	44.1 (2.0)	46.0 (1.1)	40.8 (1.6)	41.5 (2.4)	41.8 (4.1)
	Gn-co	28.4 (4.5)	40.1 (4.0)	42.3 (3.7)	27.8 (0.8)	29.3 (4.9)	29.8 (0.2)
Hot water (80˚C)	Gw	39.5 (2.8)	45.3 (4.1)	51.9 (3.3)	38.9 (0.9)	36.9 (2.8)	39.1 (4.3)
	Gn	31.3 (2.3)	32.9 (3.5)	36.9 (1.5)	21.2 (0.8)	21.1 (3.4)	21.3 (4.9)
	Gw-co	43.5 (0.6)	44.9 (4.7)	50.5 (4.3)	38.4 (5.4)	39.8 (0.2)	41.6 (2.4)
	Gn-co	37.3 (2.6)	42.6 (3.1)	47.5 (7.7)	28.3 (0.8)	28.5 (3.8)	31.4 (3.8)
NaOH (80˚C)	Gw	44.3 (3.4)	49.0 (0.7)	52.0 (5.9)	36.0 (0.4)	36.3 (3.1)	36.9 (1.9)
	Gn	36.9 (0.7)	36.9 (3.0)	40.8 (4.2)	22.7 (3.6)	18.9 (1.4)	17.6 (0.8)
	Gw-co	45.7 (3.3)	49.3 (2.5)	53.6 (0.7)	38.4 (2.8)	41.9 (1.5)	40.6 (1.1)
	Gn-co	43.0 (1.5)	42.8 (2.5)	45.6 (2.2)	27.5 (2.3)	29.2 (1.4)	29.6 (2.9)

Coefficient of Variation between brackets (CoV in %)

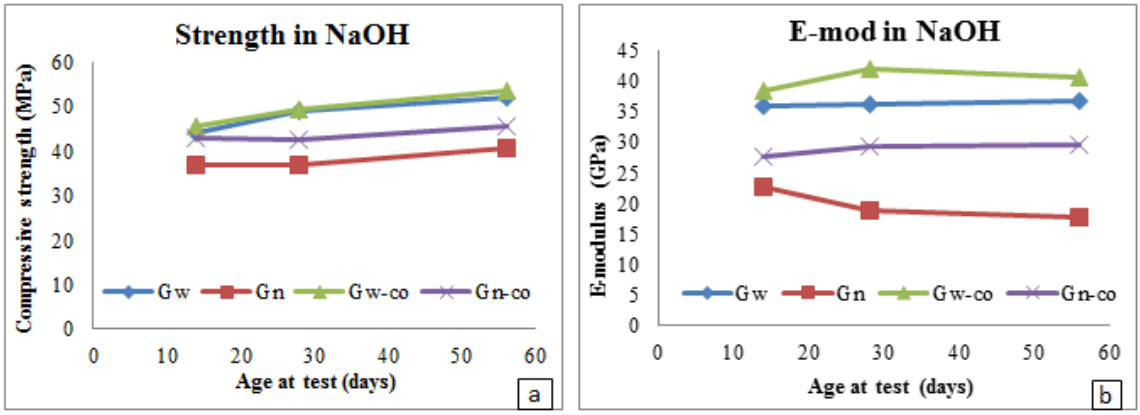

Figure 4-6 Comparison of all mixtures at different ages in NaOH: a. compressive strength and b. modulus of elasticity.

4.4 Mechanical properties testing series 2 (subjected to ASTM C 1293 condition)

ASTM C 1293 is a standard test to determine the length change of concrete due to ASR by using concrete prisms. In this experiment, the concrete cylinders were subjected to both conditions (submerged in water and exposed to high humidity) to determine the change of mechanical properties induced by ASR deterioration in this series test.

4.4.1 Test procedure

The same procedures of casting and moulding the specimens as in series 1 were followed in these series. After the specimens had been demoulded, they were placed in the two conditions. Twelve samples of each mixwere submerged in water at 38 °C, and the other twelve were exposed to high humidity at the same temperature. From each of the four mixes, a quarter of the specimens were extracted from their condition after one month to undergo the compression testing. To determine E_c, the same procedure as in Section 4.3.1 was followed. These procedures were conducted again on a quarter of the specimens at the end of 3, 7 and 12 months.

4.4.2 Tests results and discussion

To determine the ultimate strength and modulus of elasticity, static compressive tests were conducted on the specimens containing high alkali and subjected to the two mentioned conditions. The tests were carried out after 1, 3, 7 and 12 months. After 12 months of exposure to their conditions, cracks could be seen on the submerged specimens which were larger than in those exposed to humidity and in those specimens containing Corex slag. Figure 4-7 shows the cylinders of four different mixes submerged in water, whereas Figure 4-8 shows the same mixes subjected to humidity. The figures show that larger cracks are present in Gw/w mixes.

4.4.2.1 Compressive strength

The results of compressive strength and E-modulus were determined from the stress-strains curves. The compressive strength results of cylinders after 1 year of exposure are shown in Figure 5-9a for mixes made with Greywacke stone, both submerged in water and exposed to humidity and without Corex slag (Gw/w, Gw/H) and with Corex slag (Gw-co/w, Gw-co/H). The strengths have increased significantly over the first 7 months and then only slightly increased in Gw/H and Gw-co/w and slightly decreased in Gw/w and Gw-co/H. The strength changes between the 7^{th} and the 12^{th} months were -2.1, 3.0, 4.2 and -4.7% for Gw/w, Gw/H, Gw-co/w and Gw-co/H respectively. The mixes made with Granite stones Gn/w and Gn/H and mixes with Corex slag Gn-co/w and Gn-co/H are illustrated for both conditions in Figure 4-9b. The strength increased dramatically until the 7^{th} month, and then slightly changed from the 7^{th} month to the 12^{th} month. The changes in the last 5 months were -2.6, 3.8, 3.6 and 3.7 for Gn/w, Gn-co/w and Gn-co/H respectively. Comparing the strength changes in all four mixes submerged in water as shown in Figure 4-10a, it can be seen that the rates of strength-increase during the first seven months in Granite mixes were higher than those in Greywacke mixes. After seven months, a small decrease of strength in Gw/w and Gn/w can be seen, while there was a slight increase in strength of the mixes that contain Corex slag. Figure 4-10b shows that the strength of specimens exposed to humidity after seven months increased slightly in all mixes.

Gw/w Gn/w Gw-co/w Gn-co/w

Figure 4-7 Cylinder specimens submerged in water at 38 °C after 12 months.

Gw/H Gn/H Gw-co/H Gn-co/H

Figure 4-8 Cylinder specimens exposed to >90% humidity at 38 °C after 12 months.

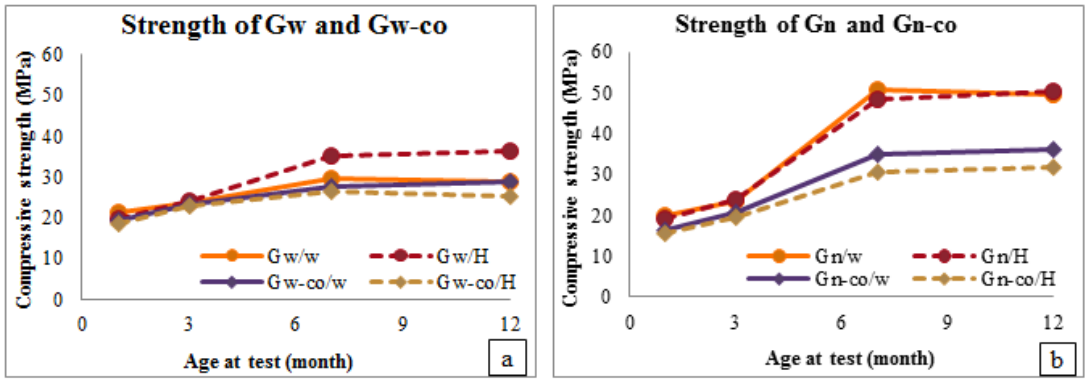

Figure 4-9 Compressive strength under ASR at different ages in water and humidity, a. Greywacke stone mixes and b. in Granite stone mixes.

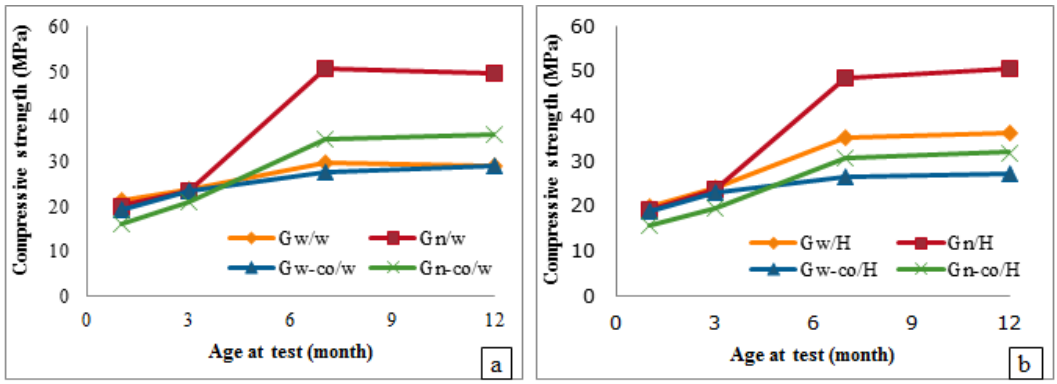

Figure 4-10 Comparing the strength of all mixes a. submerged in water and b. exposed to high humidity.

4.4.2.2 Modulus of elasticity

The E-modulus decreased over time due to ASR in the mixes made of Greywacke stone as illustrated in Figure 4-11a. The largest decrease was in Gw/w and was less when the same mix was exposed to humidity and, the decrease was less when Corex slag was added to the mix. The reductions in E-modulus at the end of 12 months when compared with reduction over 1 month were 51.9, 18, 9.2 and 11.8% for Gw/w, Gw/H, Gw-co/w and Gw-co/H respectively. In the mixes made of Granite stone, the E-moduli increased until the 7th month and then decreased as shown in Figure 4-11b. The increasing rates of Gn/w, Gn/H, Gn-co and Gn-co/H from the 1st month to the 7th month were 20.3, 23.2, 17.6 and 17.2% respectively and the decreasing rates after that until the 12th month were -8.6, -5.8, -0.5 and -4.0% respectively. The decreases in E-modulus over time under ASR for the specimens submerged in water are illustrated in Figure 4-12a, and for those exposed to humidity are shown in Figure 4-12b. In general, the E-modulus in mixes made of Greywacke stone was affected when the ASR reaction started, while in Granite mixes it was only affected some months later.

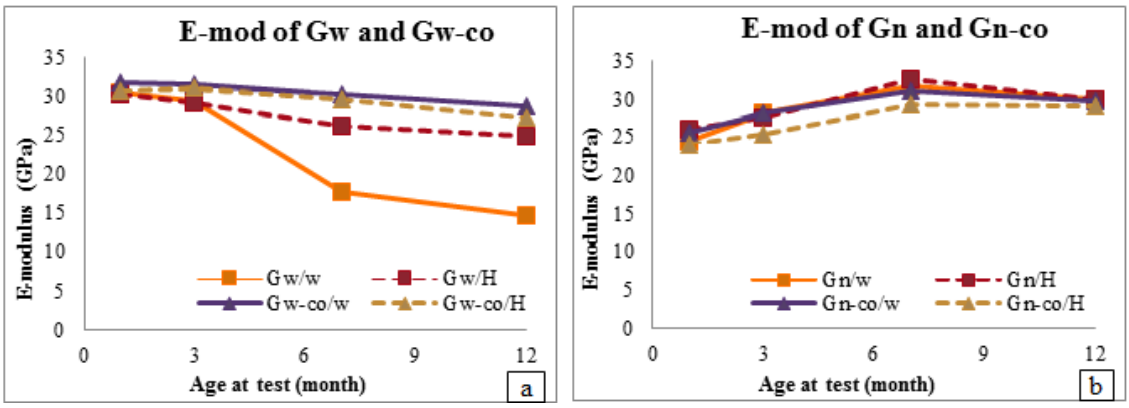

Figure 4-11 Modulus of elasticity under ASR at different ages in water and humidity, a. Greywacke stone mixes and b. in Granite stone mixes.

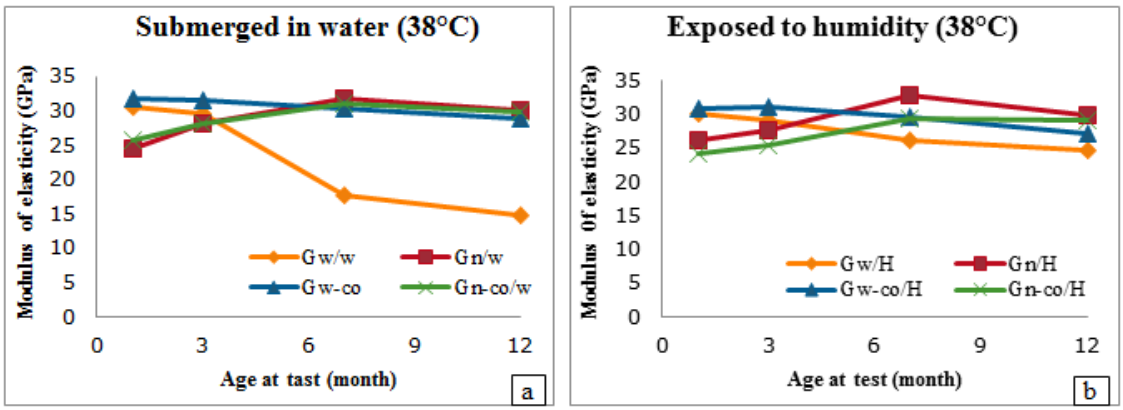

Figure 4-12 Comparing the E-modulus of all mixes a. Submerged in water and b. exposed to high humidity.

Despite an increase in the compressive strength of those specimens subjected to both conditions, the modulus of elasticity of concrete decreased soon during exposure time for the specimens containing highly reactive aggregate and those containing modestly reactive aggregate, decreased later. The experimental results show that ASR affects changes in the engineering properties of concrete, based on aggregate reactivity and exposure conditions. Some authors have confirmed this fact. In the early stage of the ASR reaction, the compressive strength test is not such a good indicator as the E-modulus, which provides a good indication of concrete deterioration (Swamy and Al-Asali, 1986). Swamy et al. (1988) first performed experiments on the mechanical properties of concrete affected by ASR and concluded that the degradations of the engineering properties do not occur at the same rate. Esposito (2012) has compared the results of some literature regarding the degradation of the mechanical properties of ASR-affected concrete and summarized that it is not a reliable parameter to consider the compressive strength to detect the ASR deterioration.

4.5 Chemical properties of specimens series test 2 (subjected to ASTM C 1293 condition)

The study of chemical properties of concrete is significant, because of the various reactions between the concrete components. The most important of these reactions here is the subject of this research (ASR). An investigation of different mixes made from the same aggregates used in previous tests was carried out.

4.5.1 Mechanism of ASR reaction

Being a multi-stage process the ASR reaction starts with the reaction on the surface of the aggregate between reactive silica (SiO_2) in the aggregate and the (equivalent) alkali (Na and/or K) in cement or another source, in the presence of water. The negative ions (OH^-) attack the poorly crystallized silica network (Si-O-Si) resulting in silicate ions (Islam and Akhtar, 2013; Garcia, et. al., 2006). The negative charge creates a balance with the positively charged alkali ions (Na^+ or K^+). The following equations by Islam and Akhtar (2013) show the stages of the reaction process.

$$Si - O - Si + OH^- \rightarrow Si - OH + OH - Si \quad (4\text{-}1)$$

$$Si - OH + OH^- \rightarrow SiO^- + H_2O \quad (4\text{-}2)$$

$$Si - O - Si + 2NaOH\ (KOH) \rightarrow 2Si - O^- - Na^+\ (K^+) \quad (4\text{-}3)$$

Two phases of reaction components are produced, namely reaction between the reactive silica, calcium ions and water leads to calcium silicate hydrate C–S–H and/or reaction between the reactive silica, alkalis and water forms the gel (Poyet et al. 2007). Two types of component gel are produced by alkali-silica reaction (Helmuth and Stark, 1992), namely calcium alkali silicate C-N(K)-S-H (non-swelling gel) and

alkali silicate hydrate N(K)-S-H (swelling gel). The damage due to alkali-silica reactivity only occurs when both types of ASR gels form (Islam and Akhtar, 2013). The reaction usually forms dark rings surrounding the aggregate (reaction rim Rr) (Giaccio, et. al., 2008). In the presence of absorbed water, the gel fills these rings when it is growing and pressing in all directions. The gel expansion then generates micro-cracks in the reactive aggregate and afterwards in the cement paste which leads to more water permeation and thus gel swelling. Figure 4-13 illustrates the various stages of the reaction process. The chemical composition and the available alkali content in the cement matrix are the main factors in the expansion rate.

4.5.2 Microscopic examination of the concrete surface

As already mentioned, concrete Gw is composed of reactive Greywacke coarse aggregate and concrete Gn of non-reactive granitic coarse aggregate. Both of them were mixed with Philippi sand and 50% of cement was also replaced with Corex slag (co) in half of the mixes as summarized in Table 3-1. The Digi Micro Mobile Portable Camera (dnt) (see Figure 3-7) was used to take photos of the cut surface in the middle of the concrete cylinders after 65 weeks of exposure. Figure 4-14 shows the texture of two of the Greywacke mixes Gw and Gw-co in both the submerged and humidity conditions while Figure 4-15 shows the feature of the mixes made of Granite Gn and Gn-co. Clear signs indicate that in the specimens exposed to moisture, dark rings form around the aggregates and it indicates that the reaction is still continuing. In those specimens submerged in water, gels were formed around the aggregates as a result of the continuous presence of water. In the last case, the gel expansion has developed significantly in Gw/w, where clear deleterious signs are observed and micro-cracks in the aggregate appear as in Figure 4-14. In Granite specimens, it is seen that the reaction rims in humid specimens as well as the gel in submerged specimens, are smaller than those in Greywacke mixes.

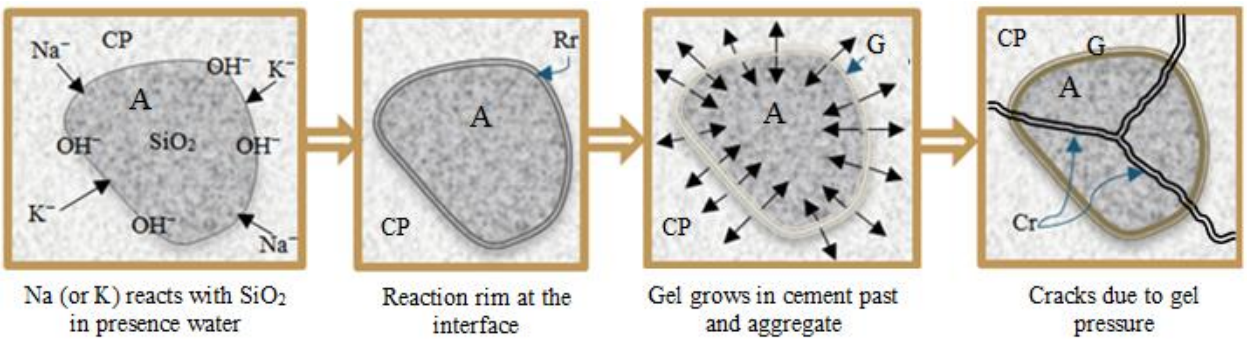

Figure 4-13 Definition of the stages of the ASR reaction A: reactive aggregate, Rr: reactive rim, G: gel, Cr: crack, CP: cement paste.

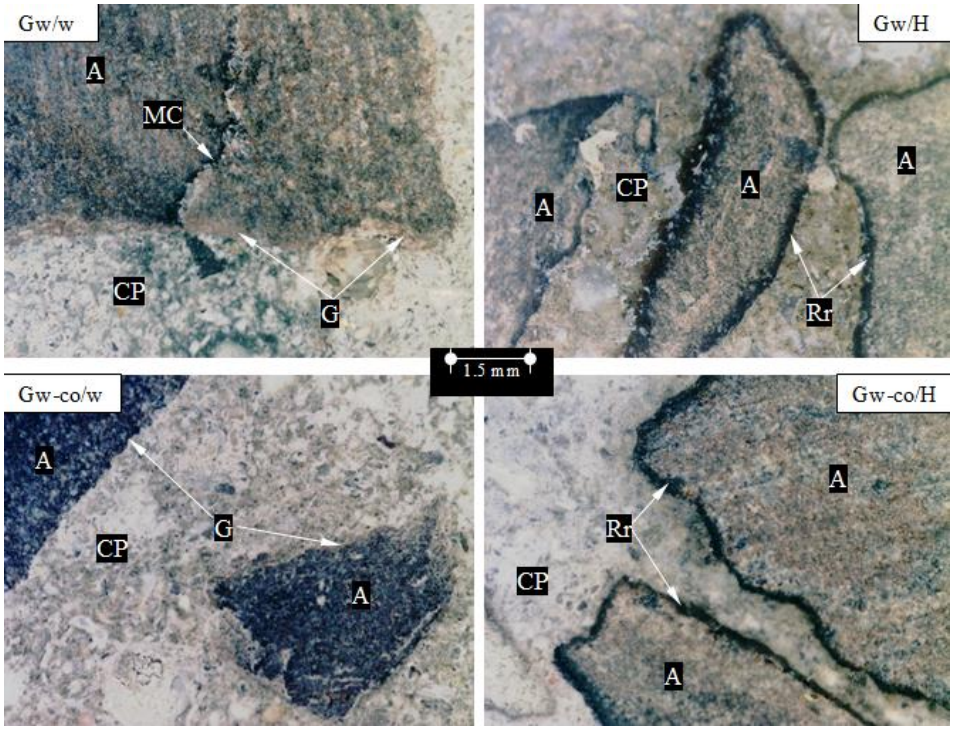

Figure 4-14 Microscopic observations of the concretes made of Greywacke. A: reactive aggregate, G: gel, Mc: micro-crack, CP: cement paste, Rr: reactive rim. The magnification factor is 35.

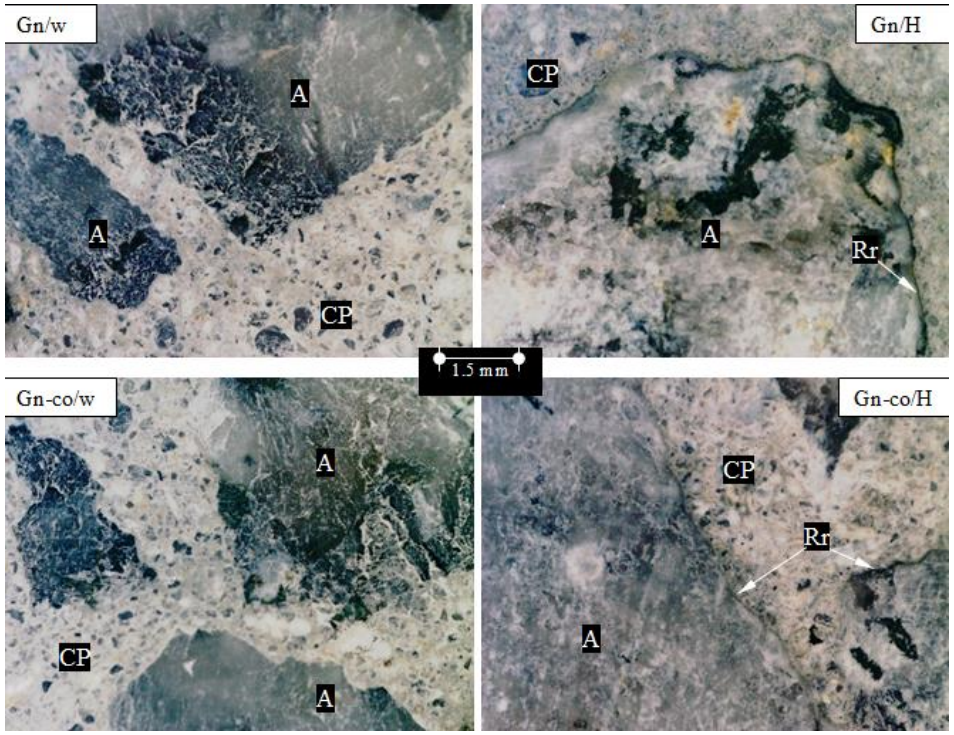

Figure 4-15 Microscopic observations of the concretes made of Granite. A: reactive aggregate, G: gel, Mc: micro-crack, CP: cement paste, Rr: reactive rim. The magnification factor is 35.

4.5.3 XRF tests of concrete mixes

Chemical component tests were carried out on specimens made as in series test 2 and the same procedure mentioned in Section 4.4.1. Cylindrical samples were cut in the middle and then the cut surfaces were crushed with a grainer machine to obtain a concrete powder from the middle surface. Figure 4-16 illustrates the surface of the four mixes as example. The powder was collected in plastic bags and sample names were written on them. The tests were carried out after 1, 8 and 12 months and the samples were taken to the chemical laboratory. XRF tests were conducted on the samples at the ICP-MS and XRF Laboratory of Stellenbosch University.

4.5.4 Chemical component (XRF) results

The results obtained at 1, 8 and 12 months are recorded in Table 4-2. Significant changes occurred after one year of exposure. These changes were based on the exposure condition and concrete materials. It is clear from the results that the calcium oxide (CaO) decreases while the silicon dioxide (SiO_2) increases over time. Figure 4-17a shows the changes in CaO and SiO_2 in normal concrete mixes Gw and Gn in both conditions. In the concrete mixed with Corex slags Gw-co and Gn-co, the chemical changes in CaO and SiO_2 are illustrated in Figure 4-17b. In Gw and Gn, the change in SiO_2 and CaO curves were soon convergent and then diverged until the 8^{th} month, after which, the curves similarly developed. In Gw-co and Gn-co, the curves stop in the rising (SiO_2), and the (CaO) decreases a little after the 8^{th} month. This difference was attributed to the presence of these oxides in concrete materials (Table 3-5), where the CaO were 65.45 and 38.13 and the SiO_2 were 20.13 and 30.50 in cement and Corex slag respectively. Despite the fact that the silica in Granite mixes is more than that in Greywacke mixes, the gels formed are less than in Granite concretes as a result of the reactivity of silica in Greywacke and moderate reactivity in Granite. The alkaline ions (K^+ and Na^+), present in the interstitial pore solution balance the low calcium ion environment (Ca^{2+}), due to negative charges (Poyet et al., 2007). Figure 4-18 shows the relationship between the CaO and alkali as Na_2Oe in all mixes. It must be noted that a reduction in CaO is off-set by an increase in Na_2Oe. Two facts may explain this - the first is compensating the loss in calcium by alkalis (Na and/or K) and the second is the calcium oxide leaches in the presence of water which is confirmed by the determination of the water pH, which transformed to alkaline concentrate at 8 months (Table 4-3). It is noted that the pH of the water in which the concrete was submerged (ASR/w) was more than that of the water in the humid condition due to the indirect touching between the concrete and water. In the same table, the pH of all mixes is recorded. The additive concretes Gw-co and Gn-co were less pH concentrated than those in normal concrete (Gw and Gn). At this stage, these results cannot be explained due to the focus on achieving the main objectives of this study. However, it is recommended to investigate these findings in future studies.

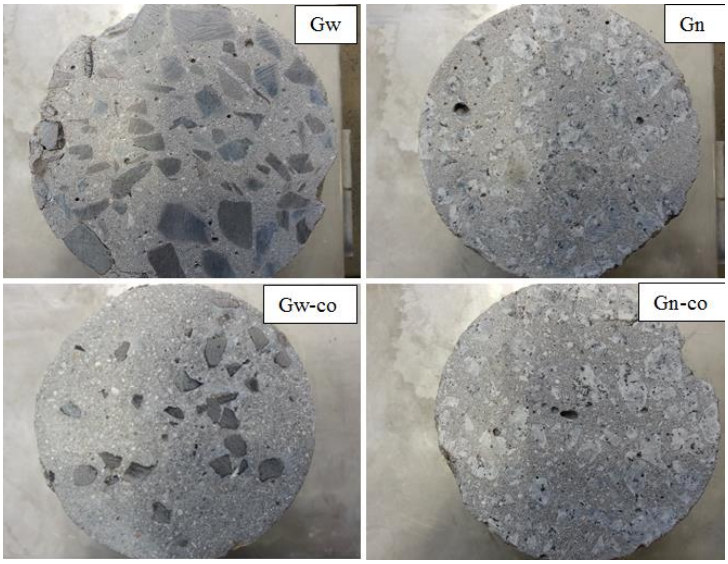

Figure 4-16 Surface texture of the four mixes (example).

Table 4-2 Chemical components of the different concrete at three ages (%).

Sample name	Time test (month)	Al_2O_3 (%)	CaO (%)	Fe_2O_3 (%)	K_2O (%)	MgO (%)	Na_2O (%)	SiO_2 (%)	L.O.I. (%)
Gw/w	1	3.32	32.62	1.75	0.66	1.09	0.45	40.59	20.40
	8	7.67	20.83	3.32	1.58	1.63	1.08	49.82	11.84
	12	6.39	25.87	2.92	1.27	1.51	1.05	54.36	4.73
Gw/H	1	3.33	33.68	1.72	0.55	1.06	0.62	39.96	19.76
	8	5.94	23.77	2.70	1.15	1.40	1.02	48.24	13.21
	12	7.30	20.48	3.22	1.59	1.62	1.26	50.66	12.10
Gn/w	1	3.89	32.00	1.46	1.00	0.71	0.75	43.73	16.75
	8	7.31	19.65	1.64	2.17	0.51	1.91	55.71	9.13
	12	7.92	18.58	1.76	2.82	0.52	1.82	56.12	9.11
Gn/H	1	3.52	33.34	1.48	1.08	0.74	0.96	41.73	17.20
	8	7.83	18.83	1.66	2.66	0.51	1.75	55.55	8.52
	12	7.50	19.26	1.68	2.69	0.54	1.77	55.81	9.26
Gw-co/w	1	4.96	23.36	1.57	0.73	2.37	0.71	51.85	14.33
	8	7.60	17.41	2.77	1.36	2.52	0.92	55.69	9.62
	12	7.32	17.60	2.63	1.39	2.51	1.01	55.66	9.95
Gw-co/H	1	4.45	23.94	1.41	0.61	2.31	0.67	52.18	14.48
	8	7.63	17.41	2.91	1.32	2.63	0.97	55.09	9.71
	12	7.71	15.35	2.79	1.37	2.38	1.16	59.07	8.99
Gn-co/w	1	5.37	19.41	1.08	1.23	1.90	0.85	59.34	10.13
	8	7.33	14.42	1.34	2.18	1.54	1.35	63.74	6.59
	12	6.56	14.52	1.15	1.96	1.56	1.26	64.78	7.27
Gn-co/H	1	4.22	20.34	0.95	0.85	1.95	0.87	58.86	11.15
	8	7.56	14.06	1.30	2.25	1.51	1.40	63.89	6.50
	12	7.75	13.62	1.34	2.52	1.42	1.60	64.26	6.45

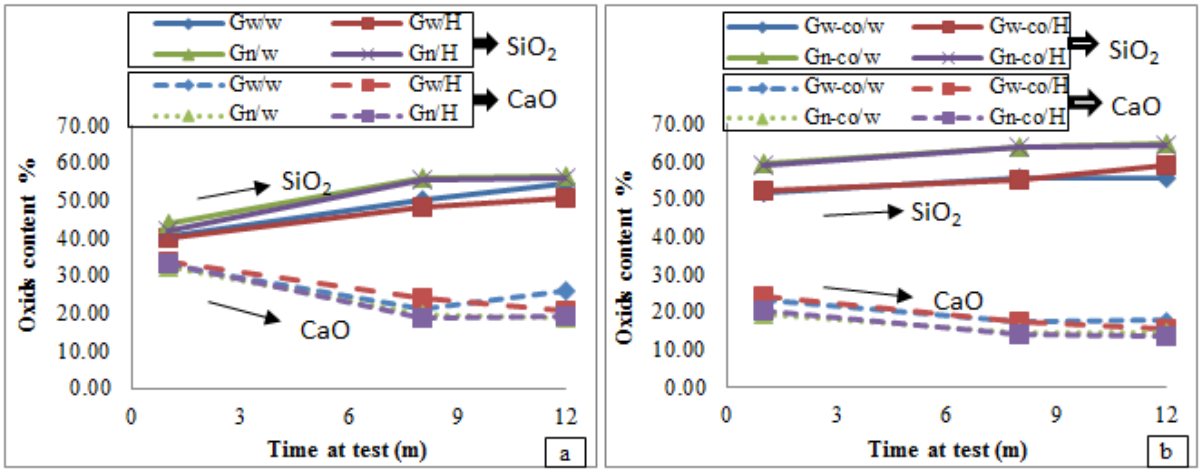

Figure 4-17 SiO_2 and CaO changes over time in both submerged and high humidity, a. normal concrete mixes Gw and Gn and b. in concrete with Corex slag added Gw-co and Gn-co.

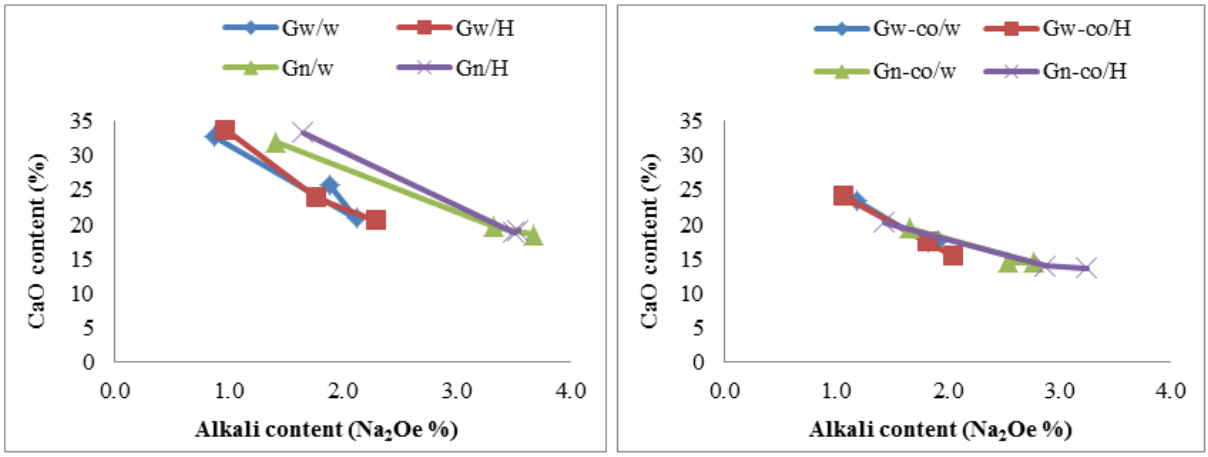

Figure 4-18 Relationship between decreasing the CaO and increasing Na_2Oe over time in both conditions, a. normal mixes (Gw and Gn) and b. concrete with Corex slag (Gw-co and Gn-co).

Table 4-3 pH of all mixes and water (normal and in conditions) at 8 months.

Concrete mix pH	Gw/w	Gw/H	Gn/w	Gn/H	Gw-co/w	Gw-co/H	Gn-co/w	Gn-co/H
	12.3	12.3	12.2	12.3	11.2	11.2	11.8	11.3
Water pH	Normal	ASR/w	ASR/H					
	6.7	12.5	11.8					

4.6 Conclusion

Concrete cylinders were prepared with different aggregates and binder compositions to investigate mechanical and chemical properties of concretes subjected to various conditions of ASR exposure. In the first condition, specimens were submerged in 1 N NaOH aqueous solution at 80 °C according to ASTM C

1260 (series test 1) and compared with others submerged in hot water (80 °C) and normal water. In the second condition, the concrete itself contained high alkaline content and was submerged in water and compared with others exposed to RH>90% and 38 °C according to ASTM C 1293 (series test 2).

4.6.1 Mechanical properties of concrete in series 1

Concrete cylinders prepared with Greywacke stone and Malmesbury sand and with Granite stone with Philippi sand were studied. Four mixes were cast, two of them made of normal concrete named Gw (Greywacke) and Gn (Granite) and in the other two 50% of the cement was replaced with Corex slag and named Gw-co and Gn-co. The specimens were submerged under three types of conditions, in 1N NaOH at 80 °C, in hot water at the same temperature and in normal water at 23±2 °C. Static compressive strength tests were performed on the cylinders after 14, 28 and 56 days. From the stress-strain curves, the ultimate strength and E-modulus were determined.

The results show that in Gw, Gw-co and Gn-co specimens, the strength in hot water was higher than that in normal temperature at 14 days, while in Gn specimens, this strength was less in hot water at the same age. Also at the early age, the strength in NaOH is slightly more than in hot water (at the same temperature of 80 ˚C) in all mixes. At 56 days, the strength of Gw specimens in ASR became almost the same as those in hot water, while the strength of Gn-co specimens reduced. These results showed that in the accelerated test, the ASR and high temperature have an effect on the strength of Gn specimens, more so than on the other mixes. E-moduli are slightly affected by ASR, where in Gw, Gn, Gw-co and Gn-co they were less than that in normal water at 14 days. It is noted that the strengths in Gn mixes were more affected by the high temperature and that the E-modulus in Gn mixes decreased with age. The 56 days submersion is not long enough to express the change in the mechanical properties of concrete according to some previous studies and these changes are based for on the reactivity and properties of the aggregate affected over time by ASR.

The accelerated method to study ASR is not a true simulation of the ASR processes in the field. Nevertheless, these accelerated exposure conditions may help in assisting to understand the behaviour of ASR in concrete.

4.6.2 Mechanical properties of concrete in series test 2

Four mixes with Greywacke and Granite stone were cast, and Philippi sand was used as fine aggregate. The ones with Greywacke were named Gw and Gw-co when Corex slag was added, and the other with Granite were named Gn and Gn-co. The specimens contained high alkali and were subjected to two conditions; submerged in water and exposed to RH>90%. Ultimate strength and modulus of elasticity were determined from static compressive tests conducted on the cylinder specimens. The tests were carried out at 1, 3, 7 and 12 months. After 12 months in their conditions, cracks were seen on the

submerged specimens, which were larger than those in high humidity and less than in specimens containing Corex slag. The largest crack was in the Gw/w specimens. The rates of strength increases after the first seven months were less in Greywacke mixes than those in Granite mixes. After seven months, there was a little decrease in the strength of Gw/w and Gn/w, and an increase in Gw-co/w and Gn-co/w. The strength of specimens exposed to humidity after seven months was slightly higher in all mixes. The E-modulus decreased over time due to ASR in the mixes made of Greywacke stone, and the largest decrease was in Gw/w. The decrease was less than in mixes under humid conditions and also in those containing Corex slags. In the mixes made of Granite stone, the E-modulus increased until the 7^{th} month and then decreased. The concrete strength in series 2 condition was not a good indicator to predict the ASR deterioration, unlike the E-modulus, which provides the signs of ASR effects.

4.6.3 Chemical properties of concrete in series test 2

The same mixes as in the last paragraph were cast to investigate the change in chemical properties over time. The XRF tests were conducted on the samples of crushed concretes taken from the middle of cylinders at 1, 8 and 12 months. The results show that increases in SiO_2 offset reductions in the CaO content for all mixes. Also, the alkali content (Na_2O and K_2O) increases, which replaces the loss in CaO. The CaO leaches in water even in the presence of humidity only where the pH of water in both conditions at 8 months transformed to high alkali concentrates.

CHAPTER FIVE

5. ASR AND CRACK WIDTH IN CONCRETE

Abstract

An experimental study was designed to investigate the role of mechanical crack formation on ASR expansion in concrete. Concrete cubes were made with a hollow along their topside and a notch in the middle of the same side. A wedge splitting test was performed on the concrete cubes to achieve a certain crack width after being subjected to accelerated ASR exposure. The concrete was made with Greywacke coarse aggregate and Philippi sand, and Corex slag in half of the samples. The samples were subjected to ASR test conditions according to ASTM C 1260 (series test 1). The specimens were immersed in 1N NaOH aqueous solution and in hot water. A comparison was made between the changes of the various crack widths when exposed to ASR-enhancing conditions. The effects caused by these ASR conditions on crack widths were compared to those cause by exposure to hot water at the same temperature (80 ˚C) to distinguish the role of thermal expansion. The digital camera (dnt) was used to measure the crack widths at the same positions after 2, 7, 14 and 28 days. Test results indicated that the mechanical crack widths reduce due to ASR and thermal expansion, with values that differ according to the initial crack widths and the concrete mix.

5.1 Introduction

ASR is not the only major source of deterioration – other sources include mechanical cracking in concrete, and other causes of cracks such as corrosion and shrinkage. These cracks may lead to many problems, such as reduced resistance to the ingress of gas, water and deleterious matter, which in turn potentially accelerate the ASR process. On the other hand, these mechanical cracks might be useful to absorb the ASR pressure. This chapter describes the design and results of experiments on concrete cubes subjected to wedge splitting performed on cubes to obtain specific crack widths and which are subsequently subjected to ASR conditions. The purpose of this experiment is to determine whether mechanical cracks play a significant role in ASR, and in particular whether the initial crack width is of importance.

5.2 Experimental programme

Two mixes of the concrete were prepared, the one containing Greywacke coarse aggregate and Philippi sand (Gw), and the second with the same aggregate, but with Corex slag (Gw-co) replacing 50% of the cement by weight. For determining the role of temperature in crack formation and volume changes, the same experiment was carried out on cubes subjected to hot water at the same temperature. Figure 5-1 shows a flow chart of the experimental programme. In the wedge-splitting test, a steel wedge with a sharp edge is forced between two rollers to convert a vertical load to a horizontal load, forcing the two upper edges of the cube apart.

5.2.1 Mixes material and test specimens

The mix proportions, by weight of cement, are shown in Table 3-1. These proportions were the same in Greywacke mixes mentioned in the series test 1 in the mentioned table, except that the Malmesbury sand was replaced by Philippi sand. The slump test result was equal to 55±5 mm for all mixes. The samples are denoted as follows: Gw/A, Gw/w, Gw-co/A and Gw-co/w (Gw = Greywacke, co = Corex Slag, w = water and A = ASR). The specimens are described in Section 3.4.2 and shown in Figure 3-3.

5.2.2 Test procedure

A total of 36 specimens of the two concrete mixes were cast. After the concrete was placed in the moulds, the specimens were covered by a plastic sheet to protect them from loss of moisture in the laboratory. The specimens were demoulded after 24 hours and placed in the chamber mentioned in Section 3.6.3 and shown in Figure 3-9. Half of the specimens of each mix was placed on the Perspex base in the hot NaOH aqueous solution (part 1) and the other half was placed in the hot water (part 2). The volume of the 1N NaOH aqueous solution, as well as that of the water was four times the volume of the concrete specimens. The lid of the device was sealed, and the thermostats' elements switched on to obtain a temperature in both sections of 80℃ in accordance with ASTM C 1260. The main pump to recycle the solution and the condenser pump were switched on. The specimens were extracted from the device after 7 days and were prepared to apply the wedge splitting load. Two LVDTs were placed at the sides of the specimens as shown in Figure 5-2. Controlled wedge splitting tests were performed in a closed-loop system, controlled by one of the LVDT readings, to achieve pre-selected residual crack widths in the unloaded state of nominally 0.1 mm, 0.2 mm and 0.4 mm, with 6 specimens per crack width (three to be placed in hot water and the other three in NaOH solution). It is possible to control the crack width during the test, but measuring the crack itself was different and was based on the measuring on the specimen face (front or rear side) and noting the position of measurement. For that, the measured crack widths after the splitting test were considered as reference for the later measurements at the same position. The load of the Instron

MTM was progressively applied until the LVDTs read the selected crack width, after which the MTM automatically stopped. Figure 5-3 illustrates the set-up of the test with the Instron MTM. The crack widths were measured on the surface by photos taken with the dnt camera (mentioned in Section 3.6.2 and shown in Figure 3-7) with a magnification factor of 35. Subsequently, the specimens were returned to the hot water and the hot NaOH aqueous solution, both at 80 °C.

The specimens were removed from the device to image them after 1, 2 and 4 weeks. Every specimen was imaged during 5±2 minutes, and subsequently returned to the device and placed in their containers. After the 4th week, all the specimens were left outside the device in the laboratory for 1 week, and then once again photos were taken. The crack width was measured on both sides in two places; one at the mouth on the top and the other in the middle of the space below the notch as shown in Figure 5-2 (right).

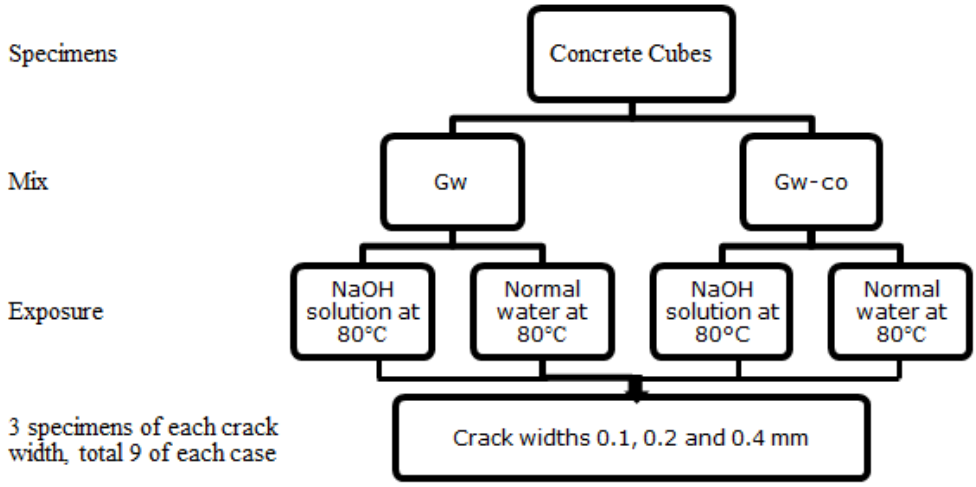

Figure 5-1 Flow chart of the experimental plan of the wedge splitting test and ASR exposure.

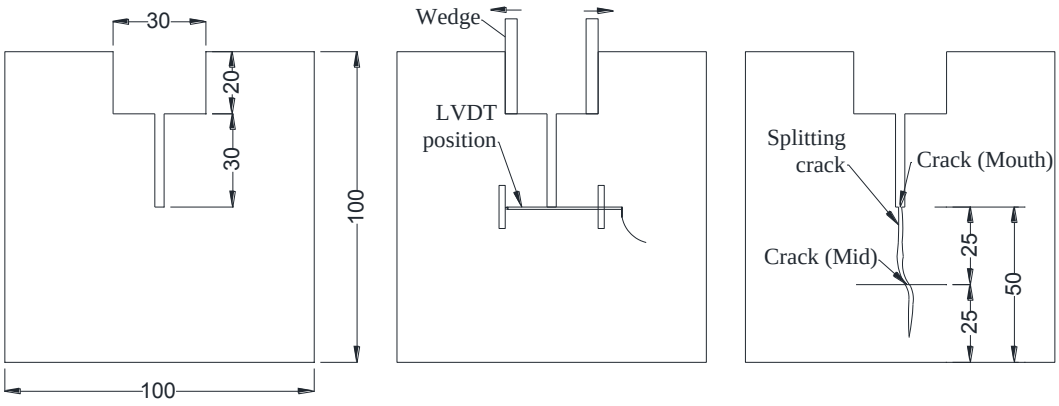

Figure 5-2 Wedge splitting specimen; dimensions, position of LVDT, crack mouth and crack mid.

Figure 5-3 Wedge splitting test set-up.

5.3 Results and discussion

The results of experiments showed that the crack widths were reduced, due to concrete expansion. The crack widths in the mixtures with Corex slag were reduced less than those in cement-only mixtures. Also, the crack widths in the specimens subjected to ASR were reduced more than those immersed in hot water. Although the wedge splitting tests were controlled to obtain specific residual crack widths (C_w = 0.1, 0.2 and 0.4 mm), the C_w was different based on the position of measurement. Table 5-1 illustrates the distribution of Cw in the different samples (4 for each sample) up to 0.7 mm, noting that some uncontrolled readings have been excluded.

Table 5-1 Distribution of the initial crack width at mouth and mid of all samples.

Sample	Gw/A		Gw/w		Gw-co/A		Gw-co/w	
Position	Mouth	Mid	Mouth	Mid	Mouth	Mid	Mouth	Mid
<100	2	1**	3*	1**	1	4*	1	2
100-200	1*	6	5	4***	3	2	3	6
200-300	3	5	1*	1*	0**	2	1*	9
300-400	7	3	1	2	3	5	3	0
400-500	1	0*	0*	2	2	3	3**	0*
500-600	1	0	1	1*	0*	1	2	0
600-700	1*	0	3	0	3	0	1	0
>700	0	0	0*	0	0*	0	0*	0
Sum	16	15	14	11	14	17	14	17
Outliers(*)	2	3	4	7	4	1	4	1
Total	18	18	18	18	18	18	18	18

** Number of uncontrolled measurements considered to be outliers and excluded.*

5.3.1 Crack reduction

The average reduction of crack widths at various ages is shown in Figures 5-4 and 5-5, where the results of both mixes (Gw and Gw-co) in both conditions (ASR and hot water) are illustrated. Each graph compares the average crack width reduction measured at the mouth of the crack (mouth) and that measured in the middle of the space under the notch (mid).

It can also be noted that there are differences between the strains in different cases. The reduction in crack width, which reflects the expansion in concrete due to ASR swelling or thermal expansion, increased dramatically in the beginning and then later increased more slowly. The maximum concrete expansions into the cracks (crack reduction) at the mid position after 4 weeks were 15.1, 8.8, 8.1 and 6.5% for Gw/A, Gw/w, Gw-co/A and Gw-co/w respectively. Since the crack widths at the mid position are smaller than those at the mouths, it leads to more significant reduction, which will be discussed later. In the 5th week when all the specimens were extracted from their exposure condition chamber, the strains in all the specimens at the mid position diminished and the above widths reduced to 12.8, 7.5, 5.7 and 4.7% respectively. The average reduction of mouth and mid is shown in Figure 5-5 and the maximum reductions after the 4 weeks of the test were 12.3, 8.3, 7.2 and 5.6% for Gw/A, Gw/w, Gw-co/A and Gw-co/w respectively, while for the same cases at the end of the 5th week, they were 9.8, 6.9, 5.4 and 4.1% respectively. These results represent the difference between the thermal and ASR expansion. Figure 5-6 shows the compression between the reductions in both mixes and both conditions. The reductions in the last figure were the average of the mouth and mid of the both sides.

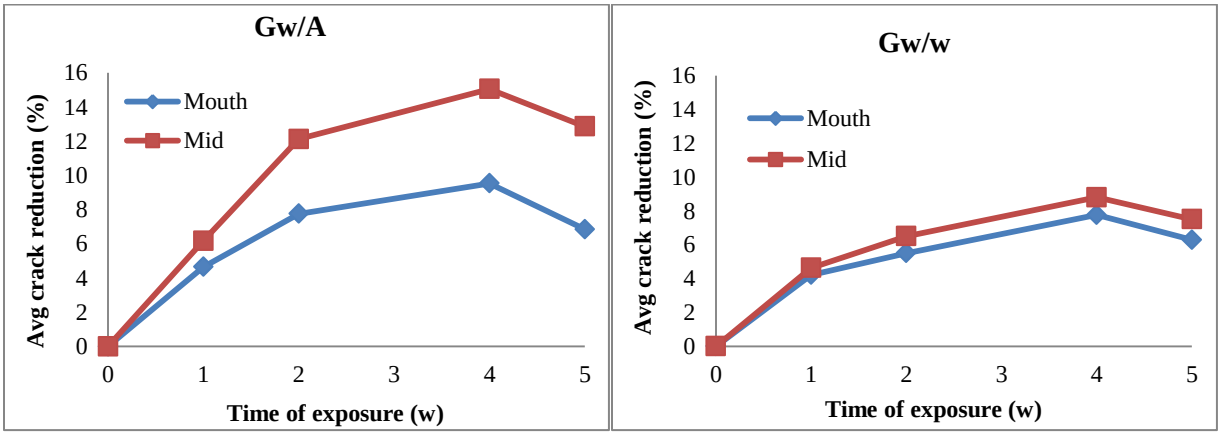

Figure 5-4 The average crack width reduction as percentage at 4 weeks of exposure and subsequently 1 week at laboratory temperature for Gw/A and Gw/w.

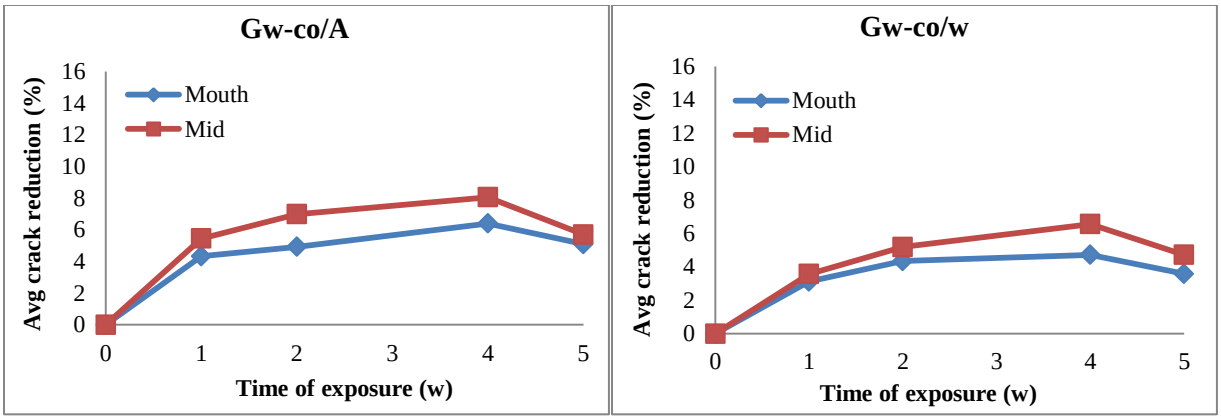

Figure 5-5 The average crack reduction as percentage at 4 weeks of exposure and subsequenlty 1 week at laboratory temperature for Gw-co/A and Gw-co/w.

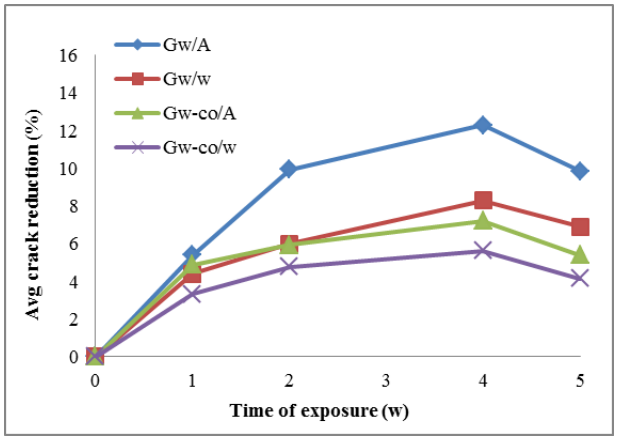

Figure 5-6 Average crack reduction for the different mixes.

5.3.2 Relationship between the crack width and crack reduction

The difference in crack width (ΔC_w) between the initial crack width and the width after 4 weeks of exposure to hot NaOH aqueous solution and to hot water, is shown in Figure 5-7. The reference measurements for the four cases were taken immediately after the wedge splitting test. The reduction of these cracks at the end of the 4th week is shown in Figure 5-7a, while in Figure 5-7b, the data is presented by an exponential curve. In the same manner, the results at the end of a further on week at laboratory temperature (23-27°C) after 4 weeks of testing are illustrated in Figure 5-8a,b. The exponential curve makes it easy to express these scattered data. The curves in Figures 5-7b and 5-8b show that the change in crack width in specimens exposed to the ASR condition is more than that of specimens submerged in hot water, and this indicates the ASR expansion. Also, when the Corex slag is added (Gw-co), the expansion was less than that of the original concrete specimen (Gw). Figure 5-9 illustrates the relationship between the crack reduction (percentage) after the 4th week and the initial crack width. It can be noted that the smaller crack widths have a greater reduction percentage than the larger ones.

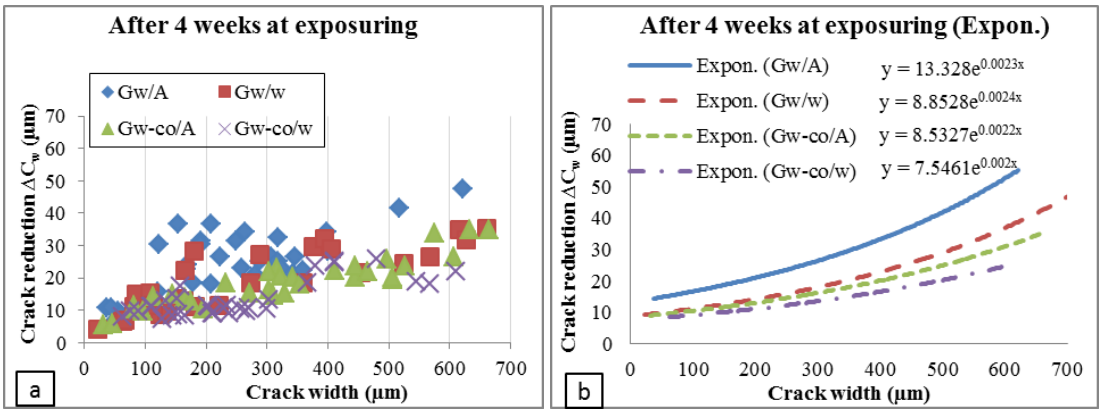

Figure 5-7 Relationship between the crack reduction and crack width at the end of 4 weeks of testing, a. crack reduction results (ΔC_w) and b. the exponential curve for the same results.

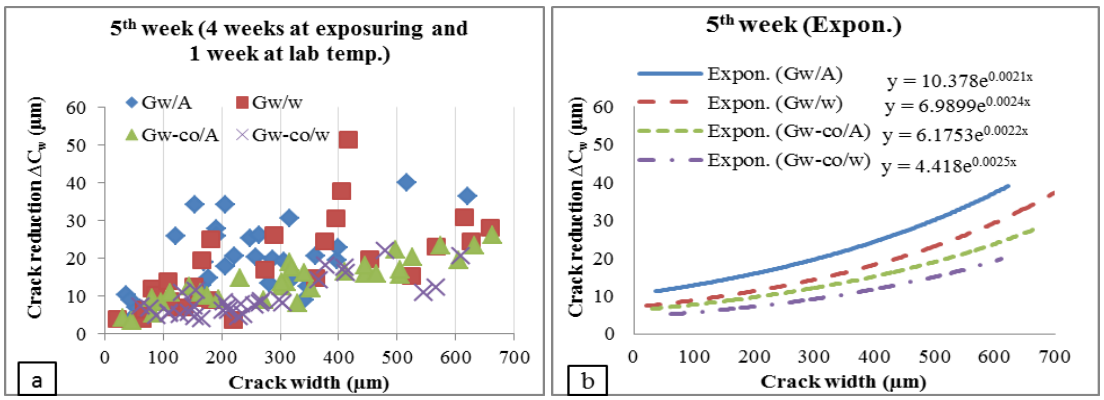

Figure 5-8 Relationship between crack reduction and crack width at the end of the 5th week (one added week at laboratory condition after 4 weeks of testing), a. crack reduction results (ΔC_w) and b. exponential curve for the same results.

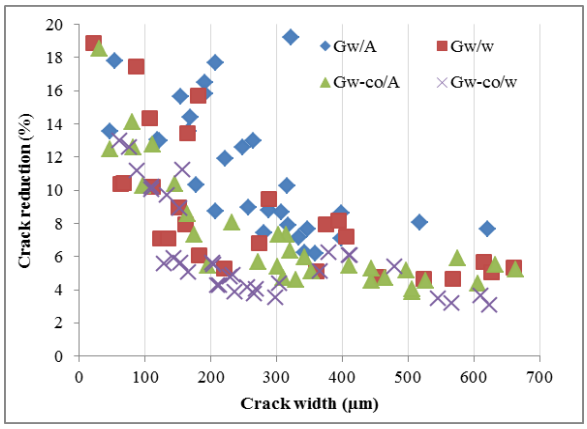

Figure 5-9 Relationship between the percentage of crack reduction and initial crack width.

This phenomenon that smaller initial crack widths reduce at a higher rate might be due to self-healing. The formation of calcium carbonate ($CaCO_3$) or calcium hydroxide ($Ca(OH)_2$) might be necessary for

self-healing to be effected and cracks may heal after some time due to continued hydration of clinker minerals (Nijland et al., 2007; Tittelboom and de Belie, 2013). Nijland et al. studied the results of self-healing of over 1000 samples of concrete and masonry mortars from different structures and found that the self-healing occurs in the presence of free lime. However, autogenous healing is only effective in the presence of water and is limited to small cracks widths (Tittelboom and de Belie, 2013). Reinhardt and Jooss (2003) developed permeability tests on high performance concrete (HPC) cells, cracked by control splitting with crack widths between 50 and 200 µm and subjected to temperatures of between 20 and 80°C, to study self-healing behaviour. They stated that a higher temperature leads to faster self-healing and that smaller cracks heal faster than larger ones. Huan et al. (2010) studied self-healing of ECC containing fly ash under cycles of wet and dry conditions. This is a fibre reinforced mortar with controlled fine cracks under tensile or flexural load. They found that ECC is an ideal material for self-healing when the crack width is less than 100 µm.

From the previous studies and the results of this dissertation, it is evident that two factors may assist ASR in the self-healing process and minimize the crack width, namely the presence of water and high temperature, which were provided in the experiment and occurs whenever there are small crack widths. The results indicate that the smaller crack widths decrease more than the larger widths. Figure 5-10 shows an example of images for the cracks that were taken by the dnt camera at the mouth and the middle of the wedge-splitting specimens. Other images taken from Gw/A specimens number VI on side 2 (Figure 5-11) show an example of self-healing in a micro-crack. In this figure, it can be seen that gel has formed in the main crack (in the yellow rectangle) after 1 week, while the secondary crack shown in the red rectangle has healed after 4 weeks of exposure.

5.4 Conclusion

The combined action of wedge splitting and ASR was studied on concrete cubes. The concrete cubes were cast and pre-cracked to study the subsequent change in mechanical cracks due to ASR. Two mixes with Greywacke stone and Philippi sand were cast, the first with cement only and the second with 50% of the cement replaced by GGCS. Wedge splitting was applied on the specimens after one week of being cast and submerged in water and NaOH at 80°C. After the wedge-splitting, the specimens were immediately returned to the same liquid in the device. Photos were taken by dnt to measure the crack widths directly after the splitting and after 7, 14 and 28 days. The specimens were then left at laboratory temperature and the photos were taken after 1 week. A comparison was also made between the crack width change in specimens subjected to ASR and those submerged in hot water at the same temperature (80 °C). Also, a comparison was made between the mixes cast with cement only (Gw) and those blended with Corex slag (Gw-co). The results showed that the crack widths were reduced due to ASR and thermal

expansion in concrete. The smaller crack widths reduce more than the larger ones due to self-healing. Generally, the crack width reduction decreased due to ASR when Corex slag was added to the mix.

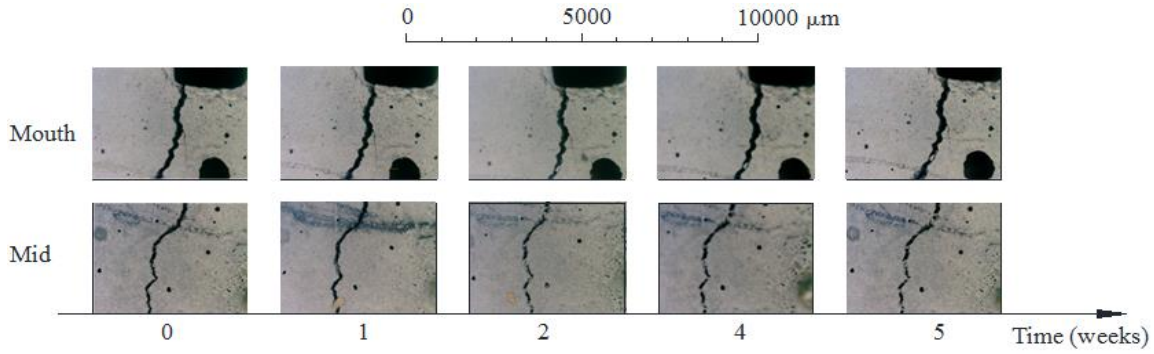

Figure 5-10 Example images of the cracks affected by ASR over the weeks, at the mouth and the middle in Gw/A specimens.

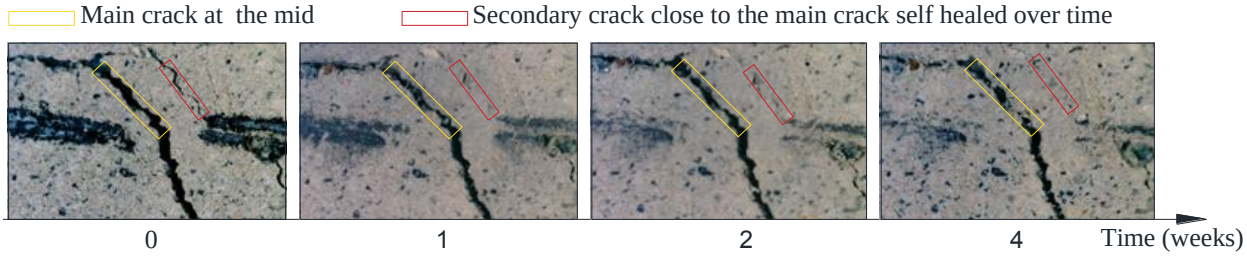

Figure 5-11 Example images illustrates the self-healing in micro-cracks in ASR over time (at 80 °C).

CHAPTER SIX

6. ASR AND MECHANICAL CRACK WIDTH IN REINFORCED CONCRETE

Abstract

An experimental study was undertaken to investigate aspects of the durability of reinforced concrete elements subjected to the combined action of mechanical loading and alkali-silica reaction (ASR). Two methods of accelerated testing, ASTM C 1260 (series test 1) and ASTM C 1293 (series test 2) were followed. In the series test 1, the reinforced concrete beams were submerged in 1N NaOH at 80 °C - half of them were subjected to mechanical tensile load to cause mechanical cracks. In the series test 2, reinforced concrete beams with high alkali content were prepared; half of them were pre-cracked in cyclic loading and subsequently submerged partially in water, or exposed to high humidity. Reactive and non-reactive aggregates were used and GGCS replaced 50% of the cement by weight in half of the specimens. The ASR expansions during the exposure time were monitored, and the crack widths were monitored in pre-cracked specimens under both humid and partially submerged conditions (in series test 2). The test results indicate that the expansion due to the combined action was significantly different from that in specimens exposed only to a high-alkaline environment. The micro and macro cracks induced by cyclic loading form ingress paths, leading to an increased ASR rate, while the macro-mechanical cracks provide regions of relatively free expansion, as can be deduced from the decreasing crack widths.

6.1 Introduction

In many cases, several deleterious mechanisms will act simultaneously or consecutively, thus contributing to the damage observed. This is particularly the case in bridges, dams or hydraulic structures that are exposed to moisture and dynamic loads, which often cause cracks and contribute to water ingress into the concrete. These aspects may contribute to increasing the damage of concrete also affected by other deleterious mechanisms. The limitation of crack width is considered to play a big role in controlling RC structural durability. Cracks act as pathways for the ingress of potentially damaging salts, moisture and gases. The presence of such water in concrete may feed and accelerate the ASR process and associated deterioration.

In order to investigate the combined action of mechanical load and ASR, a two-phase approach was followed to test concrete containing both reactive and non-reactive aggregates:

1. RC beams were submerged in 1N NaOH and compared with the same beams subjected to a pre-tension load. This test was according to series test 1. The specimens subjected to combined action were compared with same RC dimension subjected to cyclic loading and cured at laboratory conditions. Four mixes were prepared, namely Gw, Gn, Gw-co and Gn-co.
2. Pre-cracking by application of 100 000 cycles of loading was done on half of the RC beams in series test 2, to compare the total subsequent ASR expansion with those specimens subjected to ASR only. In this series, 6 specimens of each mix were partially submerged in water, denoted Gw/w, Gn/w, Gw-co/w and Gn-co/w and 6 others were subjected to RH > 90%, and denoted Gw/H, Gn/H, Gw-co/H and Gn-co/H.

The aim was to capture and describe the influence of the pre-crack on ASR response, as well as to describe clearly the strain under different conditions with reactive and non-reactive aggregates and to predict the swelling induced by ASR in mixes with and without Corex slag.

6.2 Experimental programme

Experiments were performed to investigate the expansion and behaviour of concrete containing Greywacke and Granite coarse aggregates and different sands under combined action. The procedure of these experiments consisted of: preparing the materials, chemical component tests, casting and pre-curing, applying static and cyclic mechanical tensile load, exposing specimens to ASR conditions, measurements and data recording. The experiments can be divided into two steps mentioned previously to study the pre-tension and pre-crack in RC under the two series of accelerated ASR test conditions. Figure 6-1 illustrates the flow chart of the experimental plan. The reactive and non-reactive specimen types containing the two aggregates mentioned were used throughout this experiment in the two test series. In series test 2, sodium hydroxide was dissolved in the mixing water in order to increase the Na_2Oe content to 1.25% of the mass of cement. The mix proportions by weight of both experiments are shown in Table 3-1. The RC beams dimensions were as mentioned in Section 3.4.3. To determine the yield and ultimate tensile resistance of the RC specimens, a tensile load was monotonically applied to 3 specimens of each mix at the age of 28 days. The three specimens were denoted i, ii and iii respectively. The average yield and ultimate loads were recorded and are summarised in Table 6-1, with the coefficient of variation (CoV) also given. The Instron MTM mentioned in Section 3.7 was used to perform tensile and cyclic loading on the RC specimens. To measure the change in strain over time, the devices mentioned in Section 3.6.2 were used. The Demec (Figure 3-6) was used in series 1, and the Marcator 1075R (Figure 3-5) was used in series 2.

The dnt camera (Figure 3-7) with magnification control was used to measure the cracks and monitor the concrete surface changes. The test chambers described in Section 3.6.3 were used to expose the concrete under specific conditions (see Figures 3-9 and 3-10).

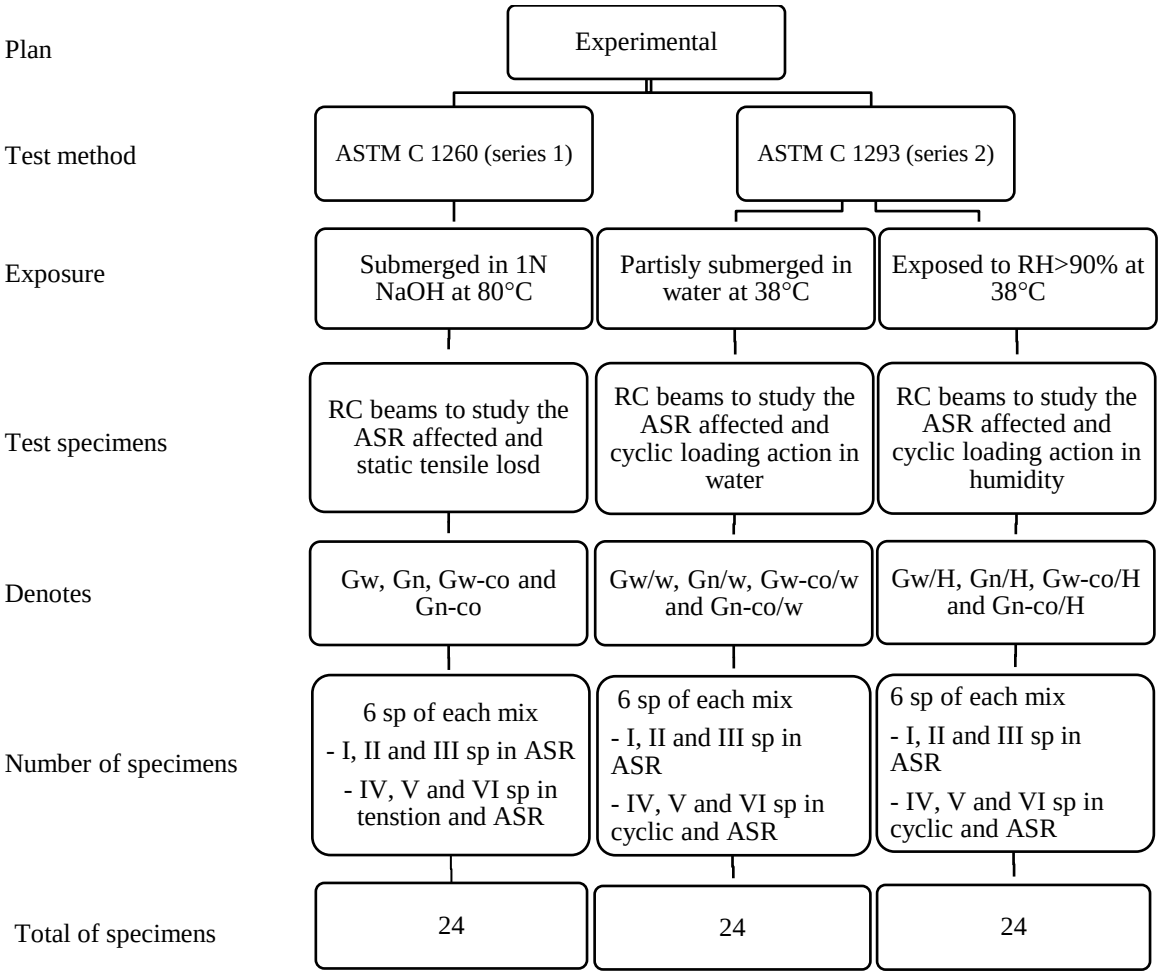

Note that: *- In the RC beam in series test 1, an extra 3 specimens (i, ii and iii) of each mix subjected to cyclic loading and left in lab conditions to compare them with those exposed to tensile loading.*

- In series test 1, an extra 3 specimens of each mix were subjected to 100 000 cycles and kept in laboratory conditions.

Figure 6-1 Flow chart of the experimental programme.

Table 6-1 Preliminary tests of RC beams for yield and ultimate strength at 28 days with Coefficient of Variation (CoV) between brackets.

Sample	Gw	Gn	Gw-co	Gn-co	Average
Yield strength (f_y) (kN)	87.9 (0.029)	90.4 (0.026)	85.8 (0.019)	89.0 (0.059)	88.3
Ultimate strength (f_t) (kN)	93.4 (0.031)	90.4 (0.028)	91.4 (0.020)	89.9 (0.065)	91.28

6.3 ASR and tension on reinforced concrete prisms in series test 1

The experiments were performed to investigate the expansion and properties of concrete containing Granite and Greywacke combined with different sands under combined action. This experiment is according to ASTM C 1260 condition.

6.3.1 Test procedure

Nine specimens of each of the four reinforced concrete mixes were cast after which the specimens were covered in the moulds to protect them from loss of moisture under laboratory conditions for 24 hours. The specimens were then removed from the moulds and cured in normal water. Four stainless steel datum discs (pins) were glued on two opposite sides of the samples I to VI, to monitor the change in the length. The strain gauge DEMEC of 200 mm length was used to do the measuring. Figure 6-2a shows the set-up of this test and Figure 6-2b shows the pins set on the specimens and DEMEC. In order to protect the outside part of the steel bar from corrosion, rubber covers were made and fitted. After 28 days, the three specimens i, ii and iii of each of the four mixes were subjected to 100 000 mechanical load cycles (as described in Section 6.4.2) and then kept in air under laboratory conditions. At 28 days, the specimens denoted IV, V and VI were subjected to 62 kN tensile load (70% of yield static tensile load in Table 6-1). Note that specimens I, II and III were not loaded mechanically. After the tension load was performed, all six samples from each mix (I to VI) were placed vertically on the Perspex base in the chamber (Figure 3-9). The specimens (pre-loaded and unloaded) were immersed in NaOH aqueous solution in accordance with ASTM C 1260 After the lid was sealed, and the condenser put in place, the heating elements were switched on to reach 80℃. The pump was switched on to recycle the solution. The measurements were taken from the second week after immersion in the solution and were recorded every week after that until the tenth week. After extracting the sample from the device and leaving it at room temperature for 24 hours, an average strain gauge reading of the four gauge lengths (two on each face) were recorded at the same time every week. At least three intermediate readings for each gauge length were made before the final reading. The measurements were taken 24 hours after the removal of the specimens from the solution in order to measure their expansion at normal temperature. After each measurement, the specimens were replaced immediately into their chamber and kept in the solution at 80 ˚C until the next measurement. Testing was carried out for 10 weeks at this temperature and in the eleventh week, the specimens were left in the same solution at laboratory temperature (23-27 ˚C). The same procedure to reading the strain gauge was performed. After the 12^{th} week, the specimens were removed from the solution and left at laboratory temperature, and their strains were measured at the 24^{th} and 36^{th} week. For the last week (37^{th}) the specimens were placed in hot water at 80˚C and then removed to cool down to laboratory temperature in order to monitor the strain after 24 hours.

Figure 6-2 Test specimens, a. set-up for the tension test, b. samples with glued pins and Demec.

6.3.2 Results and discussion

The results of both sets of experiments showed that the mixture with Greywacke stone and Malmesbury sand (Gw) was less affected than the mixture with Granite stone and Philippi sand (Gn). The ASTM C 1260 standard test results (Table 3-4) indicate that Greywacke stone was more expansive than the Granite stone and previous studies confirmed this. The results in the RC prisms however showed that the Gn mixtures were more expansive than Gw. The strain at various ages is shown in Figure 6-3, where Figure (a) illustrates the strains of the specimens that were subjected to ASR and Figure (b), the expansion of the specimens subjected to pre-tension before immersion in NaOH solution at 80˚C. The results show that expansions due to combined action are different from those due to NaOH only. As shown in the charts the Gn mix has the greatest expansion which is reduced in the same mixture when GGCS is added (Gn-co). In combined action the Gw was more expansive than the Gn-co, but less than in NaOH only. The Gw-co was not significantly affected in both cases. The maximum strains of ASR samples after ten weeks were; 0.066, 0.021, 0.016 and 0.008% for Gn, Gn-co, Gw and Gw-co mixes respectively, while in samples subjected to combined action they were; 0.071, 0.031, 0.033 and 0.016% respectively. In the 11th week the expansion still continued, although the temperature was reduced to the laboratory temperature. During the following six months, when the specimens were left at laboratory temperature, readings of the strain gauge were taken at the 24th and the 36th week and disparate shrinkage occurred in the length of the specimens. In week 37, the strain gauge was read after extracting the samples from the hot water (80 ˚C) and left for 24 hours at laboratory temperature. In this case, there was expansion in all mixes (Figure 6-3a,b). This may confirm that temperature affects volume change even after removal of the specimens to laboratory temperature for 24 hours.

Various factors may affect strain change in the concrete, including ASR, shrinkage, mechanical load, and temperature. The total strain may be considered to be the sum of strains caused by these factors:

$$\varepsilon_{Total} = \varepsilon_{ASR} + \varepsilon_{me} + \varepsilon_{T} \quad (6\text{-}1)$$

where: *me* denotes mechanical strain, and *T* denotes strain caused by variation in temperature. At early age, shrinkage or hygral strain sometimes causes cracks and could assist in increased ASR expansion later.

Two types of cracks occurred, namely shrinkage cracks and mechanically-induced cracks on half of the specimens that were pre-tensioned.

6.3.2.1 Mechanical crack

Pre-cracking under mechanical pre-tensioning allows quick ingress of NaOH, which then exacerbates ASR. Figure 6-4 shows images that were taken by the dnt camera with a magnification factor of 200 for all specimens and illustrates the comparison between the specimen cracks in ASR-accelerating conditions and others which were subjected to 100 000 tensile loading cycles and kept dry at laboratory conditions in air. The figure shows that the mechanical cracks in the samples under combined action have reduced due to expansion and gel formation. Also, self-healing of small cracks occurred, which has been discussed in Section 5.3.2. It can be noted that the self-healing had not occurred in the concrete at laboratory temperature, while it did occur in those immersed in NaOH.

6.3.2.2 Shrinkage crack

Shrinkage cracks in the early stage may contribute to the ingress of ASR as well as an increase in the volume due to cracks opening. This means that it is not only ASR playing a role in the expansion, but also the temperature, pre-cracks and other factors. Map cracking (shrinkage crack) occurring on the surface of reinforced specimens can be seen when the concrete has been wetted and is in the process of drying. These cracks were larger in Gn and Gn-co specimens than in Gw and Gw-co specimens, as shown in Figure 6-5. The digital photos in this figure were taken in the middle of the specimen's side. The illustrated specimens compare to those specimens cracked in the ASR condition with those subjected to 100 000 tensile loading cycles and kept dry at laboratory temperature. The shrinkage cracks shown have increased in the ASR condition. Cracks caused by a reacted particle will often join other cracks of nearby reacted particles. This leads eventually to a pattern of cracks resembling lines on a map (Stark, 1991).

Due to the behaviour and properties of Granite stone and Philippi sand concrete, the shrinkage cracking was more than that in the Greywacke stone and Malmesbury sand mixture. This is believed to have contributed to the larger swelling of the pre-cracked specimens when exposed to ASR and high temperature, than those that were not pre-cracked before exposure.

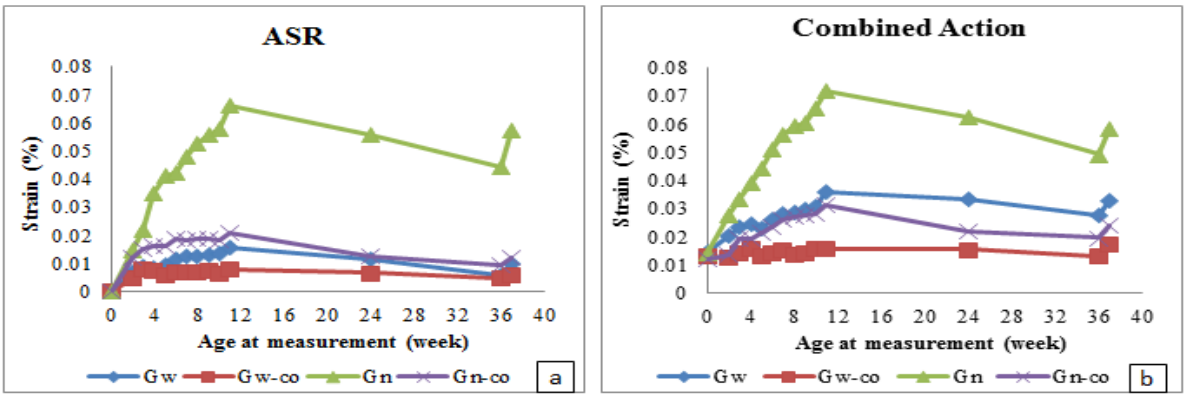

Figure 6-3 Expansion of reinforced specimens at various ages: a. only exposed to ASR condition and b. exposed to pre-tension and ASR condition (combined action).

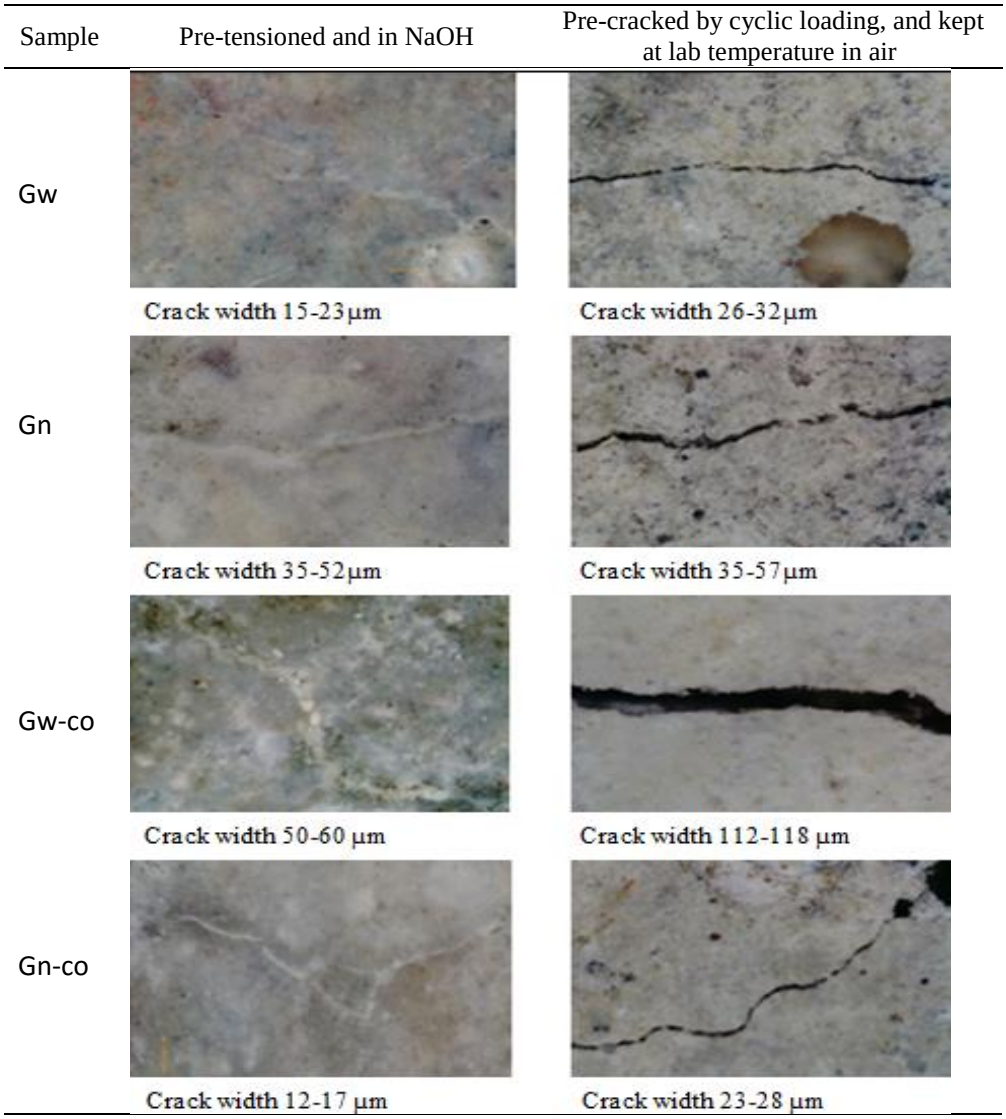

Figure 6-4 Crack formation in mechanical and combined action.

Sample	Dry shrinkage and ASR cracks	Dry shrinkage cracks
Gw		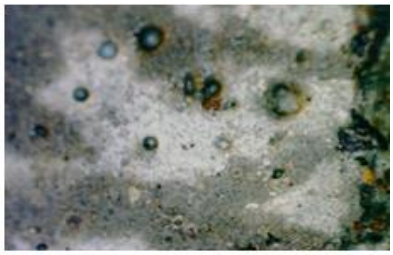
Gn	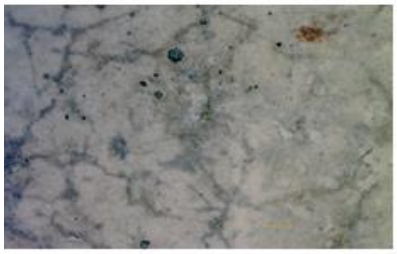	
Gw-co	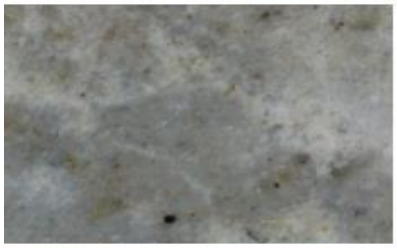	
Gn-co	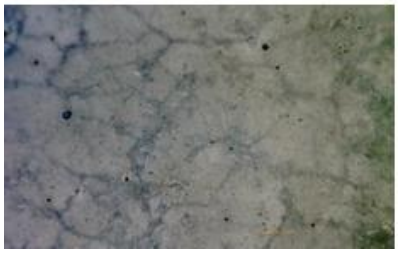	

Figure 6-5 Comparison between cracks in specimens exposed to ASR condition and specimens kept dry.

Some authors point out these expansion factors and try to explain it. The primary expansion concluded by Carles and Cyr, (2002) is not characteristic of ASR and may not occur in field conditions (normal temperature and RH< 90%). It is known that dry exposures reduce the potential for expansive cracking by alkali-silica reactivity, but it is unknown whether wet-dry cycles and continuous saturation cause more damage (Palmer 1992). The overlapping of several mechanisms of cracking complicates clear interpretation and distinction of these different mechanisms (Helmuth, et al., 1993). The aggregate size may also affect the reaction. Tests performed by Multon et al., (2008) showed that ASR expansion for coarse particles (1.25–3.15 mm) is seven times that of smaller ones (80–160 μm). Steel reinforcement may also restrain the expansion. All the factors mentioned may be a reason for changing the mechanism of ASR expansion.

6.3.3 Differences in volume change – ASTM C 1260 test results versus combined loading specimens.

The behaviour of the aggregate combination in the mixture is different when tested according to the ASTM C1260 standard. Using large particle sizes of aggregate as in RC might cause different reactions than with the ASTM C 1260 standard test, which uses aggregate sizes less than 4.75 mm. The shrinkage that occurred in the RC after the 11th week when the samples were left at laboratory temperature, also occurred in the mortar bar (singular aggregate tests) that was tested with ASTM C 1260, where the specimens measured after 1 week were kept also at laboratory temperature as shown in Table 3-4. In this test the strains of all aggregate mixes used except Greywacke, nearly returned to the initial reading before exposure to heat in water at 80 ˚C (zero reading). Although the shrinkage occurred in both tests (RC and mortar bar), it was not the same, as it depends on the aggregate and surrounding conditions. The expansions are also different in both cases, with the Greywacke mortar more expansive in the ASTM C 1260 test than the Granite one, while the mix with Greywacke and Malmesbury was less expansive than that with Granite stone and Philippi sand.

6.4 ASR and cyclic loading on RC prisms in series test 2

This experiment was made to investigate the length change in RC due to ASR and pre-cracking. Concrete prisms containing high alkali content (Na_2Oe = 1.25% of the mass of cement) were exposed to two conditions (partially submerged in water and high RH) and two actions (ASR, and combination of ASR with cyclic loading).

6.4.1 Test procedure

The same procedures of casting and moulding the specimens as previously described were followed. After demoulding, the protruding steel ends were smeared with grease and covered with rubber caps. Eight stainless steel datum discs (pins) were glued on two opposite faces of the sample (four on each face), with 100 mm between each pair to monitor the change in length. The specimens were left for 6 to 7 hours so that the glue could dry before accurately measuring the spaces between the pins. The spaces between the pins were numbered 1, 2 and 3 on one side and 4, 5 and 6 on the other side. Figure 6-6 illustrates the details and position of the datum discs (pins) on the beam. The measuring device of 100 mm length (Marcator 1075R) described in Section 3.6.3 was used to accurately measure the distances between the pins, as shown in Figure 3-5. After the zero readings were taken, the specimens were placed vertically on a Perspex base in the chamber illustrated in Figure 3-10 at a height of 100 mm from the bottom. From each mix, six specimens were partially submerged in water marked /w (part 1), and the other six were exposed to humidity marked /H (part 2). In the first part, the bottom half of the specimens

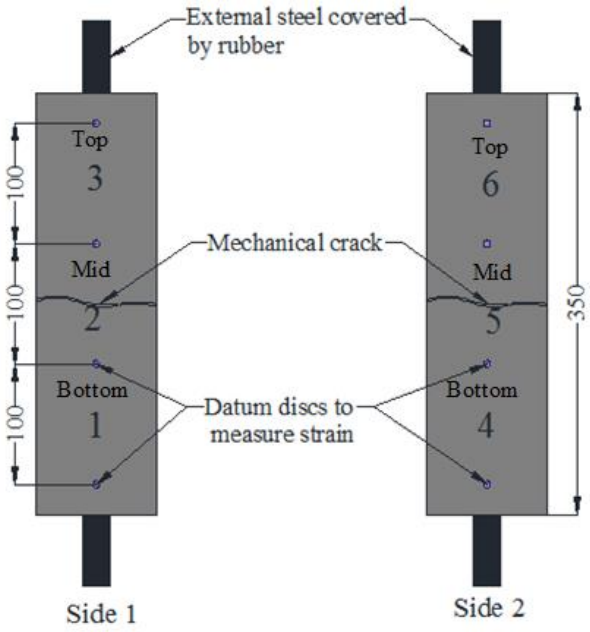

Figure 6-6 Test Specimen, positions of the pins and mechanical crack.

were submerged in water, and the top half was exposed to high humidity, while in the second part, specimens were not directly in contact with water, but were totally exposed to high humidity according to ASTM C 1293 conditions.

6.4.2 Cyclic loading and measurement

After 28 days in the mentioned condition, specimens I, II and III from each mix were extracted from the device and the distances between the pins were measured and recorded before they were returned to their condition in the device. Note that care was taken to allow a cooling and drying period of 1-2 hours after removal of each specimen from the chamber before the reading was taken. The cyclic loading was conducted on the Gw and Gn specimens IV, V and VI after 4 weeks, while this was done for the Gw-co and Gn-co after 15 weeks. For the cyclic testing, the strain readings were first recorded, after which the load cycles commenced, varying between 40 and 62 kN. The upper limit represents 70% of the yield load (the average of three samples of four mixes in Table 6-1). They were then exposed to 100 000 cycles with a 5 Hz frequency in an Instron MTM (Figure 3-4b). The same test set-up is shown in Figure 6-2a. The relationship between the applied load and deformation due to the cyclic loading is shown in Figure 6-7a, while Figure 6-7b shows the relationship between the average lengthening and the number of cycles. After the cycles had been completed, the deformation readings between the pins were taken, and the specimens were returned to the chamber in the same condition until the next measurement. The pre-cracked specimens were removed from the device after every given period to measure the deformation and crack width. The dnt camera was used to measure the crack width.

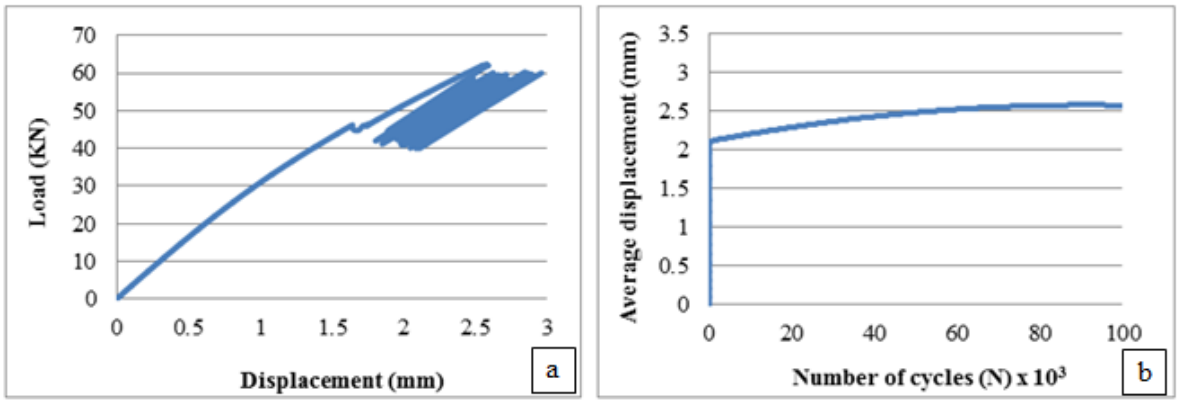

Figure 6-7 Example of the response to cyclic loading for Gw/w, showing the relationship between: a. the applied loading and displacement, b. the average displacement and number of cycles.

6.4.3 Partially submerged specimens strain results

The mechanical load caused large cracks in the middle of the specimens in the region of the reduced steel bar diameter as planned. These cracks were of different widths (0.8 to 4 mm) and extended through the cross section down to the steel bar. Micro-cracks could be caused in the skeleton of concrete due to cyclic loading. Three comparisons were made of each of the specimen types:

1. The strain in the ASR and in the combined action specimens from the start of the test.
2. The strain in both cases after mechanical cracking.
3. The strain in the lower and upper parts and neglecting the middle space (where the crack is in the combined specimens) in both cases.

6.4.3.1 Greywacke mixes (Gw/w)

The ASR cracks in the Gw mix can be seen clearly in the submerged part and is smaller in the upper part which was exposed to high humidity. The mechanical crack in the middle increased the strain dramatically after the load was applied and then started decreasing with time. The average strain readings of six spaces (both faces) for the Gw mix in both cases are illustrated in Figure 6-8. The strain increased steadily under the ASR condition, whereas under the combined action it increased before the mechanical load was applied and then became less significant than in the un-cracked specimens under the ASR condition. The maximum expansion for Gw in the ASR specimens from the first day until 65 weeks was about 0.195%, whereas the total of mechanical crack and ASR expansion in the combined specimens at 65 weeks was 0.725% for the same mix, as shown in Figure 6-8a. If the strain change is considered after the mechanical load application after four weeks in both cases (ASR and combined), thus assuming that the strain at the 4th week is zero, the maximum strain of ASR specimens was 0.184% and 0.129% in the combined specimens as illustrated in Figure 6-8b. This phenomenon can only be seen in the large mechanical cracks and therefore, if the average strain of the lower and upper spaces in both ASR and

combined action is considered, i.e. neglecting the middle space where the large crack occurs, a difference in strain can be found as shown in Figure 6-9. The expansion in the combined specimens was increasingly more than in ASR specimens. In this case, the maximum strain in combined specimens was about 0.248%, while in ASR specimens it was 0.197%. It can be noted that there are differences between the average strain of all the spaces (bottom, middle and top) as shown in Figure 6-8a and the average strain of the lower and upper spaces as shown in Figure 6-9. The first case in combined specimens, large mechanical cracks in the middle and likely also micro-cracks in the skeleton were included, whereas in the second case, micro-cracks due to cyclic loading were included.

6.4.3.2 Granite mixes (Gn/w)

The strain in Gn mixes was less than that in Gw mixes, where the Granite mixes classify as non-reactive or slowly reactive. The average strain readings of the six measurement spaces of each of three specimens in both cases of Gn mixes were recorded. The strain jumped after cyclic loading in the combined specimens and then became less than the strain in ASR specimens.

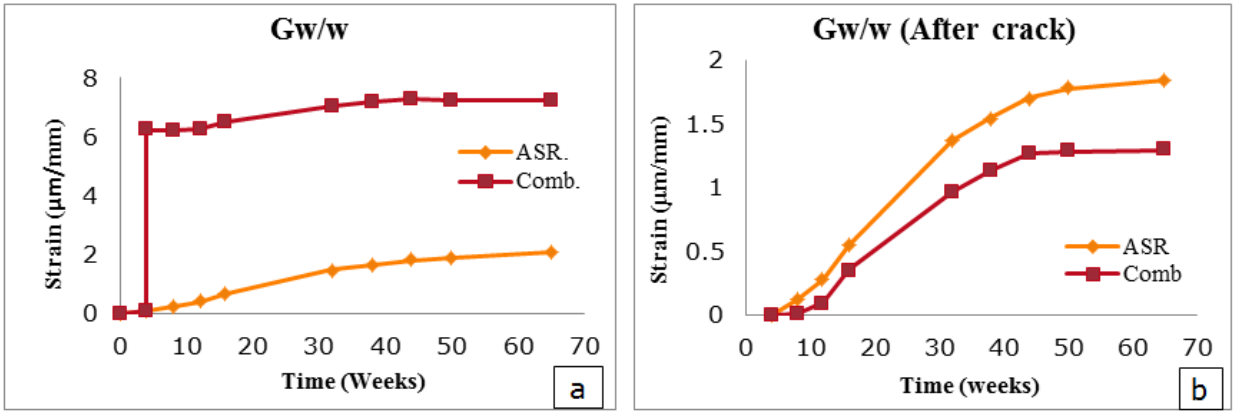

Figure 6-8 Strain against time for the Gw/w specimens subjected to ASR and exposed to combined action: a. from the start of the test and b. after cyclic loading at 4 weeks.

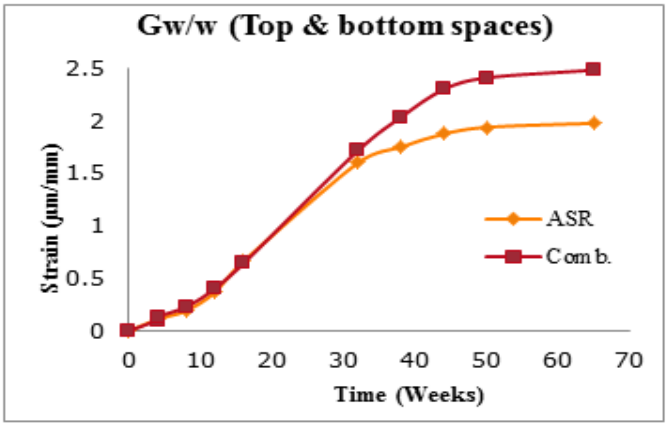

Figure 6-9 Average strain of the lower and upper spaces, neglecting the middle space in the Gw/w mix.

Figure 6-10a illustrates the maximum strain at 65 weeks and in ASR specimens was around 0.097%, while the strain due to mechanical cracking and ASR in combined specimens was 0.67%. The strain after cyclic loading (4 weeks) as illustrated in the Figure 6-10b was greater in ASR than in combined specimens due to crack spaces which allowed expansion in the crack dimension. In this case, the maximum strains were 0.0873% and 0.0308% in ASR and combined specimens respectively. The strain increased steadily in both cases and then became less after 16 weeks. The strain percentages between the combined and ASR conditions gradually diverge in the first stages and then become semi-stationary with time. In the case of no strain in the middle space where the large crack is situated, it can be seen how the effect of strain in combined action compares with the strain in the ASR condition. The difference between the strains in both conditions is shown in Figure 6-11, where there is little difference between combined action and ASR strain (unlike the Gw mix). The maximum percentages of strains were 0.094% and 0.0983% for the ASR and combined action respectively.

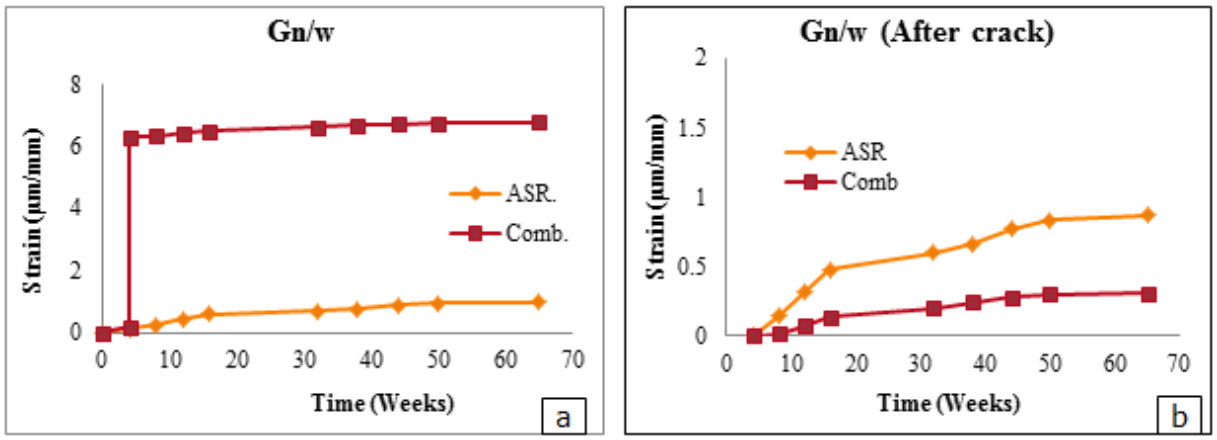

Figure 6-10 Strain against time for the Gn specimens subjected to ASR and exposed to combined action: a. from the start of the test and b. after cyclic loading at 4 weeks.

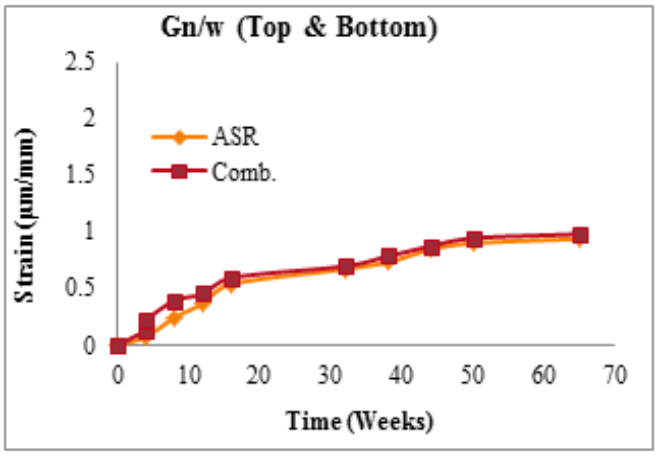

Figure 6-11. Average strain of the lower and upper spaces and neglecting the middle space in Gn.

6.4.3.3 Greywacke with Corex Slag mixes (Gw-co/w)

The cyclic loading was applied on half of the specimens after 15 weeks of being partially submerged in water, causing cracking in the middle of specimens which increased the total strain for the combined action cases. Figure 6-12a illustrates the strains in both ASR and combined mixes of Gw-co from the start of the test until 65 weeks. The maximum strains were about 0.1% in ASR and 0.38% in combined specimens including the large mechanical crack. Figure 6-12b represents the strain in both cases after cyclic loading and regards this point of strain to be equal to zero. In this case, the maximum strains at the 65th week were 0.054% and 0.0377% in ASR and combined mixes respectively. The average strains of the lower and upper spaces in both cases in Figure 6-13 do not appear to be of significant difference. In this case, the maximum strains at the 65th week were convergent, where in ASR specimens they were 0.0106%, and 0.0108% in combined specimens.

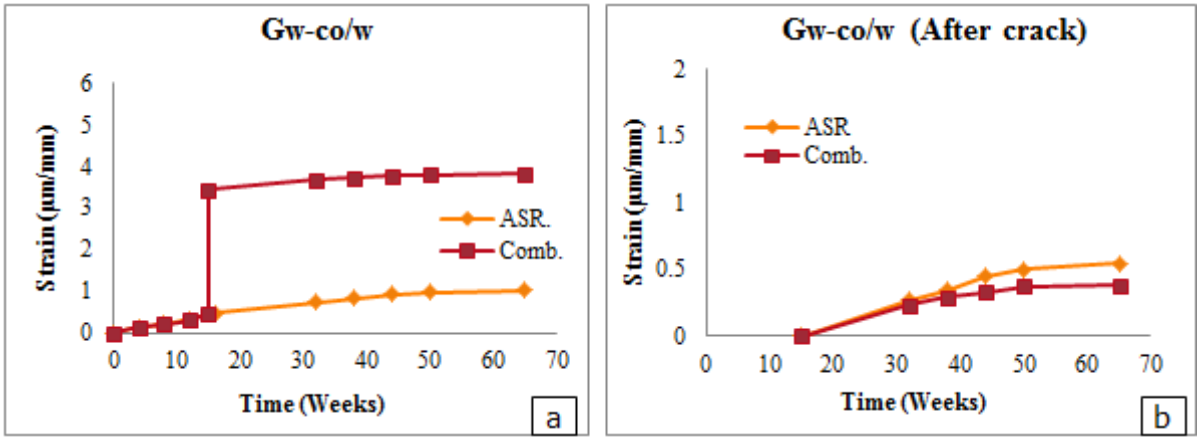

Figure 6-12 Strain against time for the Gw-co specimens subjected to ASR and exposed to combined action: a. from the start of the test and b. after cyclic loading at 15 weeks.

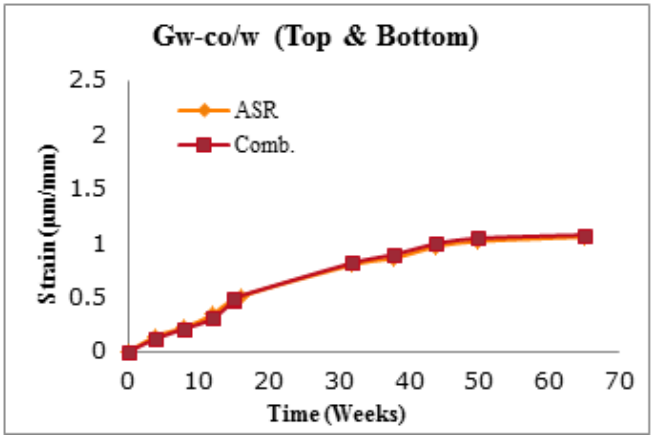

Figure 6-13 Average strain of the lower and upper spaces and neglecting the middle space in Gw-co.

6.4.3.4 Granite with Corex Slag mixes (Gn-co/w)

As in the previous mix, the cyclic loading was applied after 15 weeks of exposure, which caused mechanical cracks. The difference in strain between Gn and Gn-co can be noted in the results, where the strain in the presence of co was less than that in Gn. The average strain readings of the spaces and of the three specimens in both cases of Gn-co mixes were recorded. The strain after the cyclic loading in combined specimens was less than that in Gn due to the crack width. The maximum strain in ASR and combined specimens from the start of the test until the 65th week were 0.057, and 0.2% respectively as shown in Figure 6-14a. The strain measured after cyclic loading was applied in the combined specimens (i.e.16 weeks), were recorded at the 65th week as 0.022% and 0.023% for ASR and combined specimens respectively. As in Figure 6-14b, the strain in the combined specimens was slightly smaller than that in the case of ASR throughout the weeks. By considering the strain in the bottom and top spaces and neglecting the middle mechanically-cracked space, the maximum strains recorded at 65 weeks were 0.0585% and 0.064 for ASR and combined specimens respectively. It can be noted in Figure 6-15 that the differences between strains in both cases are semi-constant after cyclic loading was applied.

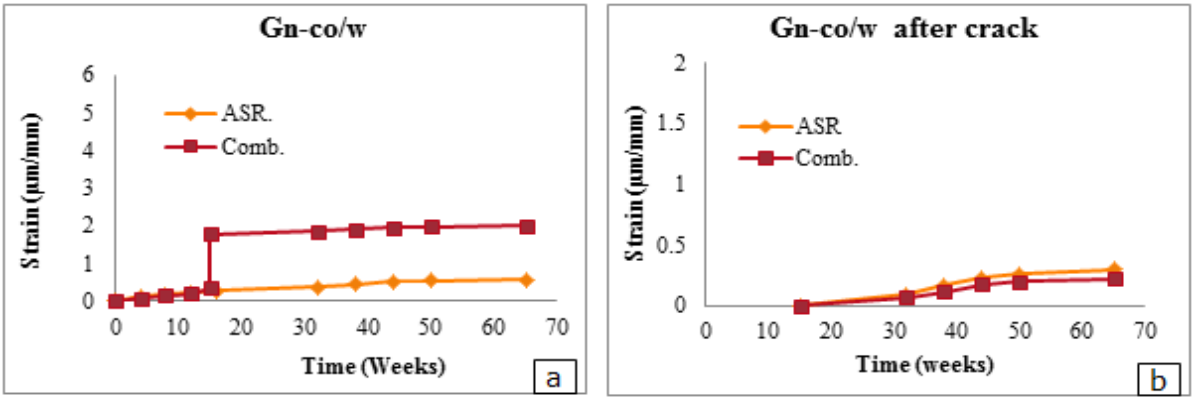

Figure 6-14 Strain against time for the Gn-co/w specimens subjected to ASR and exposed to combined action: a. from the start of the test and b. after cyclic loading at 15 weeks.

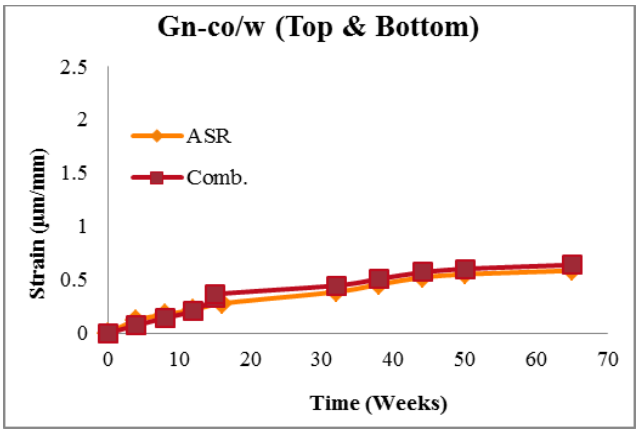

Figure 6-15 Average strain of the lower and upper spaces and neglecting the middle space in Gn-co/w.

6.4.4 High humidity specimens strain results

The experimental results confirmed that the concrete exposed to high humidity was less affected than concrete in direct contact with water. A comparison between the specimens in ASR and those pre-cracked under ASR conditions is illustrated in figures similar to those of Section 6.4.3.

6.4.4.1 Greywacke mix (Gw/H)

The specimens that were exposed entirely to high humidity (Gw/H) had fewer cracks than those that were partially submerged in water (Gw/w). The average results of the strain readings for the Gw/H mix in both cases i.e. ASR an combined, are shown in Figure 6-16 which shows that the strain increased steadily under the ASR condition, whereas in the combined action it was increasing before applying the mechanical load and then started decreasing. The maximum expansion from the first day under these conditions until 65 weeks was 0.156% in the ASR specimens and 0.62% in combined action as illustrated in Figure 6-16a. In case the strain is determined after the mechanical load was applied at 4 weeks, it is shown in Figure 6-16b that the maximum strain of ASR specimens was about 0.15% and 0.09% in the combined specimens. The strain of the lower and upper spaces in both ASR and combined action were taken and a difference in strain can be found as shown in Figure 6-17. The expansion in the combined specimens increased more than in ASR specimens. In this case, the maximum strain in combined specimens was about 0.21% while in ASR specimens it was 0.17%. This shows clearly that the Gw/w specimens underwent more expansion than those in humid conditions Gw/H. In the combined action, the strain diminished significantly for about two months, but then increased for the next month before again diminishing. On the basis of the interpretation of this behaviour, it can be assumed that the initial expansion in the concrete was influenced to a greater extent by swelling from water absorption and thermal circumstances than by ASR.

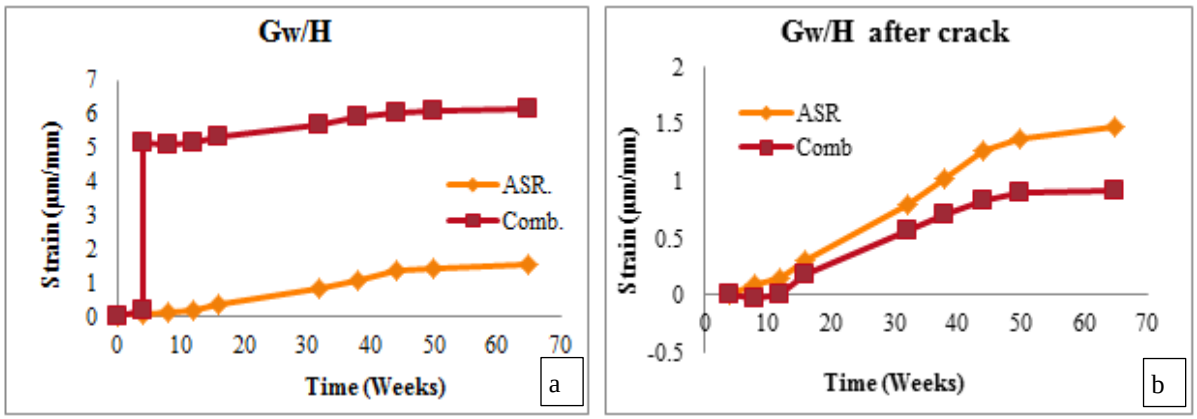

Figure 6-16 Strain against time for the Gw/H specimens subjected to ASR and exposed to combined action: a. from the start of the test and b. after cyclic loading at 4 weeks.

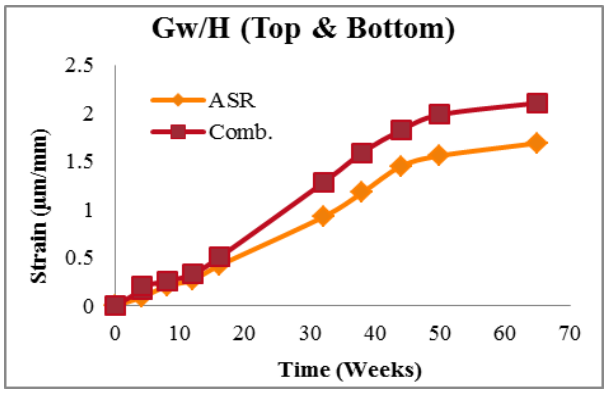

Figure 6-17 Average strain of the lower and upper spaces and neglecting the middle space in Gw/H.

6.4.4.2 Granite mix (Gn/H)

Slow expansion occurred in Gn/H compared with Greywacke in the same exposure (Gw/H). Certainly, the specimens that were exposed only to humidity (Gn/H) showed less cracking and expansion than those partially in water (Gn/w). The same steps were followed as previously when taking readings of the deformation. Figure 6-18a shows that the strain of specimens continued to increase under ASR conditions, as well as those under combined action. The maximum expansion of Gn/H in ASR and combined action was 0.45% and 0.078% respectively. The strain jumped in the combined specimens after cyclic loading, and then gradually became less than the strain in ASR specimens. The strain after cyclic loading (4 weeks) as illustrated in the Figure 6-18b was greater in ASR than in combined specimens due to crack spaces, which allowed expansion into the crack. In this case, the maximum strains were 0.058% and 0.038% in ASR and combined specimens respectively. The strain increased steadily in both cases at the beginning and after 44 weeks the expansion became less. The expansion of the specimens at 65 weeks in Gn/H- ASR is less by about 33% than in Gn/w- ASR, while in combined specimens this expansion is more in Gn/H-comb

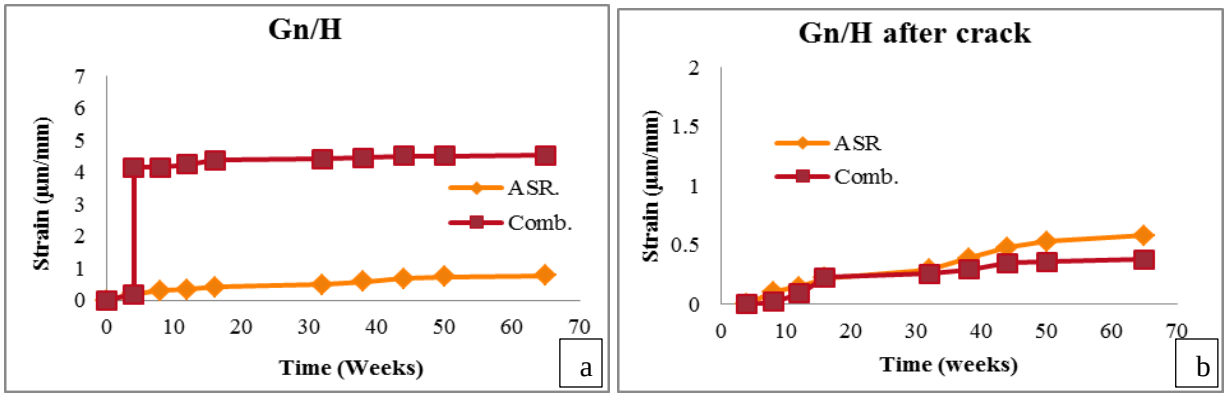

Figure 6-18 Strain against time for the Gn/H specimens subjected to ASR and exposed to combined action: a. from the start of the test and b. after cyclic loading at 4 weeks.

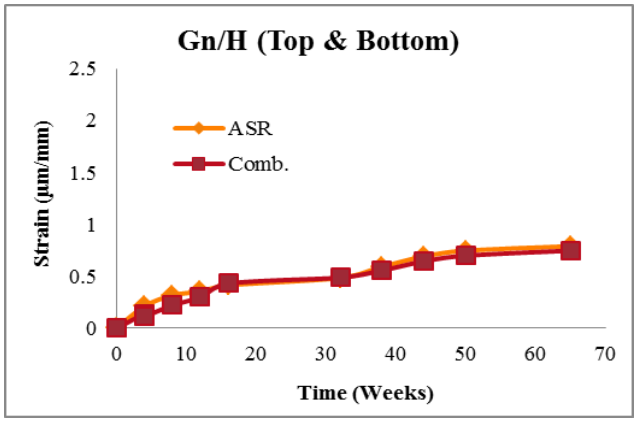

Figure 6-19 Average strain of the lower and upper spaces and neglecting the middle space in Gn/H.

than in Gn/w-comb by about 22%. This confirms the role of cracks in the assimilation of ASR pressure and therefore an increase in skeleton expansion and decrease in crack width means less total expansion. The strain in top and bottom spaces in ASR compared with combined specimens is nil as shown in Figure 6-19. The maximum percentages of strains were 0.079% and 0.075% for the ASR and combined action respectively.

6.4.4.3 Greywacke with Corex Slag mixes (Gw-co/H)

As mentioned previously, the mechanical load was applied on half of the specimens with Corex slag after 15 weeks. Figure 6-20a illustrates the strain over time until 65 weeks in both ASR and combined mixes of Gw-co/H. The maximum strains in ASR specimens were about 0.08% and 0.57% in the combined specimens affected by large mechanical crack. Figure 6-20b shows the strain in both cases after the cyclic loading at the 15th week and this is considered as the reference strain reading. The maximum strains at the 65th week were 0.052% and 0.043% in ASR and combined mixes respectively.

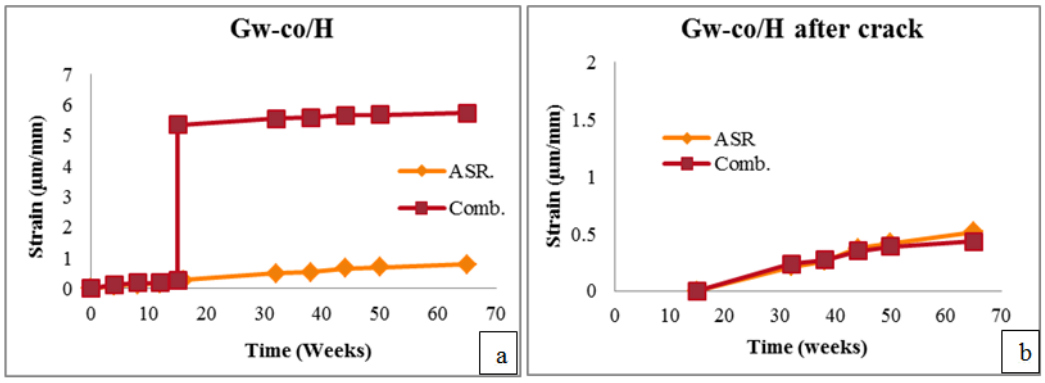

Figure 6-20 Strain against time for the Gw-co/H specimens subjected to ASR and exposed to combined action: a. from the start of the test and b. after cyclic loading at 4 weeks.

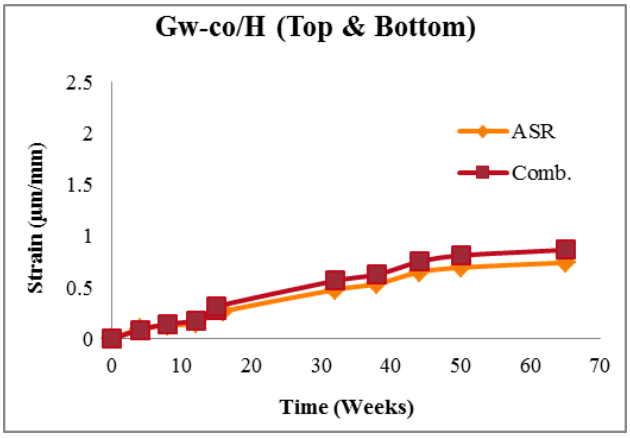

Figure 6-21 Average strain of the lower and upper spaces and neglecting the middle space in Gw-co/H.

The average strains of the lower and top spaces in both cases are shown in Figure 6-21. The figure shows that the strains in combined specimens is a little more than those in ASR. The maximum strains at the 65th week were 0.074% in ASR specimens and 0.086% in the combined specimens.

6.4.4.4 Granite with Corex Slag mixes (Gn-co/H)

After 15 weeks exposure and the application of the mechanical load for the Gn-co/H specimens, the strains in these specimens are the lowest of all the mixes. The maximum average strain in the combined action specimens is 0.31% and in ASR it is 0.061%. The readings of the strain over time are illustrated in Figure 6-22a.

The strains after the cyclic loading test of combined specimens are illustrated in Figure 6-22b. The maximum strains in ASR and combined specimens from the 15th week of the start of test until the 65th week were 0.022% and 0.30% respectively. By comparison with Gn-co/w specimens, the expansion in Gn-co/H- ASR specimens at 65 weeks is less by about 10% than in Gn-co/w- ASR specimens and in Gn-co/H-comb the expansion is more than in Gn-co/w-comb by about 22%. Figure 6-23 shows that the strain of the top and bottom spaces in the combined specimens converge with the strain in ASR throughout the weeks. The maximum strains recorded at 65 weeks were 0.0062% and 0.00626 for ASR and combined specimens respectively. It can be noted in Figure 6-23 that the difference between strains in both conditions is semi-constant after cyclic loading was applied.

6.4.5 Mechanical crack behaviour under ASR

The behaviour of cracks is dependent on the causes of the cracks and the surrounding conditions. For instance, mechanical cracks decrease when the ASR cracks increase, causing pressure in all directions. There are other causes for the cracks in concrete such as shrinkage, corrosion and thermal expansion. This study only concentrated on the mechanical and ASR cracks.

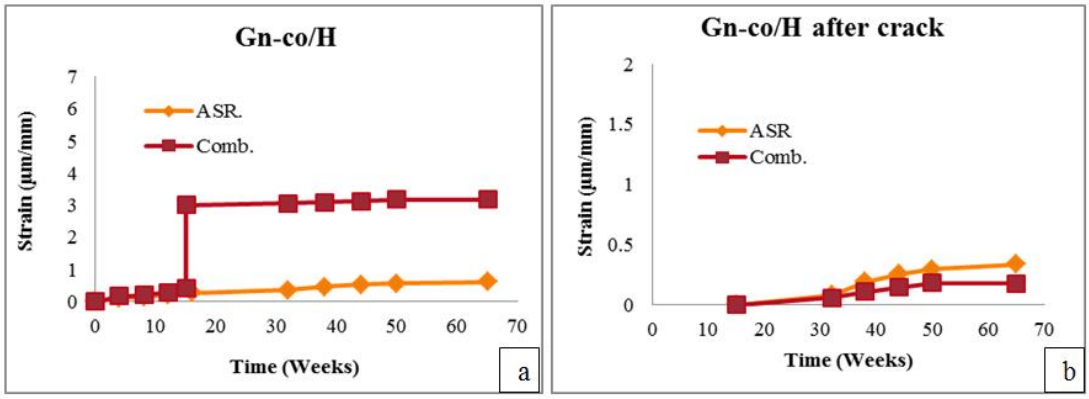

Figure 6-22 Strain against time for the Gn-co/H specimens subjected to ASR and exposed to combined action: a. from the start of the test and b. after cyclic loading at 4 weeks.

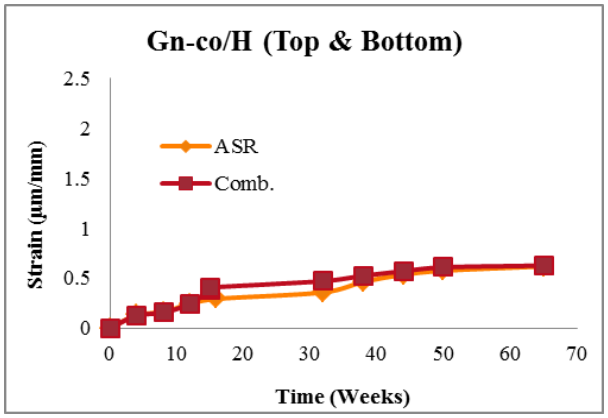

Figure 6-23 Average strain of the lower and upper spaces and neglecting the middle space in Gn-co/H.

6.4.5.1 Mechanical cracks

In the case of ASR, which causes expansion in concrete, the crack will provide space for concrete to expand. To determine the change in pre-mechanical cracks, the previously mentioned dnt camera was used. At the first reading, the position of measuring was marked to serve as a reference for every subsequent time of reading. In both conditions, the first reading in Gw and Gn specimens was at the 10th week, while in the Gw-co and Gn-co specimens it was at the 16th week. Figure 6-24a illustrates the reduction of mechanical crack widths in the middle of water submersed specimens. The largest reduction was in Gw/w, where the maximum reduction at the 65th week was around 23.7% of the crack width at the 10th week. In Gw-co/w, the reduction was less than in the Gw/w mixes, where the maximum reduction was 8.7%. In Granite mixes, the reduction at the end of the test was 7.9% in Gn/w and in the specimens containing Corex slag (Gn-co/w) it was 8.7%. The crack reduction of specimens exposed to high humidity is illustrated in Figure 6-24b. The reduction in cracks at the end of 65 weeks of Gw/H and Gn/H were 12.9 and 5.7% respectively from the 10th week, while the crack reduction in Gw-co/H and Gn-co/H

were 7.25 and 7.9% respectively from the 16th week. The stages of changes in the cracks of Gw/w and Gn/w mixes with time are illustrated in Figure 6-25 and also of Gw-co/w and Gn-co/w in Figure 6-26.

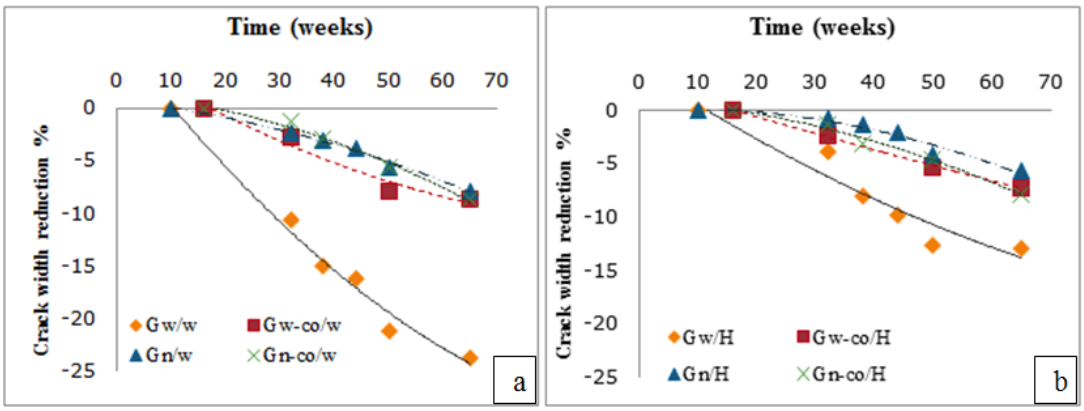

Figure 6-24 Mechanical crack widths reducing over time for specimens: a. partially submerged in water and b. exposed to high humid.

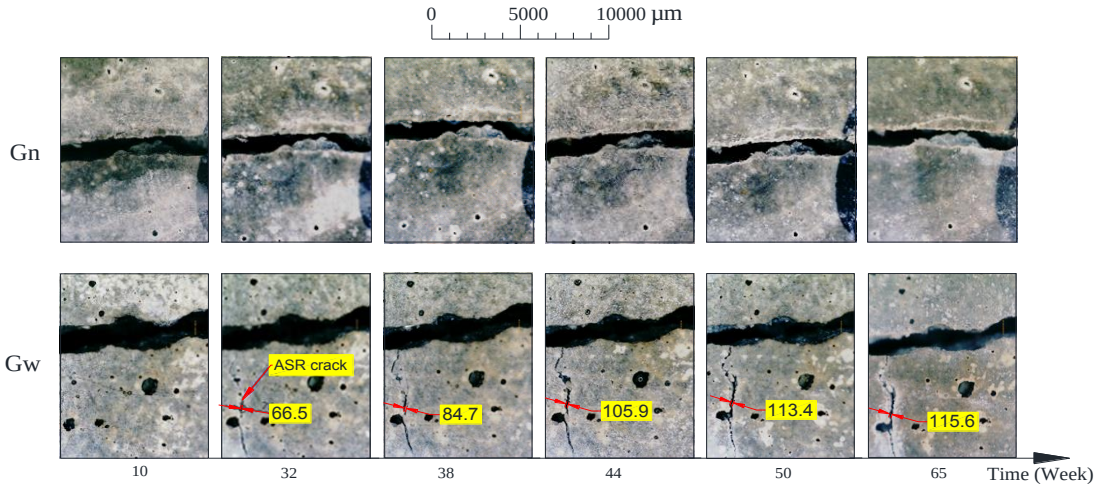

Figure 6-25 Mechanical and ASR cracks changing with time in Gw/w and Gn/w mixes.

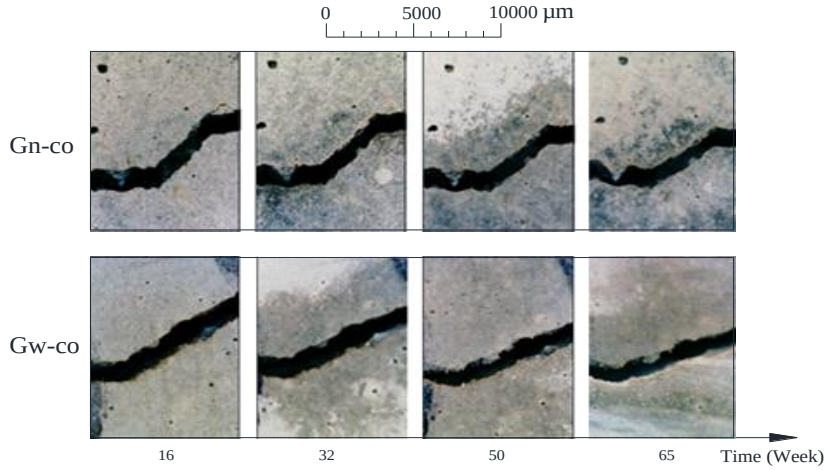

Figure 6-26 Mechanical cracks changing with the time in Gw-co and Gn-co mixes.

6.4.5.2 ASR cracks

The ASR plays a minor role in the cracking of concrete if the concrete has not been impaired previously. Due to micro-cracks caused by the mechanical degradation in concrete, the ASR expansion and thus crack forming, accelerates. The formed gel starts expanding into pores and micro-cracks of the cement matrix. As it fills up the available space, it then exerts pressure on the surrounding skeleton. ASR cracks appeared in Greywacke mixes (Gw/w) at the 32th week. The fine, vertical crack in Figure 6-27 shows the ASR cracks increasing with time in Gw/w specimens. It can be noted that the ASR crack width increased in time, while the mechanical cracks decreased. The main cracks often form in the reinforced steel direction and the crack branches in a perpendicular direction.

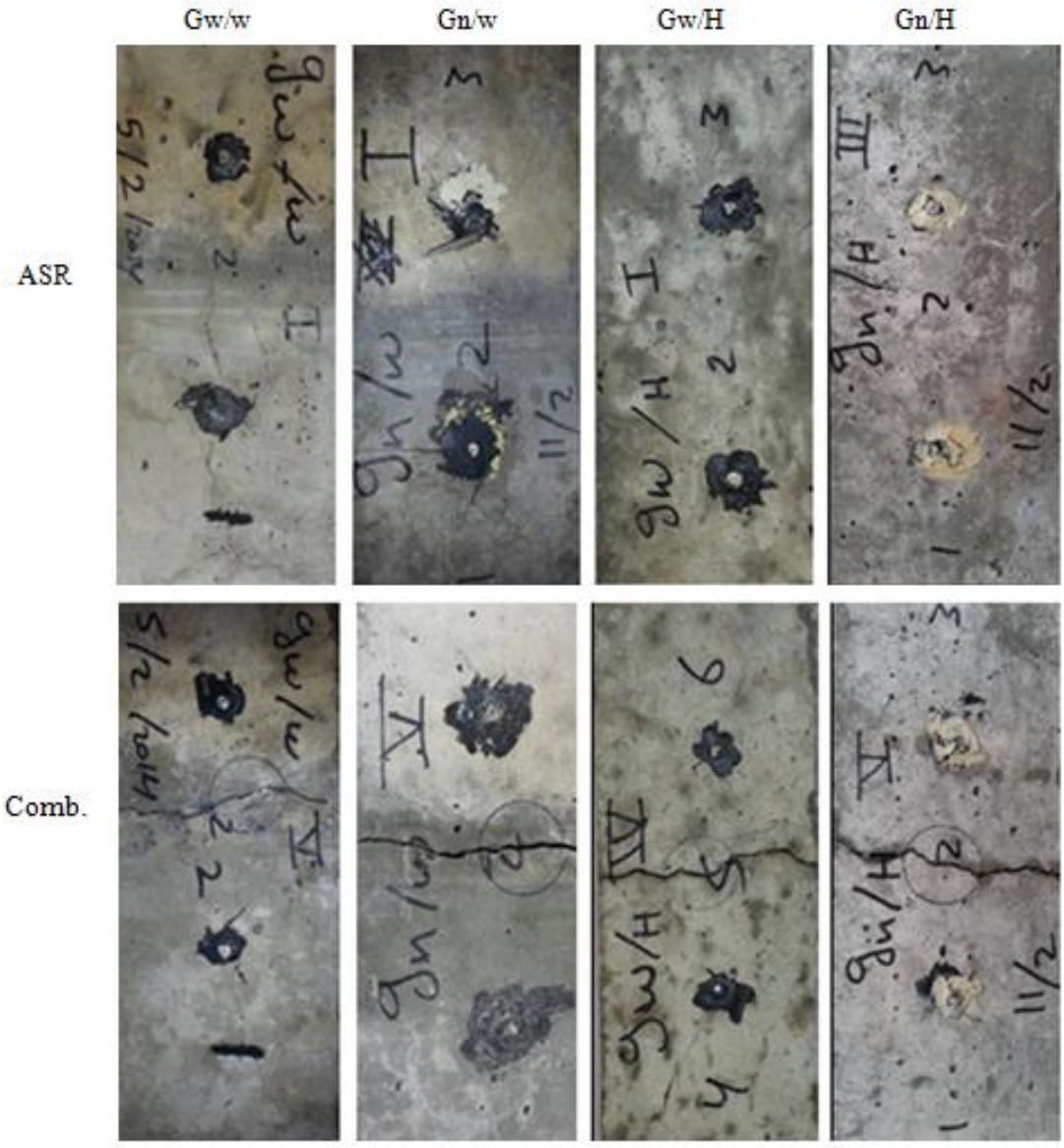

Figure 6-27 Mechanical and ASR cracks on the surface of Gw and Gn mixes in both conditions.

The ASR cracks were only seen at 44 weeks in Gn/w mixes, while there were no cracks measured at 65 weeks in the mixes with GGCS (Gw-co and Gn-co). In comparison, the specimens exposed to humidity had fewer cracks than those submerged in water and occurred later on. Figure 6-27 shows examples of the specimen surface of Gw and Gn imaged at the end of 65 weeks in ASR and combined action in both conditions. Cracks parallel with steel reinforced direction and some forked cracks occurred in Gw/w, and crack widths were less than in Gw/H. In Gn/w, micro-cracks are seen when the surface is wet and in the drying stage, and these cracks have not emerged in Gn/H.

6.4.6 Comparison between strains in different mixes

There is no doubt that there is a difference in the behaviour of expansion induced by ASR between concretes according to the exposure condition, aggregate type and whether it contained Corex slagment. Comparisons between the results of strains in the various mixes are conducted in the sections that follow.

6.4.6.1 The average strains of all spaces

The strains of the three measurement spaces including the mechanical crack (in combined specimens) were determined. Figure 6-28 illustrates the comparison between the strains of different mixes in both conditions and actions determined from the onset of observation until 65 weeks. In ASR specimens, the largest strains were in Gw mixes, while the lowest strains were in Gn-co mixes in both conditions. The strains in Gn and Gw-co were convergent in both conditions.

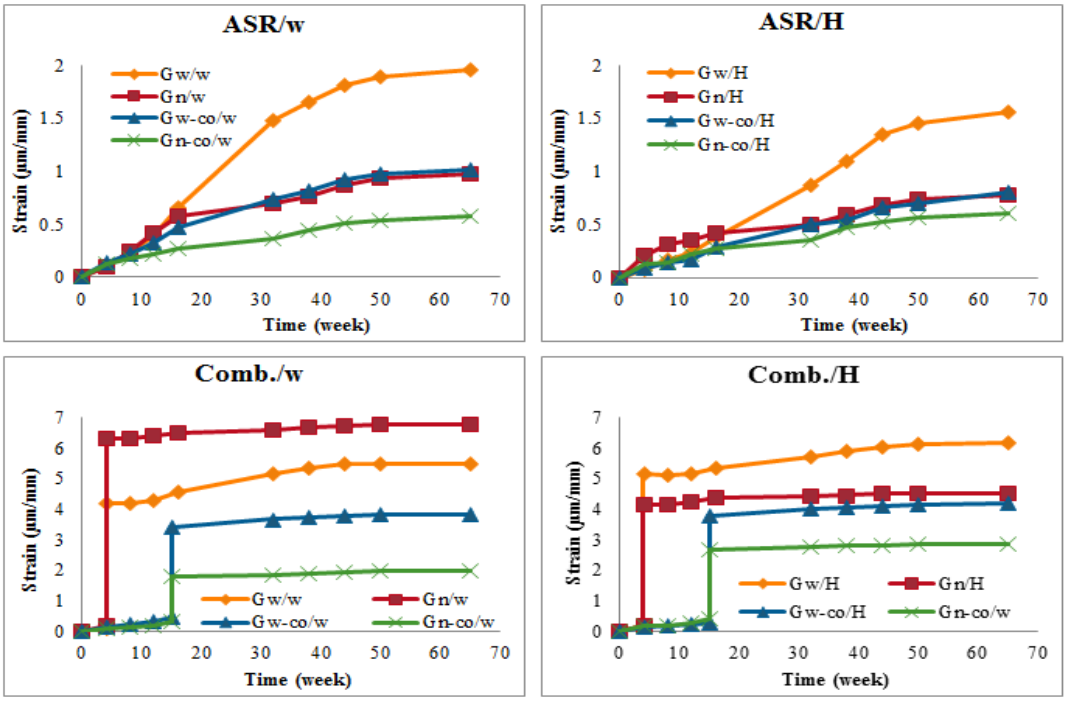

Figure 6-28 Comparison between the average strains in different mixes under ASR and combined action and in both conditions.

The specimens in submerged condition were more expanded than those in a humid environment. In ASR exposure of Gw/w, Gn/w, Gw-co/w and Gn-co/w, the maximum strains were 0.19, 0.097, 0.1 and 0.057% respectively, while in Gw/H, Gn/H, Gw-co/H and Gn-co/H they were 0.155, 0.078, 0.08 and 0.06% respectively. The mechanical crack widths were not the same in all specimens, and the total strains in combined specimens were dependent on these crack widths. The crack width in each mix was convergent (in two sides of three specimens), except one crack in Gw/H specimens which was excluded. The maximum strains in combined action of Gw/w, Gn/w, Gw-co/w and Gn-co/w were 0.55, 0.68, 0.38 and 0.2% respectively, while in Gw/H, Gn/H, Gw-co/H and Gn-co/H they were 0.6, 0.45, 0.42 and 0.29 respectively. The decrease in crack widths in the middle space after mechanical cracking decreases the slope of the curves.

6.4.6.2 The average strains of top and bottom spaces (excluding the middle space)

To compare the strains in skeletons not affected by the mechanical cracks, the top and bottom measurement spaces were considered in both actions, i.e. excluding the cracked, middle measurement space. It can be noted in Figure 6-29 that the largest strain at 65 weeks is in Gw and lowest is in Gn-co in both conditions. In ASR, the maximum strains of Gw/w, Gn/w, Gw-co/w and Gn-co/w were 0.198, 0.094, 0.1 and 0.058% respectively, while in Gw/H, Gn/H, Gw-co/H and Gn-co/H they were 0.168, 0.079, 0.074 and 0.062% respectively. These strains are close to those determined for all spaces. In combined action specimens, the maximum strains of Gw/w, Gn/w, Gw-co/w and Gn-co/w were 0.25, 0.098, 0.10 and 0.064% respectively, while in Gw/H, Gn/H, Gw-co/H and Gn-co/H they were 0.2, 0.075, 0.086 and 0.063% respectively. From these results, one can compare the strains of the specimens subjected only to ASR and of those exposed to combined action. The strains of Gw in combined action (in both conditions) were larger than those in ASR, while in the other mixes they were convergent in both cases. As in the other comparisons, the strains in partially submerged specimens were larger than those exposed to high humidity in both ASR and combined action except in Gn-co case which were convergent in both actions.

6.4.6.3 The average strains determined after mechanical crack time

In this case, the strains are considered after mechanical cracking, which means, after 4 weeks for Gw and Gn specimens and after 15 weeks for Gw-co and Gn-co specimens in both conditions. As the mechanical cracking occurred at different times, the comparisons were made between Gw and Gn and with Gw-co and Gn-co as in Figure 6-30. The maximum strains in Gw/w, Gn/w, Gw/H and Gn/H in ASR were 0.18, 0.087, 0.15 and 0.057% respectively and in combined action they were 0.13, 0.03, 0.09 and 0.038% respectively. In Gw-co and Gn-co the maximum strains at 65 weeks determined after 15 weeks in Gw-co/w, Gn-co/w, Gw-co/H and Gn-co/H were 0.054, 0.029, 0.053 and 0.033 in ASR respectively, while

they were 0.037, 0.022, 0.043 and 0.017 in combined action respectively. In all mixes, the strains in combined actions were less than those in ASR due to the pre-mechanical cracks.

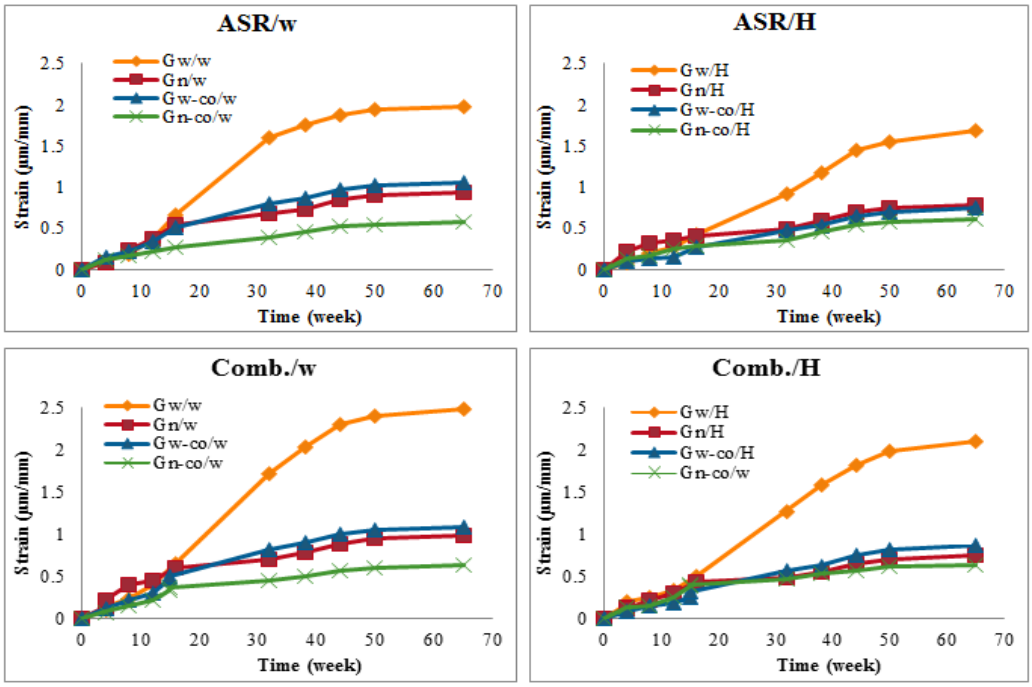

Figure 6-29 Comparison between the average strains of top and bottom spaces in different mixes under ASR and combined action and in both conditions.

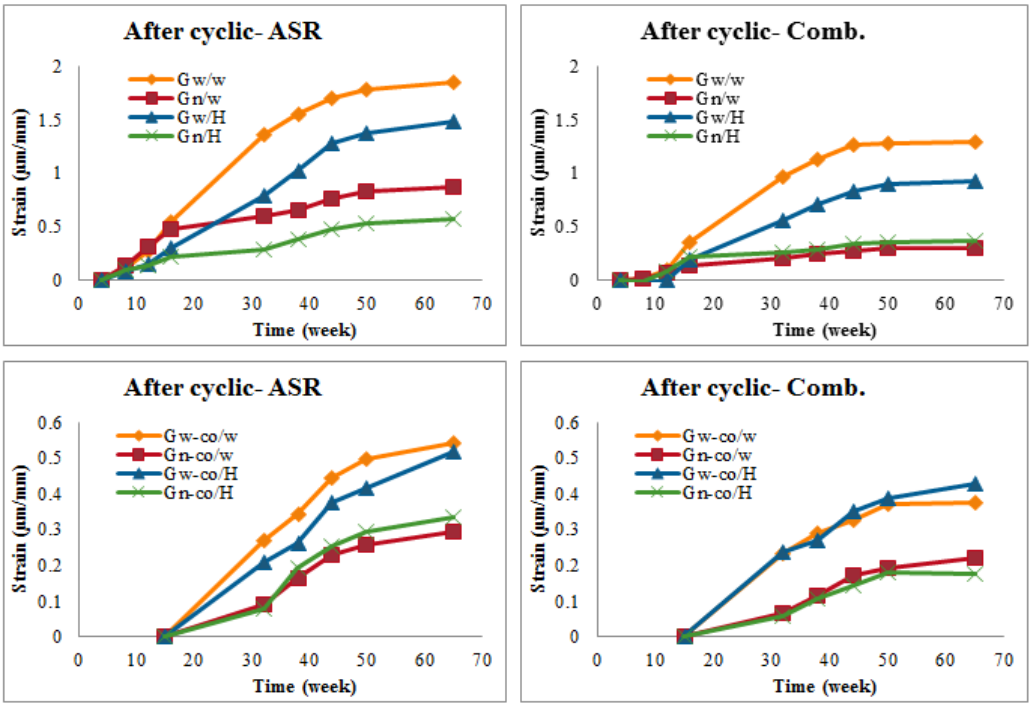

Figure 6-30 Comparison between the average strains determined after mechanical cracking time in different mixes under ASR and combined action and in both conditions.

6.4.6.4 The average strains in middle space determined after mechanical crack time

In this case, the strains are determined in the middle space where mechanical cracks occurred in combined specimens. To mechanical crack behaviour under continued ASR expansion, the expansion after the crack was imposed is considered. This means after 4 weeks in Gw and Gn and 15 weeks in Gw-co and Gn-co specimens, the respective ages at which the mechanical cracks were imposed. The relationship between the strain and time in all mixes in both ASR and combined action are illustrated in Figure 6.31. This shows clearly that the Gw/w specimens underwent more expansion than those in humid conditions (Gw/H). Under ASR conditions, the amount of expansion at 65 weeks increased by about 30.8% when the specimens were partially submerged in water (Gw/w- ASR) compared with the specimens exposed to high humidity (Gw/H- ASR). Likewise, the strain decreased in the combined action under the same conditions due to pre-cracking, whereas the strain of Gw/w- combined by the time of the test had decreased by about 47.1% more than the strain in Gw/H- combined. Under partially submersed conditions, the specimens of Gw/w- ASR expanded about 0.18%, whereas Gw/w- combined reduced by 0.216% over 65 weeks. In the same time, the specimens of Gw/H- ASR expanded by 0.125%, whereas the specimens of Gw/H- combined were reduced by 0.1%. In the combined action, the strain reduced significantly for about two months, but then expanded for the next month before starting to decline. For the interpretation of this behaviour, it can be assumed that the initial expansion in the concrete was influenced to a greater extent by swelling from water absorption and thermal expansion than by ASR. The results obtained for the specimen under the combined action confirmed that the mechanical pre-crack degradation provided more space for ASR expansion. Under ASR conditions, the Gn/w specimens expanded more than those under humid conditions (Gn/H), and also slightly more in the combined action. The expansion of the specimens at 65 weeks is more by about 35% in Gn/w- ASR compared with those exposed to high humidity (Gn/H- ASR). The strain reduced due to pre-crack in the Gn/w-combined by about 0.015% at 65 weeks, while in the Gn/H-combined it reduced by 0.014% in the same time. The ASR specimens expanded rapidly at first, and then expanded slowly. In the combined action, the strain reduced significantly for about four weeks, after which it expanded for a few weeks before slowly reducing. The maximum strain which occurred from the 15th week to 65th week in Gw-co/w –ASR was 0.052% and in Gw-co/H-ASR it was 0.044%, on average it was about 15.4% less than Gw-co/w. In combined action, the strain increased in Gw-co/H for the next 15 weeks and then decreased but did not reach a minimum value at the 65th week. In Gw-co/w, the strain was 0.02 at the 65th week. The last comparison is of Gn-co specimens in both actions, where the maximum strain of Gn-co/w and Gn-co/H in ASR were 0.27and 0.35% respectively. The strains in combined action at the 65th week were 0.06 and 0.09% for Gn-co/w and Gn-co/H respectively. Only in the Gn-co, the strains in humid condition were

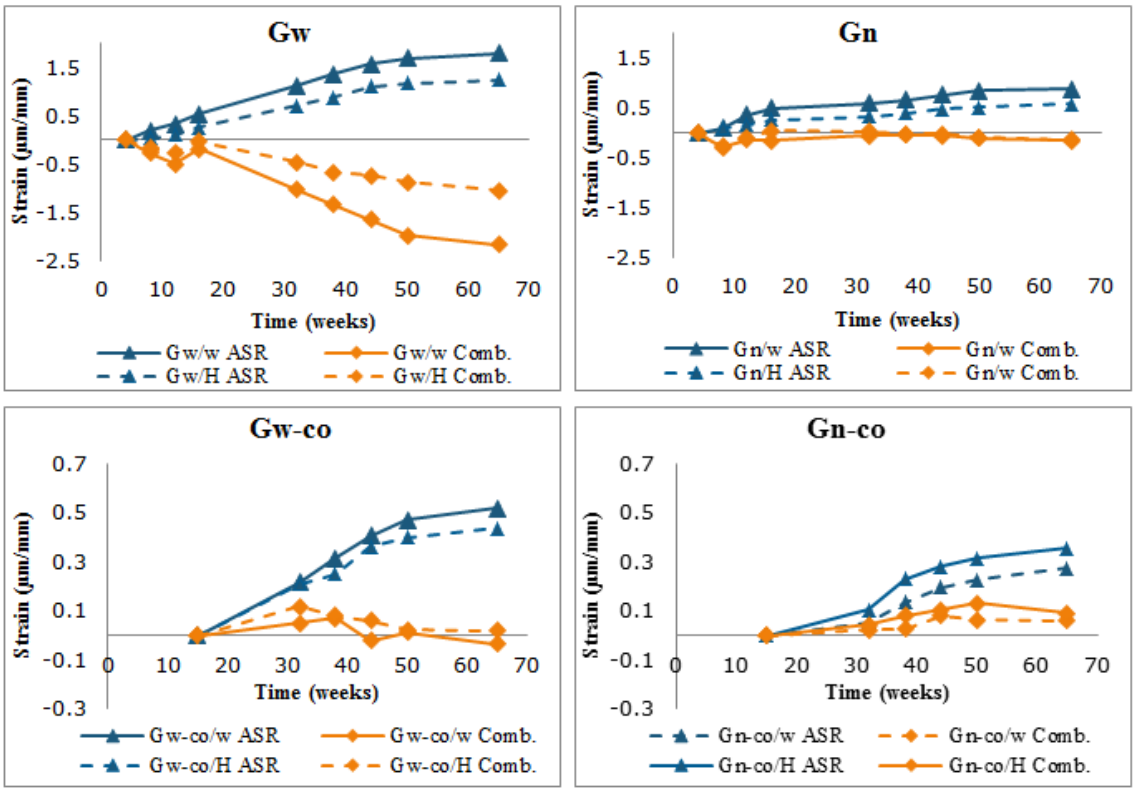

Figure 6-31 Comparison between the average strains of different mixes determined after mechanical crack time in the middle space under ASR and combined action and in both conditions.

larger than the one submerged in water. In general, the ASR in the specimens under the combined action differed from the specimens under ASR only.

6.4.7 Discussion

The cyclic mechanical loading of concrete prisms has been shown to have a significant influence on crack widths and the strain of ASR-affected concrete. Throughout the results shown in the foregoing figures, the Granite specimens (Gn) were more effective in controlling cracking than Greywacke mixes (Gw) in concrete exposed to ASR. In concrete with both Greywacke and Granite aggregates under various conditions, the widths of the cracks caused by cyclic mechanical loading were reduced considerably upon subsequent, continued ASR expansion. This was more significant in the reactive aggregate of Gw specimens and could be detected easily with the dnt camera (i.e. at relatively low magnification) as early as 10 weeks after the specimens had been submerged in water and to a lesser extent in those specimens exposed to high humidity. An explanation for the crack reduction is that the mechanical crack provides space for ASR expansion into the un-cracked regions. The cracks also contribute to increase the permeability and allow the ingress of undesirable gases, salts and water into the concrete, which may lead to further degradation of the concrete. Mechanical and ASR cracks together decrease the durability of

concrete, although concrete that is pre-cracked mechanically, allows the ASR to expand and possibly fill the small cracks. The ASR expansion of both sides (bottom and top) takes place in all directions including in the direction of the crack in the middle space. In the other cases shown in Figure 6-29 the measuring of the bottom and top spaces and neglecting the middle space which contains the large crack, the strain in the combined mixes increases more with time than the strain in the ASR mixes. This phenomenon can be caused by the fact that (i) part of the expansion is absorbed by the mechanical cracks in the middle distance and that expansion occurs in the terminal distances due to micro-cracks likely caused by the cyclic mechanical loading and (ii) that mechanical micro-cracks interconnect flow paths and increase concrete permeability, allowing more water or aggressive chemical ions to penetrate into the concrete, facilitating deterioration (Wang et. al., 1997). In the last case (ii), water liquid or vapour entering the concrete by way of the micro-cracks will be the additional factor which forms the ASR gel. The large mechanical cracks seem to be the main reason for the decrease in the expansion of the concrete due to the presence of enough space to expand. Therefore, the pre-crack might be useful in this case, but at the same time may lead to the impairment of the concrete properties, which in turn may lead to an untimely deterioration of the concrete. Other factors might have an effect on crack width changing such as the thermal expansion and self-weight of the upper part. The mechanism of strain changing in ASR and combined action is illustrated in Figure 6-32. This phenomenon happens in the initial reaction when the ASR gels form and find enough space to expand without cracking the cement paste (Charpin and Ehrlacher, 2012). The gel may expand into pores and cracks in the cementitious skeleton, being in a sufficiently humid environment (Bangert and Meschke, 2001). At a later age, some substances from the leaching of calcium hydroxide into concrete could block small pores on the surface of the concrete, thereby decreasing the permeability (Wang et al., 1997). The quantity of water plays a significant role as the solvent for the silica and is a necessary compound for the formation of gels, precipitates, crystals, etc. (Ulm, 2000). The dissolved silica may diffuse away from the reactive aggregate particles when the internal humidity elevated and the subsequent reaction in solution-forming amorphous gel or precipitates may then take place anywhere in the concrete (Steffens, Li and Coussy 2003). Also, the formation of basic gel and increase of particle value are accelerated by an increase of permeability (Pazant and Steffens 2000). It is not only the ASR expansion that is involved in changing the crack width but for example, self-weight may contribute to reducing the crack width (especially when the crack direction is horizontal in the case of these specimens that were kept in vertical orientation in the respective exposure chambers) affected by the upper part. An important role in the anisotropy of the expansion is also fulfilled by micro-cracks when the concrete structure is loaded (Charpin and Ehrlacher, 2012). Therefore, many factors may effect on crack width changing over time.

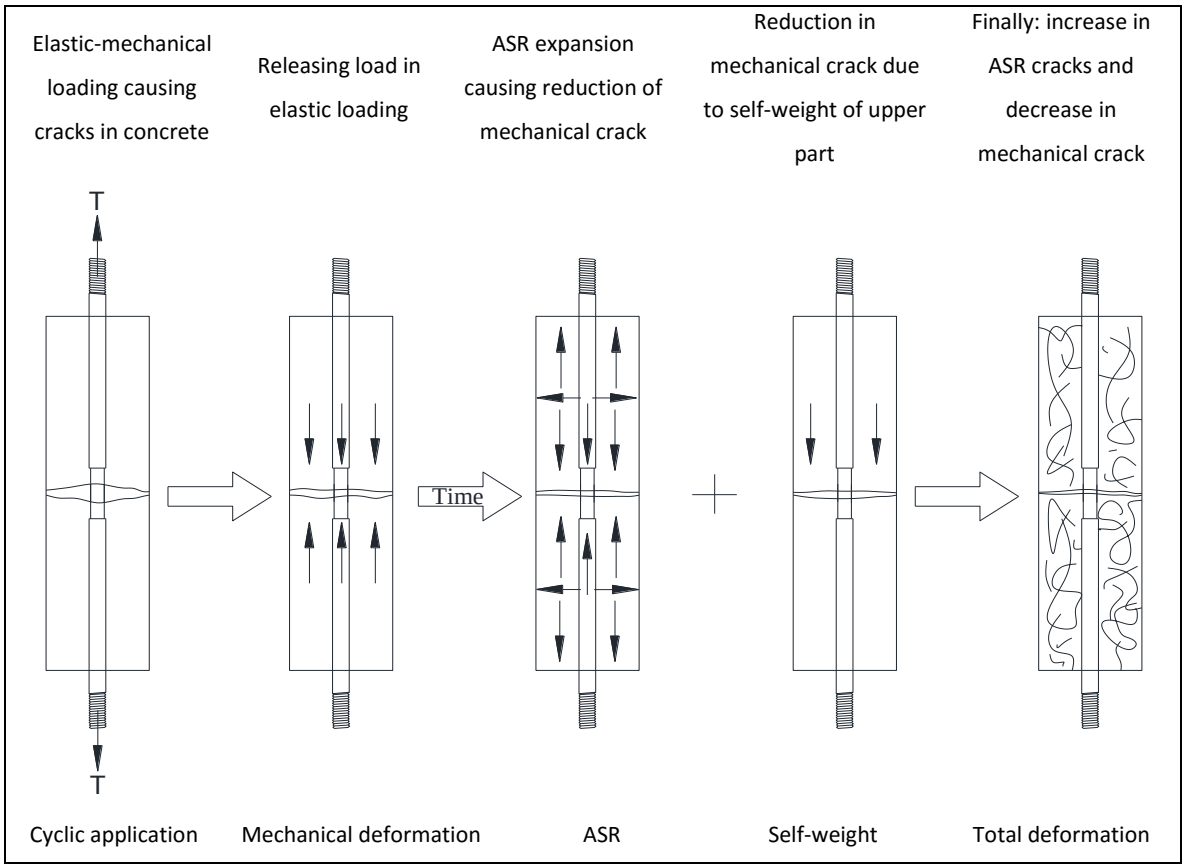

Figure 6-32 Transfer of the concrete specimens to different stages.

6.5 Summary and conclusion

The combined action on concrete prepared with aggregates of different rock types were studied under accelerated ASR tests according to ASTM C 1260 and 1293 (series tests 1 and 2). In series 1, the experiment was divided into two sub-series; firstly, mortar bars on which to conduct ASTM C 1260 standard tests, secondly, RC prisms, immersed in 1N NaOH, half of them exposed to mechanical pre-tension (phase 3). In series 2, RC prisms were subjected to two conditions (partially submerged in water and exposed to RH higher than 90%) and two actions (ASR exposure, and mechanical cyclic loading combined with ASR exposure).

6.5.1 ASR and tension on RC in series test 1

From the final results on RC specimens in series 1, it can be observed that the mixture Gn expanded more than Gw and the expansion decreased when GGCS was added in Gn-co. Although the Greywacke is classified as a reactive aggregate and the accelerated test ASTM C 1260 confirmed that, the results here show that the Granite indicated more weaknesses due to some factors namely:

1. The shrinkage, crack started in Gn and Gn-co and developed more than in Gw and Gw-co, which led to larger expansion.
2. Pre-cracking can allow ingress of alkalis and water, which then exacerbates ASR as do other mechanisms such as shrinkage.
3. Large mechanical cracks allow the ASR expansion to proceed in both directions, which might reduce the crack width.
4. The mixture with Granite stone and Philippi sand (Gn) may be affected by temperature more than the mixture with Greywacke stone and Malmesbury sand (Gw), as became apparent when the specimens were removed from the NaOH and kept at laboratory temperature. It was also observed that after one week in hot water, the Gn specimens were more expanded.
5. The strain in the concrete must be calculated for all actions that caused changes in its dimensions, as mechanical, ASR, shrinkage and temperature.

The condition in the accelerated method to test for potential ASR (ASTM C 1260 test) is not a true reflection of ASR in the field and therefore using the same condition may give unreliable results. It can, however, help in assisting to understand the behaviour of ASR in concrete.

6.5.2 ASR and cyclic loading on RC in series test 2

The potential of ASR was tested on RC prisms containing high alkaline content (NaOH), half of them were exposed to cyclic loading causing a macro-crack in the middle and micro-cracks in the skeleton in series test 2. Greywacke stone denoted (Gw) as reaction aggregate and Granite stone denoted (Gn) as non-reaction aggregate were used in the concrete mix. Ground granulated Corex slag (GGCS) denoted (co) was used in half of the 12 specimens of both aggregates. The prism specimens with cracks of widths between 0.8 and 4 mm, which were induced by a tensile cyclic load, were named “combined” and “ASR” specimens. Then all the specimens were partially submersed in water at 38 ˚C and the upper half was exposed to >90% relative humidity. The results obtained at the end of 65 weeks showed that the mechanical pre-cracks play a significant role in concrete strain due to the ASR. The macro-cracks in the middle of the specimens were reduced due to certain factors such as ASR pressure, self-weight of the upper part of the concrete and thermal expansion. The reduction of the central crack width and the expansion of concrete were of different values for the various mixes. These reductions and expansions were more in Gw than in Gn specimens. Also, replacing 50% of the cement mass with GGCS led to a reduction and expansion that was less than in its concrete counterpart without GGCS. The crack-width decrease at the end of 65 weeks was around 23.7% in Gw/w compared with 7.9% in Gn/w and around 8.7% in both Gw-co/w and Gn-co/w. In humid conditions, the crack reductions were 12.9, 5.7, 6.2 and

7.9% for Gw/H, Gn/H, Gw-co/H and Gn-co/H respectively. On the other hand, the greatest expansion from the beginning of testing was in Gw in both combined and ASR specimens and the lowest in Gn-co. When considering that the expansion starts after the mechanical load is applied, the maximum combined strains were less than those in ASR specimens due to the macro-crack in the middle of combined specimens, while when neglecting the middle space and only considering the lower and upper spaces, the maximum strains in combined action were more than those in ASR specimens in Gw mixes. It can be concluded that the mechanical macro-cracks reduce due to ASR pressure whereas the micro-cracks may lead to more expansion in combined action compared to ASR specimens. This phenomenon suggests possible change in the concrete volume exposed to the ASR by the presence of the mechanical micro- and macro-cracks.

CHAPTER SEVEN

7. MODELLING ASR AND MECHANICAL CRACK INTERACTION

Abstract

Two series of experiments were performed to study the combined effect of ASR expansion and mechanical cracks, as reported in Chapters 5 and 6. Here in Chapter 7, modelling approaches are elaborated to simulate the ASR expansion and mechanical cracks. In Series model 2, the length change in the mechanically cracked RC specimens, which were subsequently subjected to ASR inducing exposure, is considered over the central length of 100 mm containing the macro mechanical crack. The stiffness of concrete in the specimens containing Greywacke stone is also considered. The changes in the crack widths due to this expansion are also modelled. The specimen was also simulated with a finite element (FE) model to monitor the expansion behaviour of the concrete with or without the mechanical crack, as well as with or without steel bar restraint. The experimental and the FE model results were convergent. In Series model 1, crack reduction (ΔC_w) of pre-cracked plain concrete cubes (described in Chapter 5) subjected to NaOH and hot water at 80°C is computed. The results of the crack width reduction at four weeks of exposure are simulated. The ΔC_w due to ASR is refined by subtracting the effect of thermal expansion from the total deformation.

7.1 Introduction

Chemical, physical and mechanical models have been used by researchers to model ASR cracking. These models do not consider the mechanism of the crack formation by cyclic tensile load, which is a different, mechanical mechanism. Many studies have adopted the basis of ASR reaction and the relationship between the rate of reaction and some characteristics, such as the kind of silica, the amount of alkali in the cement as equivalent (Na + 0.658 K), size of aggregate, presence of admixture, as well as the surrounding environment. The concentrations of ionic species are roughly homogeneous in the cement paste at each time step, although there are some changes in composition with age (Multon et al., 2009). The composition of the gels depends on many parameters, such as gel position in the concrete (inside or outside the aggregate) and its age. It is usually assumed that old gels contain more calcium than new gels.

The alkaline ions (K^+ and Na^+) present in the interstitial pore solution balance the low calcium ion environment (Ca^{2+}), due to negative charges (Ulm et al., 2000). Bangert and Meschke (2001) describe the process of gel formation phenomenologically by the extent of non-dimensional reaction, assuming that the kinetic law ($\partial\xi/\partial t = k(1-\xi)$) of gel formation governs the alkali-silica reaction (formation of gel + swelling of gel). The extent of reaction $\xi\epsilon$ [0, 1] is ξ = 0 in the beginning, and in the end of the dissolution process ξ = 1. For constant environmental conditions, the characteristic velocity of the process k is constant. The extent of the ASR reaction ξ can be written as a function of time t: $\xi = 1 - e^{-kt}$. In this chapter, models represent the role of ASR swelling, leading to change in the mechanical crack width based on this kinitic law.

7.2 Chemo-mechanical modelling

ASR expansion has been modelled differently by different researchers. Bangert and Meschke (2001) concluded that the skeleton swelling induced by ASR results from the variation of the material density ρ^s of the skeleton, whereby the expansive strain $\varepsilon_{asr}$is defined as:

$$\varepsilon_{asr} = \left(\frac{\rho^u}{\rho^r} - 1\right)\xi \tag{7-1}$$

where ρ^u denotes the initial material density of the skeleton (unswollen state ξ=0), and ρ^r final material density (fully swollen ξ=1). The term in brackets $\left(\frac{\rho^u}{\rho^r} - 1\right)$ expresses the asymptotic ASR strain in a stress-free expansion test.

Ulm et al. (2000) modelled the stress with the Chemo-elastic Pressure-Spring Device analogy of ASR Swelling. Their model is based on two springs: the elastic spring of stiffness E_s, denoted by $\sigma_\mu = E_s\,\varepsilon$; and the chemical swelling pressure, denoted by $P_g = -E_g(\varepsilon - c\xi)$. Considering the extent of this chemical reaction ξ, and neglecting the free expansion space in which the products can freely expand, the stress equilibrium in this chemoelastic device reads

$$\sigma = \sigma_\mu - P_g = E_s\varepsilon + E_g(\varepsilon - c\xi) \tag{7-2}$$

where c is the intrinsic dilatation coefficient of the reaction products, and E_g and E_s are spring moduli of the chemoelastic device, that represent the modulus of elasticity of gel and skeleton respectively.

The rate equation of kinetic law relates the reaction affinity $A_m(\xi)$, and it is assumed to decrease progressively from the initial affinity $A_m(\xi = 0) = A_{m0}$ to equilibrium state $A_m(\xi = 1) = 0$, and the linear affinity is $A_m(\xi) = A_{m0}(1 - \xi)$. The linear relationship between the reaction rate $d\xi/dt$ and reaction affinity at free-stress can be expressed as follows:

$$A_m(\xi) = C_d \frac{d\xi}{dt} \tag{7-3}$$

$$\frac{d\xi}{dt} = \frac{1}{t_c}(1-\xi) \tag{7-4}$$

where $1/t_c = k$ and $t_c = C_d / A_{m0}$ define a characteristic of reaction time, $C_d > 0$ is a kinetic coefficient. Also, if $\sigma = 0$, the total strain ε measurable in such an experiment and neglecting the thermal expansion (i.e. assuming the temperature is constant) is thus related through a chemical dilatation coefficient β to the extent ξ of the ASR as follows:

$$\varepsilon_{asr} = \beta\xi \tag{7-5}$$

and

$$\beta = \frac{cE_g}{E} \tag{7-6}$$

Where $E = E_s + E_g$ and c is the intrinsic dilatation coefficient of the reaction products. By equating Eqs. (7-1) and (7-5) at free stress, the chemical dilatation coefficient β can be written:

$$\beta = \frac{cE_g}{E} = \left(\frac{\rho^u}{\rho^r} - 1\right) \tag{7-7}$$

and

$$c = \frac{E}{E_g}\left(\frac{\rho^u}{\rho^r} - 1\right) \tag{7-8}$$

The ASR strain is related to the ratio of modulus of elasticity for the concrete to gel and the density of swollen at non-reactive to swollen at fully reactive of concrete.

7.3 Length changing and crack reduction model in RC beams

In the experiments of this research project, it can be considered that the strains are caused by four phenomena: ASR strain ε_{ASR}, thermal expansion ε_T, shrinkage ε_{sh}, and mechanical strain ε_{me}. The total strain in concrete can be de-composed as follows:

$$\varepsilon = \varepsilon_{asr} + \varepsilon_T + \varepsilon_{me} + \varepsilon_{sh} \tag{7-9}$$

The stages of transferring the concrete under combined mechanical crack and ASR are postulated to be associated with the following processes:

1 In the starting reaction, the small pores are filled by gel produced before it starts to press on the paste.

2 Tensile loading on the beam has an elasticity limit, which may cause cracks in the concrete and, when the load is released, the steel reverts to its original length, and the concrete crack that is bigger on the external side may remain.

3 Cyclic loading could cause micro-cracks in the concrete besides the main crack, leading to undesirable gases and humidity entering, thereby resulting in more deterioration.

4 After filling the small pores, ASR expansion will be faster until a certain stage and then expand slowly.

5 ASR expansion, thermal expansion, shrinkage and self-weight will contribute to reducing the mechanical crack width and to the expansion of the skeleton of the concrete.

However, it is not quite as simple. The phenomena in Eq. (7-8) have different mechanisms and depend on certain parameters. For example, in the experiments of this project, only the upper part of the self-weight of the concrete had an effect on the crack width, while the effect of the other strains came from both directions (upper and lower). All strains in Eq. (7-8) are a function of time. The relationship between the strain and the time cannot be considered as constant, which complicates the understanding of the strain mechanism. In order to model the ASR in concrete induced with a mechanical crack, it should divide the period into two stages: before the mechanical crack and thereafter. Neglecting the change in cross-section, the longitudinal change Δl in concrete due to ASR and mechanical actions can be described by:

$$\Delta l(t) = \Delta l_{ini}(t_{ini}) + C_w(t_{cr}^m) + \Delta l_f(t_f) \tag{7-10}$$

with Δl_{ini}, initial expansion, C_w, crack width, Δl_f, longitudinal change after the mechanical crack occurred and t_{ini}, t_{cr}^m, t_f the initial reaction time, mechanical crack time and the final reaction time respectively as summarised in Table 7-1. Figure 7-1 shows the change stages in length at the time induced by combined action. Deformation before the mechanical crack was induced can be expressed as follows:

$$\Delta l_{asr} = \beta \xi l_g \tag{7-11}$$

with $\xi = (1 - e^{-kt})$ and k a constant for each mix; β is the variable that depends on chemical properties of concrete and the ASR exposure condition.

After the mechanical crack arises, the ASR expansion still continues due to retained ASR affinity. The release of restraint to ASR expansion at the crack is believed to induce the subsequent ASR-induced deformed shape shown in Figure 7-2. This implies that the overall length in the central gauge area will vary as follows before and after the crack is induced:

$$\Delta l = \begin{cases} \beta\left(1 - e^{-kt}\right) l_g & for\ \ 0 < t > t_{cr}^m \\ \beta\left(1 - e^{-kt_{cr}^m}\right) lg + C_w - 2\beta\left(1 - e^{-k(t - t_{cr}^m)}\right) l_a & for\ t > t_{cr}^m\ \ and\ \Delta C_w \leq C_w \end{cases} \tag{7-12}$$

Later, the deformation may close the crack, which means that continued ASR swelling will cause overall lengthening of the gauge length over the crack again from that point onward. This is reflected in the

condition of the second part of Eq. (7-12). The crack will be closed when the deformation in overall crack width $\Delta C_w = 2\beta\left(1 - e^{-k(t-t_{cr}^m)}\right)l_a = C_w$.

From the same graph, the surface crack width reduction in time can be expressed as:

$$C_w(t) = C_w - 2\beta\left(1 - e^{-k(t-t_{cr}^m)}\right)l_b \qquad for\ t > t_{cr}^m\ and\ C_w(t) \geq 0 \qquad (7\text{-}13)$$

Table 7-1 The period of experimental stages.

Time	Initial time (t_{ini})		Mechanical crack time (t_{cr}^m)		Final time (t_f)	
	From	To	From	To	From	To
Period	The reaction starts (t_0)	Mechanical crack (t_{cr}^m)	The period of mechanical crack (t_{cr}^m)		End of mechanical crack (t_{cr}^m)	The reaction end (t_f)
Time (weeks)	0	4 or 15	4 or 15		4 or 15	65

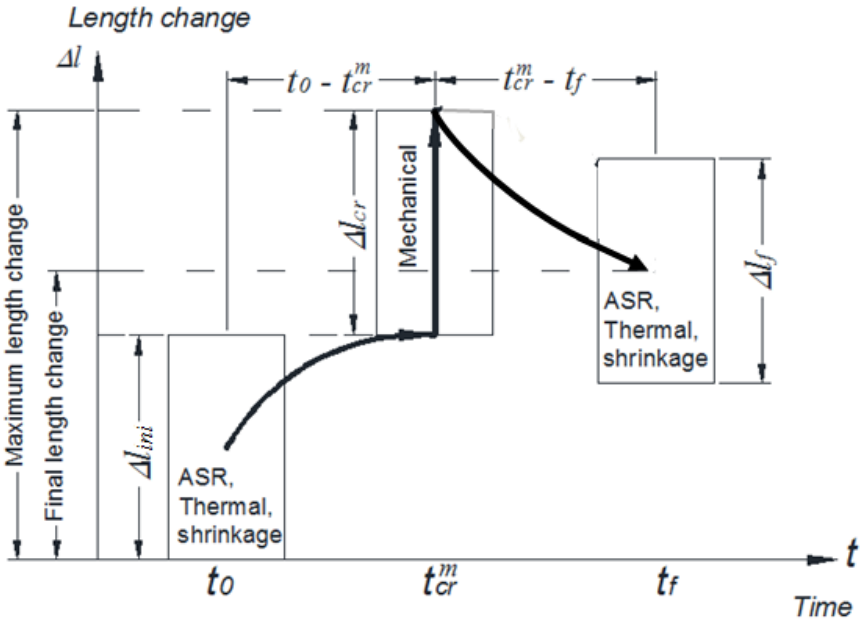

Figure 7-1 Length changes stages of concrete under ASR and pre-mechanical crack.

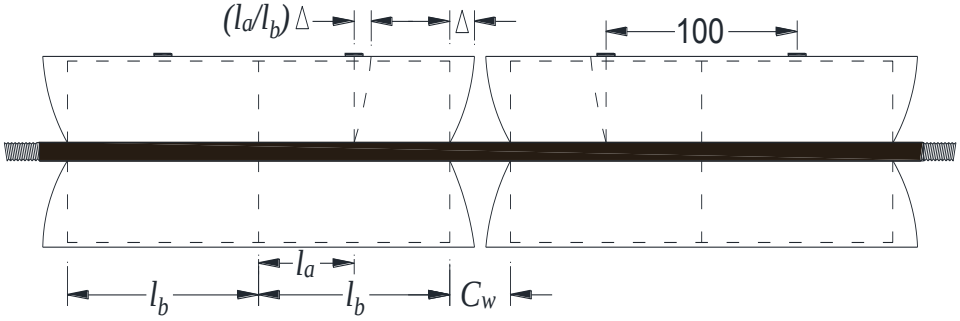

Figure 7-2 The deformation mechanism due to combined action.

In Eq. (7-12) deformation due to self-weight has been considered negligible. Figure 7-3 illustrates the experimental and computed deformation over the central gauge length due to ASR, and Figure 7-4 shows the deformation due to combined action. For different mixes and conditions, k and β values used are given in the figures.

Note that partial delamination from the steel bar in the cracked vicinity may slightly alter the expression in Eq. (7-13), as well as the crack shape, also reducing the crack width to an extent at the steel bar interface.

The averages of crack widths C_w (at 4th week in Gw and Gn and at 15th week in Gw-co and Gn-co) in both conditions were computed from the difference between the total gauge length change before and after the cyclic loading causing the crack.

Table 7-2 illustrates the average values of C_w recorded in mm with the coefficient of variation (CoV) given between brackets. To verify the computed crack width changes in Eq. (7-13), the actual crack widths were measured at specific times by the digital camera (dnt). The crack widths were measured at the middle of the crack line on the surface of two opposite sides, and the average of four readings (two on each side) were taken for each specimen, and then the average of the three specimens were determined. Figure 7-5 shows the reduction of crack widths computed by Eq. (7-13) compared with those measured, noting that the widths were measured from the 10th week only in Gw and Gn specimens while in Gw-co and Gn-co were from 16th week.

Young's modulus (E) was determined on cylinder specimens 100 mm in diameter and 200 mm high (Chapter four). The results are shown in Figure 7-6 for the respective mixes, normalised with initial value E_0 at 28 days, unaffected by ASR exposure. In concrete containing Greywacke stone, E reduced under ASR exposure, while in Granite mixes it continued to increase and after roughly 200 days started decreasing. By defining ω as the ratio between the current, affected value of E_t and its initial value E_0 as shown in Figure 7-6, the change in E due to ASR over time can be written as follows:

$$\omega = \frac{E_0}{E_t} = e^{-\alpha t} \tag{7-14}$$

From the Greywacke results here, it appears that the change in E-modulus is directly related to the ASR-related volume increase. In Granite mixes tested here, the hydration-related rise in E appears to dominate for an extended period of accelerated ASR-inducing exposure, postponing the time of refraction, i.e. when the E-modulus begins to decline. In Greywacke mixes, the strain can be written as:

$$\varepsilon = \beta(1 - e^{-kt}/\omega) \tag{7-15}$$

$$\varepsilon = \beta(1 - e^{-\varphi t}) \tag{7-16}$$

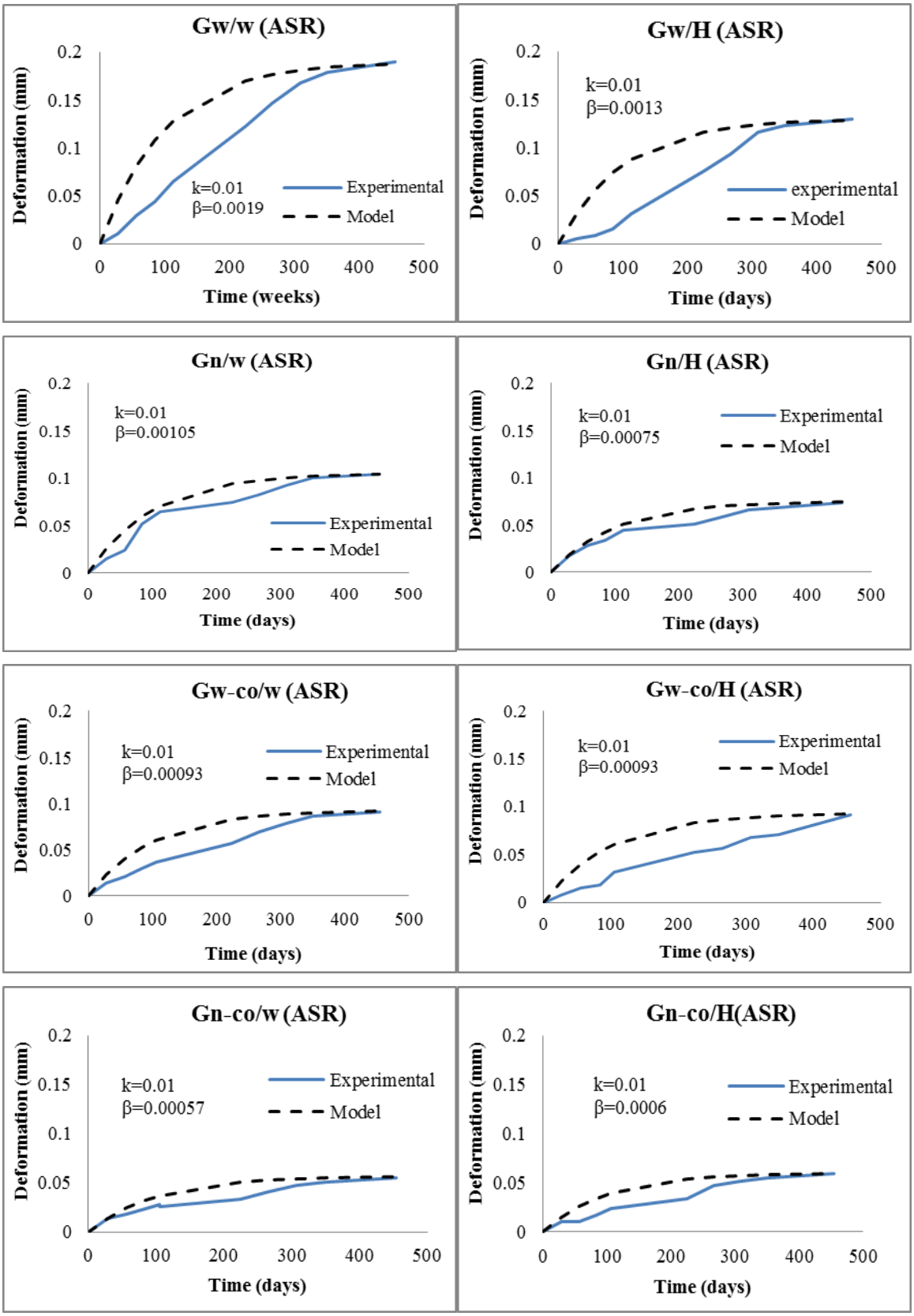

Figure 7-3 Experimental and model deformation due to ASR.

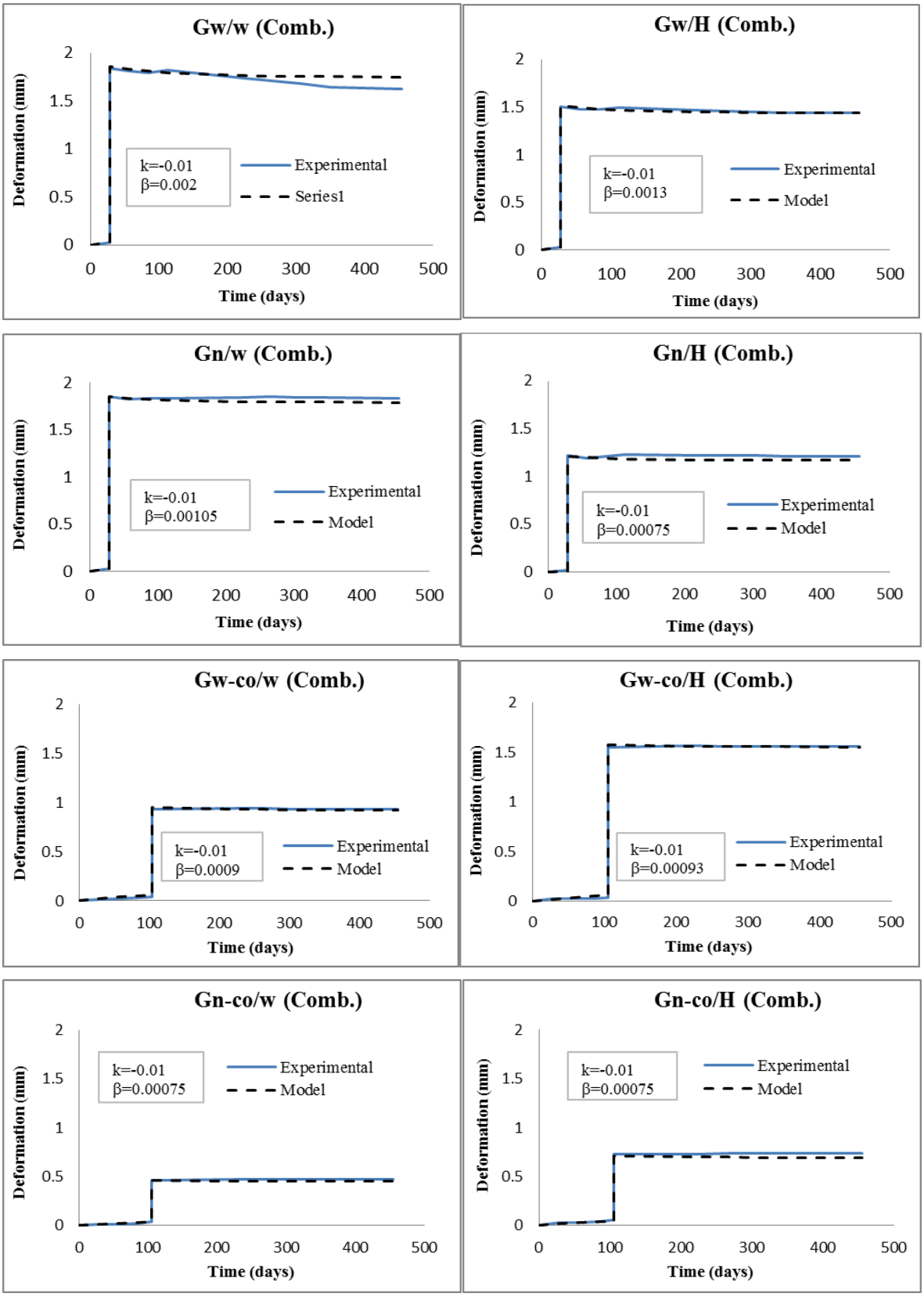

Figure 7-4 Experimental and model deformation due to ASR and mechanical loads (combined action).

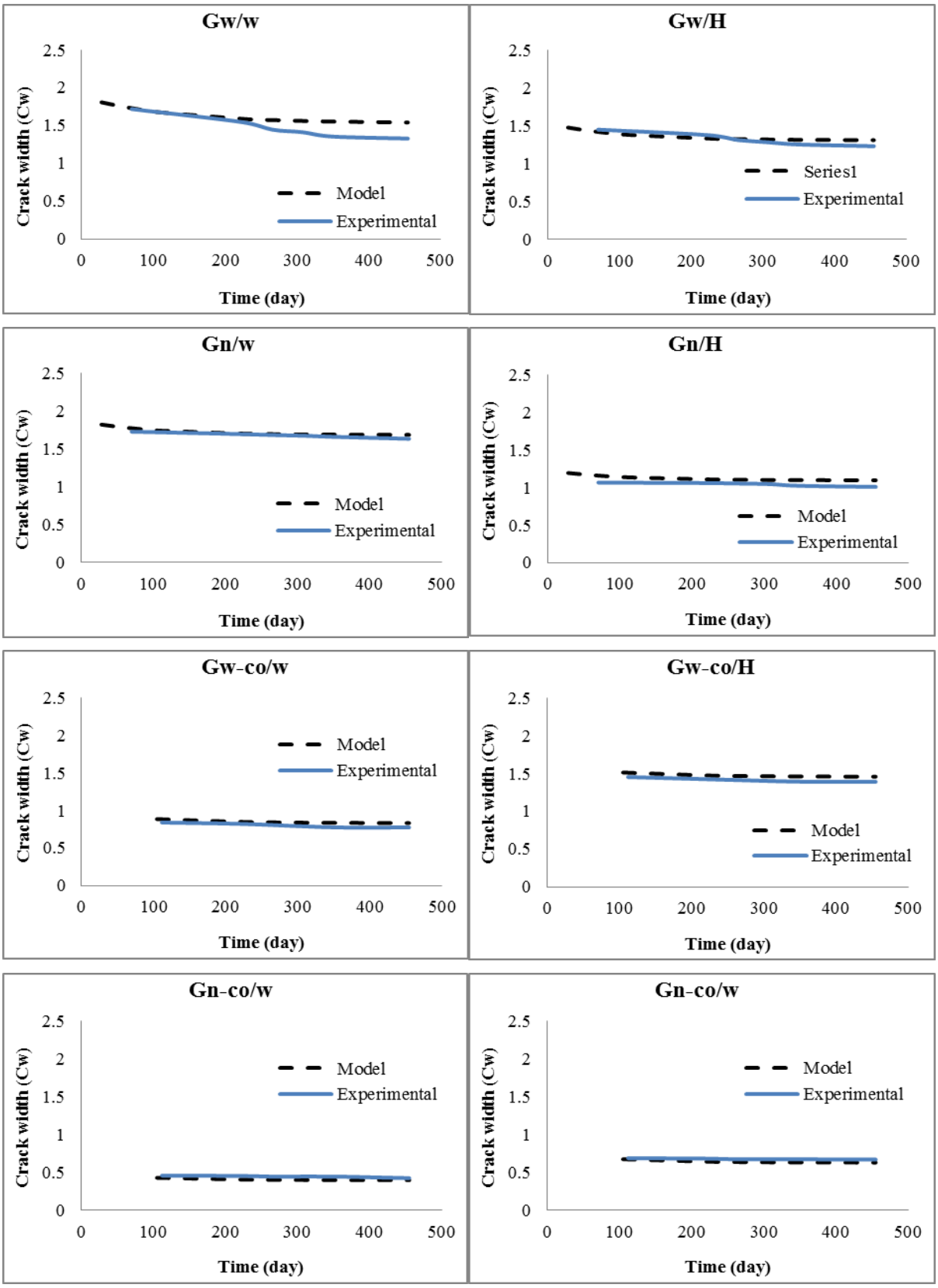

Figure 7-5 Experimental and modelled mechanical crack width change under ASR expansion.

Table 7-2 The average mechanical crack widths of the beams (mm) and coefficient of variation between the brackets (%).

Mix	Gw/w	Gw/H	Gn/w	Gn/H	Gw-co/w	Gw-co/H	Gn-co/w	Gn-co/H
Average crack width (CoV) %	1.84 (0.01)	1.48 (0.12)	1.82 (0.18)	1.20 (0.21)	0.89 (0.07)	1.52 (0.16)	0.64 (0.25)	0.67 (0.74)

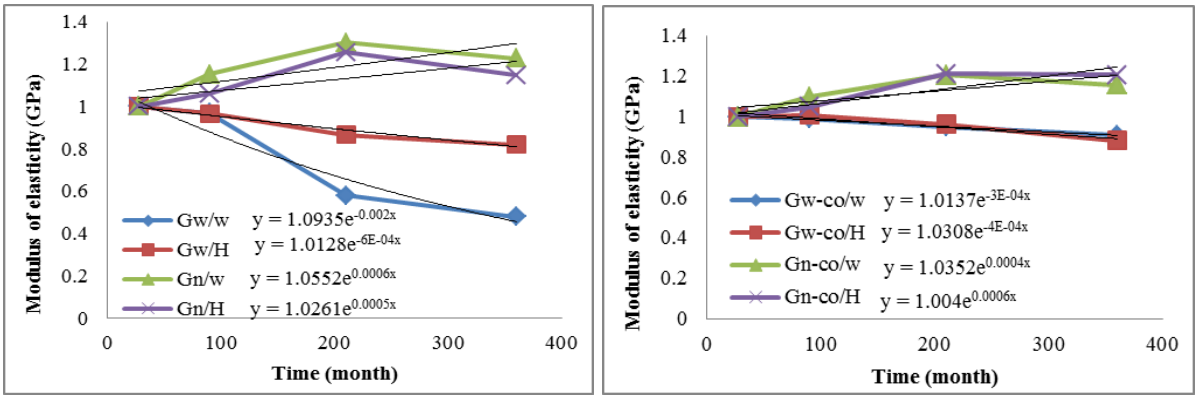

Figure 7-6 Degradation of E-modulus ratio vs. time.

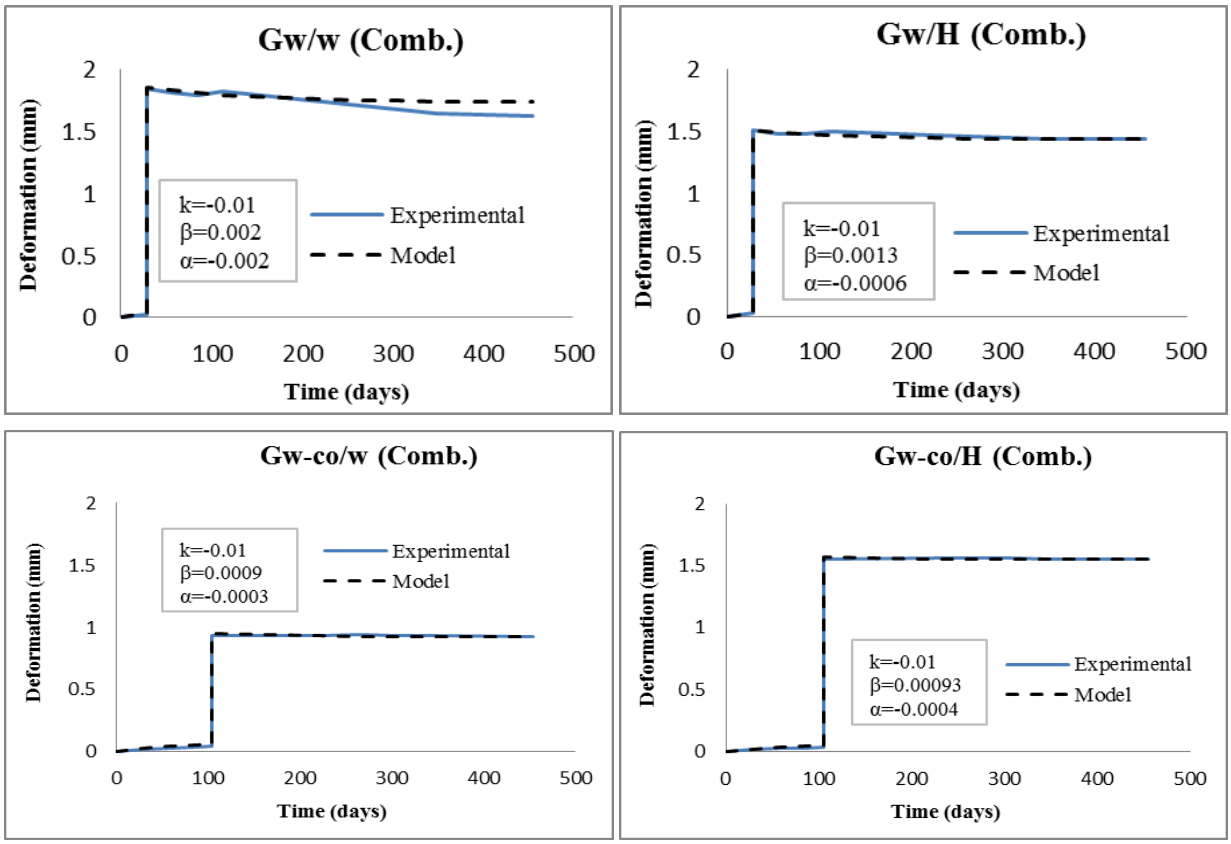

Figure 7-7 Experimental and computed deformation due to ASR and mechanical loads considering reduced E-modulus.

where $\varphi = k - \alpha$, and the deformation in Eq. (7-12) can be rewritten as:

$$\Delta l = \begin{cases} \beta(1 - e^{-\varphi t})lg & for\ 0 < t > t_{cr}^{m} \\ \beta\left(1 - e^{-\varphi t_{cr}^{m}}\right)lg + C_w - 2\beta^{*}\left(1 - e^{-\mu(t - t_{cr}^{m})}\right)l_a & for\ t > t_{cr}^{m}\ and\ \Delta C_w \leq C_w \end{cases} \quad (7\text{-}17)$$

where:

$$\beta^{*} = \beta e^{-\varphi(t_{cr}^{m})} \quad (7\text{-}18)$$

$$C_w(t) = C_w - 2\beta^{*}\left(1 - e^{-\varphi(t - t_{cr}^{m})}\right)l_b \qquad for\ t > t_{cr}^{m}\ and\ C_w(t) \geq 0 \quad (7\text{-}19)$$

Figure 7-7 illustrates the deformation in Greywacke mixes considering the reducing E-modulus induced by ASR deterioration using Eq. (7-19).

7.4 Finite element model to monitor and determine the expansion behaviour

The finite-element (FE) simulations for expansion that have been often performed are dependent on assuming fictitious thermal loading conditions, on a trial-and-error basis (Huang and Pietruszczak, 1999). In this section, FE modelling is used in an attempt to understand the behaviour of reinforced concrete subjected to expansion, and to study the mechanism of deterioration related to ASR either with or without a mechanical crack. A comparison between restrained and un-restrained concrete expansion is also considered in this model. The ASR expansion is simulated by thermal expansion. The model was applied on the Greywacke partially submerged specimens (Gw/w) described in Section 6.4.

7.4.1 Boundary conditions of the finite-element model

The simulated geometrical parts for the cracked and un-cracked samples are illustrated in Figure 7-8. A quarter of the RC prism was simulated due to symmetry. The concrete and steel were modelled, as shown in Figures 7-8(c) and (d). The reduction in steel bar diameter at the middle was considered. The model was simulated with quadratically interpolated solid, three dimensional elements. General static linear elastic analysis was performed for thermal action and the self-weight was neglected. The connection between the two surfaces of the concrete and steel was considered to be retained during the ASR process, i.e. no de-bonding or slip was allowed. This was modelled as a pinned constraint between the steel and concrete parts. The boundary conditions of the mechanical crack line in the cracked part were simulated free for concrete and continuous (i.e. fixed vertically at the symmetry boundary) for the steel bar, while in the un-cracked model it was considered as continuous for both. The same boundary condition was applied for the restrained and un-restrained model. For the latter, no steel reinforcing bar was included in the model.

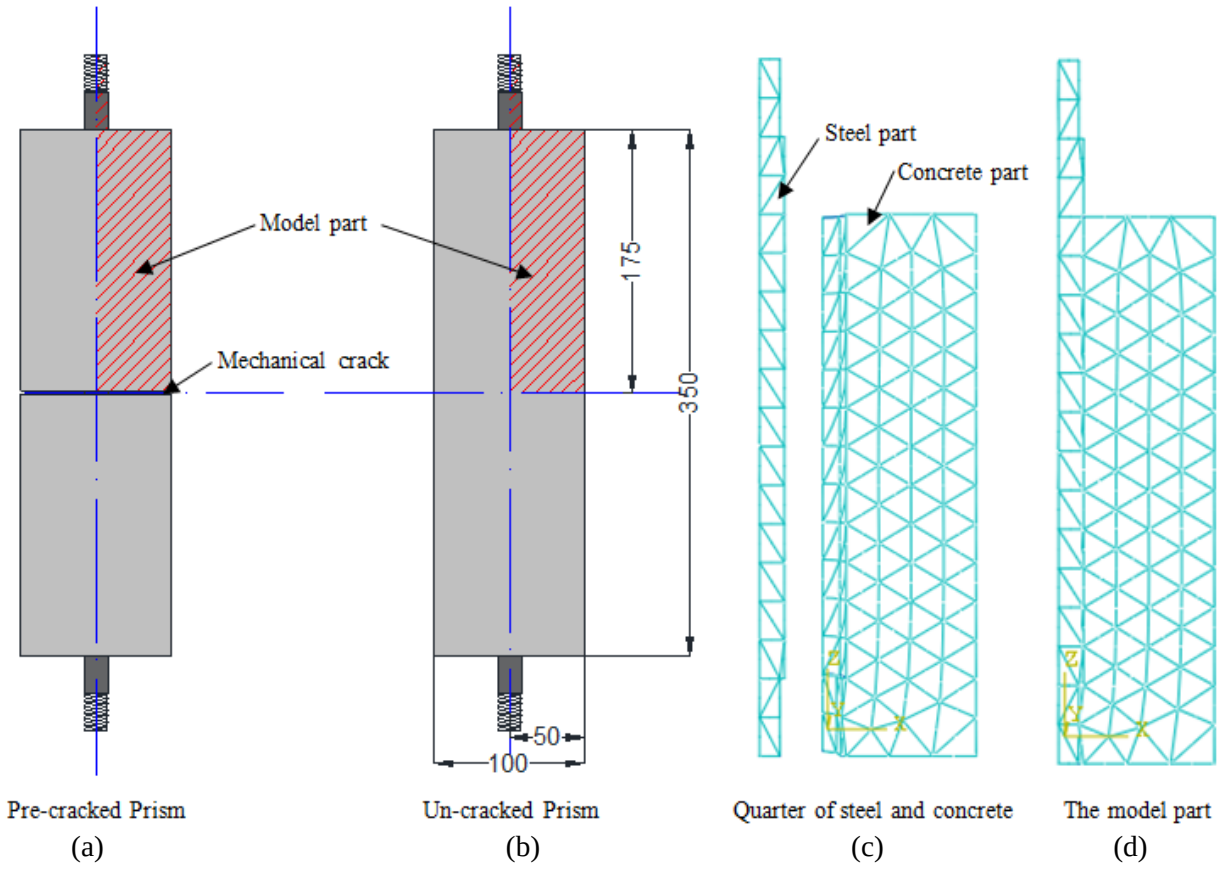

Figure 7-8 FE model schematization for (a) cracked and (b) un-cracked RC specimens, showing (c) the FE models for the rebar and concrete separately, and (d) combined.

7.4.2 Model parameters

The numerical simulations were performed based on constitutive model parameters of concrete from the experimental results in Table 7-3. Compared with the normal thermal coefficient of concrete (Section 3.7.2), the thermal expansion coefficient which simulated ASR expansion in the upper part of the specimen (in humidity) was found to be about 6.5 times, while in the lower one (in water) it was about 8.5 times. The same coefficient was used in the pre-cracked and un-cracked specimen as well as for the restrained and un-restrained specimens. The coefficients were determined in correspondence with the ASR expansion at 65 weeks according to the experimental results of the Gw/w mix. The ASR expansion in this case was calculated from the total expansion measured over 100 mm between the two pins 1 and 2 in the un-cracked regions (the top space in humidity and the bottom one in the submerged case refer to Figure 6-6). The reference temperature was considered to be 20°C and the defined temperature during the analysis was 38 °C as stipulated in the experimental condition.

Table 7-3 Finite-element properties and parameters for ASR swelling in Gw/w mix.

Properties and parameters	Calibrated values
Concrete density (kg/m^3)	2400
Steel density (*kg/m^3*)	7850
Young's modulus of concrete (*GPa*)	27
Young's modulus of steel (*GPa*)	202
Poisson's ratio υ for concrete	0.3
Poisson's ratio υ for steel	0.2
Thermal expansion coefficient simulated for concrete in humidity *(m/m °C)*x *10^{-6}*	54.5*
Thermal expansion coefficient simulated for concrete in water *(m/m °C)*x *10^{-6}*	70*
Thermal expansion coefficient of steel *(m/m °C)*x *10^{-6}*	12
Reference temperature	20 °C
Defined temperature	38 °C

**This coefficient was calculated to account for the total expansion of the concrete after 65 weeks of accelerated ASR exposure.*

7.4.3 Structural degradation and expansion mechanisms

It can be noted from the results obtained by the proposed model in Figure 7-9 that a very different behaviour occurs at the crack line in the pre-cracked RC specimen (the upper case) from that in the un-cracked specimen (lower case). In the pre-cracked case, the concrete expansion at the crack line has a curve with displacements close to zero at the reinforcement due to the restraint, while the maximum expansion is at the surface of the concrete. The expansion in the un-cracked prism at the middle was almost zero, because the expansion direction is only horizontally. The displacements at the pins were measured, and the expansive strain between the two pins at top and bottom spaces were determined by the difference between the two pins divided by the 100 mm space. In the middle space, the deflections at the crack line were identified above the crack from the upper half and under the crack from the lower half. The expansion in this space was considered as a summation of the two displacements divided by the 100 mm space including the crack. These displacements in the submerged part under the crack were larger than those above due to this more severe exposure condition. Table 7-4 shows the deformation pattern of expansion and results at different points in the pre-cracked specimen. It can be noted in this table that the middle space expansion with negative sign reflects the reduction in the pre-crack width. The calculations of the expansion in the model were compared with those from the experimental results. The expansions at the top and the bottom spaces were 0.206 and 0.263% respectively from the FE model, which are almost the same as the experimental results (0.206 and 0.264%). At the middle space, the summation of the expansion determined from both sides was 0.246%, which also nearly equal to the experimental result (0.244%).

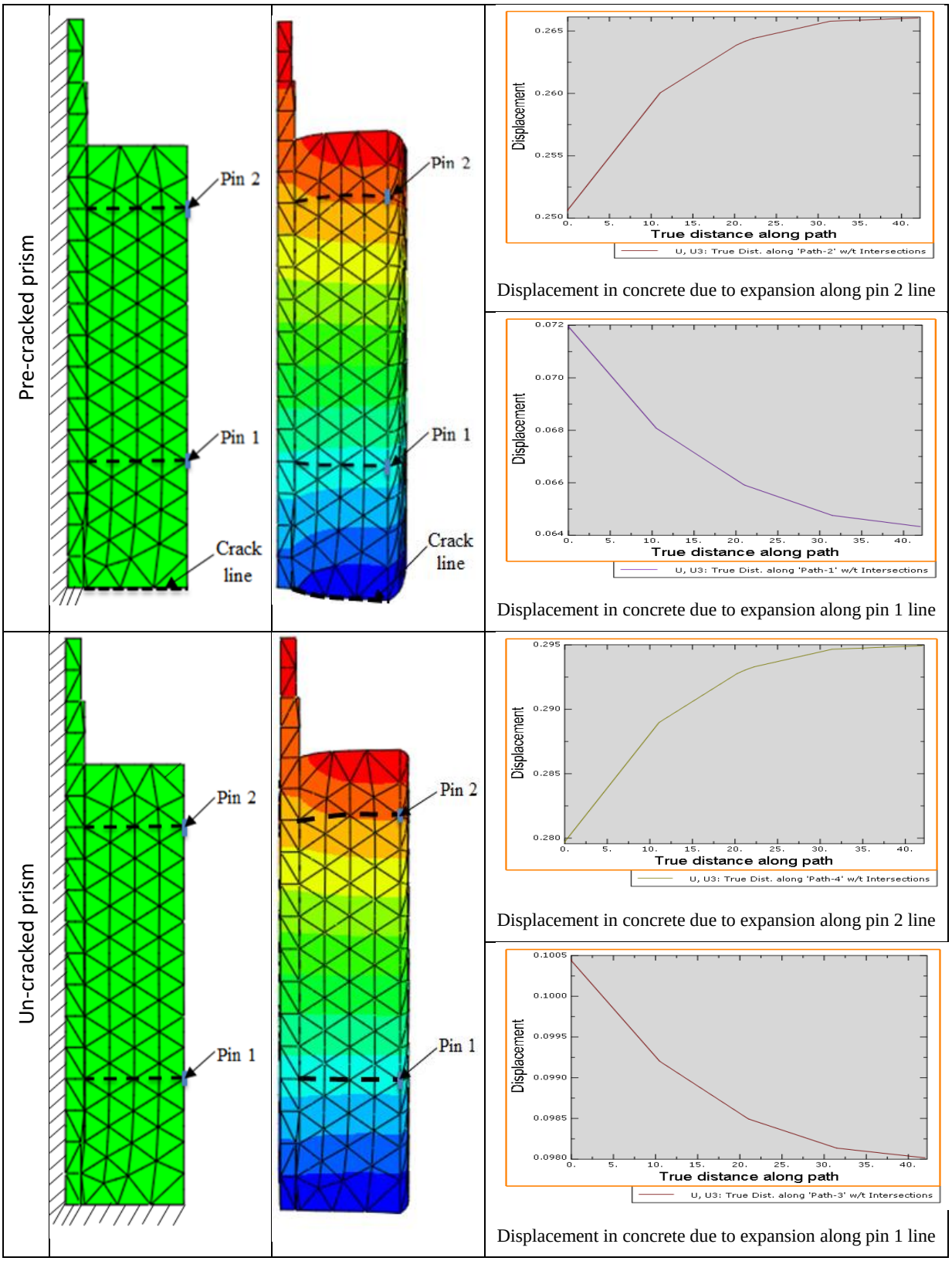

Figure 7-9 Mechanism of the expansion in concrete, for the case of mechanical crack (the upper) and for un-cracked (the lower).

Table 7-4 Finite-element deformation and expansion compared with experimental results.

Half of the specimens	Exposure	Expansion at the ends	Coefficient of expansion model	Deflection at ends Δ (mm)	Expansion between two pins over 100 mm (%)		
						Model	Exp.
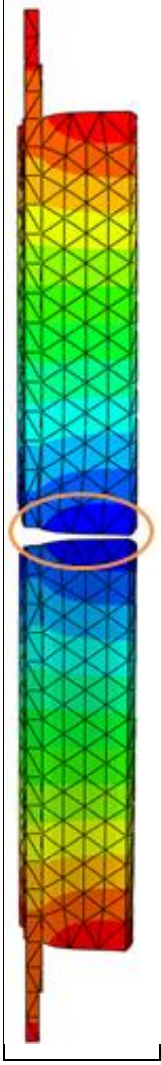	The upper half exposed to humidity >90%	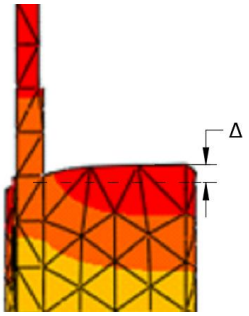	$54.5x10^{-6}$	+ 0.320	Top space	+ 0.206	+ 0.206
	The part above crack exposed to humidity and the under one in water	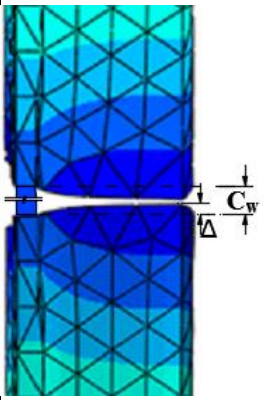		- 0.042 + 0.058	Middle space	- 0.246	- 0.244
	The lower half submerged in water	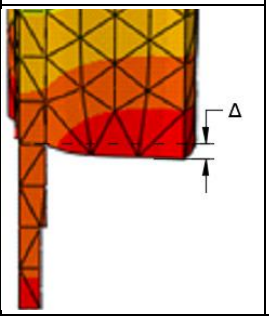	$70x10^{-6}$	- 0.408	Bottom space	+ 0.263	+ 0.264

7.4.4 Restrained and un-restrained model

Normal concrete with the same dimensions as the reinforced concrete specimen was modelled to monitor the role of the steel restraint in expansion. The same parameters, boundary conditions and mesh as for the restrained sample were applied. Figure 7-10 illustrates the deformation pattern in both cases. The expansion results on the top space of the un-restrained model were 0.229%, and 0.298% in the bottom space, i.e. more than the restrained model (0.206 and 0.263% respectively). From these results, it can be noted that the restraint of concrete reduced the ASR expansion by about 10 and 12% in humidity and submersion exposure respectively. These reduction percentages compare well with the expansion

percentage between the restrained and un-restrained concrete obtained from the thermal coefficient tests of the Gw mix in Section 3.7.2, which was about 13%. It should be noted that, the restrained and un-restrained specimens in the FE model and the thermal coefficient tests were the same. Furthermore, a different size or reinforcement level may give different ratios, for which further tests and analyses in various cases are needed.

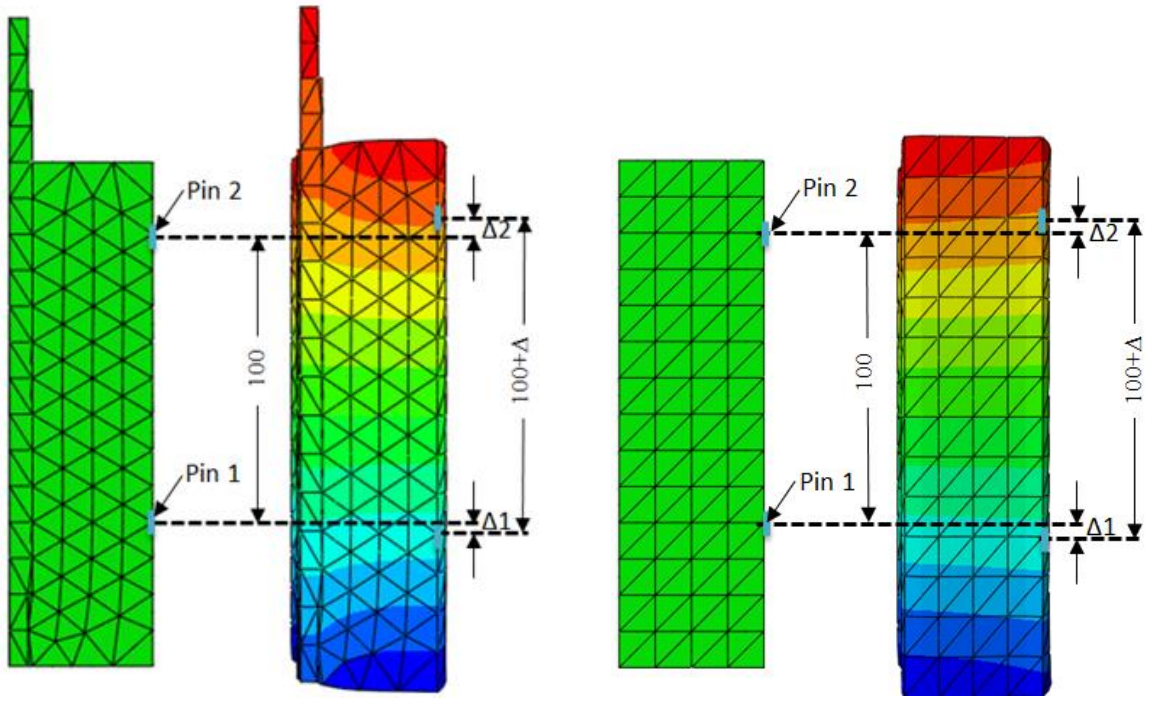

Figure 7-10 Comparison the concrete deformation between the restraint (left) and unrestraint (right)

7.5 The change in mechanical crack induced by the wedge splitting test under ASR expansion

Different measurements of wedge splitting cracks C_w were obtained as described in Chapter 5. The C_w at the mouth varied up to 700 µm as summarized in Table 5-2. An expansion occurs in the concrete due to NaOH at 80 °C and thermal expansion leads to reduction in the pre-mechanical cracks. This means the total strain ε is equal to the summation of ASR strain ε_{asr} and thermal expansion ε_T. Therefore, the ASR strain can be determined from:

$$\varepsilon_{asr} = \varepsilon - \varepsilon_T \tag{7-20}$$

At the mechanical crack area, it can be considered that half of the total strain expands into the crack namely, crack reduction (ΔC_w), and the other half expands into both side directions (see Figure 7-10 left). In constrained concretes, the ASR swelling starts to fill the spaces of the mechanical cracks. After the

mechanical cracks were filled, the ASR cracks formed. The measurements of the C_w taken by dnt camera were recorded at four weeks exposure in NaOH and hot water at 80 °C and the results are presented by exponential curves in Figures 5-7 and Figure 5-9 presented the percentage of reduction. The mechanism of the ΔC_w in Figure 7-10 (right) is represented by an exponential curve, indicating that the small cracks are faster reducing than larger crack widths. The ΔC_w in the plan and free stress can be written:

$$\Delta C_w = \tfrac{1}{2}\varepsilon l \tag{7-21}$$

With l is width of the concrete sample. To determine ΔC_w, the expansion due to hot water (80 °C) is subtracted from the total strain recorded at exposure of NaOH at 80 °C as follows:

$$\Delta C_w = \tfrac{1}{2}((\varepsilon_{asr} + \varepsilon_T) - (\varepsilon_T)l \tag{7-22}$$

The total ΔC_w recorded of mouth and mid in Figure 5-9 is presented in Figure 7-11 (right: Gw/A and Gw/w while in the left: Gw-co/A and Gw-co/w). Reduction of the narrower cracks (<200 µm) is presented by linear trend, and the larger cracks presented by a power trend. The same data are presented alternatively by the exponential curve in Figure 7-12. The ΔC_w is considered as the areas between the two curves. By subtracting the curves induced by temperature from those induced by NaOH and temperature (Figure 7-12 left and right) by substituting these curves in Eq. 7-22, the ΔC_w induced by ASR in Gw mix can be written:

$$\Delta C_w(Gw) = 4.4957e^{0.002(C_w)} \tag{7-23}$$

And for Gw-co mix, the ΔC_w is equal to:

$$\Delta C_w(Gw - co) = 2.9589e^{0.002(C_w)} \tag{7-24}$$

The results from Eqs. (7-23 and 7-24) are presented in Figure 7-13.

Note that the crack width starts at 50 µm and ends at 700 µm which is based on the recorded crack widths. The time of exposure is four weeks. Different exposure times might produce different results. To represent the crack width Cw(t) at any time, the kinetic law can be used by considering that the reduction of the cracks is changed according to the crack width. The crack width at a particular time can be written as a function of time and crack width induced by ASR:

$$C_w(t) = C_w - \tfrac{1}{2}\beta\left(1 - e^{-kt}\right)l \times (he^{-iC_w}). \tag{7-25}$$

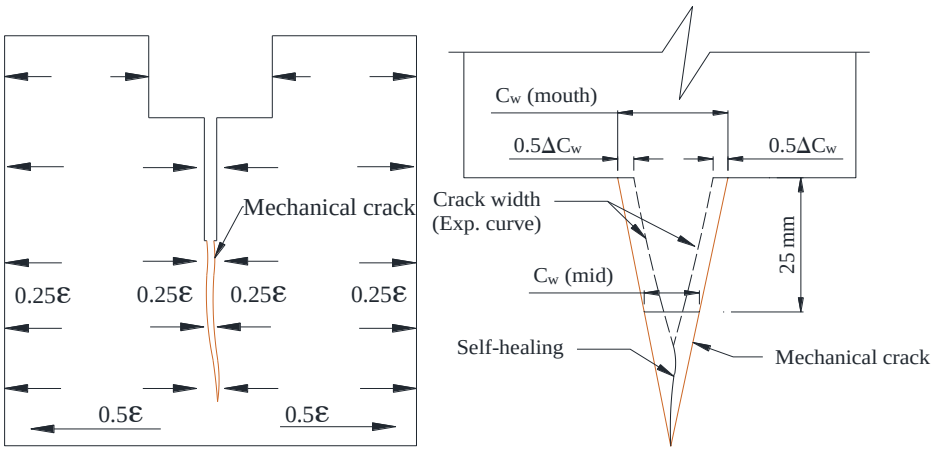

Figure 7-11 The supposed mechanism of the concrete specimen deformation due to pre-cracking and ASR, left: distribution the expansive ASR and thermal strain and right: distribution and mechanisms of crack reduction.

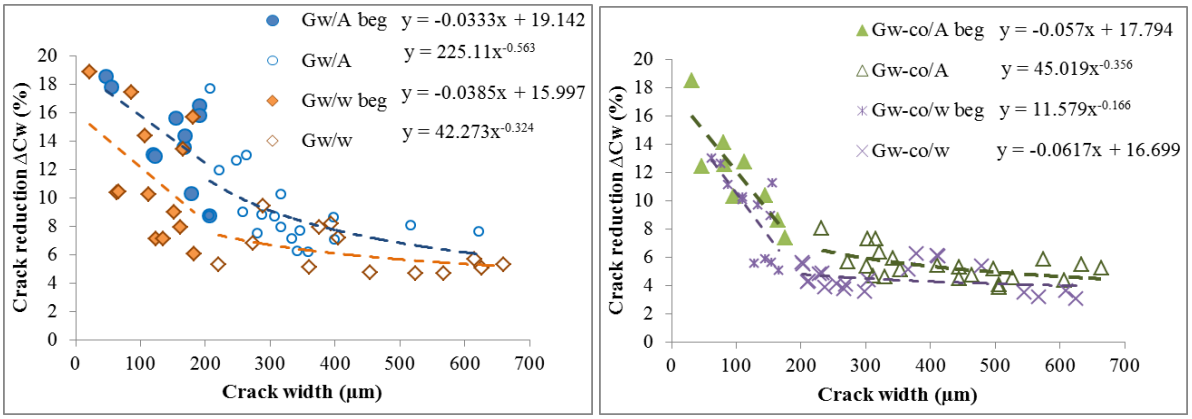

Figure 7-12 The reduction of all the crack widths ΔC_w (mouth and mid) vs crack width due to ASR and water at 80 °C after 4 weeks of exposure. The narrower cracks (<200 µm) presented by linear trend and the larger cracks presented by power trend.

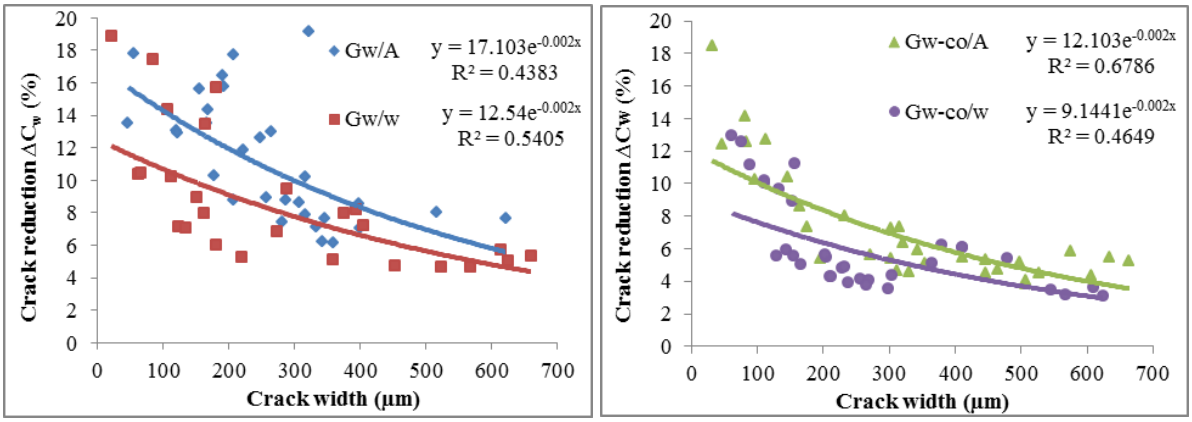

Figure 7-13 The reduction of all the crack widths in last figures presented alternatively by the exponential curve.

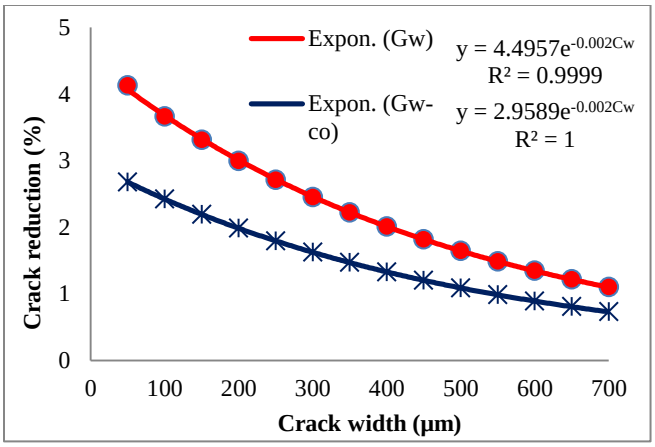

Figure 7-14 The reduction of the crack width ΔC_w vs crack width due to ASR.

The last part (he^{-iC_w}) is the crack reduction determined in Figure 7-13. The difficulty here is finding the experimental crack width caused by only ASR over time to compare the results with this model. The parameters k and β are supposed to have different values than for the previous model in RC due to the different conditions (temperature and exposure time).

7.6 Conclusion

Two series models were proposed to simulate the ASR expansion in presence of mechanical cracks. The first Series model was on the RC beams described in Chapter 6 which were subjected to ASTM C 1293 conditions. This model simulates the change over the central length of 100 mm (middle space) of the specimens in ASR and combined action based on kinetic law. Some characteristics were identified from the experimental results and compared with the model proposed. The degradation of the E-modulus was taken into account for the mixes containing Greywacke stone as it reduced under ASR exposure, while for the mixes containing Granite stone it was not considered, because it continued to increase and after roughly 200 days, it started decreasing. The quarter of the prism was simulated by finite element model to monitor the behaviour of the concrete expansion with and without pre-crack, as well as with and without restraint. Results obtained from both, the experimental and the FE model were in close agreement. The second Series model was only applied on the pre-cracked plain concrete cubes subjected to ASTM C 1260 conditions. The equations obtained from this model were used to determine the width reduction of the pre-crack under ASR expansion after 4 weeks of exposure to ASR conditions. The role of thermal expansion was taken into account by subtracting the crack reduction (ΔC_w) of the specimens subjected to hot water from those subjected to NaOH aqueous solution at the same temperature (80 °C). The ΔC_w equation, represented by the exponential curve, showed that the width of smaller crack is reduced more than that of larger cracks.

CHAPTER EIGHT

8. CONCLUSION

8.1 Introduction

In this study an experimental study was designed to investigate the combined action of mechanical loading and ASR on concrete. Reactive (Greywacke) and non-reactive (Granite) stone types were used as coarse aggregates, while Malmesbury and Philippi were used as the fine aggregates. Ground Granulated Corex Slag (GGCS) was used to replace 50% by weight of the cement (CEM I 52.5) in half of the specimens. Two methods of accelerated testing, ASTM C 1260 (series test 1) and ASTM C 1293 (series test 2) were used. The flow diagram in Figure 8-1 illustrates the experimental program. The specimens in different mixes are denoted: Gw, Gn, Gw-co and Gn-co, for Greywacke, Granite, Greywacke with slag and Granite with slag mixes respectively. The /w, /H and /A present the exposure in water, humidity and ASR respectively.

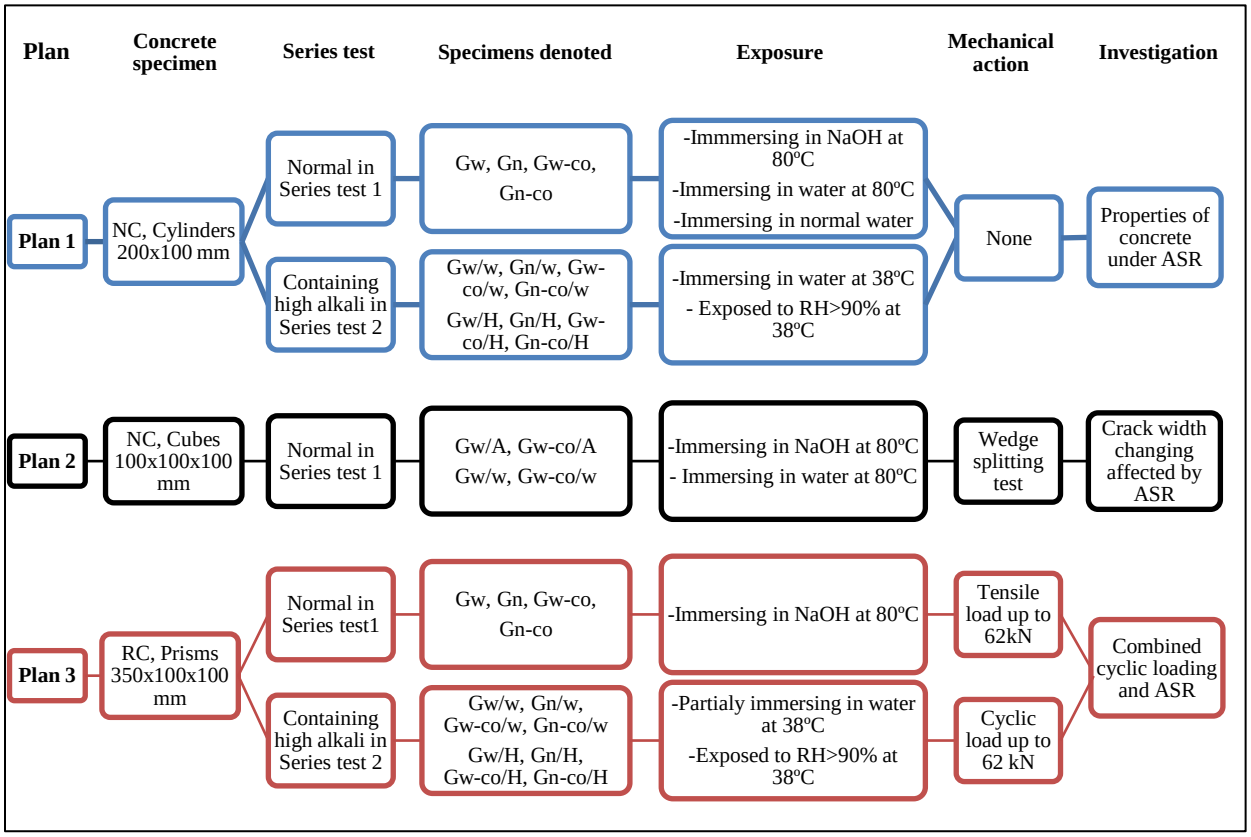

Figure 8-1 Flow chart of the experimental work

8.2 Summary of findings

8.2.1 Preliminary tests

The most important tests that were conducted in the experiments are:

1. **ASTM C 1260 test**: to conduct this test, mortar bars of 25x25x260 mm were made of cement combined with Greywacke, Granite, Malmesbury or Philippi aggregates. The test results show that the Greywacke stone causes the highest expansion while the Philippi and Malmesbury sands were not affected by the ASR condition. The expansion of Greywacke aggregate at 14 days was 0.30% and can be classified as nocuous and deleterious in field performance, while the Granite expansion was less than 0.1% which is indicative of innocuous behaviour in most cases.
2. **Coefficient of thermal expansion test:** this test were conducted according to Danish T1-B method and performed on restrained and un-restrained concrete prisms of 100x100x350 mm. The restraint was provided by a central, embedded steel reinforcing bar with 16 mm diameter. The concrete test specimens contained Greywacke and Granite coarse aggregate. The results show that the thermal expansion in restrained concrete was less than that of un-restrained concrete. The thermal coefficient for restrained and un-restrained Gw specimens were $8.4x10^{-6}$ and $9.7x10^{-6}$ respectively, while for the Gn specimens were $9.4x10^{-6}$ and $10x10^{-6}$ respectively.

8.2.2 Plan 1 –properties of ASR affected concrete

Concrete cylinders in Plan 1 were prepared with different aggregate and binder compositions to investigate mechanical and chemical properties of concretes subjected to various conditions of ASR exposure.

1. In the Series 1 test, the cylinders were submerged in 1 N NaOH at 80 °C and compared with others submerged in hot water (80 °C) and normal water (23±2 ^{o}C). The results at 14, 28 and 56 days showed that in these accelerated test conditions, the ASR and high temperature have an effect on the strength degradation of Gn specimens more so than in the other mixes. The E-modulus is slightly affected by NaOH. In all mixes, the E-moduli were lower than those of specimens cured in normal water at 14 days. It is observed that the strength in Gn mixes was more affected by the high temperature and that the E-modulus in Gn mixes decreased with age.
2. In the Series 2, the concrete itself contained high alkaline content and was submerged in water and compared with others in RH>90% at 38 °C. The tests were carried out at 1, 3, 7 and 12 months. The strengths after seven months were slightly decreased in Gw/w and Gn/w and increased in Gw-co/w and Gn-co/w. The strength of specimens after seven months exposure to humidity was slightly higher in all mixes. The E-modulus decreased over time due to ASR in the mixes made of Greywacke stone, with the largest decrease observed for Gw/w. However, this decrease was less in the mixes under

humid conditions than in those submerged in water. It was also less in the mixes containing Corex slag. On the other hand, the E-modulus in the mixes made of Granite stone, showed an increase until the 7th month and then started decreasing. Similar to Greywacke mixes, the humidity and slag content in Granite mixes also showed less reduction in E-modulus.

3. XRF tests were only monitored in Series 2 and conducted on the samples of crushed concretes taken from the middle of cylinders according to Series test 2 at 1, 8 and 12 months. The results indicate that there are increases in SiO_2 and reductions in the CaO content for all mixes. Also, the alkali content (Na_2O and K_2O) increases which replaces the loss in CaO. The CaO leaches in the water even in the presence of humidity only where the pH of water in both conditions at 8 months transformed to high alkali concentrates.

8.2.3 Plan 2 – ASR effect on mechanically cracked concrete

Two concrete mixes made of Greywacke stone and Philippi sand namely Gw and Gw-co were cast. The cubes were submerged in NaOH solution according to Series 1 test, 24 h after casting. The specimens were extracted from NaOH after 7 days and subjected to wedge splitting to obtain cracks with pre-determined widths and then returned to their exposure. High resolution photographs were taken with a dnt camera to measure the crack widths directly after 1, 2 and 4 weeks of being cast. Subsequently, the changes in mechanical cracks due to NaOH were compared with the same cracks in the specimens that were submerged in hot water (both at 80 °C). Also, a comparison was made between the mixes cast with cement only (Gw) and those blended with Corex slag (Gw-co). The results showed that the splitting crack widths were reduced due to ASR and thermal expansion in concrete. The smaller crack widths reduced more than the larger ones due to self-healing. Generally, the crack width reduction decreased due to ASR in concrete specimens containing Corex slag.

8.2.4 Plan 3 – ASR effect on mechanically cracked reinforced

The concrete prisms were prepared with different aggregates and subjected to combined action in Series tests 1 and 2. The following observations are made:

1. The final results of the expansion in the RC specimens in Series 1 subjected to ASR or combined action of ASR and tensile load show that the Gn specimens expanded more than the Gw specimens. These results are unlike those obtained from the ASTM C 1260 test and may be due to the following reasons:
   a. The mixture with Granite stone and Philippi sand (Gn) was affected by temperature more than the mixture with Greywacke stone and Malmesbury sand (Gw), as became apparent when the specimens were removed from the NaOH and kept at laboratory temperature. It was also observed

that after one week in hot water, the Gn specimens were more expanded. This was confirmed by the higher coefficient of thermal expansion for Gn than for Gw;

b. The stiffness of Gn is affected more by high temperature than Gw according to the tests results in Section 8.2.2.

2. RC prisms containing high alkaline (NaOH) were tested in Series test 2 for the ASR potential and combination of ASR with cyclic loading which caused crack widths between 0.8 and 4 mm in the middle of the samples. The results obtained at the end of 65 weeks showed that the mechanical pre-cracks played a significant role in concrete deformation due to the ASR. The reduction of crack widths and the expansion of concrete were of different values for the various mixes. These reductions and expansions were largest in Gw and the smallest in Gn-co specimens. Also, the expansions were affected by water more than in humid conditions. When considering that the expansion starts after a mechanical load is applied, the maximum combined deformations were less than those in ASR specimens due to the macrocrack in the middle of combined specimens.

Table 8-1 compares the expansions of ASR in Gw and Gn concrete samples in both series tests at different conditions and exposure times.

8.2.5 The different results from the two series tests

The two series tests (ASTM C 1260 and ASTM C 1293) produced different results. These differences have been observed in ASR affected mechanical properties, as well as mechanical crack width reduction. Table 8-2 summarizes the comparison of mechanical properties and the expansion investigated by the two series tests. There is a difference between the two series methods. These are:

1. The 56 days submersion in Series 1 may not be long enough to reach the change in the mechanical properties of RC, unlike in the Series 2;
2. Reduction and self–healing occur more in small cracks than the larger ones due to ASR expansion and more at high temperature. Therefore, the healing is more in Series 1.

Table 8-1 Comparing the expansion due to ASR in the two series methods (%).

Series test	According to ASTM C 1293 (series1)		According to ASTM C 1260 (series 2)	
Conditions	Submerging in 1N NaOH at 80°C		Partially submerging in water /w (38 °C)	Exposed to humidity close to 100% /H (38 °C)
Sample	Standard test (mortar bar)	RC (prism)	RC (prism)	RC (prism)
Exposure time (d)	14	70	455	455
Gw	0.300	0.016	0.190	0.155
Gn	0.030	0.066	0.097	0.078

Table 8-2 Comparing the mechanical properties degradation and expansion due to ASR in the two Series methods.

Parameters	Series test 1	Series test 2
Condition	• Submersing in 1N NaOH at 80 °C	• Fully or partially submerging in water at 38 °C • Exposed to humidity close to 100% and 38 °C
E-modulus (Cylinders)	Concrete with Granite (Gn) reduces after 14 days while those containing Greywacke and those containing Granite with Corex slag are not significantly changed during the exposure days (56).	Concrete containing Greywacke reduce significantly more than those containing Granite. Greywacke mixes decreased from early age while Granite mixes only decreased after about 7 months. In particular the case for Greywacke concrete submerged in water reduced significantly more than exposed to high RH.
Strength (Cylinders)	Granite mix (Gw) had the lowest strength of all mixes. The Granite with Corex slag (Gn-co) was almost the same strength as Greywacke mixes at 14 days of exposure. At 56 days, the two Greywacke mixes are slightly more increased than the two Granite mixes. The strength is not significantly affected by ASR expansion.	All Granite and Greywacke concrete strengths in both conditions are almost the same and increase over the first 3 months of exposure. Strength of Granite mixes is increased more significantly than Greywacke mixes after 3 months. All mixes (submerged or humid) from 7 to 12 months are not significantly changed.
Expansion (prisms)	Gn at 70 days is more expansive than Gw, Gw-co and Gn-co mixes by 75.7, 87.8 and 68% in ASR exposure and by 53.5, 77 and 56% in combined action respectively. At 70 days, the mixes Gn, Gn-co, Gw and Gw-co in combined action were more expansive than the same mixes in ASR by 7, 32, 51.5 and 50% respectively.	In partially submerged at 455 days, Gw/w is most expansive, more than Gn/w, Gw-co/w and Gn-co/w by 52, 46 and 70% in ASR and 60, 56 and 74% in combined action respectively. In humidity exposure at 455 days, Gw/H more expansive than Gn/H, Gw-co/H and Gn-co/H by 53, 56 and 63% in ASR and 64, 58.9 and 70% in combined action respectively. The submerged mixes Gw/w, Gn/w, Gw-co/w and Gn-co/w were more expansive than the same mixes in humidity Gw/H, Gn/H, Gw-co/H and Gn-co/H by 14.6, 16, 30 and -5.8% in ASR respectively and by 15, 23.9, 19.7 and 1.8 in combined mixes respectively.
Wedge splitting (cubes)	The mechanical cracks were reduced due to ASR expansion in Gw more than that in Gw-co. The narrower cracks were faster reduced than the larger ones.	Not tested

8.3 Conclusion

The evaluation of the potential reactivity in the concrete affected by ASR and mechanical loading depends on the test conditions. Different outcomes have been obtained from the two series methods. The phenomena observed in this experimental program can be divided into: mechanical crack reduction induced by ASR, the effects of concrete properties under ASR expansion and the difference in the results between the two series tests.

8.3.1 Mechanical crack width reduction affected by ASR

It is observed from the experiments that the mechanical crack reduces over time due to ASR expansion. The reduction in the mechanical cracks can be captured by the following factors.

8.3.1.1 Geometrical deformation assumed in crack reduction and modelling

The two experiments to investigate the change in crack width (RC beam and split cubes) have different assumed geometries of deformation. The model of crack reduction in RC beams at 38 °C and submerged or exposed to high RH is assumed as straight formed from the surface to the reinforcement. Subsequently, considering that the concrete affected by ASR is constrained at the reinforcement and expanded on the surface into the mechanical crack leads to reduction in this crack. In-plain concrete, subjected to wedge splitting and submerged at 80 °C, the mechanical cracks are assumed to be formed as a triangle, free at the mouth and constrained at the bottom.

8.3.1.2 Effect of exposure on the crack reduction

The widths of mechanical cracks in specimens under ASR are varied in different samples and exposure. The change in crack width according to the various concrete samples can be described as:

1. In Series 1 of Plan 3, the RC beams subjected to 62 kN of static tensile load and submerged in NaOH at 80 °C caused small cracks (12-60 µm). These cracks were self-healed after weeks of exposure in all mixes and the change in the crack width has not been investigated. In Series 2 of Plan 3, the RC specimens were subjected to 62 kN of tensile cyclic loading caused macro-cracks (800-4000 µm). In this series, the investigated crack widths were reduced in the submerged specimens more than those exposed to the moisture in the same sample types at the same temperature (38 °C).
2. The crack widths in cubes (wedge splitting test) were reduced in the specimens submerged in NaOH at 80 °C more than the others submerged in hot water at the same temperature.

From the two exposures above, it can be deduced that the temperature and submersion are the factors that contribute to more crack width reduction with ASR expansion.

8.3.1.3 Effect of aggregate reactivity and concrete restraint on the crack reduction

More reactivity in aggregates to ASR leads to further expansion and consequently to a reduction in the crack width. The mechanical crack width in RC specimens with Greywacke stone were reduced more than those in the Granite specimens at 38 °C in Series test 2. From the FE analyses and thermal coefficient test, the results confirmed that the restrained concrete experiences less expansion than the un-restrained concrete.

8.3.1.4 Effect of the initial crack width on the crack reduction

The initial crack width also plays a role in the crack reduction over time due to ASR. The relationship between the initial crack width and the crack reduction was only investigated in the wedge splitting cracks at 80 °C. It is found that the small initial cracks reduced more than larger cracks. The crack reduction in percentage has been modelled as an exponential curve decreasing with increased initial crack width.

8.3.1.5 Effect of the concrete binder composition on the crack reduction

The reductions of mechanical cracks are affected by binder composition in concrete. In both series tests RC beams at 38 °C and plain concrete cubes at 80 °C, the mechanical crack width reduction has been found to increase less when Corex slag was added to the mixes than those only containing CEM I.

8.3.2 Effects of mechanical concrete properties under ASR expansion

The mechanical properties of concrete are affected by ASR deterioration. Compressive strength and E-modulus were investigated in two series tests (at 80 °C and 38 °C).

8.3.2.1 Degradation of the concrete compressive strength due to ASR

To determine the effect of ASR exposure to concrete, reference specimens were made and tested at the same ages as ASR exposed specimens. At high temperature (80 °C), the compressive strength at 56 days in Granite mixes increased less than the Greywacke mixes. At 38 °C after 455 days, the compressive strength of Greywacke mixes were more degraded. In Series test 1, adding Corex slag to both mixes of Granite and Greywacke increases the strength more than those without slag, while, in Series test 2 the compressive strength is the lowest when the Corex slag is added to the same mixes.

8.3.2.2 Degradation of the concrete E-modulus due to ASR

There are relationships between the expansion of ASR and stiffness degradation, where the increase of ASR expansion leads to decrease in the E-modulus. The E-modulus were reduced in Granite mixes over time and increased in Greywacke mixes at 80 °C (Series 1) until 56 days in NaOH. However, the Greywacke mixes at 38 °C (Series 2) were reduced from an early age (a few weeks after exposure) and in

the Granite mixes were reduced after roughly 200 days at the same temperature. The Young's modulus (E) is less affected by ASR when the slag is added in both mixes in series test 1. It is noted that the Granite mixes in Series 1 were more expansive than the Greywacke mixes. In Series 2 the Greywacke mixes were more expansive, and this confirms that more expansion (thermal or ASR) means more E-modulus degradation.

8.4 General concideration of the experimental program

The general conception of the experimental series can be concluded to be:

1. The conditions in the accelerated method to test for ASR potential (ASTM C 1260 test) do not present a true simulation of ASR in the field and, therefore, using the same condition may give unreliable results. It may nevertheless help in understanding the behaviour of ASR in concrete;
2. The compressive strength is not a good indicator to predict the ASR deterioration, unlike the Young's modulus (E), which provides the signs of ASR effects;
3. ASR deteriorations are more when the concrete is submerged than when exposed to the moisture;
4. Greywacke mixes expand more than Granites mixes due to ASR;
5. The mechanical crack reduces over time due to the ASR swelling. Self-healing in small cracks appears to lead to faster reduction in crack width than in larger cracks.

8.5 Summary of Contributions

The work presented in this thesis contributes to improving the assessment and understanding of the mechanisms of ASR effects under mechanical loading. The main findings are:

1. Indication of what tests should be carried out on a given aggregate to determine its potential reactivity and usually what criteria should be followed to assess methods of mitigating aggregate reactivity if needed;
2. Indication of what materials and mixture proportions could be used to control ASR;
3. Models to estimate the ASR expansion in presence of mechanical cracks. The estimation is based on knowing the mechanical crack width and concrete materials, noting that the parameters in these models were found for Greywacke and Granite stone;
4. Devising models for estimating the reduction of mechanical crack width induced by ASR expansion, based on original crack width and remaining reactivity of the aggregate used;
5. Confirming that the ASR process in presence of mechanical action that leads to cracking is altered from when it is evaluated as a separate action. The mechanical loading may cause micro-cracks that lead to ingress of moisture into the concrete;

6. Indication that the small mechanical cracks, roughly less than 0.2 mm wide in concrete affected by ASR are self-healed unlike the large cracks. The remaining open cracks may lead to undesirable ingress of gases and/or water into the concrete, which must be addressed by repair intervention strategies.

8.6 Future Research

Further research aimed at evolving studies on the effects of the mechanical and ASR actions to promote the understanding of the combined action as an integral part of the problems in concrete. These include studies on:

1. The role of the temperature in the ASR expansion especially when using a fine aggregate with the Granite stone in ASTM C 1293 series test;
2. The changes in wedge splitting cracks under Series test 2 conditions.
3. The combined action of ASR affected concrete in marine conditions (salt water and high humidity) and investigating the change in corrosion rate;
4. The combined action on other concretes such as fiber concrete;
5. Validation of the models for crack reduction by other tests on different types of aggregates;
6. Identifying elastic materials which to be used to fill the mechanical cracks and which allow ASR expansion to freely close the crack without further pressure build-up, while preventing deleterious matter from entering the concrete through the cracks.

8.7 Recommendation

There are two opportunities to prevent or mitigate ASR and mechanical cracks. The first is through the appropriate design by taking the necessary precautions for structural performance and through the proper use of materials in the new concrete mixture to prevent the deterioration of the concrete. The second is the repair and structural strengthening once cracks or ASR deterioration occur and depend on the outcome of the structural condition assessment.

Standard methods to prevent ASR are to limit total alkali content, or to avoid the use of reactive aggregate, or to carefully match the alkali content to the level of reactivity of the available aggregate. The major treatment of ASR-affected structures is to prevent water ingress, one prerequisite for the reaction. The treatment should permit the water already in the structure to leave the concrete to ensure that the reaction does not continue. This means that the treatment must be permeable to water vapor and impermeable to liquid water.

Further information about suggested methods for ASR and crack mitigation is described in Appendix A.

References

Abe, Michihiko, Mikio Wakasugi, Masashi Tanaka, and Hideki Kamimoto, 1992, "The Effect of Surface Coating on Inhibition of Alkali-Silica Reaction, Rehabilitation of Concrete Structures" , *International RILEM/CSIRO/ACRA Conference* (Melbourne, Australia): 409–414.

ACI Committee 221. 1998, "State-of-the-Art Report on Alkali-Aggregate Reactivity", *American Concrete Institute (ACI)*, 98, (Reapproved, R-98):1–31.

ACI Committee 224, 2001, "Control of Cracking in Concrete Structures", *American Concrete Institute (ACI)* (R-01): 1–46.

Aldea, C., S. Shah, and A. Karr, 1999, "Effect of Cracking on Water and Chloride Permeability of Concrete." in *J. Mater. Civ. Eng* : 181–197.

Alexander, MG, H. Jaufeerally, and JR Mackechnie, 2003, "Structural and Durability Properties of Concrete Made with Corex Slag", *Published by the Department of Civil Engineering, University of Cape Town* (6): 1–30.

ASTM C1293, 2008, "Determination of Length Change of Concrete Due to Alkali-Silica Reaction", *American Society for Testing and Materials (ASTM) international*, Annual Book of ASTM Standards, 100 Barr Harbor Drive, PO Box C700, West'; Conshohocken, PA 19428·2959, United States.

ASTM C 1260, 2007, "ASTM, Standard Test Method for Potential Alkali Reactivity of Aggregates (Mortar-Bar Method, D)", *American Society for Testing and Materials (ASTM) international*, Annual Book of ASTM Standards, 100 Barr Harbor Drive, PO Box C700, West'; Conshohocken, PA 19428·2959, United States.

Bangert, Falko and Gunber Meschke, 2001, "A Coupled Hygro-Chemo-Mechanical Damage Model for ASR-Affected Concrete", *Institute for strctural mechanics, Ruhr University Bochum, Germany*: 1-8

Carles-Gibergues, André and Martin Cyr, 2002, "Interpretation of Expansion Curves of Concrete Subjected to Accelerated Alkali-Aggregate Reaction (AAR) Tests", *Cement and Concrete Research* 32(5):,691–700.

Cavalcanti, A.J.C.T. and Silveira, J. F. A, 1989, "Investigations on the Moxoto Powerhouse Concrete Affected by Alkali-Silica Reaction.", in *Proceedings of the 8th International Conference on Alkali-Aggregate Reaction in Concrete, Kyoto, Japan*,797–802.

Charpin, Laurent and Alain Ehrlacher, 2012, "A Computational Linear Elastic Fracture Mechanics-Based

Model for Alkali-Silica Reaction" , *Cement and Concrete Research* 42(4): 613–25. Retrieved (http://dx.doi.org/10.1016/j.cemconres.2012.01.004).

Chen, Jingru, Xiaocui Song, Tiejun Zhao, and Li Tian, 2010, "Service Life Prediction of Lining Concrete of Subsea Tunnel under Combined Compressive Load and Carbonation", *Journal Wuhan University of Technology, Materials Science Edition* 25(6):1061–64.

Croce, Pietro, Malakatas N., 2010 "EN 1991 – Actions on Bridges." in *Eurocodes Background and application, Vienne, 4-6 October*.

Cyr, Martin and André Carles-Gibergues, 2002, "Normalized Age Applied to AAR Occurring in Concretes with or without Mineral Admixtures" , *Cement and Concrete Research* 32(11):1771–82.

Davis, D. and M. Alexander. 1989. "Properties of Aggregate in Concrete", Part 1, *Hippo Quarries Technical Publication, An Anglo-Alpha Company*, South Africa, ISBN: 0620139897.

Davis, D. and W. Coull. 1991. "Alkali-Aggregate Reaction", Second edition, *Hippo Quarries Technical Publication, An Anglo-Alpha Company*, South Africa, ISBN:0-62015826-X.

Ekolu, S. O., 2009. "Contribution to Diagnosis of Alkali-Silica Reaction in a Bridge Structure." in *2nd international conference on Concrete Repair, Rehabilitation and Retrofitting (ICCRRR)*. London: Taylor & Francis Group, ISBN 978-0-415-46850-3: 597–602.

Eskridge, Amy E., Jeremy T. Klahorst, Richard E. Klingner, and Michael E. Kreger, 2005, "Mitigation Techniques for In-Service Structures with Premature Concrete Deterioration", *Synthesis Report, conducted for the Texas Department of Transportation*, Research Project 0-4069,*October* 7(106): 273–281.

Esposito, R. and M. A. Hendriks, 2012, "Degradation of the Mechanical Properties in ASR-Affected Concrete : Overview and Modeling." Pp. 1–11 in *Numerical Modeling Strategies for Sustanable Concrete Stractures (SSCS)*, Aix-en-Provence, France.

Fan, Shenfu and John M. Hanson, 1998, "Effect of Alkali Silica Reaction Expansion and Cracking on Structural Behavior of Reinforced Concrete Beams" , *ACI Structural Journal* 95(5): 498–505.

Feng, X., M. D. A. Thomas, T. W. Bremner, K. J. Folliard, and B. Fournier, 2010, "Summary of Research on the Effect of $LiNO_3$ on Alkali-Silica Reaction in New Concrete" , *Cement and Concrete Research* 40(4):636–642. Retrieved (http://dx.doi.org/10.1016/j.cemconres.2009.08.021).

FHWA, Federal HighWay Administration, 2010, "Alkali-Silica Reaction in Transportation", *FHWA-HIF-09-001*, Retrieved (http://www.pdhengineer.com/pages/C-6011.htm).

Folliard K.J., M.D.A. Thomas, B. Fournier, K.E. Kurtis, J. H.Ideker, 2007, "The Use of Lithium to

Prevent or Mitigate Alkali-Silica Reaction in Concrete Pavements and Structures." *Federal Highway Administration* (FHWA-HRT-06-133):47.

Fournier, B., M. Bérubé, M. Thomas, N. Smaoui, and K. Folliard, 2004, "Evaluation and Management of Concrete Structures Affected by Alkali–Silica Reaction - A Review." *Seventh CANMET/ACI International Conference on Recent Advances in Concrete Technology*, Farmington Hills, Michigan.

Fournier, B., M. D. A. Thomas, K. J. Folliard, M. A. Bérubé, and A. Seminário, 2010, "Recent Developments in the Prevention and Mitigation of AAR in Concrete Outline of the Presentation." in *Alkali-aggregate reaction - Causes, diagnosis and solutions, CBC IBRACON*.

Franz-Josef Ulm, Olivier Coussy, Li Kefei, Catherine Larive, 2000, "Thermo-Chemo-Mechanics of ASR Expansion Concrete Structures." *Journal of Engineering Mechanics* 126 (March):233–242.

Fulton's Concrete Technology, 2009, "Deformation and Volume Change of Hardened Concrete", Edited by: Alexander M., Beushausen, Hans, Pp. 111–54 in Ninth edition.

Fujii, Manabu, Kasuo Kobayashi, Toyoaki Miyagawa, and Makoto Hisada. 1989. "Surface Treatment for Concrete Structures Damaged By Alkali-Aggregate Expansion," Proceedings." Pp. 875–880 in *International Conference on Alkali-Aggregate Reaction*.

Garcia-Diaz, E., J. Riche, D. Bulteel, and C. Vernet, 2006, "Mechanism of Damage for the Alkali-Silica Reaction." *Cement and Concrete Research* 36(2):395–400.

Gerhardus H. Koch, Michiel P. H. and and Neil G.Thompson; Y.Paul Virmani; J. H.Payer Brongers, 2002, "Corrosion Costs and Preventive Strategies in the United States." *Federal Highway Administration FHWA* (Publication No. FHWA-RD-01-156):1–12. Retrieved (papers2://publication/uuid/4D469A9D-07D6-4543-B217-3A15873793CF).

Giaccio, G., R. Zerbino, J. M. Ponce, and O. R. Batic, 2008, "Mechanical Behavior of Concretes Damaged by Alkali-Silica Reaction." *Cement and Concrete Research* 38(7):993–1004.

Giordano, Luca, Giuseppe Mancini, and Francesco Tondolo, 2011, "Durability of R/C Structures under Mechanical and Environmental Action", *Key Engineering Materials Vols.*462–463:949–954, Retrieved (www.scientific.net/KEM.462-463.949)

Grabe, P. J.and Oberholster R. E, 2000, "Programme for the Treatment and Replacement of ASR Affected Concrete Sleepers in the Sishen-Saldanha Railway Line" , Pp. 1059–1068 in *In Proceedings of the 11th International Conference on Alkali-Aggregate Reaction in Concrete*, edited by B. F. and B. D. M.A. Bérubé. Quebec City, Canada.

Helmuth, R., D. Stark, S. Diamond, and M. Moranville-Regourd, 1993, *Alkali-Silica Reactivity: An*

Overview of Research, Retrieved (http://onlinepubs.trb.org/onlinepubs/shrp/SHRP-C-342.pdf).

Hobbs, D. W., 1988, "Alkali-Silica Reaction in Concrete" , *Thomas Telford* (London, England):183.

Ichikawa, Tsuneki, 2009, "Alkali-Silica Reaction, Pessimum Effects and Pozzolanic Effect", *Cement and Concrete Research* 39(8):716–726. Retrieved (http://dx.doi.org/10.1016/j.cemconres.2009.06.004).

Institution of Structural Engineers (lSE). 1992. *Structural Effects of Alkali-Silica Reaction: Technical Guidance on the Appraisal of Existing Structures*. 11 Upper Belgrave Street, London SW1X 8BH.

Islam, Mohammad Shahidul and Sazeda Akhtar. 2013. "A Critical Assessment to the Performance of Alkali-Silica Reaction (ASR) in Concrete." *Canadian Chemical Transactions* 1(4):253–66. Retrieved (http://canchemtrans.ca/uploads/journals/CCT-2013-0026.pdf).

Jason Williams P., Joseph J. Biernacki, Larry R. Walker, Harry M. Meyer, Claudia J. Rawn, Jianming Bai, 2002, "Microanalysis of Alkali-Activated Fly Ash- CH Pastes", *Cement and Concrete Composites* 32:963–972.

Kawamura, Mitsunori and Hirohito Fuwa. 2003. "Effects of Lithium Salts on ASR Gel Composition and Expansion of Mortars." *Cement and Concrete Research* 33(6):913–919.

Kesler, C. E., 1953, "Effect of Speed of Testing on Flexural Fatigue Strength of Plain Concrete", *Proceedings, Highway Research Board* 32:251–258.

Kessy, J. G., M. G. Alexander, and H. Beushausen, 2015, "Concrete Durability Standards: International Trends and the South African Context." *South African Institution of Civil Engineering* 57(Day 2005):47–58.

Knudsen, A., F. M. Jensen, O. Klinghoffer, and T. Skovsgaard, 1998, "Cost-Effective Enhancement of Durability of Concrete Structures by Intelligent Use of Stainless Steel Reinforcement", Proceedings, Conference on Corrosion and Rehabilitation of Reinforced Concrete Structures, Florida, US.

Kunieda, Minoru and Keitetsu Rokugo, 2006, "Recent Progress on HPFRCC in Japan Required Performance and Applications", *Journal of Advanced Concrete Technology* 4(1):19–33.

LCPC (Laboratoire Central des Ponts et Chaussées), 1997, "Détermination de l'indice de fissuration D'un parement de béton. Méthode d'essai", *Techniques et méthodes des Laboratoire des Ponts et Chaussées*. *Ministère de l'équipement, des transports et du logement* No. 47, 58 bd Lefebvre F75732 Paris cedex 15, octobre 1997.

Li, V. C., 1993, "From Micromechanics to Structural Engineering - the Design of Cementitious Composites for Civil Engineering Applications", *Structural Mechanics and Earthquake Engineering* (JSCE, 10(2)):37–48.

Marzouk, H. and S. Langdon, 2003, "The Effect of Alkali-Aggregate Reactivity on the Mechanical Properties of High and Normal Strength Concrete", *Cement and Concrete Composites* 25(4–5 SPEC):549–56.

Mechtcherine, Viktor, Lieboldt, Matthias, 2011, "Permeation of Water and Gases through Cracked Textile Reinforced Concrete", *Cement and Concrete Composites* 33(7):725–34. Retrieved (http://dx.doi.org/10.1016/j.cemconcomp.2011.04.001).

Multon, Stéphane, Martin Cyr, Alain Sellier, Paco Diederich, and Laurent Petit, 2008, "Coupled Effects of Aggregate Size and Alkali Content on ASR Expansion", *Cement and Concrete Research* 38:350–59.

Multon, Stéphane, Alain Sellier, and Martin Cyr, 2009, "Chemo-Mechanical Modeling for Prediction of Alkali Silica Reaction (ASR) Expansion". *Cement and Concrete Research* 39(6):490–500. Retrieved (http://dx.doi.org/10.1016/j.cemconres.2009.03.007).

Neeraj, Buch and Shervin Jahangirnejad, 2007, "Quantifying Coefficient of Thermal Expansion Values of Typical Hydraulic Cement Concrete Paving Mixtures", *Final Report performed by Michigan State University, Department of Civil and Environmental Engineering, 3546, Engineering Building, East Lansing, MI 48824*, Retrieved (https://www.michigan.gov/documents/mdot/MDOT_Research_Report_RC1503_228603_7.pdf).

Nijland, Timo G., Joe a Larbi, Rob P. J. Van Hees, and Barbara Lubelli, 2007, "Self Healing Phenomena in Concretes and Masonry Mortars : A Microscopic Study." *Proceedings of the First International Conference on Self Healing Materials 18-20 April 2007, published by Springer*, Noordwijk aan Zee, The Netherlands:1–9.

Oberholster, R., & Davies, G, 1986, "An Accelerated Method for Testing the Potential Alkali Reactivity of Siliceous Aggregates", *Cement and Concrete Research* 16 (2):181–89.

Olsson, Karin and Josef Pettersson, 2010, "Fatigue Assessment Methods for Reinforced Concrete Bridges in Eurocode Comparative Study of Design Methods for Railway Bridges", *M.Sc., Department of Civil and Environmental Engineering, Chalmers University of Technology*, Göteborg, Sweden, 167.

Ostertag, C.P., Blunt, J., Grubb, J. 2007. "Mitigation of Expansive Deterioration Processes through Crack Control." in *6th International Conference on Fracture of Concrete or Concrete Structures (FRAMCOS 6)*. Catania, Italy, Taylor & Francis.

Owsiak, Z., J. Zapała-Sławeta, and P. Czapik, 2015, "Diagnosis of Concrete Structures Distress due to Alkali-Aggregate Reaction", *Bulletin of the Polish Academy of Sciences Technical Sciences* 63(1):23–29. Retrieved (http://www.degruyter.com/view/j/bpasts.2015.63.issue-1/bpasts-2015-

0003/bpasts-2015-0003.xml).

Palmer, D, 1992, "The Diagnosis of Alkali-Silica Reaction: Report of a Working Party", *BCA, Slough*. Retrieved (http://linkinghub.elsevier.com/retrieve/pii/S0950061889800212).

Pazant, Zdene K. and Alexander Steffensb, 2000, "Mathematical Model for Kinetics of Alkali – Silica Reaction in Concrete", *Cement and Concrete Composites* 30:419–428.

Paul S.C. and van Zijl G.P.A.G., 2013, "Mechanically Induced Cracking Behaviour in Fine and Coarse Sand Strain Hardening Cement Based Composites (SHCC) at Different Load Levels", *Journal of Advanced Concrete Technology* 11:301–11.

Pedneault, A, 1996, "Development of Testing and Analytical Procedures for the Evaluation of the Residual Potential of Reaction, Expansion, and Deterioration of Concrete Affected by ASR.", M.Sc. Memoir, Laval University, Québec City, Canada, 133.

Pellant, Chris, 2000, "Rocks and Minerals", *(DK Hand books), DK ADULT*, ISBN:15648061X 1995-07-01.

Poyet S., Sellier A., Capra B., Foray, G., Torrenti, J. M., Cognon, H. and Bourdarot E., 2007, "Chemical Modelling of Alkali Silica Reaction: Influence of the Reactive Aggregate Size Distribution." *Materials and Structures* 40(2):229–239.

Reinhardt, Hans Wolf and Martin Jooss, 2003, "Permeability and Self-Healing of Cracked Concrete as a Function of Temperature and Crack Width", *Cement and Concrete Research* 33(7):981–85.

Rodrigo Del Hoyo, 2007, "Alkali Aggregate Reactions", *Special work shop on Chemical expansion of concrete in dam and hydro projects*, Grnada, Spain.

Rokugo, K., Takada, H., Onda, Y., Fujishiro, M., Kobayashi, K., Asano, Y., 2013, "Chemical Pre-Stressing of Steel Bar-Reinforced Concrete Beams Using SHCC That Retains ASR Expansion for a Long Time", Pp. 43–50 in *3rd International Conference on Strain hardening Cement-based Composites (SHCC3)*, Dordrecht, The Netherlands,: RILEM Publications S.A.R.L., 3-5 November.

Rokugo, Keitetsu, Minoru Kunieda, and Lim S. C., 2005, "Patching Repair with ECC on Cracked Concrete Surface", *Proc. of ConMat05*, Vancouver, Canada. Retrieved (http://citeseerx.ist.psu.edu/viewdoc/summary?doi=10.1.1.146.2838).

Roylance, David, 2001, "Fatigue", *Department of Materials Science and Engineering , Massachusetts Institute of Technology*, Cambridge, MA 02139):2–10.

Şahmaran, Mustafa and Victor C. Li., 2008, "Durability of Mechanically Loaded Engineered Cementitious Composites under Highly Alkaline Environments", *Cement and Concrete Composites*

30(2):72–81. Retrieved: (http://linkinghub.elsevier.com/retrieve/pii/S0958946507001485).

Schladitz F, Lorenz E, Jesse F, Curbach M, 2009, "Strengthening of a Barrel-Shaped Roof Using Textile Reinforced Concrete", Pp. 416–17 in *33rd symposium of the international association for bridge and structural engineering, IABSE*, Bangkok, Thailand.

Shehata, M.H. and Thomas, M. D. A., 2000, "The Effect of Fly Ash Composition on the Expansion of Concrete Due to Alkali Silica Reaction", *Cement and Concrete Research* 30(7):1063–72.

Slag Cement Association, 2013, "Mitigating Alkali-Silica Reaction." 2(8):2. Retrieved (http://www.slagcement.org/news/pdf/no8_mitigation_reaction.pdf).

Song, Gao. 2005. "Matrix Manipulation to Study ECC Behaviour", *M.Sc. Department of Civil Engineering, University of Stellenbosch*.

Stanton, T. E., 1940, "Expansion of Concrete through Reaction between Cement and Aggregate", *Proc. Am. Soc. Civ. Eng.* 66:1781–1811.

Steffens, Alexander, Kefei Li, and Olivier Coussy, 2003, "Aging Approach to Water Effect on Alkali–Silica Reaction Degradation of Structures", *Journal of Engineering Mechanics* 129(1):50–59.

T. M. A. Ahmed, E. Burley, S. R.Rigden, 1999, "The Effect of Alkali-Silica-Reaction on the Fatigue Behaviour of Plain Concrete Tested in Compression, Indirect Tension and Flexure", *Magazine of Concrete Research* 51(6):375–90.

Thomas, M. D. A., and Innis, F. A., 1998, "Effect of Slag on Expansion due to Alkali-Aggregate Reaction in Concrete", *ACI Materials Journal* 95(No. 6):716–24.

Thomas, M., 2007, "Optimizing the Use of Fly Ash in Concrete", *Portland Cement Association*, 24.

Thomas, Michael D. a., Kevin J. Folliard, Benoit Fournier, Patrice Rivard, and Thano Drimalas, 2013, "Methods for Evaluating and Treating ASR-Affected Structures", *Results of Field Application and Demonstration Projects*; *Volume I: Summary of Findings and Recommendations*. I:1–80. Retrieved (http://www.fhwa.dot.gov/pavement/concrete/asr/pubs/hif14002.pdf).

Thomas, Michael, Benoit Fournier, Kevin Folliard, Jason Ideker, and Medhat Shehata, 2006, "Test Methods for Evaluating Preventive Measures for Controlling Expansion due to Alkali-Silica Reaction in Concrete", *Cement and Concrete Research* 36(10):1842–56.

Van Tittelboom, Kim and Nele De Belie, 2013, "Self-Healing in Cementitious Materials-a Review", Materials 2013, 6, 2182-2217; doi:10.3390/ma6062182. Retrieved (www.mdpi.com/journal/materials).

Van Zijl, G. and F. H. Wittmann, 2011, "Durability of Strain-Hardening Fibre-Reinforced Cement-Based

Composites (SHCC) ", chapter 2 (Durability under Mechanical Load – Micro-crack Formation (Ductility)), © RILEM 2011:9-39.

Wang, Kejin, Daniel C. Jansen, Surendra P. Shah, and Alan F. Karr, 1997, "Permeability Study of Cracked Concrete", *Cement and Concrete Research* 27(3):381–93.

Wood, J.G.M. and Angus, E.C., 1995, "Montrose Bridge: Inspection, Assessment and Remedial Work to a 65 Year Old Bridge with AAR", Structural faults and Repair – 95, 6p.

Yi, C. K. and C. P. Ostertag, 2005, "Mechanical Approach in Mitigating Alkali-Silica Reaction", *Cement and Concrete Research* 35(1):67–75.

Yu, Jia Huan, Wei Chen, Ming Xin Yu, and Yang En Hua., 2010, "The Microstructure of Self-Healed PVA ECC under Wet and Dry Cycles", *Materials Research* 13(2):225–31.

APPENDIXES

A. SUGGESTED METHODS FOR ASR AND CRACK MITIGATION

A.1. Introduction

Developing a comprehensive, structure-specific strategy for the design and implementation of repair or retrofitting intervention due to concrete deterioration is a challenge to engineers. This must be based on true identification and understanding of the deterioration mechanism in each part of the structure. The eventual overall costs resulting from poorly designed or executed repairs will be higher than the costs associated with primary repair of deteriorating concrete structures. The success of technical and economical repair projects rely on an appropriate condition assessment of the structure, careful and appropriate design and carrying out of remedial measures, and maintenance strategies. The required concrete performance during its service life and the as-built structural concrete properties should be specified prior to construction. However, it should be noted that there are only a few instances in practice where actual in-situ or as-built properties are measured (Kessy et al., 2015). Up to now, it is not possible to develop a definitive, step-by-step methodology for selecting mitigation measures for ASR for some reasons (FHWA, 2010), including:

1. A limited number of studies have been done in this area, with satisfying observations, that would quantify accurately the benefits of various mitigation options.
2. Some emerging technologies are still at present in their experimental and devolopment stage.
3. Due to the fact that every structure is different, the option of a “one size fits all” approach that will be universal, has not been achieved.

The emphasis of this study is on the effect of crack control on expansive deterioration processes of ASR. The following sections describe the types and methods of mitigating concrete cracks and suggested methods to repair the concrete cracked due to ASR, with the focus on optimal subsequent performance of the repaired structural elements.

A.2. Proper use of materials in the new concrete

The best option to mitigate ASR is to prevent its occurrence through appropriate use of materials in new construction. Three main options to limit the effect of alkali content in the concrete are (i) to use cement

with low alkali content and/or un-reactive aggregate; (ii) to use supplementary cementing materials, lithium-based admixtures or restrained mixture such as ECC and; (iii) keep the concrete surface dry. Figure A-1 summarises ways of mitigating ASR in new concrete.

A.2.1 Control alkali content

One of the options to mitigate alkali effectively is using cement with a low amount of alkali (Na_2Oe < 0.60% of portland cement or < 2.8 kg/m^3 of concrete). The amount of Na_2Oe is determined by Equation 2-1. Another method is to use non-reactive aggregate. Figure A-2 shows the limitation of Na_2Oe in percentage of cement (left) and in kg/m^3 of concrete (right).

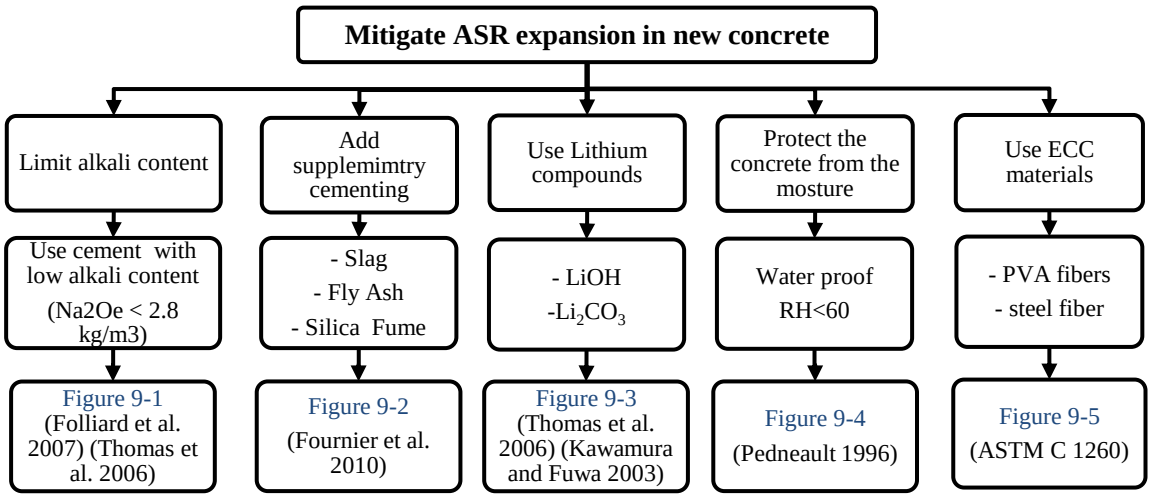

Figure A-1 Methods of mitigating ASR expansion in concrete

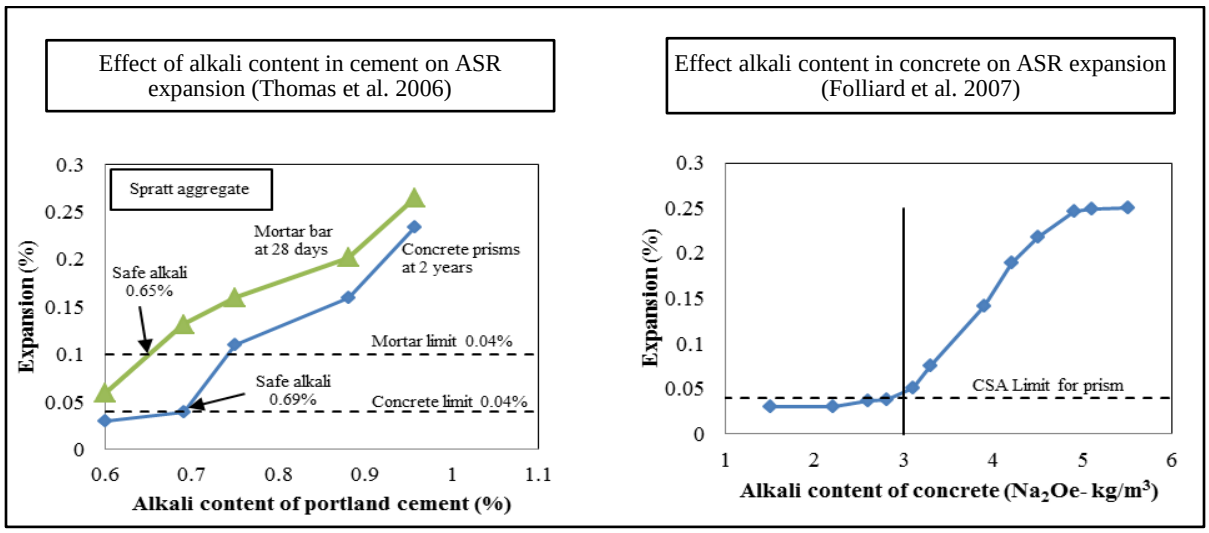

Figure A-2 Effect of Alkali content on ASR expansion, left: for mortar and concrete in cement as % (Thomas et al., 2006) and right: in concrete prisms asNa_2Oe (Folliard et al., 2007).

A.2.2 Concrete additives and cement supplementary materials

Supplementary materials are used in concrete to reduce the amount of alkali in the system that is available for reaction with the aggregate. Materials such as fly ash, silica fume or slagment are typically used as supplementary materials to reduce the high alkali-containing cement content. Figure A-3 illustrates the effects of different options and dosages of the supplements.

Lithium compounds are used to reduce/prevent the reaction between the reactive silica and alkali in concrete. The effect of these compounds on the ASR expansion is illustrated in Figure A-4.

A.2.3 Restraint to ASR expansion

Using SHCC materials leads to increased tension strain capacity and reduced crack widths. However, this is not applicable if the SHCC is not saturated. This is the situation in capillary absorption tests, and it has been shown that water (or chlorides) enter cracks very quickly in this condition, even in cracks with widths as small as 30 – 50 micrometer (Paul and van Zijl, 2013).

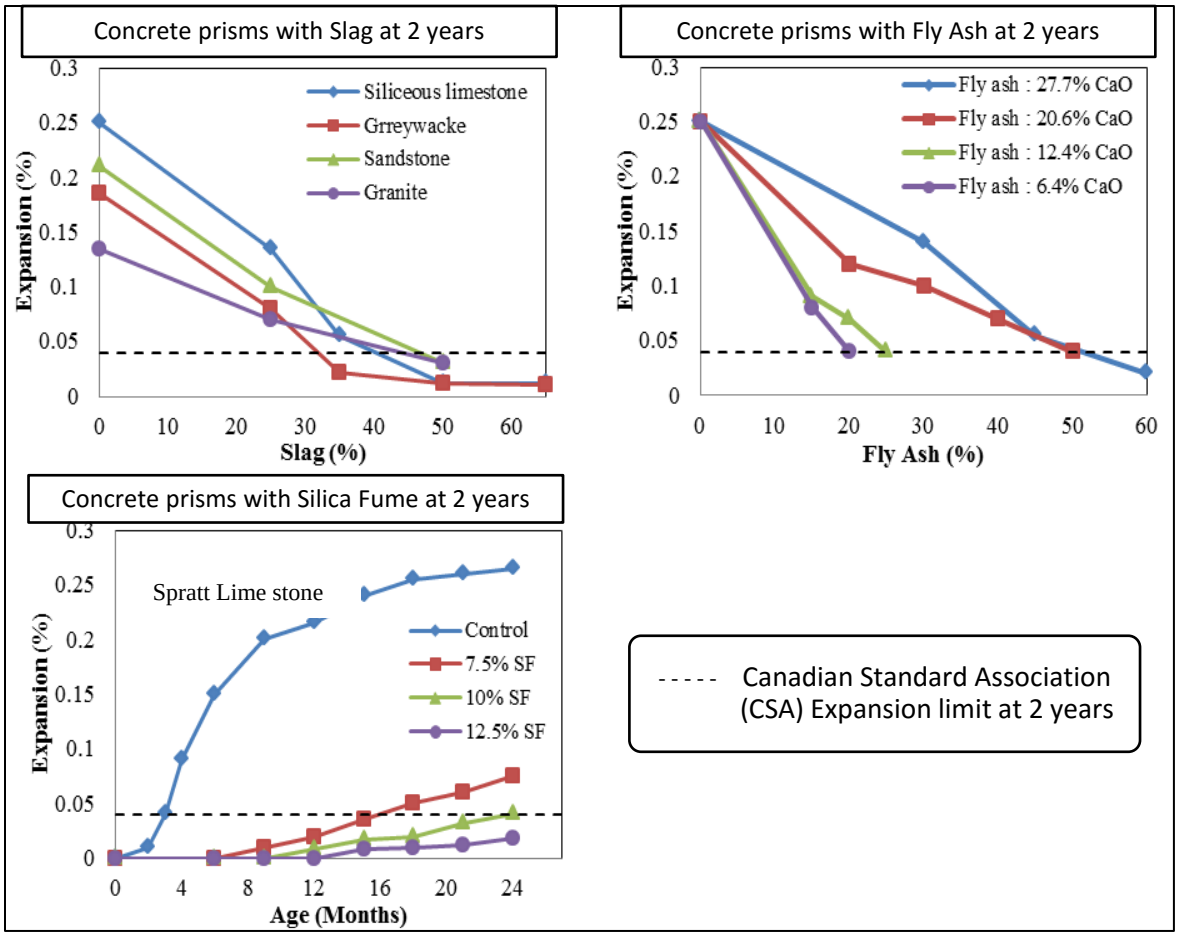

Figure A-3 Effect of supplementary materials on ASR expansion in concrete prisms (Fournier et al., 2010)

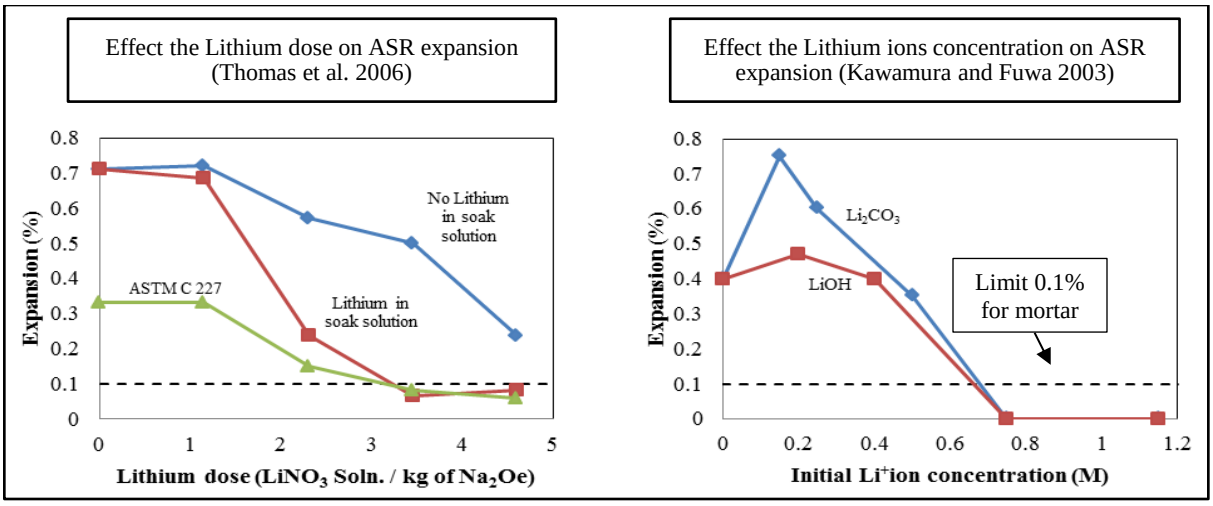

Figure A-4 Effect of Lithium compounds on ASR expansion in mortar.

Figures A-5 shows the effect of ECC on the ASR expansion reported by Şahmaran and Li (2008). The role of HPFRCC in controling the cracks by Kunieda and Rokugo (2006) is shown in Figure A-6. Ostertag et al. (2007) showed that fibres reduce ASR expansion rate, by controlling crack widths and preventing the ASR product from leaving the region. A recent paper studied ASR swelling in SHCC by Rokugo et al., (2013) shows that ASR can occur in SHCC (ECC) if reactive sand is used.

The main role of reinforcement is to bear tensile loads to strengthen the structure according to the loads acting on the structure. However, steel reinforcement is also usefull to reduce the ASR expansion of concrete due to the restraint it provides. The results from the thermal coefficient test in Sec. 3.7.2 and FE model in Section 7.4.4 confirmed that the steel restraint reduces the expansion by about 10 to 13% of the potential free expansion for the geometry and reinforcement level used in this research. This step cannot be considered as alternative method to prevent ASR expansion because the reinforcement depends on the mechanical concrete structure as needed.

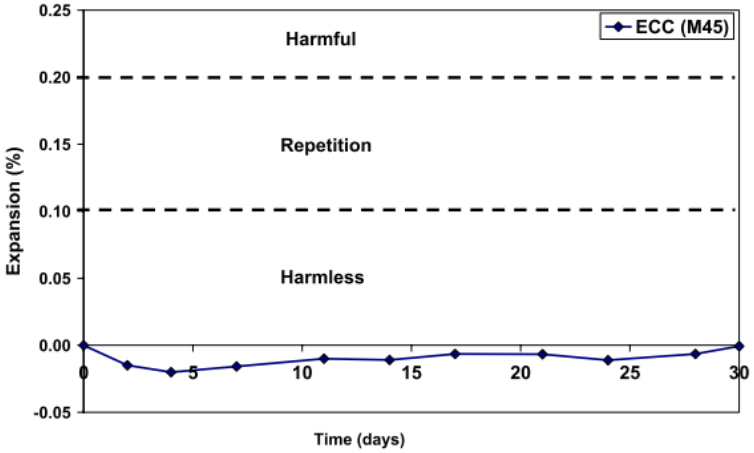

Figure A-5 Expansion time histories for ECC mixture (Şahmaran and Li, 2008).

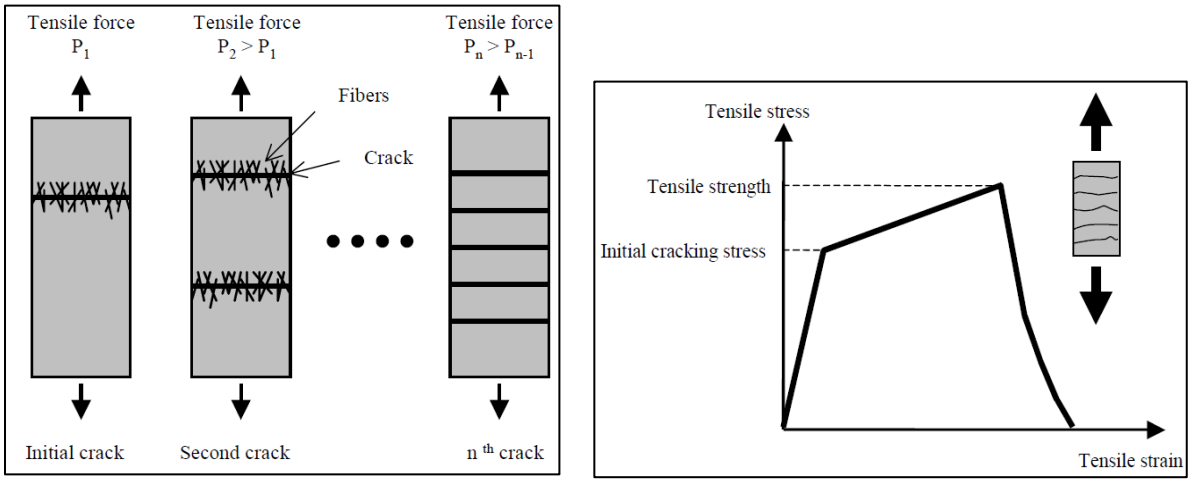

Figure A-6 Role of HPFRCC in tensile strength and cracks, left: multiple crack, and right: the material response of HPFRCC under uniaxial tension (Kunieda and Rokugo, 2006).

Steel reinforcement is not a mitigating measure for ASR so much as reducing ASR crack width. This reduction should be considered by the designer when the reinforcement provides restraint which causes tension in the steel, which must be added to tension caused by mechanical load.

A.2.4 Protect the concrete surface

This step comes directly after the casting of concrete. Seal the surface of the concrete structure to prevent or limit ingress of water in order to prevent the reaction process of the reactive silica with alkalis. Other possible way to reduce the moisture level is improving drainage conditions. The limits of the humidity allowed for some aggregates are illustrated in Figure A-7. The concrete made with four different types of aggregates in the graph displayed very small expansion at a relative humidity less than 80%. The expansion increases exponentially when RH increases above 80%.

A.3. Repair the damage in existing concrete

There is no simple way to halt the ASR reaction once it begins. The most appropriate way is to prevent water ingress, as discussed in the previous section. This can be done by sealants, or depending on the requirement for removal of affected material, other repair materials may be introduced. The main performance requirements for the repair material are strength, dimensional stability, shield ability, durability, bond to the substrate concrete, ductility (Rokugo et al., 2005).

The options for mitigating measures are divided into two groups according to whether they are prepared to treat the causes of ASR or the symptoms of the deleterious reaction, as illustrated in Figure A-8. Typically, both the cause and symptoms must be addressed, and management action against ASR and mechanical cracks must continue by regular monitoring and periodical inspections.

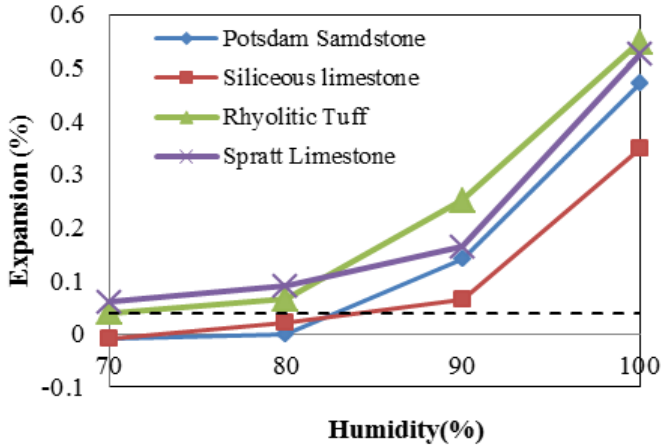

Figure A-7 Effect of relative humidity on ASR expansion in concrete prisms using the ASTM C 1293 (Pedneault, 1996)

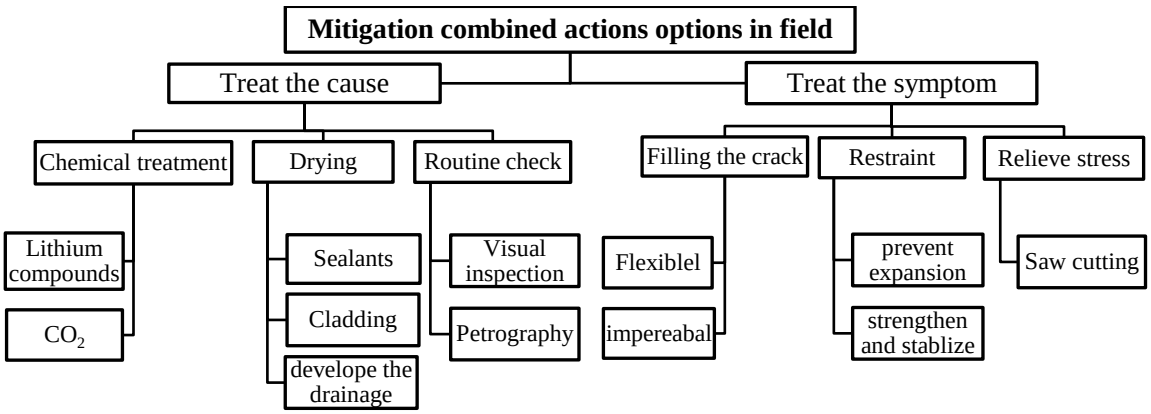

Figure A-8 Flow chart for options to mitigate the combined mechanical and ASR expansion and cracks

Before any repair or mitigation of deterioration, assessment and evaluation must be performed. The flow chart in Figure A-9 shows the routine inspection and diagnosis for the structure damaged under combined action of mechanical load and ASR.

A.3.1 Anticipatory detection of the problem

Detection of the problem at an early stage can be the main factor to mitigate any expected damage. The procedure of protecting the structure from ASR or mechanical cracks consists of one or more of the following.

A.3.1.1 Routine check

Visual inspection is typically done prior to detailed petrographic examination to observe concrete features. Factors must be considered to a detailed visual inspection of the structure before drawing conclusions about the distress under investigation such as moisture accessibility, and region environment. After these , evaluate whether ASR or mechanical action have caused it.

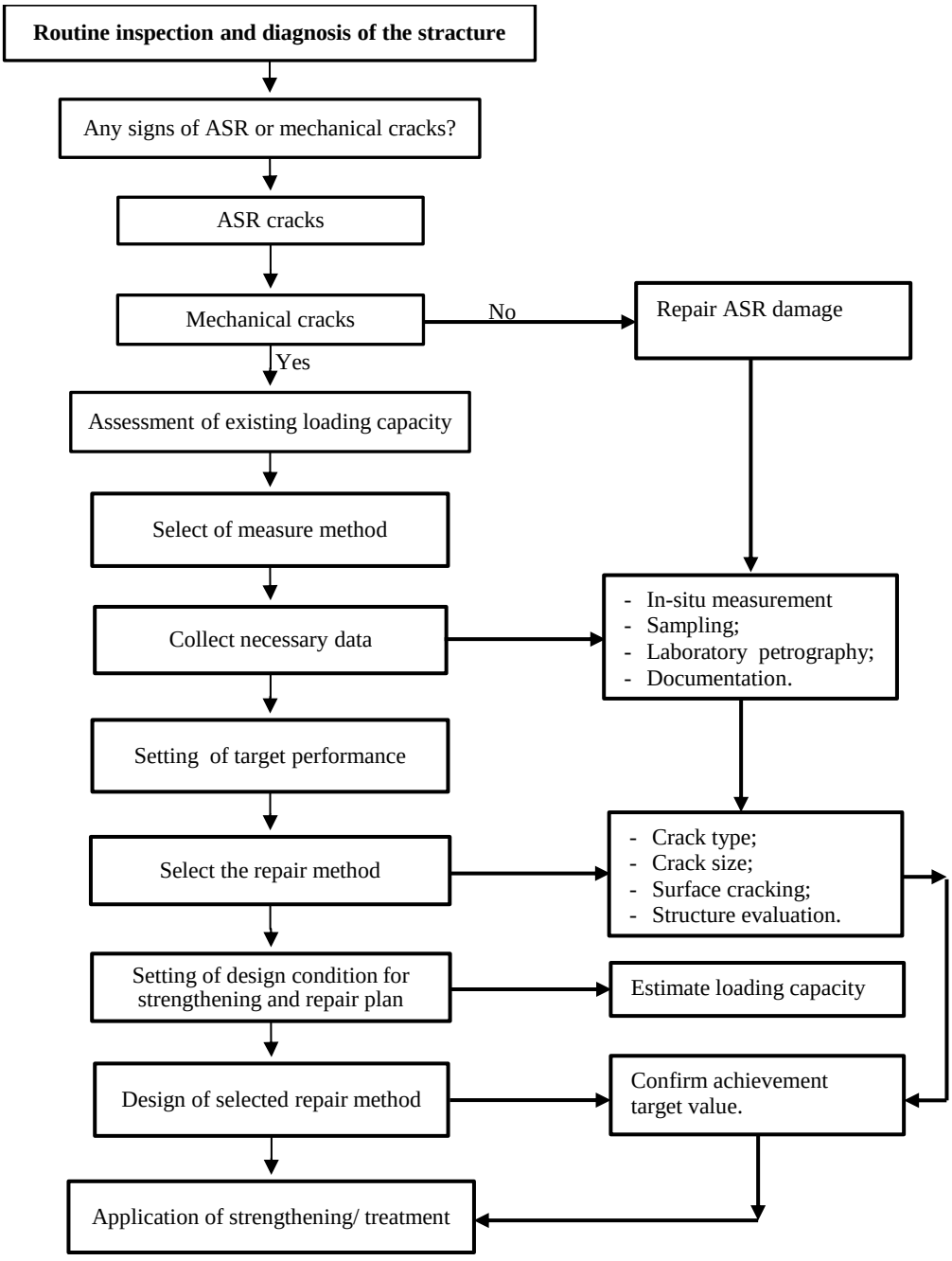

Figure A-9 Flow chart for the evaluation and repair management of combined mechanical and ASR cracks in concrete structures

A.3.1.2 Reduce ASR reaction

The reduction of ASR reaction is suitable only for ASR at the beginning of the reaction or when micro-cracks appear. A coating technique can accomplish this decrease and/or chemically neutralizing the reactive surface (ACI 221 Committee, 1998). Lithium compounds could be spread on the surface of ASR-affected concrete or introduced into the concrete by vacuum impregnation to reduce the ASR reaction.

To reduce the ASR extent, attempts have also been made to minimize the pH of the concrete pore fluid level by injecting CO_2 into the concrete (Cavalcanti and Silveira, 1989). Implementation of this process is not practical or economical for most concrete structures and can lead to carbonation (Fournier and Thomas, 1991).

A.3.1.3 Insulate the concrete surface

Precautions must be taken to protect the concrete surface from the external conditions such as humidity or water which feed the ASR reaction. Minimizing moisture or water ingress and the associated deterioration could be achieved by insulating the concrete surfaces with sealants, impermeable coating or mortar layer. Ventilated cladding might reduce ingress of the moisture and permits the drying of concrete, unlike coatings which can trap moisture (Wood and Angus, 1995). Modifications might be implemented to allow water to drain away from the structure rather than onto or through parts of it (Hobbs, 1988).

A.3.2 Treatment of structures affected by combined ASR and mechanical cracks

The method selected to deal with the structure cracked will depend on distress in a structure or pavement that classified as non-structural or structural in nature. Structural repair needs considerably more study and analysis to ensure enough safety (ACI Committee 221, 1998). ASR deterioration at the beginning stages can be classified as a non-structural and mechanical or combined action as a structural.

A.3.2.1 Relief stress

Saw cutting or removal of sections of concrete near the expansion joints in certain applications such as a pavement suffering from ASR-induced expansion can be a viable option to accommodate stresses and joint-related failures, therefore, prolong the service life (FHWA, 2010). Sound concrete could be used in the sections that have been removed, with careful attention paid to restoring the intended joint details. Narrow mechanical cracks (typically less than 0.2 mm wide) might be useful in reducing the pressure caused by ASR expansion and may self-heal in the presence of water or water damp. In the large cracks that affect the service life of the concrete structure, it is advisable to follow another approach to repair the structure.

A.3.2.2 Filling cracks and water repellent

The method selected to repair the structures affected by ASR could depend on the crack widths. To restore structural continuity or to limit water penetration, the macrocracks or construction joints are filled with cement grout or epoxy resin before applying a waterproof sealing or water repellent agent (Fournier et al., 1991). However, a flexible epoxy or other crack-filler might be more efficient than a rigid filler in a

concrete where ASR expansion is still active. The filler should absorbed the expansion without causing build-up of pressure. It should clog the cracks and also extend when the crack width increases under mechanical load. Figure A-10 (left) illustrates an example of an ASR crack in the Good Hope Center in Cape Town that was filled with rigid epoxy in 1993. The filler size in this example was not changed while the crack width has increased which caused a new space in the crack. The filling of cracks is commonly performed before applying a water repellent agent or waterproof sealing.

The coating such as waterproofing of silane on a concrete surface must be impermeable and bridge the narrow cracks that were not filled. Figure A-10 (right) shows an example of the management program to treat the concrete sleepers cracked in the Sishen-Saldanha railway line, South Africa (Grabe and Oberholster, 2000). The monitoring of the treated elements with silane showed that the rate of ASR deterioration was reduced.

A.3.2.3 Strengthening damaged structure

Both results of field and laboratory studies are needed in the management of concrete structures affected by combined action. These investigations are required to check whether the damaged part provides sufficient strength and stiffness to the structure. To reduce deleterious expansion due to ASR or combined action, it can perform by strengthening the damaged member with some approaches depending on deterioration degree:

1. Encapsulate the affected member by high-performance fiber reinforced cement composites (HPFRCC). The cracks in the region adjacent to the interface (within HPFRCC layer) is distributed to fine-cracks. Kunieda et al. (2005) have performed HPFRCC layer on the concrete surface of retaining wall. They found that a number of cracks had distributed on the repair surface layer (Figure A-11 left).
2. Encasement of the affected members with layers of textile concrete reinforced (TRC) made of carbon fiber. Distribution of fine cracks form in the TRC layer alternatively the larger crack as shown in Figure A-11 (right) (Mechtcherine et al., 2011). These fine cracks lead to less permeability in comparison with cracked ordinary concrete. An example of placing the TRC is shown in Figure A-12 to repair a building in Zwickau, Germany (Schladitz et al., 2009).
3. Removing the infected concrete and replacing with new steel reinforced concrete that will not have ASR. This step aims to replace the externally damaged concrete induced by ASR and to provide sufficient stiffness to the structures. As mentioned previously in the experiments, the restraint by reinforcement reduces the expansion to a certain extent. Therefore, using this reinforcement could also be useful in the mantainance. Figure A-13 shows two examples of the cracked concrete strengthed by steel reinforced concrete. The steps of this approach start by removing the externally

damaged layer. The second step is by adding steel reinforcement around the member; then non-reactive concrete is placed in the form.

Figure A-10 Crack treatment, left: the crack width increased while a rigid epoxy has not changed in Good Hope Centre, Cape Town, and right: a part of treating the concrete sleepers with silane in the Sishen-Saldanha railway line, South Africa (Grabe and Oberholster, 2000).

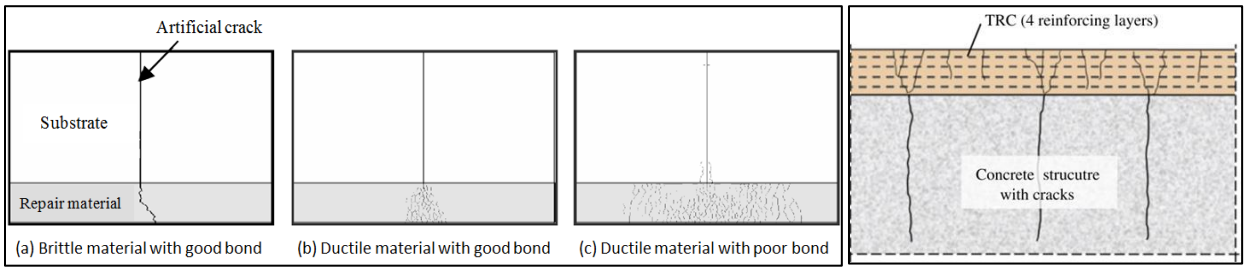

Figure A-11 Schematic view of transferring crack patterns through the repair layer, left: different materials with and without bonding in the artificial crack (Kunieda and Rokugo, 2006), and right: cracked concrete member with TRC with four reinforcing layers.

Figure A-12 Placing of the textile reinforcement (Schladitz et al., 2009)

Figure A-13 Strengthening damaged by steel reinforced concrete, left: a highway structure affected by ASR in South Africa, and right: electricity tower concrete foundation affected by ASR in Quebec City, Canada (Fournier et al., 1991).

B. STRAIN AND DEFORMATION DATA

B.1. Average strain in 200mm gauge lengths for different exposures and times in test Series 1.

Table B-1 Average strain of four spaces (two on each side) during exposures time for the four mixes exposed to ASR (the average of three specimens and CoV between brackets)

ASR specimens

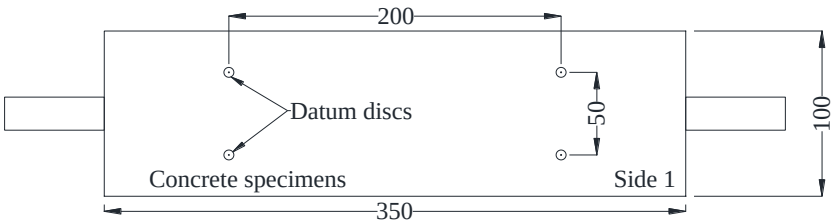

Age at measurement (w)	Exposure	Gw	Gw-co	Gn	Gn-co
1	Before exposure in NaOH (80°C)	0.000	0.000	0.000	0.000
2	After exposure in NaOH (80°C)	0.007 (0.07)	0.005 (0.08)	0.015 (0.14)	0.012 (0.04)
3		0.009 (0.11)	0.008 (0.08)	0.022 (0.08)	0.015 (0.01)
4		0.008 (0.10)	0.007 (0.13)	0.035 (0.07)	0.016 (0.01)
5		0.009 (0.08)	0.006 (0.18)	0.041 (0.07)	0.016 (0.04)
6		0.012 (0.11)	0.007 (0.19)	0.042 (0.06)	0.019 (0.05)
7		0.012 (0.12)	0.007 (0.22)	0.048 (0.05)	0.019 (0.07)
8		0.013 (0.10)	0.007 (0.18)	0.053 (0.05)	0.019 (0.01)
9		0.013 (0.07)	0.007 (0.13)	0.056 (0.06)	0.019 (0.05)
10		0.014 (0.07)	0.007 (0.24)	0.058 (0.01)	0.018 (0.00)
11	After week in NaOH at (23±2°C)	0.016 (0.07)	0.008 (0.07)	0.066 (0.03)	0.021 (0.05)
24	After 13 weeks in air	0.011 (0.07)	0.007 (0.13)	0.056 (0.02)	0.012 (0.04)
36	After 25 weeks in air	0.006 (0.07)	0.005 (0.14)	0.044 (0.05)	0.010 (0.05)
37	1 week in water at (80°C)	0.010 (0.07)	0.006 (0.21)	0.057 (0.01)	0.012 (0.10)

Table B-2 Average strain of four spaces (two on each side) during exposure time for the four mixes exposed to combined action (the average of three specimens and CoV between brackets)

Combined action

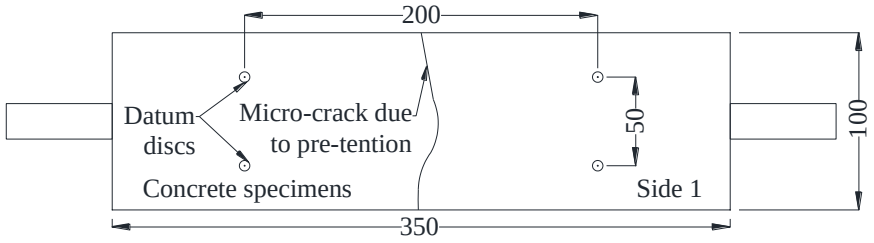

Age at measurement (w)	Exposure	Gw	Gw-co	Gn	Gn-co
1	Before tension	0.000	0.000	0.000	0.000
1	After tension in NaOH (80°C)	0.015 (0.10)	0.013 (0.04)	0.014 (0.03)	0.012 (0.10)
2		0.020 (0.22)	0.013 (0.07)	0.028 (0.02)	0.014 (0.05)
3		0.024 (0.20)	0.014 (0.03)	0.034 (0.07)	0.020 (0.04)
4		0.025 (0.22)	0.016 (0.04)	0.039 (0.13)	0.019 (0.06)
5		0.023 (0.09)	0.013 (0.04)	0.044 (0.15)	0.022 (0.00)
6		0.026 (0.18)	0.014 (0.09)	0.051 (0.19)	0.024 (0.03)
7		0.028 (0.19)	0.015 (0.13)	0.056 (0.17)	0.026 (0.10)
8		0.029 (0.14)	0.014 (0.13)	0.060 (0.13)	0.027 (0.09)
9		0.030 (0.15)	0.014 (0.03)	0.061 (0.17)	0.028 (0.20)
10		0.031 (0.12)	0.016 (0.15)	0.066 (0.18)	0.028 (0.16)
11	After week in NaOH at (23±2°C)	0.036 (0.10)	0.016 (0.14)	0.072 (0.14)	0.031 (0.12)
24	After 13 weeks in air	0.033 (0.06)	0.016 (0.11)	0.063 (0.11)	0.022 (0.16)
36	After 25 weeks in air	0.028 (0.06)	0.013 (0.16)	0.049 (0.08)	0.020 (0.05)
37	1 week in water at (80°C)	0.033 (0.13)	0.018 (0.15)	0.058 (0.08)	0.024 (0.06)

B.2. Deformation over 100 mm gauge lengths of specimens partially submerged in water at different exposure times in test Series 2.

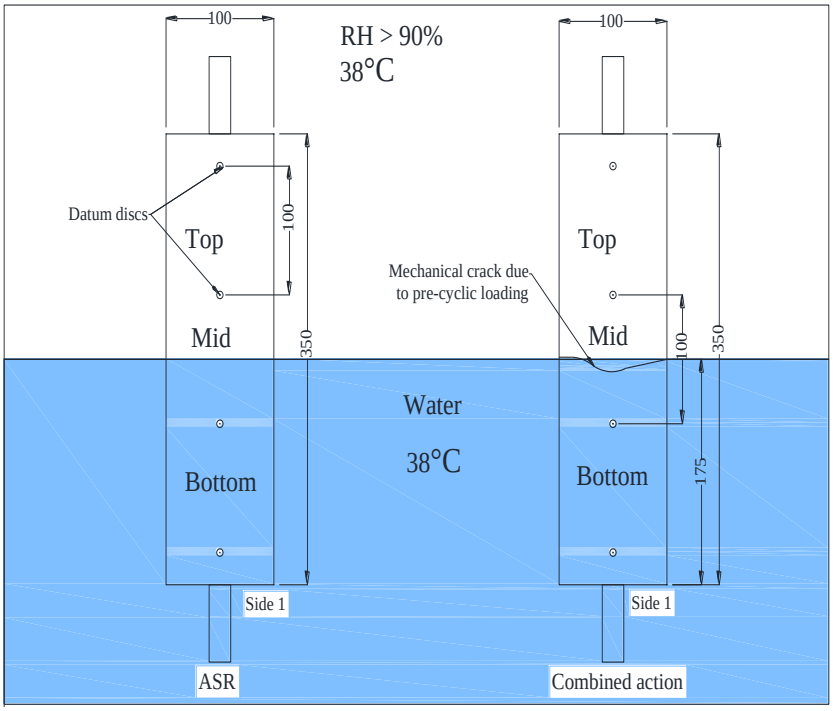

Figure B-1 Set of ASR and combined concrete prisms in chamber (partially submerged in water)

Table B-3 Average strain gauge readings in 100 mm gauge lengths during exposure time for the **Gw/w** specimens in test series 2 (average of three samples)

In ASR				In combined action			
Exposure time (w)	Average for gauge region			Exposure time (w)	Average for gauge region		
	Bottom	Mid	Top		Bottom	Mid	Top
2d	0.000	0.000	0.000	2d	0.000	0.000	0.000
4	0.014 (0.50)	0.011 (0.27)	0.008 (0.06)	4*	0.006 (0.75)	0.003 (0.29)	0.005 (0.29)
8	0.018 (0.14)	0.030 (0.12)	0.020 (0.15)	4#	0.018 (0.38)	1.865 (0.01)	0.011 (0.13)
12	0.033 (0.09)	0.044 (0.09)	0.040 (0.12)	8	0.024 (0.17)	1.831 (0.01)	0.016 (0.26)
16	0.067 (0.07)	0.065 (0.01)	0.066 (0.05)	12	0.047 (0.07)	1.786 (0.00)	0.038 (0.19)
32	0.199 (0.24)	0.123 (0.02)	0.122 (0.04)	16	0.068 (0.03)	1.831 (0.00)	0.070 (0.09)
38	0.211 (0.24)	0.147 (0.06)	0.140 (0.08)	32	0.212 (0.14)	1.745 (0.00)	0.197 (0.22)
44	0.223 (0.20)	0.168 (0.04)	0.152 (0.09)	38	0.246 (0.13)	1.712 (0.00)	0.244 (0.24)
50	0.230 (0.16)	0.179 (0.04)	0.158 (0.09)	44	0.276 (0.14)	1.683 (0.00)	0.271 (0.21)
65	0.233 (0.16)	0.191 (0.03)	0.163 (0.09)	50	0.287 (0.15)	1.670 (0.02)	0.283 (0.20)
				65	0.294 (0.14)	1.655 (0.02)	0.284 (0.18)

** Before cyclic load*
 # After cyclic load

Table B-4 Average strain gauge readings in 100 mm gauge lengths during exposure time for the **Gn/w** specimens in test series 2 (average of three samples and CoV between brackets)

In ASR				In combined action			
Exposure time (w)	Average for gauge region			Exposure time (w)	Average for gauge region		
	Bottom	Mid	Top		Bottom	Mid	Top
2d	0.000	0.000	0.000	2d	0.000	0.000	0.000
4	0.013 (0.39)	0.015 (0.17)	0.004 (0.33)	4*	0.015 (0.13)	0.029 (0.42)	0.012 (0.10)
8	0.028 (0.16)	0.024 (0.24)	0.022 (0.14)	4#	0.023 (0.10)	1.848 (0.18)	0.020 (0.24)
12	0.051 (0.16)	0.052 (0.09)	0.031 (0.17)	8	0.035 (0.09)	1.819 (0.18)	0.044 (0.07)
16	0.062 (0.12)	0.065 (0.12)	0.049 (0.13)	12	0.039 (0.00)	1.834 (0.18)	0.052 (0.05)
32	0.091 (0.14)	0.075 (0.05)	0.059 (0.11)	16	0.053 (0.04)	1.833 (0.18)	0.067 (0.02)
38	0.103 (0.15)	0.082 (0.04)	0.065 (0.11)	32	0.070 (0.04)	1.843 (0.18)	0.070 (0.02)
44	0.118 (0.15)	0.092 (0.05)	0.074 (0.11)	38	0.076 (0.03)	1.844 (0.18)	0.081 (0.02)
50	0.126 (0.16)	0.100 (0.02)	0.077 (0.10)	44	0.087 (0.00)	1.843 (0.18)	0.088 (0.01)
65	0.130 (0.14)	0.104 (0.02)	0.081 (0.09)	50	0.093 (0.01)	1.837 (0.18)	0.096 (0.04)
				65	0.097 (0.01)	1.833 (0.18)	0.100 (0.03)

** Before cyclic load*
 # After cyclic load

Table B-5 Average strain gauge readings in 100 mm gauge lengths during exposure time for the **Gw-co/w** specimens in test series 2 (average of three samples)

In ASR				In combined action			
Exposure time (w)	Average for gauge region			Exposure time (w)	Average for gauge region		
	Bottom	Mid	Top		Bottom	Mid	Top
2d	0.000	0.000	0.000	2d	0.000	0.000	0.000
4	0.014 (0.30)	0.015 (0.27)	0.015 (0.25)	4	0.012 (0.30)	0.013 (0.26)	0.015 (0.17)
8	0.022 (0.20)	0.021 (0.25)	0.022 (0.26)	8	0.019 (0.16)	0.014 (0.26)	0.027 (0.16)
12	0.038 (0.09)	0.029 (0.07)	0.030 (0.15)	12	0.036 (0.19)	0.029 (0.21)	0.040 (0.26)
16	0.061 (0.13)	0.041 (0.10)	0.041 (0.18)	15*	0.044 (0.11)	0.037 (0.22)	0.050 (0.11)
32	0.098 (0.06)	0.062 (0.03)	0.062 (0.23)	15#	0.049 (0.07)	0.909 (0.08)	0.050 (0.08)
38	0.103 (0.10)	0.072 (0.03)	0.070 (0.21)	32	0.084 (0.06)	0.926 (0.08)	0.081 (0.10)
44	0.113 (0.07)	0.081 (0.03)	0.082 (0.15)	38	0.093 (0.02)	0.929 (0.08)	0.089 (0.13)
50	0.117 (0.07)	0.088 (0.03)	0.087 (0.15)	44	0.109 (0.04)	0.922 (0.08)	0.092 (0.12)
65	0.121 (0.07)	0.093 (0.02)	0.091 (0.15)	50	0.114 (0.03)	0.927 (0.08)	0.097 (0.13)
				65	0.119 (0.03)	0.922 (0.07)	0.098 (0.10)

** Before cyclic load*
 # After cyclic load

Table B-6 Average strain gauge readings in 100 mm gauge lengths during exposure time for the Gn-co/w specimens in test series 2 (average of three samples)

In ASR				In combined action			
Exposure time (w)	Average for gauge region			Exposure time (w)	Average for gauge region		
	Bottom	Mid	Top		Bottom	Mid	Top
2d	0.000	0.000	0.000	2d	0.000	0.000	0.000
4	0.013 (0.17)	0.014 (0.30)	0.011 (0.17)	4	0.006 (0.25)	0.013 (0.30)	0.009 (0.30)
8	0.018 (0.16)	0.018 (0.21)	0.017 (0.16)	8	0.014 (0.17)	0.015 (0.24)	0.013 (0.24)
12	0.022 (0.14)	0.024 (0.19)	0.021 (0.22)	12	0.021 (0.19)	0.020 (0.14)	0.022 (0.24)
16	0.029 (0.25)	0.028 (0.16)	0.026 (0.20)	15*	0.034 (0.18)	0.038 (0.15)	0.032 (0.14)
32	0.040 (0.04)	0.033 (0.19)	0.037 (0.05)	15#	0.039 (0.25)	0.441 (0.23)	0.034 (0.15)
38	0.047 (0.05)	0.041 (0.16)	0.044 (0.02)	32	0.046 (0.25)	0.446 (0.21)	0.045 (0.23)
44	0.054 (0.06)	0.047 (0.16)	0.050 (0.03)	38	0.051 (0.25)	0.447 (0.19)	0.054 (0.21)
50	0.057 (0.06)	0.050 (0.15)	0.053 (0.03)	44	0.056 (0.25)	0.452 (0.19)	0.059 (0.19)
65	0.060 (0.06)	0.055 (0.14)	0.057 (0.02)	50	0.060 (0.24)	0.453 (0.18)	0.062 (0.18)
				65	0.064 (0.25)	0.456 (0.16)	0.067 (0.16)

** Before cyclic load*
 # After cyclic load

B.3. Deformation of 100 mm gauge lengths in specimens exposed to high humidity at different exposure times in test Series 2.

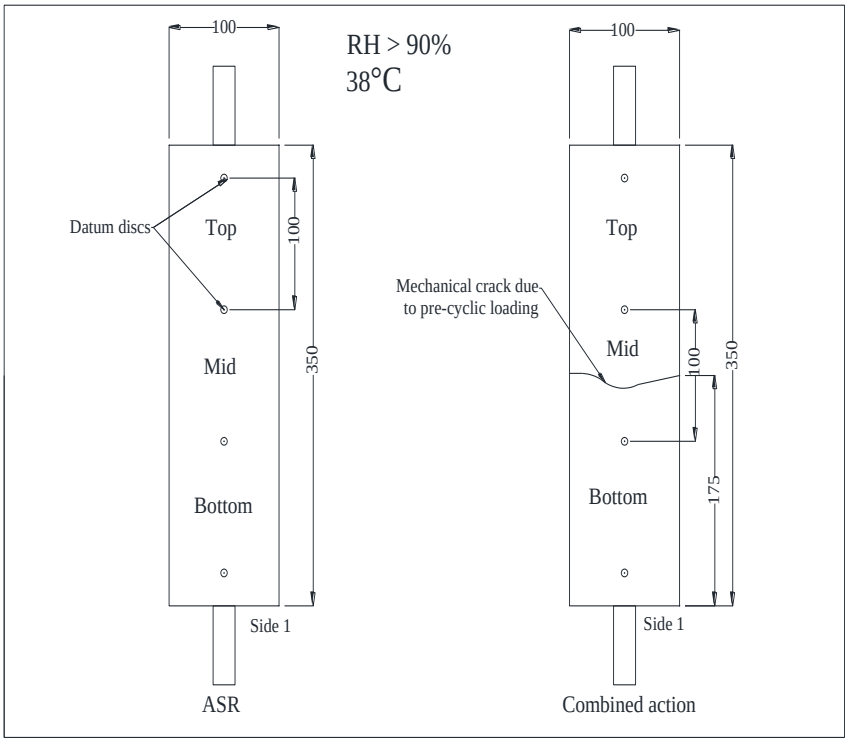

Figure B-2 Set of ASR and combined concrete prisms in chamber (exposed to high humidity)

Table B-7 Average strain gauge readings in 100 mm gauge lengths during exposure time for the **Gw/H** specimens in test series 2 (average of three samples)

In ASR				In combined action			
Exposure time (w)	Average for gauge region			Exposure time (w)	Average for gauge region		
	Bottom	Mid	Top		Bottom	Mid	Top
2d	0.000	0.000	0.000	2d	0.000	0.000	0.000
4	0.004 (0.06)	0.005 (0.31)	0.013 (0.28)	4*	0.013 (0.29)	0.030 (0.48)	0.011 (0.34)
8	0.012 (0.26)	0.009 (0.25)	0.029 (0.12)	4#	0.015 (0.26)	2.409 (0.53)	0.015 (0.29)
12	0.017 (0.25)	0.015 (0.15)	0.036 (0.06)	8	0.021 (0.12)	2.392 (0.54)	0.018 (0.29)
16	0.032 (0.14)	0.032 (0.17)	0.052 (0.07)	12	0.025 (0.16)	2.384 (0.54)	0.025 (0.17)
32	0.078 (0.08)	0.076 (0.18)	0.106 (0.14)	16	0.035 (0.14)	2.406 (0.54)	0.040 (0.15)
38	0.103 (0.05)	0.094 (0.16)	0.132 (0.14)	32	0.092 (0.19)	2.363 (0.54)	0.099 (0.22)
44	0.127 (0.03)	0.116 (0.11)	0.163 (0.13)	38	0.117 (0.20)	2.343 (0.54)	0.122 (0.16)
50	0.136 (0.04)	0.123 (0.10)	0.175 (0.13)	44	0.138 (0.19)	2.335 (0.54)	0.136 (0.15)
65	0.145 (0.05)	0.129 (0.13)	0.192 (0.14)	50	0.146 (0.19)	2.322 (0.54)	0.152 (0.14)
				65	0.157 (0.17)	2.305 (0.54)	0.159 (0.17)

** Before cyclic load*
 # After cyclic load

Table B-8 Average strain gauge readings in 100 mm gauge lengths during exposure time for the **Gn/H** specimens in test series 2 (average of three samples)

In ASR				In combined action			
Exposure time (w)	Average for gauge region			Exposure time (w)	Average for gauge region		
	Bottom	Mid	Top		Bottom	Mid	Top
2d	0.000	0.000	0.000	2d	0.000	0.000	0.000
4	0.024 (0.07)	0.018 (0.33)	0.018 (0.33)	4*	0.012 (0.30)	0.028 (0.34)	0.016 (0.14)
8	0.036 (0.30)	0.028 (0.08)	0.028 (0.14)	4#	0.006 (0.30)	1.225 (0.21)	0.017 (0.27)
12	0.038 (0.27)	0.034 (0.07)	0.033 (0.05)	8	0.014 (0.09)	1.199 (0.23)	0.029 (0.06)
16	0.043 (0.29)	0.044 (0.06)	0.040 (0.02)	12	0.020 (0.15)	1.215 (0.22)	0.038 (0.07)
32	0.051 (0.25)	0.051 (0.11)	0.046 (0.05)	16	0.030 (0.18)	1.229 (0.22)	0.050 (0.07)
38	0.061 (0.19)	0.058 (0.11)	0.058 (0.02)	32	0.034 (0.19)	1.227 (0.22)	0.056 (0.07)
44	0.070 (0.18)	0.066 (0.12)	0.068 (0.06)	38	0.041 (0.14)	1.223 (0.22)	0.063 (0.09)
50	0.076 (0.18)	0.070 (0.12)	0.073 (0.06)	44	0.049 (0.12)	1.222 (0.23)	0.073 (0.07)
65	0.081 (0.18)	0.076 (0.12)	0.077 (0.06)	50	0.056 (0.10)	1.215 (0.23)	0.076 (0.09)
				65	0.062 (0.09)	1.211 (0.23)	0.080 (0.09)

** Before cyclic load*
 # After cyclic load

Table B-9 Average strain gauge readings in 100 mm gauge lengths during exposure time for the **Gw-co/H** specimens in test series 2 (average of three samples)

In ASR				In combined action			
Exposure time (w)	Average for gauge region			Exposure time (w)	Average for gauge region		
	Bottom	Mid	Top		Bottom	Mid	Top
2d	0.000	0.000	0.000	2d	0.000	0.000	0.000
4	0.011 (0.37)	0.008 (0.34)	0.009 (0.39)	4	0.012 (0.37)	0.025 (0.37)	0.004 (0.36)
8	0.013 (0.27)	0.015 (0.29)	0.013 (0.36)	8	0.017 (0.25)	0.029 (0.29)	0.007 (0.24)
12	0.016 (0.19)	0.018 (0.34)	0.014 (0.24)	12	0.018 (0.25)	0.029 (0.28)	0.011 (0.27)
16	0.027 (0.17)	0.031 (0.15)	0.026 (0.21)	15*	0.023 (0.20)	0.037 (0.26)	0.021 (0.28)
32	0.049 (0.21)	0.052 (0.18)	0.046 (0.08)	15#	0.026 (0.23)	1.555 (0.16)	0.023 (0.26)
38	0.055 (0.20)	0.056 (0.15)	0.052 (0.02)	32	0.037 (0.20)	1.566 (0.16)	0.061 (0.08)
44	0.065 (0.16)	0.067 (0.13)	0.065 (0.08)	38	0.044 (0.14)	1.563 (0.16)	0.067 (0.09)
50	0.070 (0.16)	0.071 (0.11)	0.069 (0.08)	44	0.056 (0.06)	1.561 (0.15)	0.077 (0.11)
65	0.075 (0.15)	0.092 (0.13)	0.074 (0.07)	50	0.061 (0.03)	1.557 (0.16)	0.084 (0.10)
				65	0.067 (0.03)	1.557 (0.16)	0.090 (0.09)

** Before cyclic load*
 # After cyclic load

Table B-10 Average strain gauge readings in 100 mm gauge lengths during exposure time for the **Gn-co/H** specimens in test series 2 (average of three samples)

In ASR				In combined action			
Exposure time (w)	Average for gauge region			Exposure time (w)	Average for gauge region		
	Bottom	Mid	Top		Bottom	Mid	Top
2d	0.000	0.000	0.000	2d	0.000	0.000	0.000
4	0.008 (0.18)	0.010 (0.31)	0.019 (0.28)	4	0.012 (0.13)	0.031 (0.27)	0.009 (0.30)
8	0.012 (0.23)	0.011 (0.26)	0.020 (0.03)	8	0.019 (0.16)	0.030 (0.18)	0.011 (0.24)
12	0.019 (0.23)	0.017 (0.24)	0.031 (0.13)	12	0.028 (0.13)	0.039 (0.16)	0.017 (0.26)
16	0.024 (0.18)	0.024 (0.23)	0.035 (0.12)	15*	0.043 (0.16)	0.055 (0.27)	0.031 (0.23)
32	0.031 (0.16)	0.034 (0.25)	0.041 (0.09)	15#	0.045 (0.14)	0.823 (0.72)	0.035 (0.15)
38	0.041 (0.13)	0.047 (0.18)	0.052 (0.07)	32	0.051 (0.09)	0.826 (0.72)	0.041 (0.13)
44	0.048 (0.18)	0.052 (0.18)	0.060 (0.06)	38	0.057 (0.06)	0.825 (0.71)	0.047 (0.12)
50	0.051 (0.09)	0.055 (0.18)	0.064 (0.06)	44	0.062 (0.06)	0.827 (0.70)	0.051 (0.13)
65	0.056 (0.06)	0.059 (0.17)	0.068 (0.05)	50	0.064 (0.06)	0.833 (0.71)	0.057 (0.14)
				65	0.068 (0.07)	0.828 (0.70)	0.057 (0.12)

** Before cyclic load*
 # After cyclic load

C. CALCULATIONS, CURVES AND RELATIONSHIPS

C.1. Calculation of the modulus of elasticity E

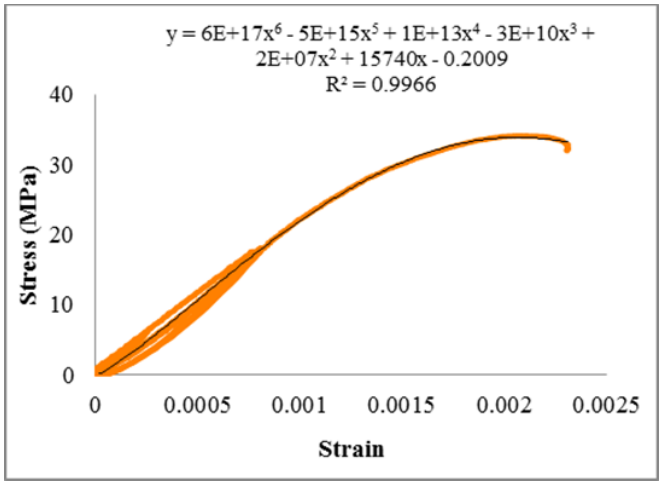

Figure C-1 Stress-strain relationship for 100x200 mm concrete cylinders (example of Gw specimens)

$$E = \frac{\sigma_{40\%} - \sigma_{50\mu\varepsilon}}{\varepsilon_{40\%} - 50\mu\varepsilon} \quad \text{(B-1)}$$

Where: $\sigma_{40\%}\ and\ \varepsilon_{40\%}$ are the 40% of the ultimate stress and its corresponding strain and $\sigma_{50\mu\varepsilon}$ is calculated from curve formula y that correspond micro strain x = 0.00005.

C.2. Steel bars test in tension

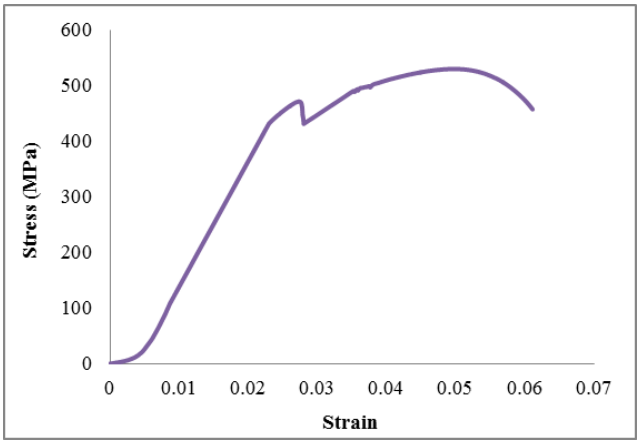

Figure C-2 Stress-strain relationship of the steel bar used in the experimental work

C.3. Relationship between load and displacement in tensile beam tests

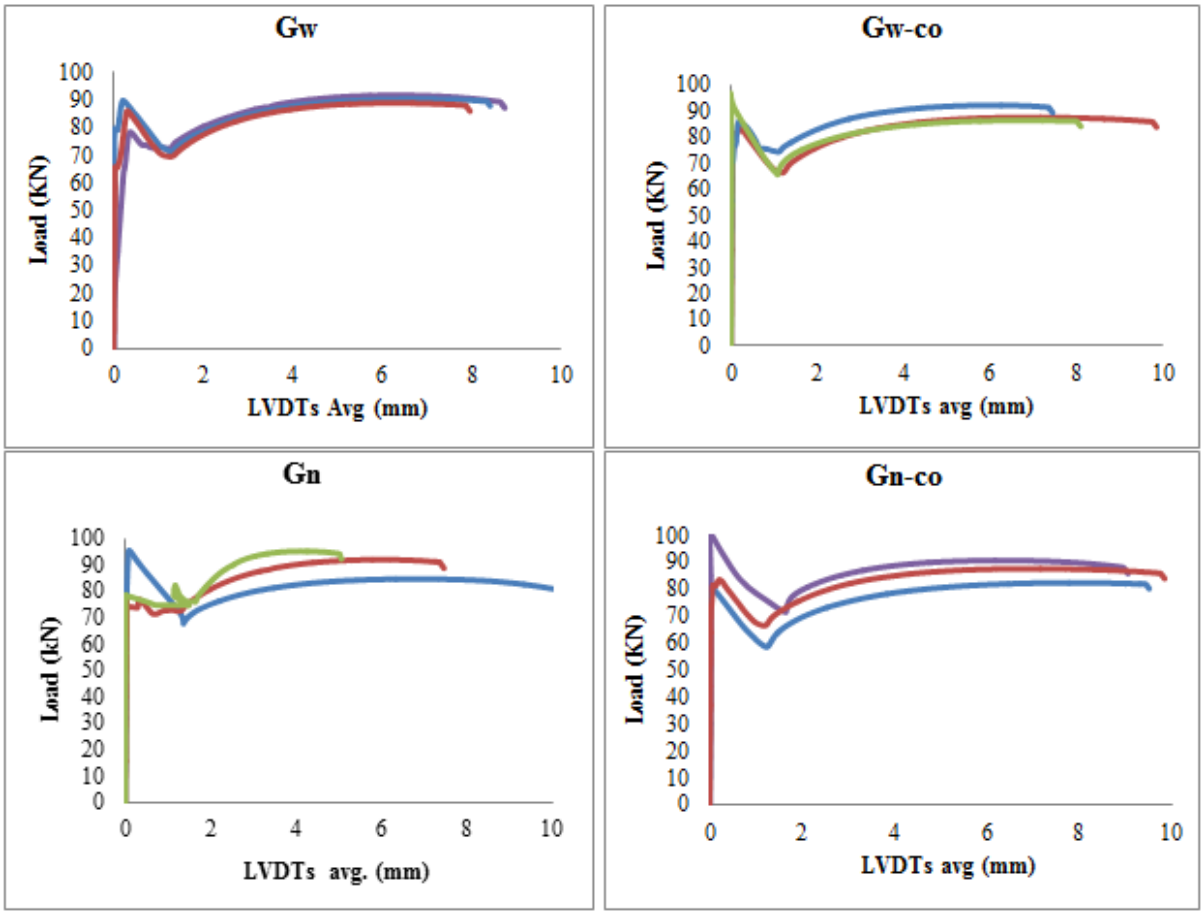

Figure C-3 Load-displacement relationship of direct tensile of the reinforced beams (3 sps of each mix)

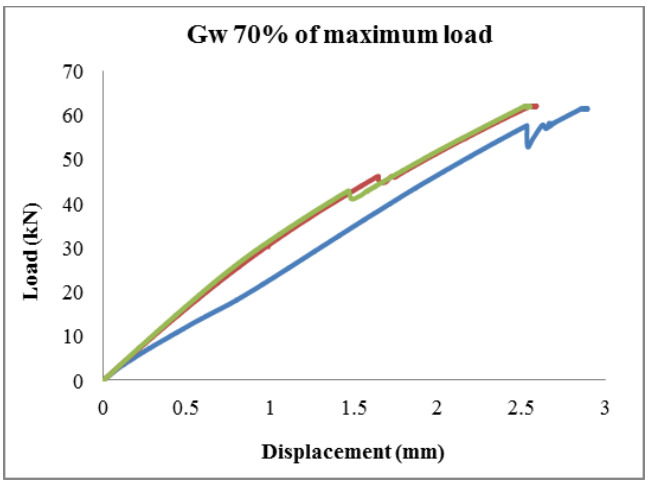

Figure C-4 Load-displacement relationship of 70% ultimate tensile of the reinforced beams (3 specimens of Gw mix, example)

C.4. Relationship between load and crack width in wedge splitting test

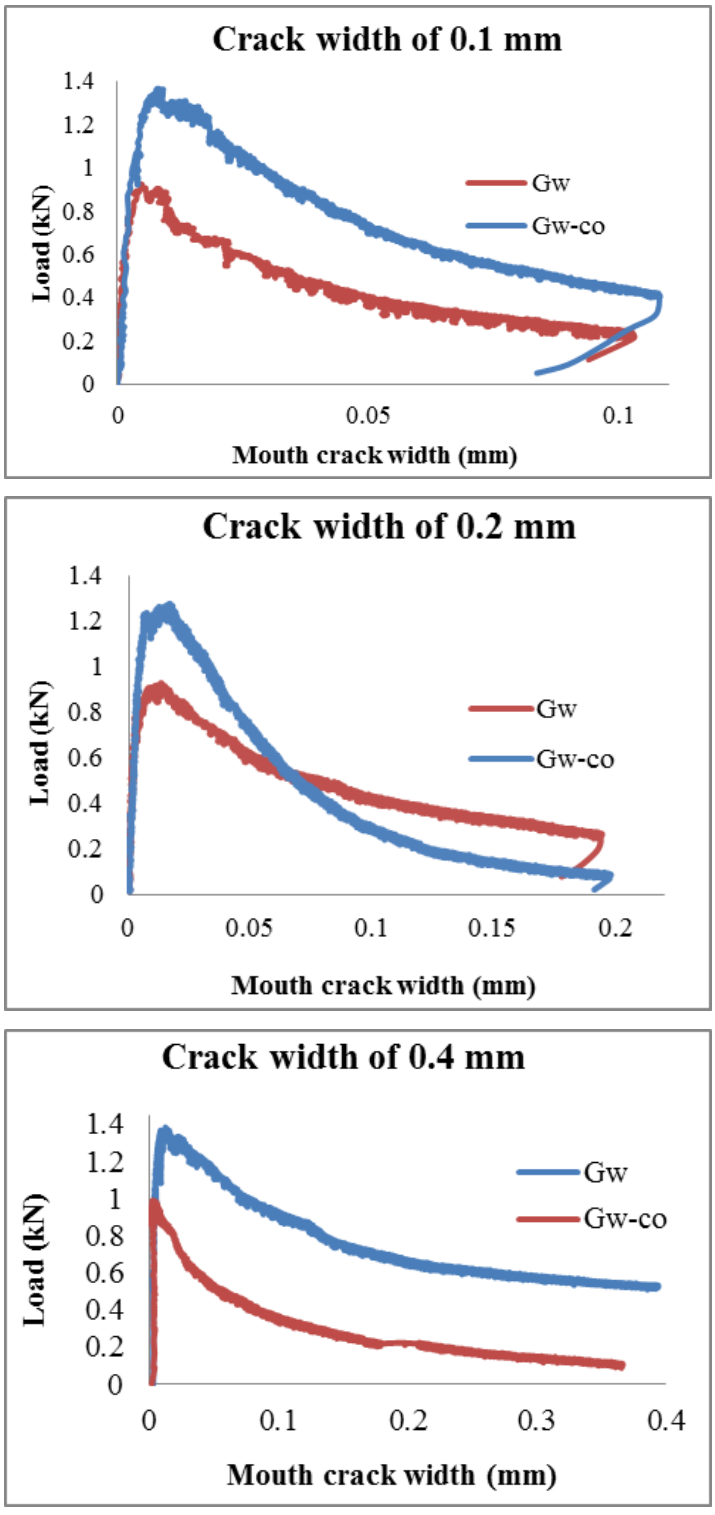

Figure C-5 Load-crack width relationship for wedge splitting of 100 mm3 concrete cubes (example) with controlled crack of: upper = 0.1, mid = 0.2 and lower = 0.4 mm

C.5. Sieve analysis of the aggregates used in the experimental

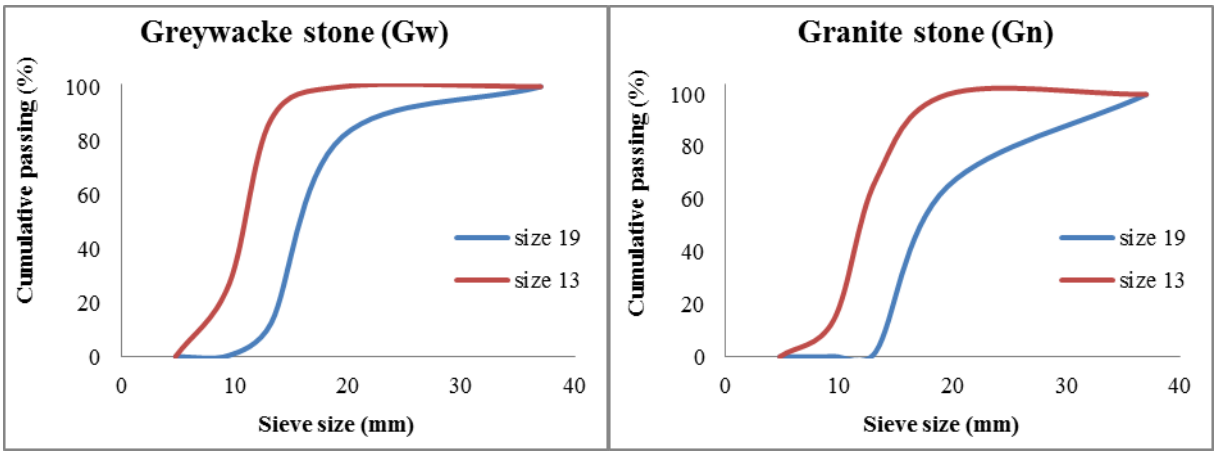

Figure C-6 Sieve analysis of 19 and 13 mm of coarse aggregates (Greywacke and Granite)

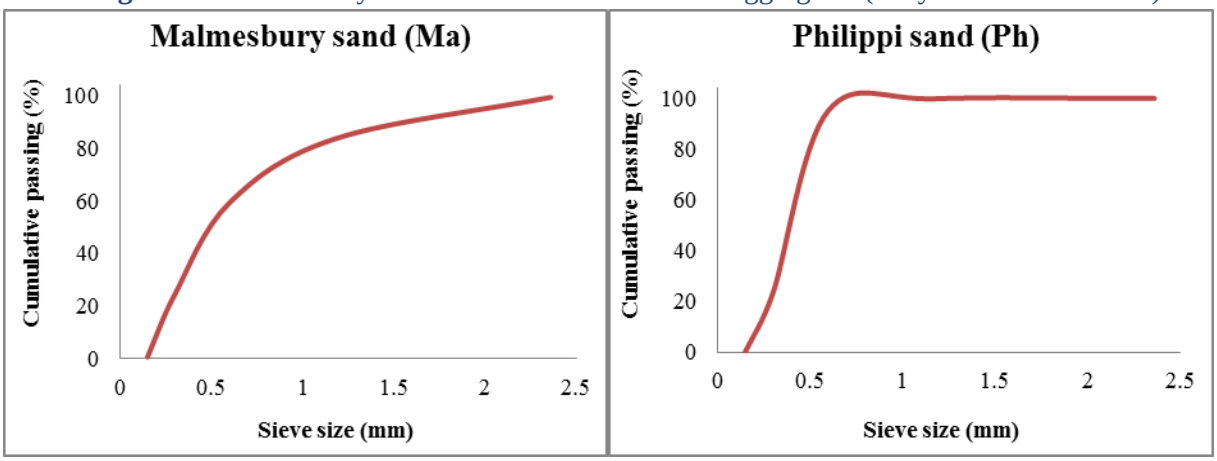

Figure C-7 Sieve analysis of fine aggregates (Malmesbury and Philippi)

APPENDIXES

D. PHOTOS OF DEVICES AND SPECIMENS

D.1. Curing devices

Figure D-1 NaOH and hot water chamber with controlled temperature (80°C)

Figure D-2 Chamber for submerged in water (part 1) and exposed to humidity (part 2), RH >90% & 38 °C

Figure D-3 Submerged the specimens in water at 23±2 °C

D.2. Cutting devices

Figure D-4 Devices to cut the specimens; left: Grinding table and right: Sawing table

D.3. Measurement devices

Figure D-5 Devices to read the change in the specimens during the tests; left: Spider 8 data logging equipment and right: LVDT (HBM WA/50MM-T)

Figure D-6 Devices to measure the linear deformation; left: digital strain gauge of 100 mm (resolution 0.001 mm) and right: Mechanical Strain Gauge of 200 mm (resolution 0.002 mm)

D.4. Cylinders specimens

Figure D-7 Greywacke mixes submerged in water at 38 °C

Figure D-8 Greywacke mixes exposed to humidity >90% at 38 °C

Figure D-9 Granite mixes submerged in water at 38 °C

Figure D-10 Granite mixes exposed to humidity >90% at 38 °C

D.5. Destruction of the cylinders

Figure D-11 Destruction of Greywacke specimens after compressive strength test mixes

Figure D-12 Destruction of Granite specimens after compressive strength test mixes

D.6. Marking the specimens

Figure D-13 Denoted the samples in series test 2 (specimens name, condition, date and number of the specimens and spaces between the Pins)

Figure D-14 Denoted the samples in series test 1(specimens name, date and number of the specimens and spaces between the Pins)